Technical Report IRRP-98-3
March 1998

US Army Corps of Engineers
Waterways Experiment Station

Installation Restoration Research Program

Vertical Migration Potential of Metal Contaminants at Small Arms Firing Ranges, Camp Edwards Military Reservation, Massachusetts

by R. Mark Bricka, Yilda B. Rivera, Patrick N. Deliman

19980514 137

Approved For Public Release; Distribution Is Unlimited

DTIC QUALITY INSPECTED 4

Prepared for Massachusetts Military Reservation

The contents of this report are not to be used for advertising, publication, or promotional purposes. Citation of trade names does not constitute an official endorsement or approval of the use of such commercial products.

The findings of this report are not to be construed as an official Department of the Army position, unless so designated by other authorized documents.


PRINTED ON RECYCLED PAPER

Installation Restoration Research Program

Technical Report IRRP-98-3
March 1998

Vertical Migration Potential of Metal Contaminants at Small Arms Firing Ranges, Camp Edwards Military Reservation, Massachusetts

by R. Mark Bricka, Yilda B. Rivera, Patrick N. Deliman

U.S. Army Corps of Engineers
Waterways Experiment Station
3909 Halls Ferry Road
Vicksburg, MS 39180-6199

Final report

Approved for public release; distribution is unlimited

Prepared for Massachusetts Military Reservation
Reading, MA 01867-1999

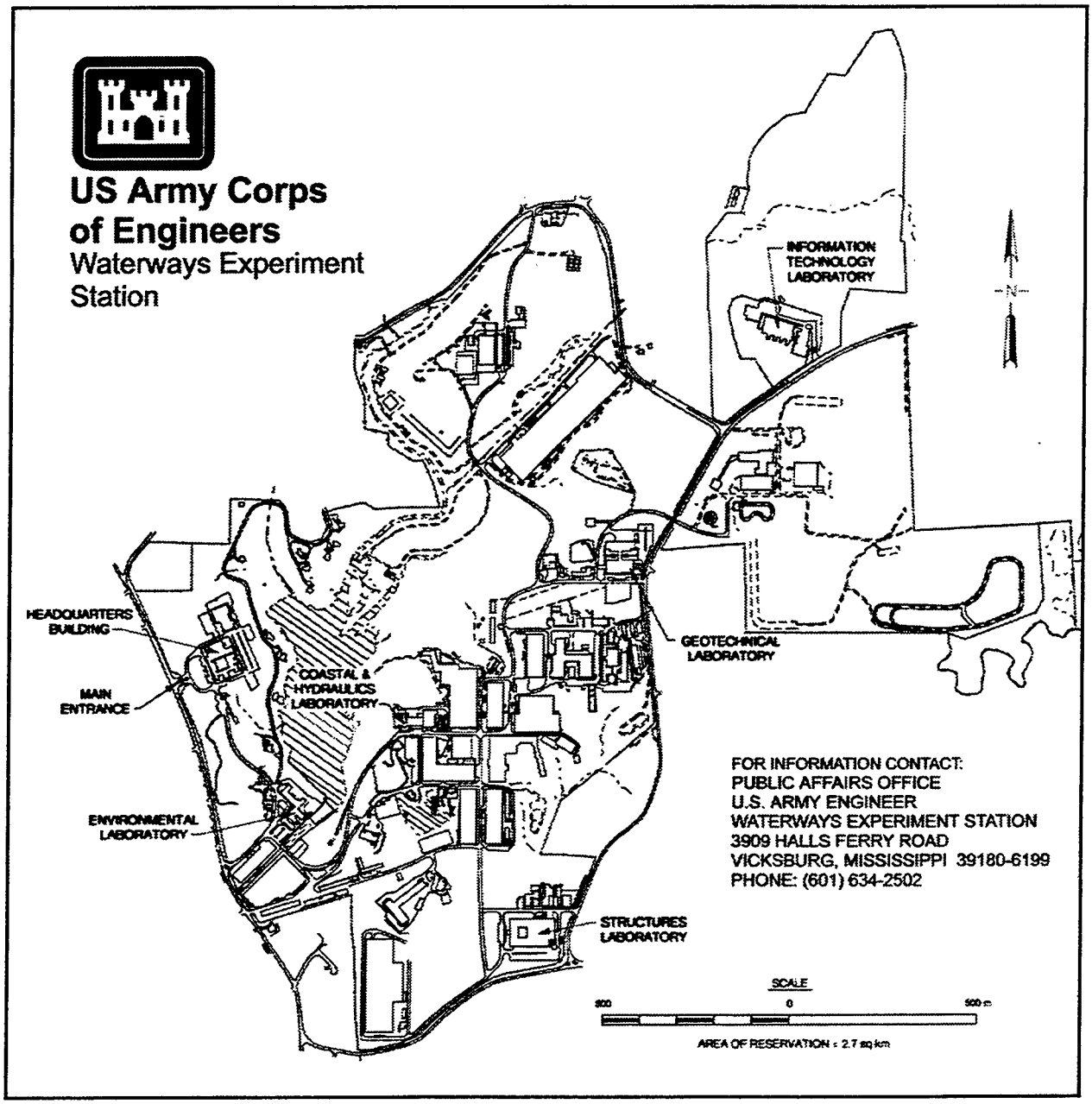

Waterways Experiment Station Cataloging-in-Publication Data

Bricka, R. Mark.

Vertical migration potential of metal contaminants at small arms firing ranges, Camp Edwards Military Reservation, Massachusetts / by R. Mark Bricka, Yilda B. Rivera, Patrick N. Deliman ; prepared for Massachusetts Military Reservation.

198 p. : ill. ; 28 cm. — (Technical report ; IRRP-98-3)

Includes bibliographic references.

1. Metals — Impact testing — Environmental aspects. 2. Rifle-ranges — Massachusetts — Camp Edwards. 3. Projectiles — Environmental aspects. 4. Camp Edwards (Mass.) — Firearms — Environmental aspects. I. Rivera, Yilda B. II. Deliman, Patrick N. III. United States. Army. Corps of Engineers. IV. U.S. Army Engineer Waterways Experiment Station. V. Installation Restoration Research Program. VI. Series: Technical report (U.S. Army Engineer Waterways Experiment Station) ; IRRP-98-3.

TA7 W34 no.IRRP-98-3

Contents

List of Figures

List of Tables

Preface

This report was prepared for the Army National Guard Bureau, Massachusetts Military Reservation (MMR), Environmental Office, and as part of the Installation Restoration Research Program (IRRP), by the U.S. Army Engineer Waterways Experiment Station (WES). Captain Tracy Norris served as the MMR project manager for this investigation. This study was conducted as part of an investigation to examine the potential for vertical migration of lead from small arms training activities conducted at MMR.

The report was prepared by Mr. R. Mark Bricka of the Environmental Restoration Branch (ERB), Environmental Engineering Division (EED), Environmental Laboratory (EL), and Yilda B. Rivera, Environmental Resources Engineering Branch (EREB), EL, WES. Chemical analyses were performed by the Environmental Chemistry Branch under the supervision of Ms. Ann Strong. Modeling support was provided by Dr. Patrick Deliman of the Water Quality and Contaminant Modeling Branch of the Environmental Process and Effects Division, EL, under the supervision of Dr. Mark Dortch.

Collection of the samples was overseen by Mses. Trudy J. Olin and Yilda B. Rivera, EL, and sampling support was provided by the U.S. Army Corps of Engineers, Vicksburg District, under the guidance of Mr. Jimmy Gray. Technician support for this project was provided by Mr. Mike Marino and Mses. Julie Rosado and Carla Guimbellot, of the ERB.

The study was conducted under the direct supervision of Mr. Daniel E. Averett, Chief, ERB, and under the general supervision of Mr. Norman R. Francingues, Chief, EED, and Dr. John Harrison, Director, EL.

During publication of this report, Dr. Robert W. Whalin was Director of WES. COL Robin R. Cababa, EN, was Commander.

This report should be cited as follows:

Bricka, R. M., Rivera, Y. B., and Deliman, P. N. (1998). "Investigation of the Vertical Migration Potential of Metal Contaminants at Small Arms Firing Ranges, Camp Edwards Military Reservation, Massachusetts," Technical Report IRRP-98-3, U.S. Army Engineer Waterways Experiment Station, Vicksburg, MS.

The contents of this report are not to be used for advertising, publication, or promotional purposes. Citation of trade names does not constitute an official endorsement or approval of the use of such commercial products.

1 Introduction

The primary goal of the U.S. Military is to train and equip troops to maintain military readiness. Training range areas represent a major element in keeping the Army ready to accomplish this mission. Training ranges represent considerable investments in time, land, money, and other resources (U.S. Army 1992). It is critical for the Army to maintain and operate such training ranges. Training range activities have negatively impacted the environment; thus, it is necessary to conduct research and development to minimize any environmental impact while meeting Army training requirements.

A wide variety of training ranges are currently owned and/or operated by the Army. Such ranges include (but are not limited to) small arms ranges, gunnery ranges, hand grenade ranges, mortar ranges, and large impact training ranges. Operations at each of these ranges are widely varied, as are the types of weapons and projectiles used during training exercises.

Of recent concern is the impact of training activities on the environment. Military training activities, and spent munitions remaining after the conclusion of training activities, have come under recent review. There is a concern that these activities result in long-term environmental degradation. Regulations are currently being drafted (U.S. Environmental Protection Agency (USEPA) 1995) to regulate such activities.

Small Arms Ranges

Small arms ranges (SAR) include a vast array of ranges. Specifically excluded from the SAR category are impact areas. While SAR may include mortar ranges and grenade ranges, in this report SAR will only refer to outdoor pistol and rifle training ranges.

A typical SAR consists of a firing position (the point of weapon firing), a cleared down range area, a target position, and an impact berm, as shown in Figure 1. The Army has a variety of SAR as listed in Table 1 (U.S. Army 1992), but generally these ranges can be grouped into the following three classes:

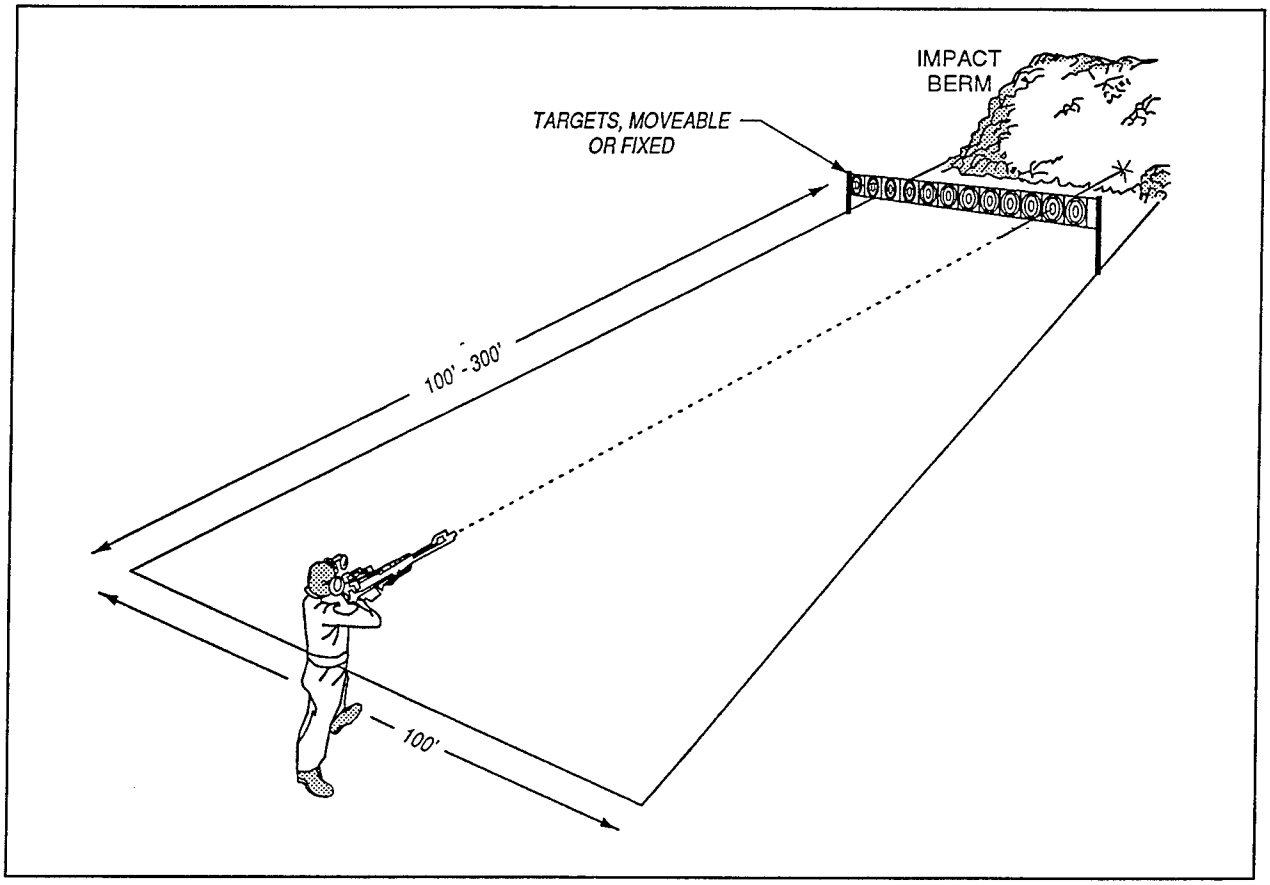

Figure 1. Typical small arms range

Table 1
Types of Small Arms Training Ranges Utilized by the Army

Range/Facility	Type
Combat Pistol Qualification Course/Military Police Firearms Qualification Course (MPFQC)	M
Multipurpose Indoor Range (Small Arms)	M
Basic 25-m (82-ft) Range (Zero)	M
Automated Field-Fire Range	M
Automated Record-Fire Range	M
Modified Record-Fire Range	M
Sniper Field-Fire Range	S
Night-Fire (Small-Arms) Range	S
Known-Distance (KD) Range	S
Machine Gun 10-m (32.8-ft) Range	S

Note: S = Armywide Standard, M = Modernized Armywide Standard.

a. Zeroing ranges.

b. Famaliarization ranges.

c. Qualification ranges.

Typically the weapons utilized at these SAR are 50-caliber or smaller munitions with the largest percentage currently utilized at these ranges consisting of 9-mm pistol rounds, M16-5.56-mm machine gun rounds, and M60-7.62 machine gun rounds. Historically, 45-caliber pistol and M1 carbine rounds have also been extensively used. A schematic of a typical 25-m (82-ft) zeroing range is presented in Figure 2, and while a distinction was previously made between familiarization and qualification ranges, these typically have the same general configuration, as shown in Figure 3.

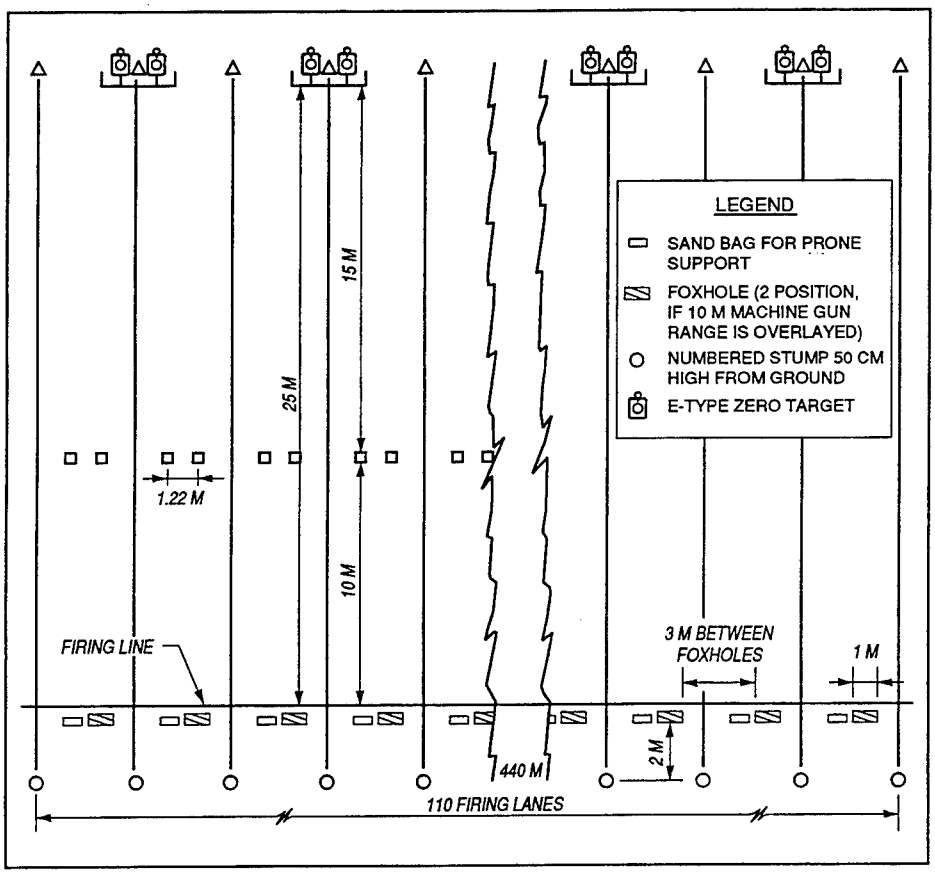

Figure 2. A 25-m (82-ft) zeroing range

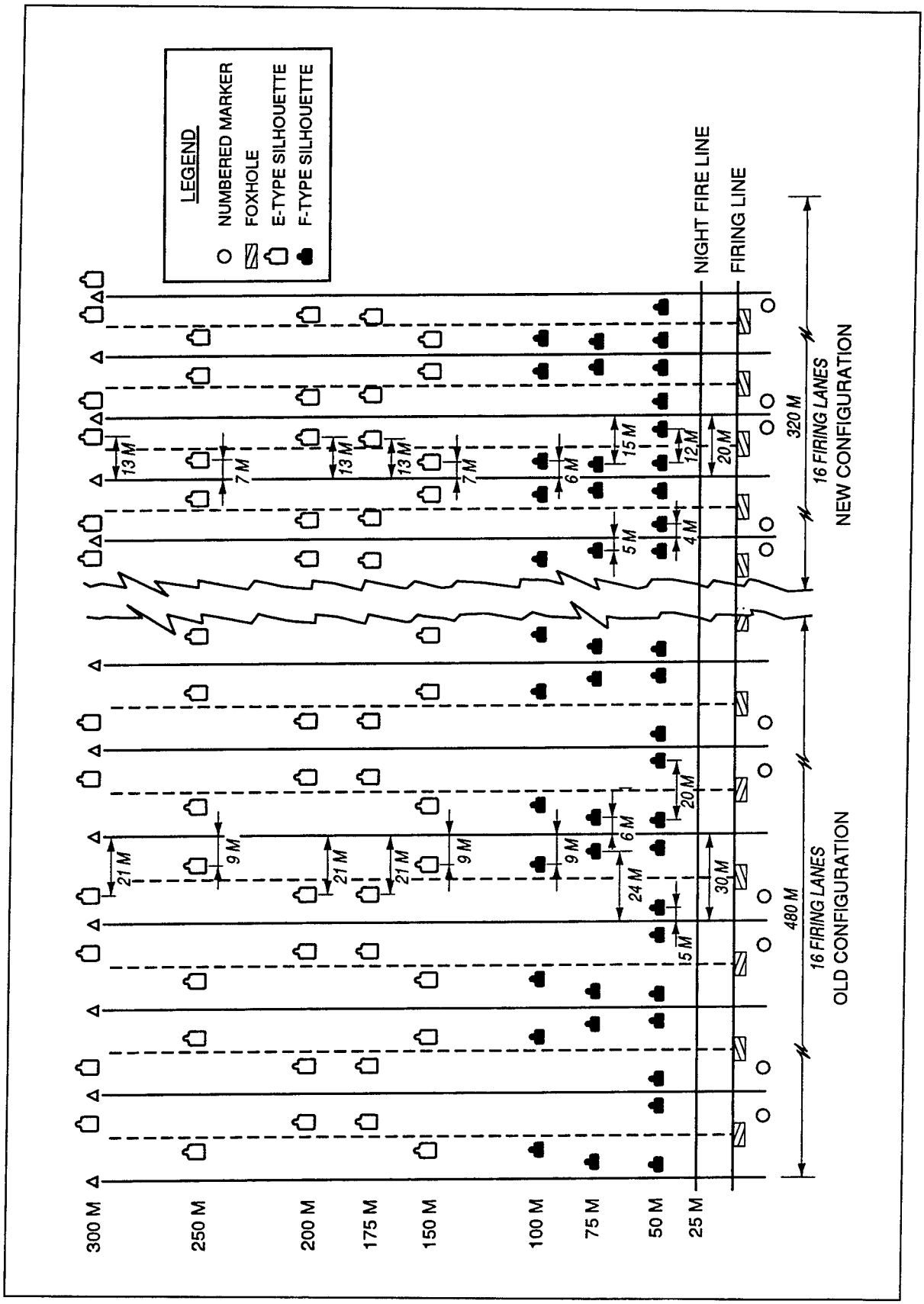

Figure 3. Schematic of a typical familiarization and/or qualification range

Environmental Issues at SAR

The main environmental concern associated with SAR involves spent munitions. Typically projectiles are fired at a target and after passing through the target, projectiles are stopped in a berm or the soil located behind the targets. After years of use, the projectiles from the small arms activities build up in the soil. The projectile rounds utilized at SAR typically consist of a copper-jacketed bullet and a lead core. As shown in Table 2 and Figure 4, the majority of the projectiles are comprised of a lead (Pb) antimony (Sb) alloy, and copper (Cu) metal. Military specifications for the rifle projectiles are provided in Appendix A. As illustrated in Table 2, lead accounts for up to 75 percent of the weight of the projectile and constitutes the greatest environmental concern.

Table 2
Typical Metal Composition of 5.56-mm and 7.62-mm Projectiles

Ball Type	Weapon	Metal Concentration in Weight Percent			
		Antimony	Copper	Iron	Lead
5.56 mm	M16	1.4	31.3	--	67.3
7.62 mm	M60	1.5	23.2	--	75.3
5.56 mm (Hardened Tip)	M16	1.0	35.4	12.7	50.9

The quantity of lead and copper which can accumulate in an SAR berm is massive. Based on conservative estimates and assuming only weekend training at CEMR, it is estimated that approximately 12,000 lb of Pb will accumulate in the berm of a single SAR on an annual basis (calculations are provided in Appendix B). At active duty, SAR lead accumulation is expected to be higher due to higher usage.

Summary of Metal Toxicity

Over the years, a large number of studies have been conducted investigating lead and its health consequences. One popular belief is that the fall of the Roman Empire, in part, may have been caused by the use of Pb alloys for drinking vessels and aqueducts. The ingestion of lead-contaminated wine and drinking water resulted in health problems and mental impairment of the society. Regardless of the Roman history, modern medicine identifies Pb as having major impacts on human health, particularly for children (Sax 1984).

The Safe Drinking Water Act passed by Congress sets the U.S. public drinking water action level to a stringent 15 µg/ℓ of (USEPA 1996) and the Clean Water Act sets the standard for Pb at 50 µg/ℓ (USEPA 1986b). Lead blood levels of >0.05 mg/kg or urine levels >0.08 µg/ℓ are associated with lead poisoning. Serious brain, kidney, and nervous system damage has been documented even at levels in drinking water below the maximum contaminant level goal of 50 ppb (Gale, Liu, and Bricka 1994).

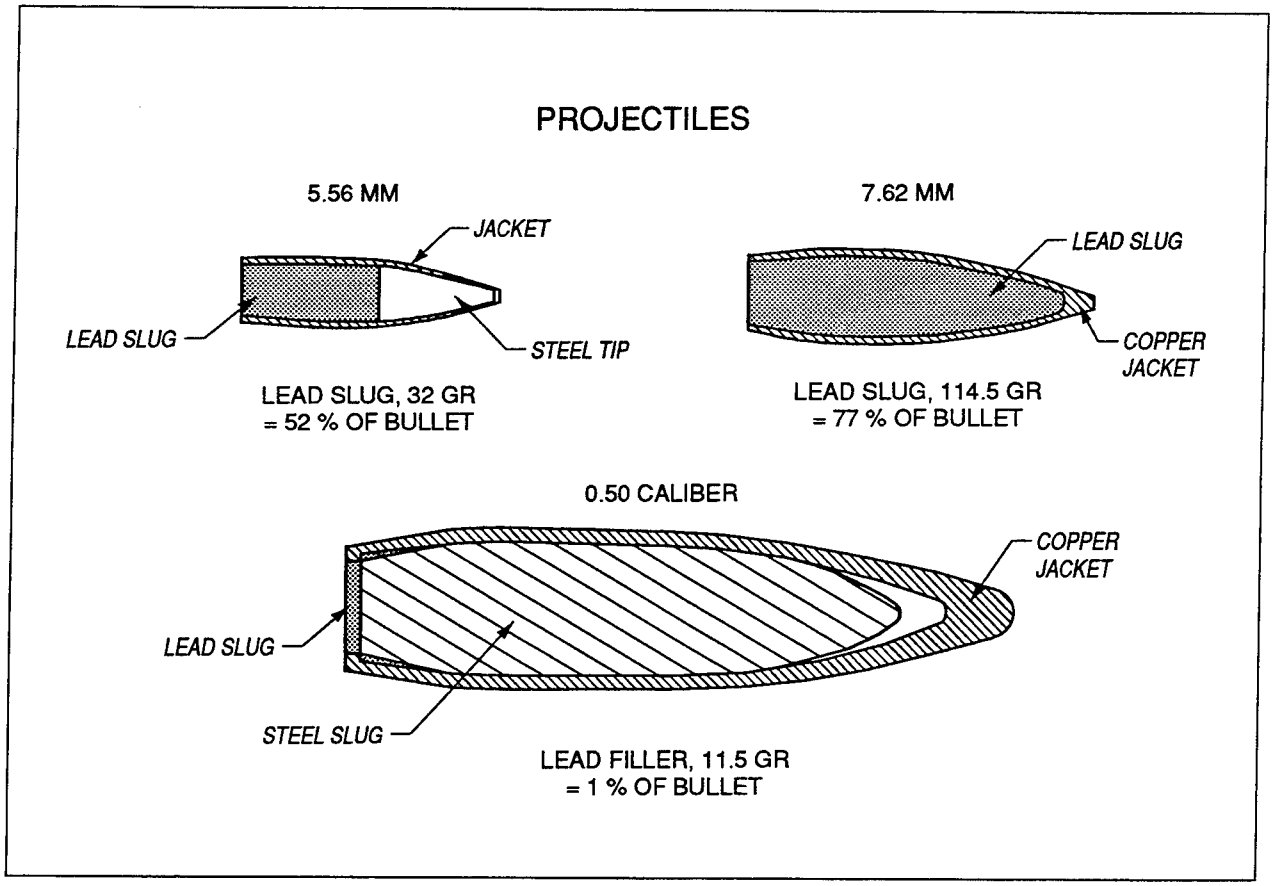

Figure 4. Drawing showing cross sections of bullets

Copper, in contrast, has little or no human toxicity. Cu is known to have effects on the biotia and has been used as a fungalcide in many industrial and agricultural applications (Gale, Liu, and Bricka 1994). The drinking water standard for Cu is 1 part per million (ppm).

Metals Migration at SAR

Metals have two primary mechanisms of transport from an SAR. They can be transported from the range via horizontal migration, resulting in surface water contamination, and they can migrate vertically, potentially impacting the groundwater.

Horizontal transport

Horizontal migration generally occurs during heavy precipitation events where particulate metals are transported through quick-moving surface runoff to nearby streams. Metal particulates transported though this type of migration generally

result in localized contamination since the density of the metals exceeds that of water. As the velocity of the transporting water slows, the metal particles originally suspended drop from solution and are deposited on the surface. Horizontal metal migration also occurs via sediment transport. Dissolved metal ions tend to sorb to the fine material in the soil. Lab tests indicate (Bricka 1996a) that in many instances metals concentrate in the fine fraction of the soils (less than 63 μm). Small soil particles heavily contaminated with metals are easily transported in the suspended and dissolved solid fraction of the water. Colloidal materials, having electrostatic charge and containing large concentrations of heavy metals, may remain suspended indefinitely in the water column. This allows the metals to be transported long distances in the surface water. Suspended matter containing metal contamination may settle from the water column far from the range resulting in substantial accumulation of metals in the sediment of local streams near SAR.

Vertical transport

Metals also have the potential to migrate from the SAR to groundwater via vertical transport. This occurs because the metals are in constant contact with the soil pore water, which can become saturated with dissolved metals. The infiltration of rainwater can flush the pore water and carry contamination to the groundwater. However, the capillary action of the soil and evapotranspiration may mitigate downward contaminant migration. During this vertical migration, the contaminants pass through the vadose zone to groundwater; thus, the metals must move through an unsaturated condition prior to impacting the groundwater. After the contaminant enters the groundwater, subsurface horizontal transport in the groundwater will be the predominant transport mechanism, disseminating the contaminant from the source.

Many factors influence the rate of vertical transport of the metal contaminants: soil chemistry, water chemistry, metal speciation, atmospheric precipitation, site topography, wetting and drying cycles, freezing and thawing cycles, groundwater depth and velocity, and projectile type. Water chemistry effects including pH, redox potential (Eh), and the presence of complex-forming ligands (carbonates, sulfates, and various organic acids, etc.) will also affect the metal migration. Soil chemistry, water chemistry, and metal speciation are closely intertwined. As shown in Figure 5, once the metal is dissolved, factors such as the soil organic content, presence of metal oxides, carbonates, sulphide, soil clay content, and soil cation exchange capacity can affect metal solution chemistry.

In general, soil chemistry will affect the sorption behavior of the metal. For example, soils with high clay contents or containing large fractions of organic matter will exhibit high sorption capacity for the metals. Water chemistry, on the other hand, governs metal solubility and coprecipitation. In addition, water chemistry will affect the redox potential and the metal speciation. Each of these factors contributes to the retention or release of the metals by the soils. In summary, vertical transport of metal contaminants is a complicated process involving many soil and pore water interactions. A detailed discussion of soil and pore water interactions is provided in Chapter 6, "Theory of Metal Migration at CEMR."

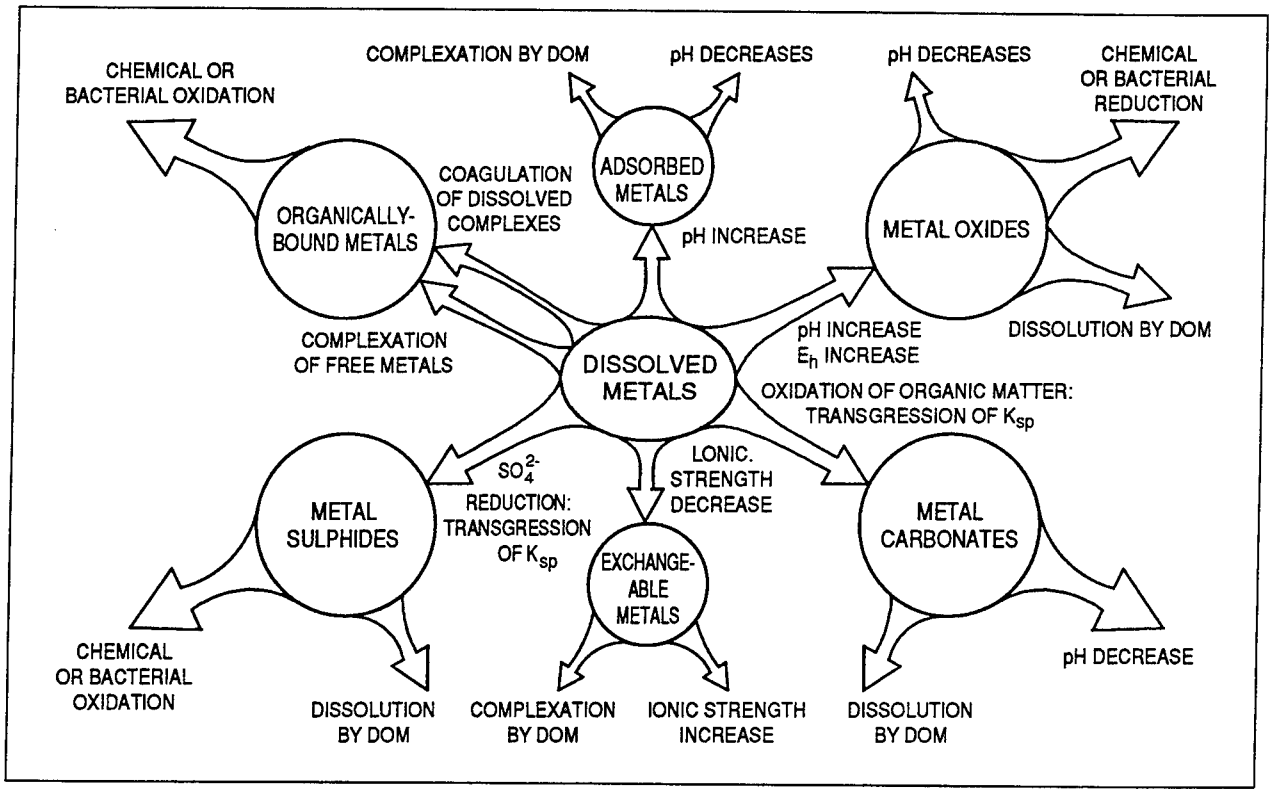

Figure 5. Factors contributing to metal distribution in soils

2 Objective of This Report

The objective of this report is to determine the potential impact of the vertical migration of metals from SAR located at Camp Edwards Military Reservation (CEMR). This report attempts to combine theory, site sampling data, and two modeling efforts to support this objective. In addition to supporting the issues at CEMR, results of this study will serve as a basis to support prediction of contaminant migration potentials at active duty ranges. Answers to basic questions in this study will provide a basis for additional research.

3 Site Location and Description

CEMR is located on upper Cape Cod about 60 miles southeast of Boston (Figure 6). CEMR consists of about 22,000 acres. Approximately 14,000 acres, occupying the northern 70 percent of CEMR, make up the Camp Edwards range, maneuver, and impact areas. Camp Edwards is primarily utilized as a training area for National Guard troops.

The sites selected in this study are located approximately 0.8 m (1/2 mile) south of the impact area just off of Pocasset Forestdale Road. The SARs investigated in this study include Range G (southwest of Opening Pond), Range H, and Range K (as shown in Figure 7).

Range G is a 25-m (82-ft) zeroing range consisting of approximately 27 firing points. Range G measures approximately 60 m (196.9 ft) wide by approximately 35 m (114.8 ft) long. A large berm is located approximately 6 m (19.7 ft) behind the targeting area. This berm collects the majority of the projectiles fired, although some projectiles are observed behind the berm area. It appears as though this range is used mostly for training involving M-16 rifles, using the 5.56-mm jacketed ball projectile, although some ball projectiles from 9-mm pistol training were observed in the impact berm.

Range H is a 25-m (82-ft) zeroing range located just east of Range G. Range H is a 25-m (82-ft) zeroing range, which is similar in design to Range G and is used for similar training activities.

Range K appears to be a modified record-fire range located approximately 1 mile southeast of Range G. Range K is approximately 50 m (164 ft) wide and 125 to 150 m (410 to 492 ft) long and has approximately 30 firing points. Fewer projectiles were observed in the berm of Range K than Range G or H. Most of the projectiles found at Range K appeared to be of the 5.56-mm jacket ball type. No pistol rounds were observed at this range. It should also be noted that there was a berm located at this site, but range control personnel indicated that this berm may have only been in place for a short period. Site personnel were unsure of the berm's age, but it appeared that some recent earthwork had been performed on the berm. The berm was located approximately 10 to 15 m (32.8 to 49.2 ft) behind the target area. It should also be noted that the berm appeared to be eroded. The toe of the

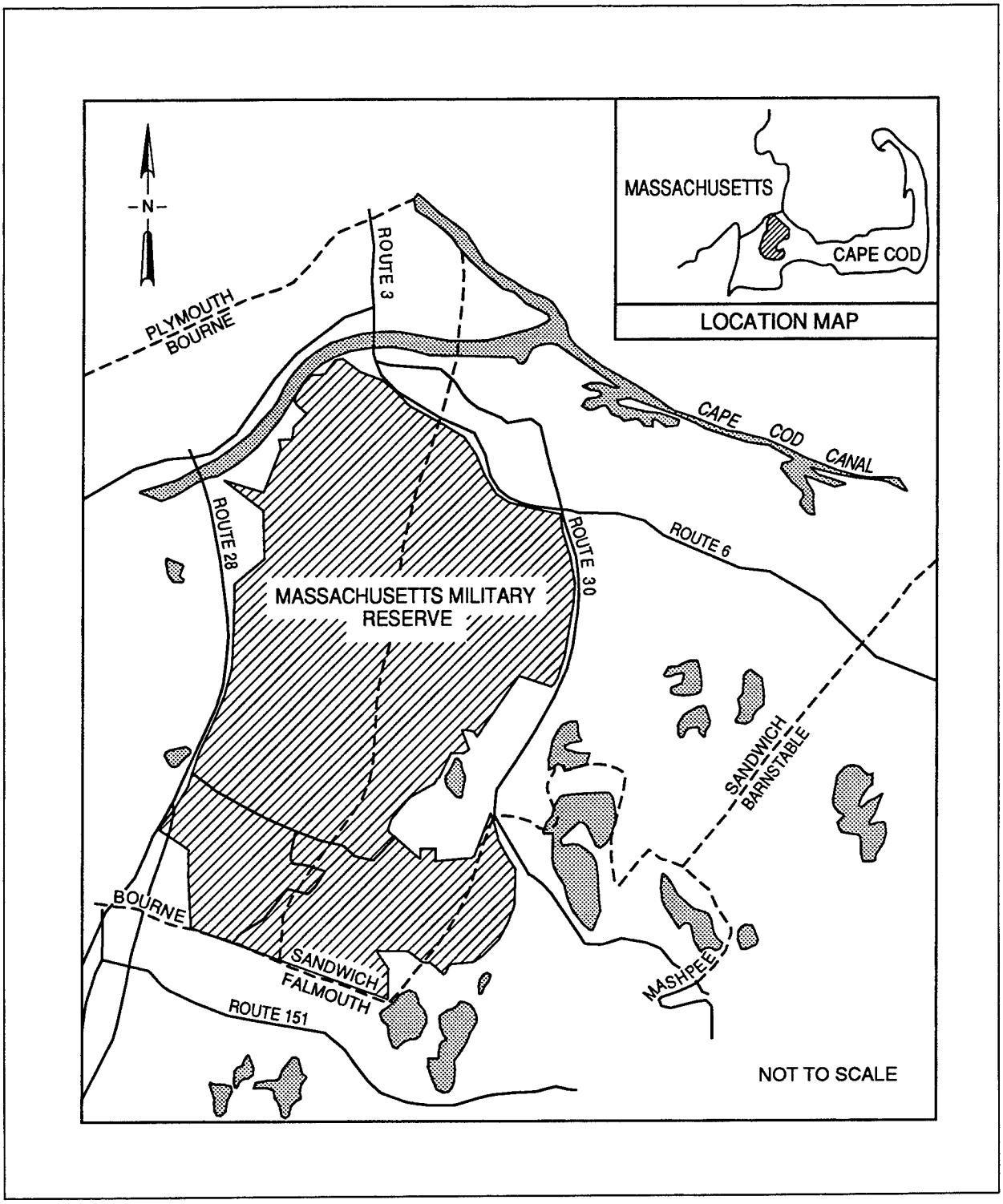

Figure 6. Location of Camp Edwards Military Reservation (CEMR)

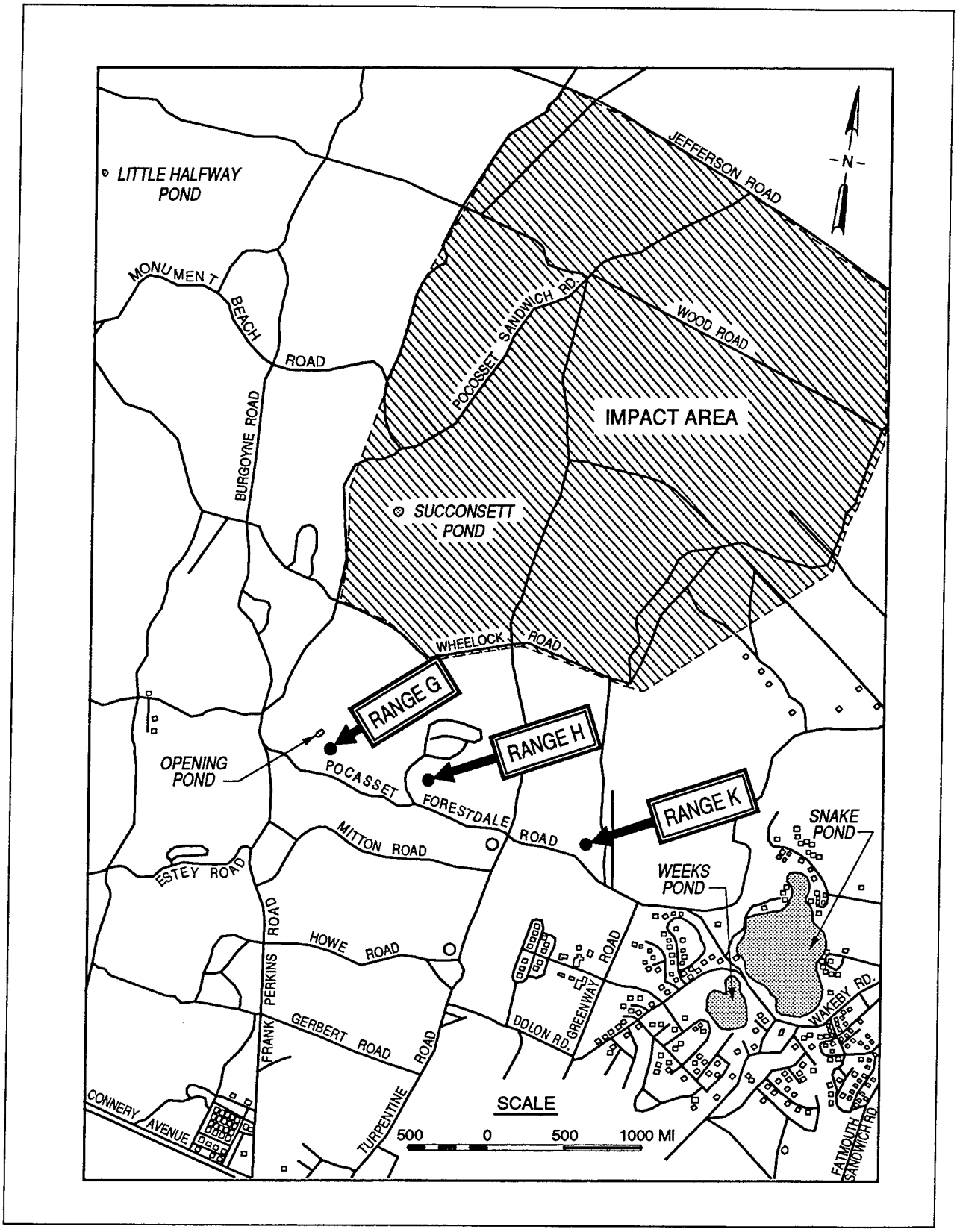

Figure 7. Locations of small arms Ranges G, H, and K

berm had a fine sediment buildup typical of ranges where rain events have washed the fines from the slope to the toe of the berm.

The ranges at CEMR were selected for testing because it was expected that the berms at Ranges G, H, and K would serve to concentrate the projectiles. If vertical migration of the metals is occurring, the berms at these ranges would act as a point source. Vertical contaminant migration near the berms constitutes a worst-case scenario for transport of the metals into the soil. Sample borings were collected approximately in the middle of the ranges at the toe of the berms. Figures 8-10 indicate the sampling locations at Ranges G, H, and K, respectively.

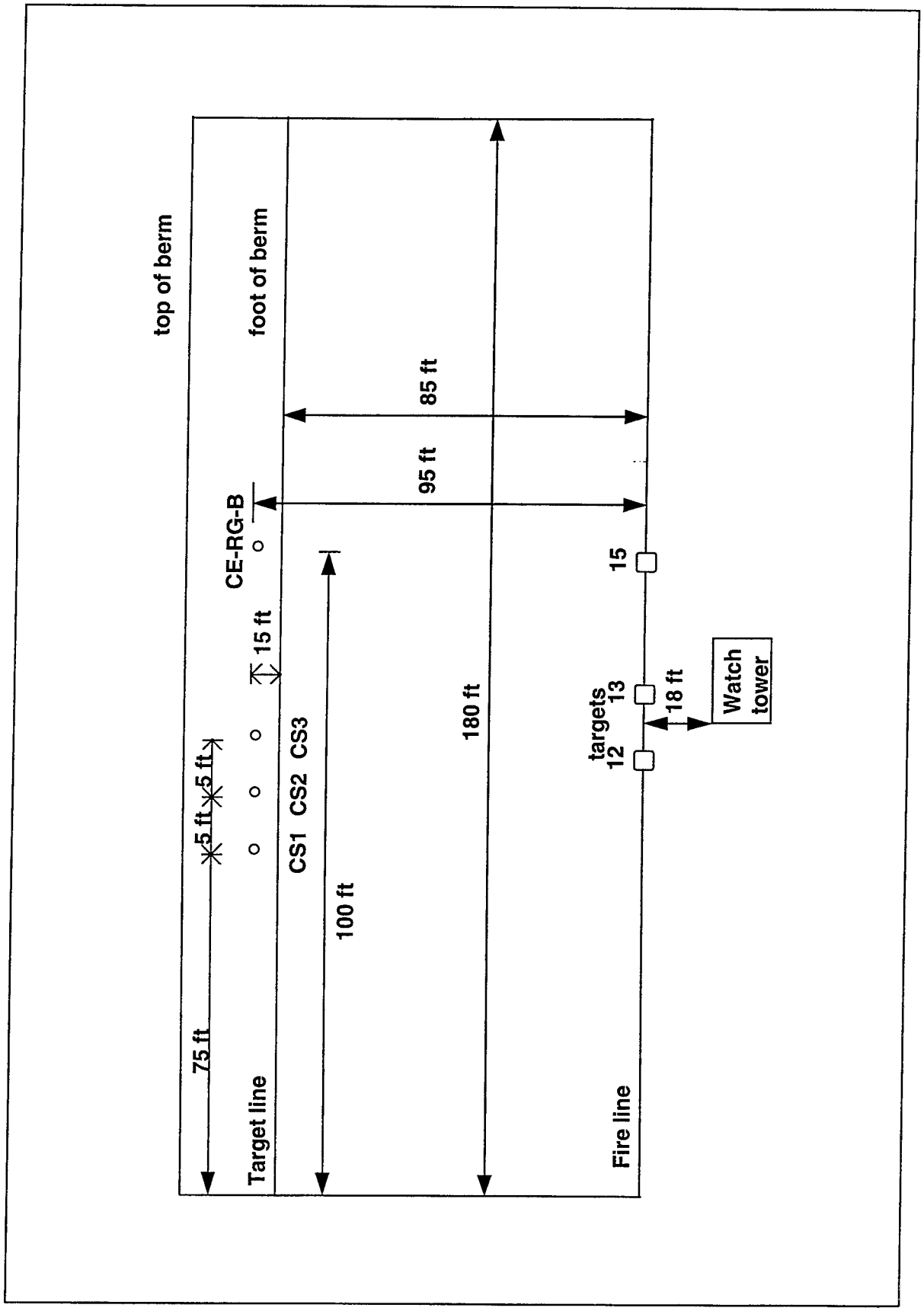

Figure 8. Locations of core Samples CS-G-1, CS-G-3, and CE-RG-B at Range G

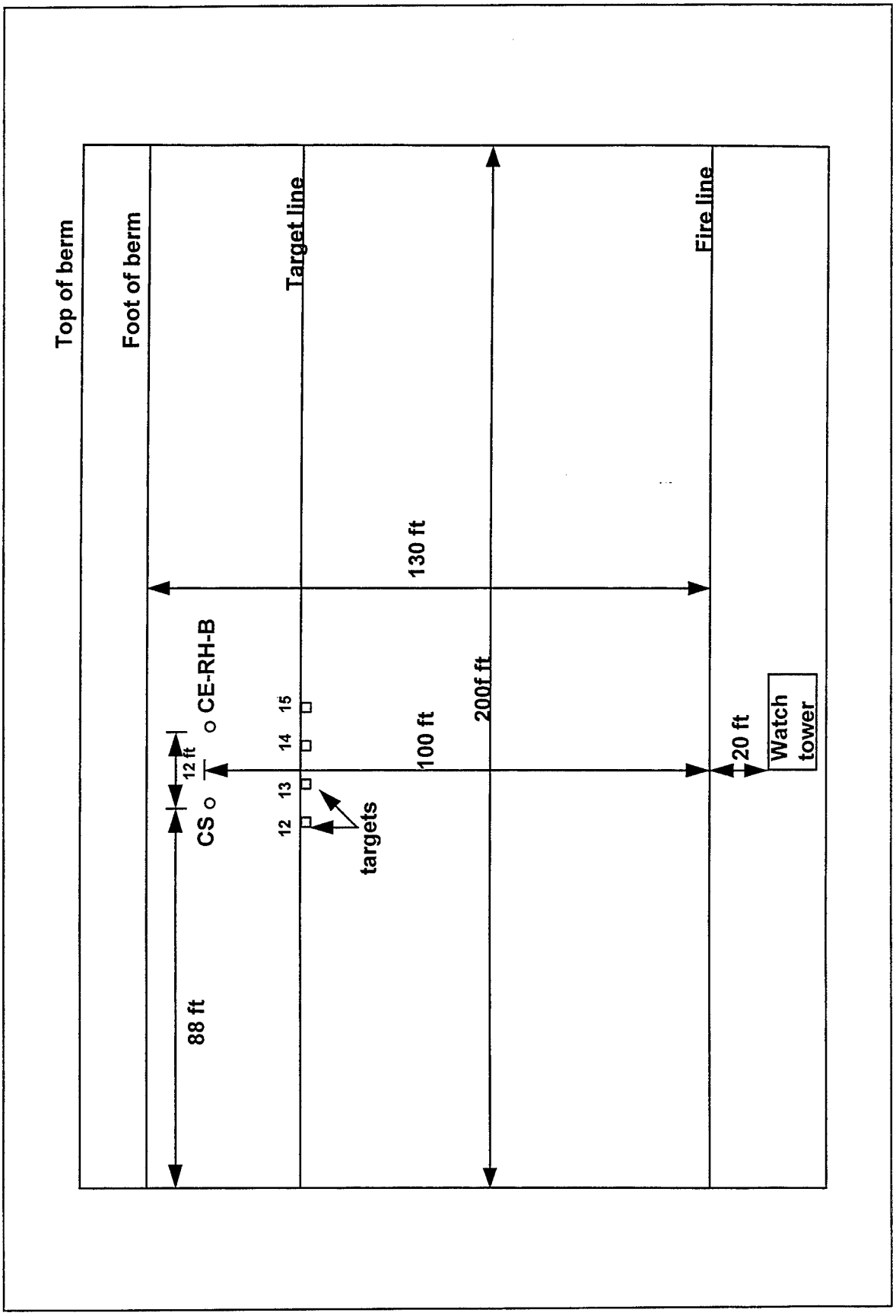

Figure 9. Locations of core Samples CS-H-1 and CE-RH-B at Range H

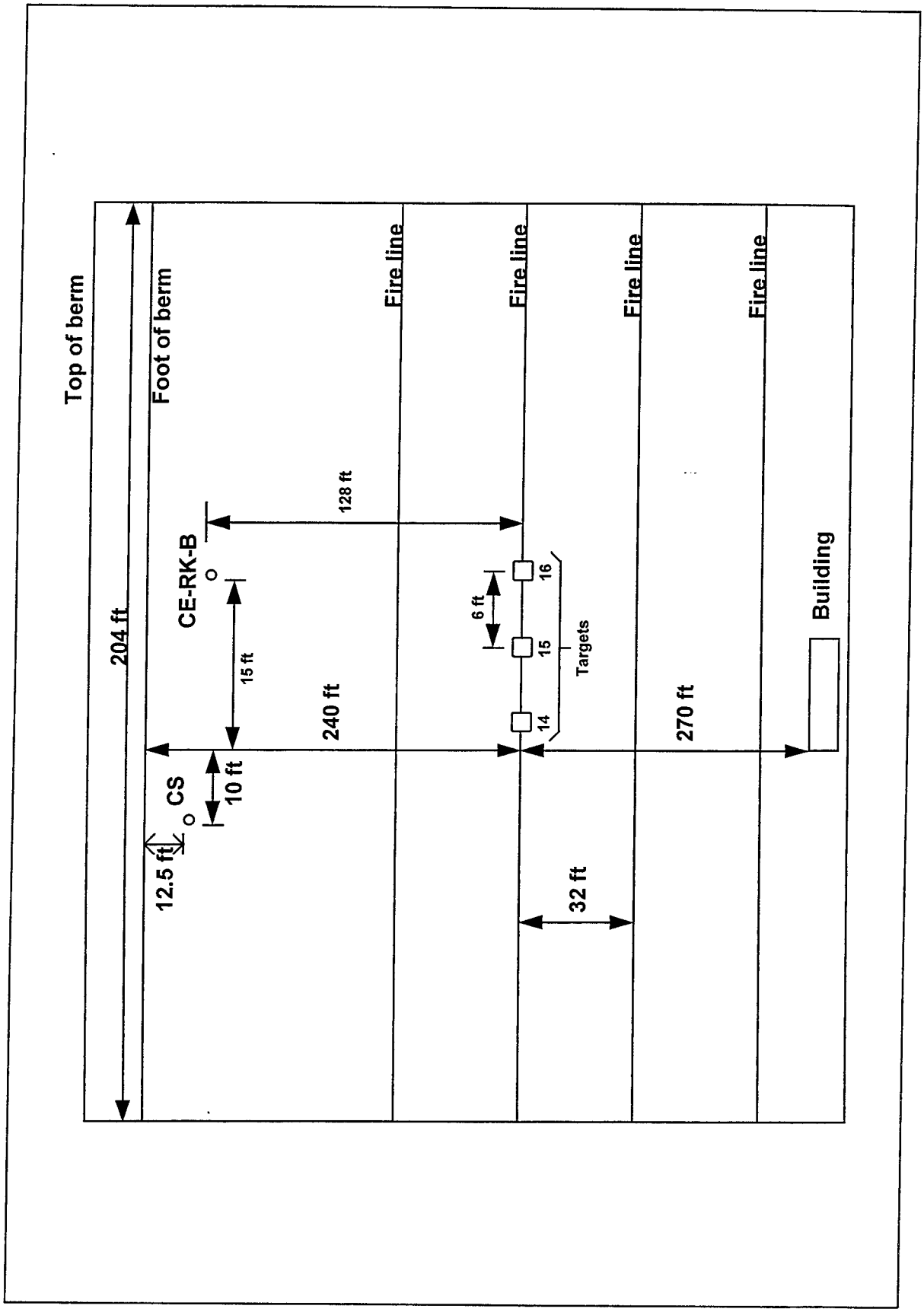

Figure 10. Locations of core Samples CS-K-1 and CE-RK-B at Range K

4 CEMR SAR Site Information

Site Hydrology

Little information regarding site hydrology was available at the time this report was prepared. Based on limited information provided by CEMR personnel, it appears that there is a perched water table located under CEMR, which flows radially from CEMR to the shoreline surrounding the Cape. Figure 11 illustrates this regional groundwater flow (Martin Marietta 1992). This is further supported by other reports showing local groundwater flow. Groundwater at site CS-19 flows in a westerly direction (Figure 13). This report also indicates that the groundwater was encountered at depths ranging from 35.4 to 35.7 m (116-117 ft) or elevations of 23.2 m (76 ft) mean sea level (msl) (U.S. Army 1994b). Groundwater flow from site GP-9 (Figure 14) is almost directly west (Figure 15) (U.S. Army 1994a). Using this information, it appears that various sources are in agreement regarding the groundwater flow direction. Combining information from the topographic map prepared by the 175th Engineering Company and data from site CS-19, it is estimated that the groundwater at sites G, H, and K is encountered at 27.4 m (90 ft), 25.9 m (85 ft), and 18.3 m (60 ft), respectively. Using a hydraulic conductivity of 1.4×10^{-4} ft/hr (estimated for a sand material), and the information provided in Figure 11, it is estimated that the approximate groundwater velocity at SAR Sites G, H, and K is 0.08 cm/sec (9.5 ft/hr).

Soil Description

Based on information provided in the Soil Survey of Barnstable County, Massachusetts (Fletcher 1993), the soils at the range area are described as follows:

Range G

This soil is described as a Merrimac Sandy Loam (MeB). It is classified using the Unified Soil Classification System as an SM to a GP (Appendix C). The soil is generally described as "very friable," containing leaf and pine litter in the top 7.6-cm (3-in.) layer. From a depth of 7.6 to 53.3 cm (3 in. to 21 in.), the soil is

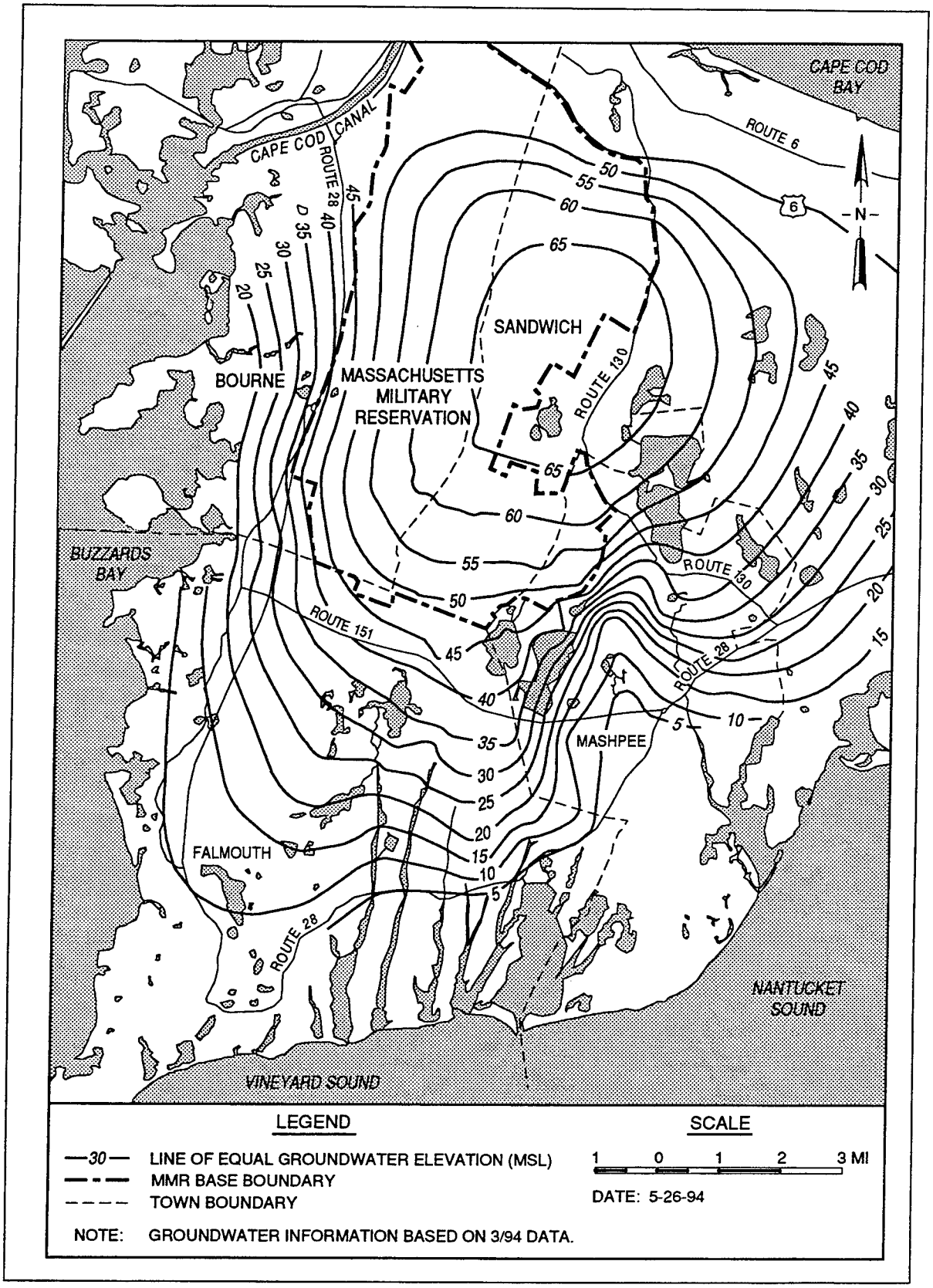

Figure 11. Regional groundwater table map indicating groundwater flow

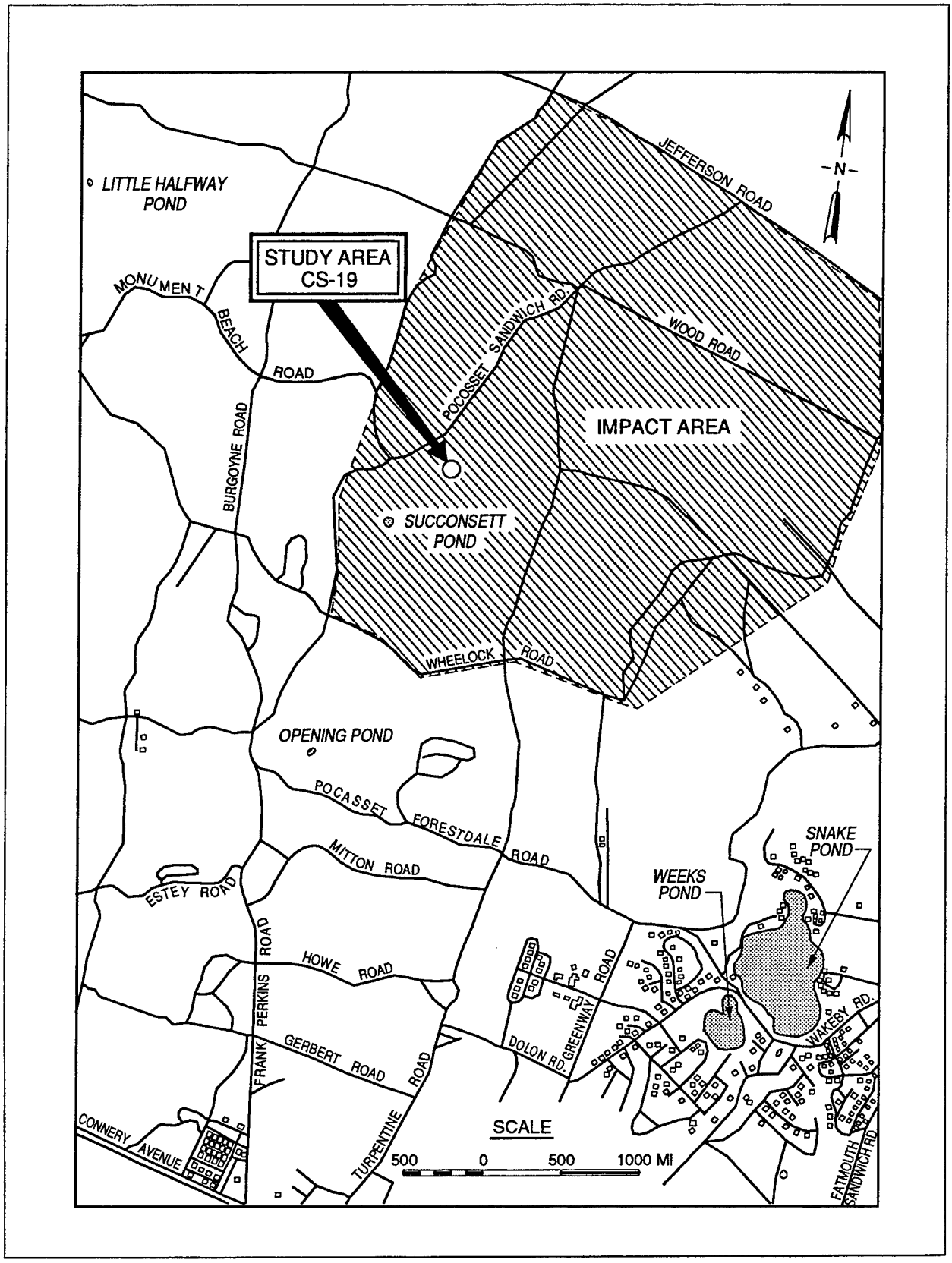

Figure 12. Location of study area CS-19

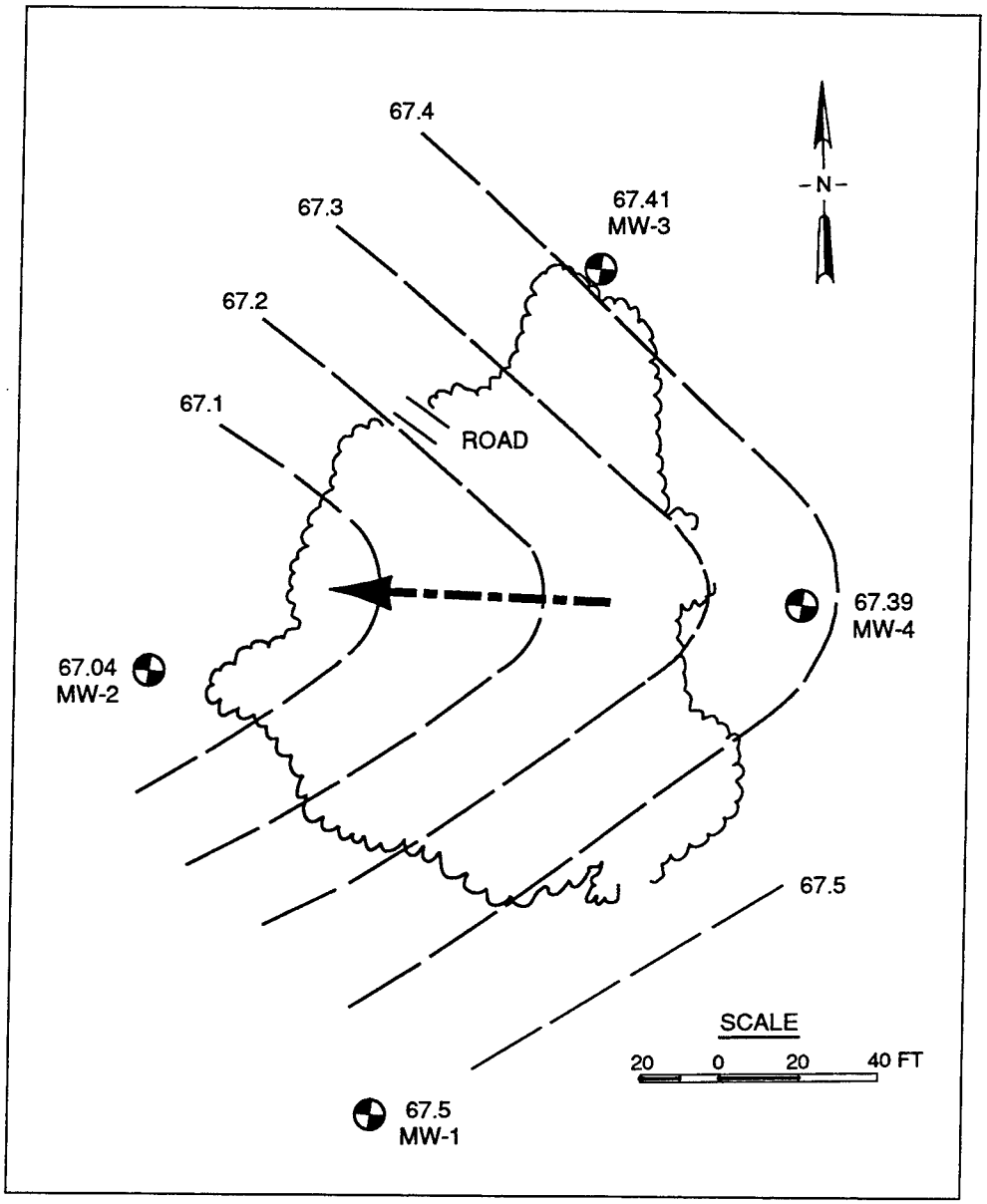

Figure 13. Groundwater table map indicating groundwater flow at Site CS-19

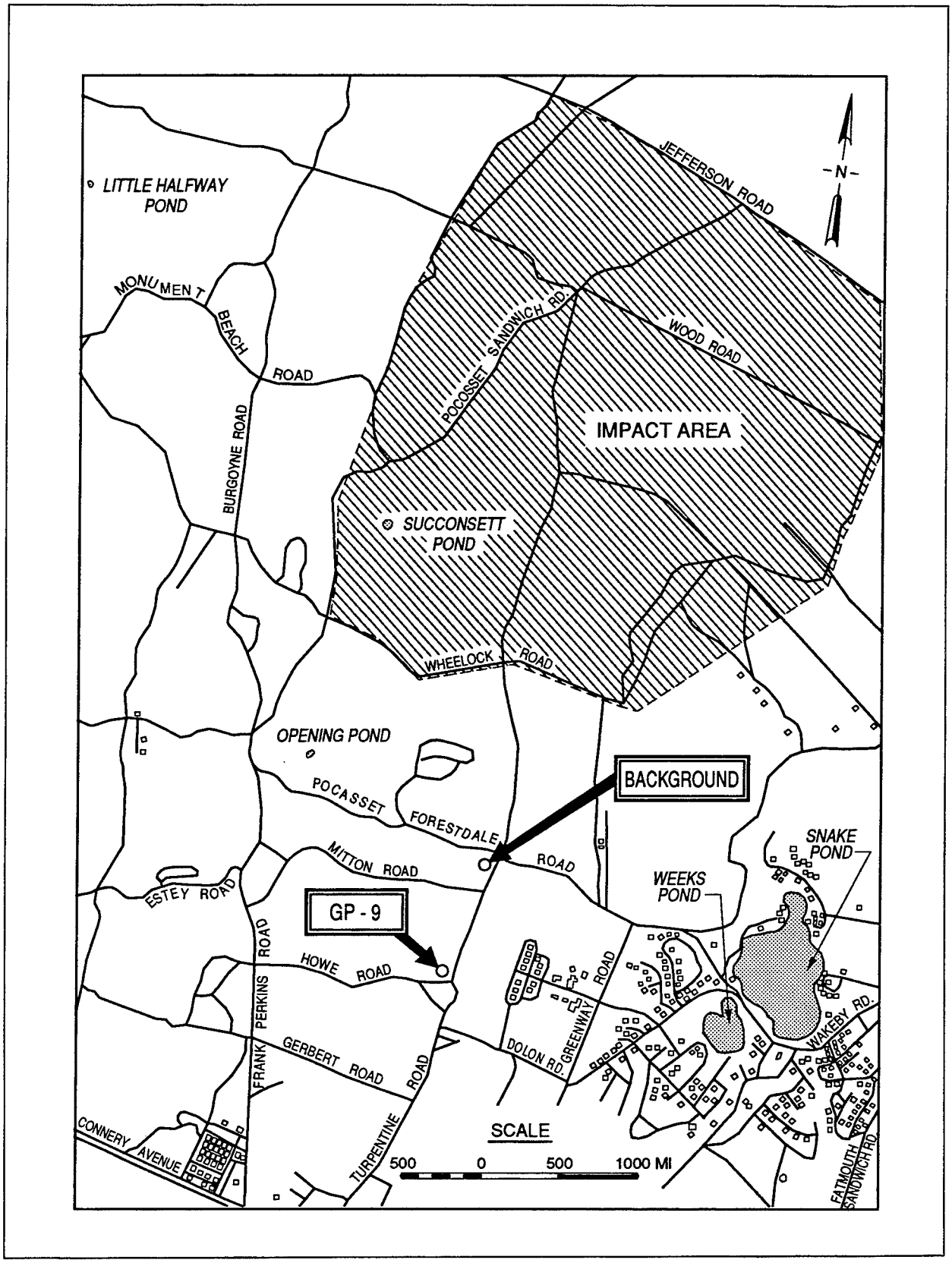

Figure 14. Location of study area GP-9

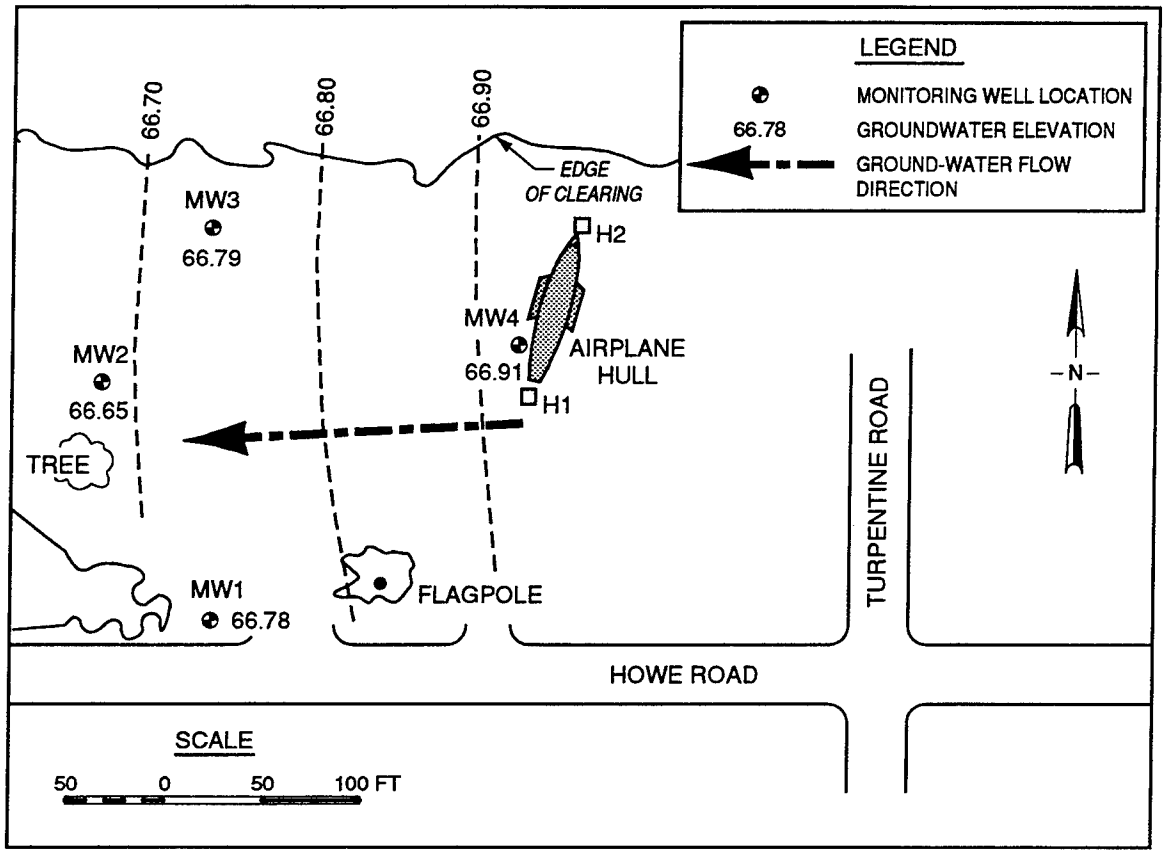

Figure 15. Groundwater table map indicating groundwater flow at Site GP-9

described as a sandy loam, and from 53.3 to 165.1 cm (21 to 65 in.), a loose coarse sand. Table 3 lists some properties of Range G soil.

Table 3
Soil Properties for Range G

Soil Property	Value
Clay content	1-4%
Bulk density	1.2-1.4 g/cc
Permeability	2.0-6.0 in./hr 1.4×10^{-3} 4.2×10^{-3} cm/sec
Soil pH	3.6-6.0
Organic content	1-5%
Corrosion risk	High

Source: Fletcher (1993).

Range H

Range H soil is described as an Enfield Silt Loam (EnB). It is classified using the Unified Soil Classification System as an SM (Appendix C). The soil is generally described as having a 2.5-cm (1-in.) layer of organic matter. From a depth of 2.5 to 165.1 cm (1 to 65 in.) the soil is described as a friable silty loam. Table 4 lists some properties of this soil.

Table 4
Soil Properties for Range H

Soil Property	Value
Clay content	3-6%
Bulk density	1.3-1.5 g/cc
Permeability	6.0-20 in./hr (1.4×10^{-3}-4.2×10^{-3} cm/sec)
Soil pH	3.6-5.5
Organic content	1-2%
Corrosion risk	High

Source: Fletcher (1993).

Range K

Range K soil is described as an Eastchop Loamy Fine Sand (EnA). It is classified using the Unified Soil Classification System as an ML to an SP (Appendix C). The soil is described as having a 2.5-cm (1-in.) top layer of organic matter. From a depth of 2.5 to 48.3 cm (1 to 19 in.), the soil is described as a friable loamy fine sand, and from 48.3 to 165.1 cm (19 to 65 in.) the soil is a loose, very fine sand. Properties for this soil are the same as presented in Table 4 for Range H.

First Sampling Activity at CEMR

During the time period of 06 Nov 95 - 11 Nov 95, samples were collected at CEMR from Ranges G, H, and K. These samples were collected using a drill rig and a 6.4-cm-diam (2.5-in.-diam) drive tube and/or a split spoon sampler. The drilling hole was uncased and core samples were placed in plastic sampling vessels as withdrawn from the borehole. Samples were collected and prepared for shipment to WES for analyses. Samples were collected continuously (every 15.2 cm (6 in.)) the entire depth of the bore hole, except where site conditions prevented sample collection.

The original intent of this effort was to collect a minimum of two cores (sampling continuously every 15.2 cm (6 in.)) to a depth of 27.4 m (90 ft). But, large rocks prevented the drive tube from being driven into the soil, and small rocks plugged the split spoon sampler. Thus, procedural modifications were required to collect valid samples. As a result, three types of samples were collected. These

included the drive tube samples, split spoon samples, and samples collected at the surface using a hand-driven sampler 3.6 cm (1.4 in.) in diameter.

A total of three attempts were made to collect the deep core from Range G. Two attempts only penetrated to depths of 66 and 96.5 cm (26 and 38 in.) prior to encountering resistance to drilling. A third attempt to sample Range G was conducted using a backhoe to excavate the soil as the samples were collected. A total of seven hand core samples were also collected at Range G at depths up to 1.1 m (3.5 ft). A single core sample was collected at Range H to a depth of 137.2 cm (54 in.). A single deep sample was collected at Range K to a depth of 17.2 m (56.5 ft) as well as six hand core samples at depths up to 0.9 m (3 ft).

Selected samples were analyzed. Several samples were suspected to have been jeopardized due to the rigorous drilling means required. More samples were collected than could be analyzed due to time or project fund constraints. These additional samples were archived for later research purposes.

All sample results that are presented as part of this effort were submitted to the U.S. Army Engineer Waterways Experiment Station (WES's) analytical lab and analyzed for Pb, Cu, Zn, Ba, and Sb according to EPA SW846 (USEPA 1986a) methods. While all the metals were analyzed, the concentration of the Zn or Ba analyses are not presented here due to the low concentration of these contaminants. Results of the analysis are presented in Figures 16-24.

Discussion—First Sampling Activity

Range G

Analyses of the three cores collected at Range G are presented in Figures 16-18. These cores are labeled:

CS-G-1
CS-G-2
ERB-3

Samples CS-G-1 and CS-G-2 were collected with the drilling rig using the drive tube. For those samples collected with the drill rig the soil surface was removed prior to drilling to provide a flat surface for the drilling rig. Thus, as shown in Figures 16-17, analytical data are not available for the 0- to 20.32-cm (0- to 8-in.) depths. The sample is highly contaminated to a depth of approximately 50.8 cm (20 in.), but contamination "falls off" at depths below 50.8 cm (20 in.).

Sample ERB-G-3 was collected high upon the berm. As expected, the berm "wall" is contaminated at greater depths than the berm's toe due to projectile penetration. It is suspected that the high value at 48.3-63.5 cm (19-25 in.) is due to a bullet particulate in the sample.

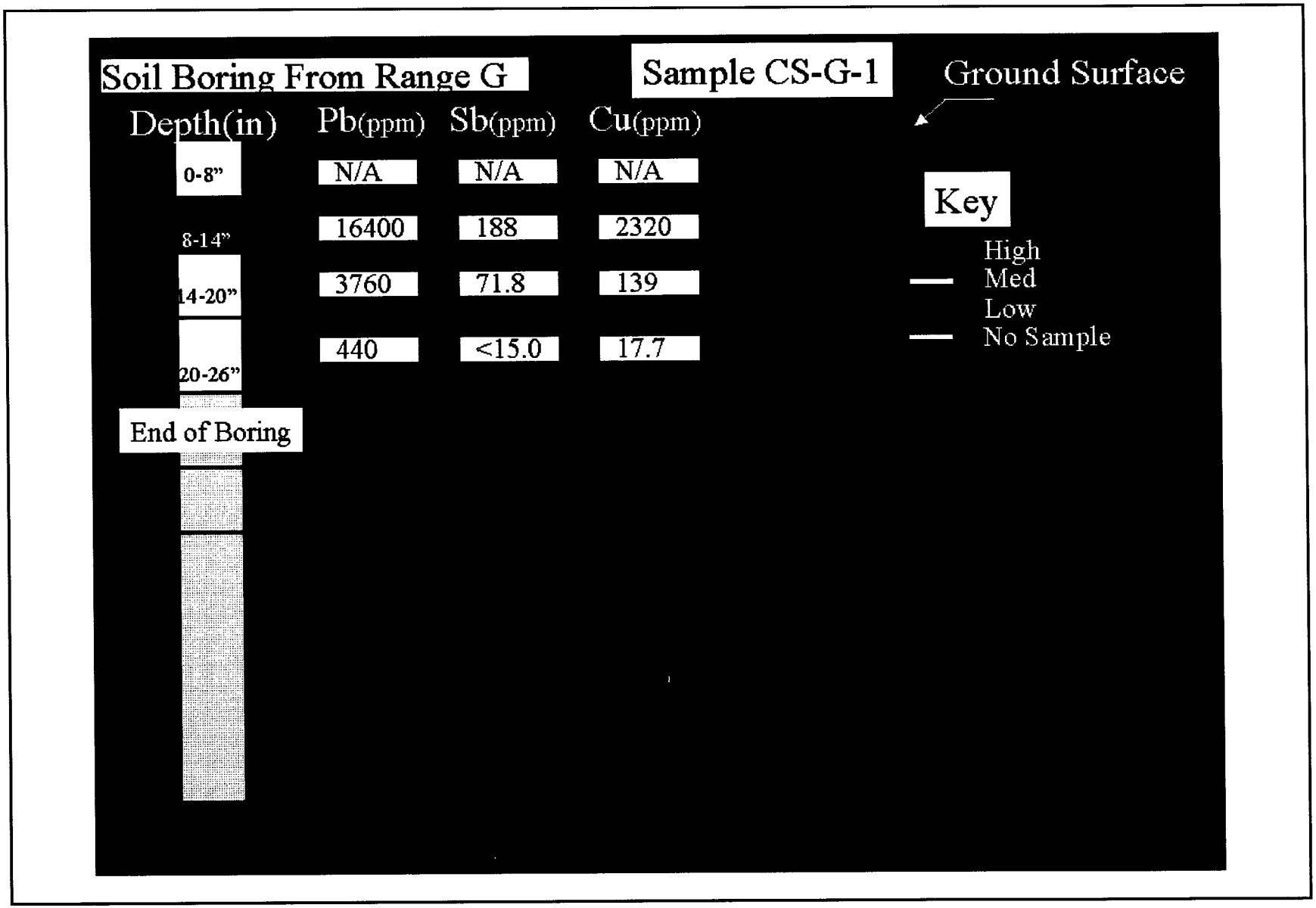

Figure 16. Sampling results for core Sample CS-G-1 from CEMR Range G

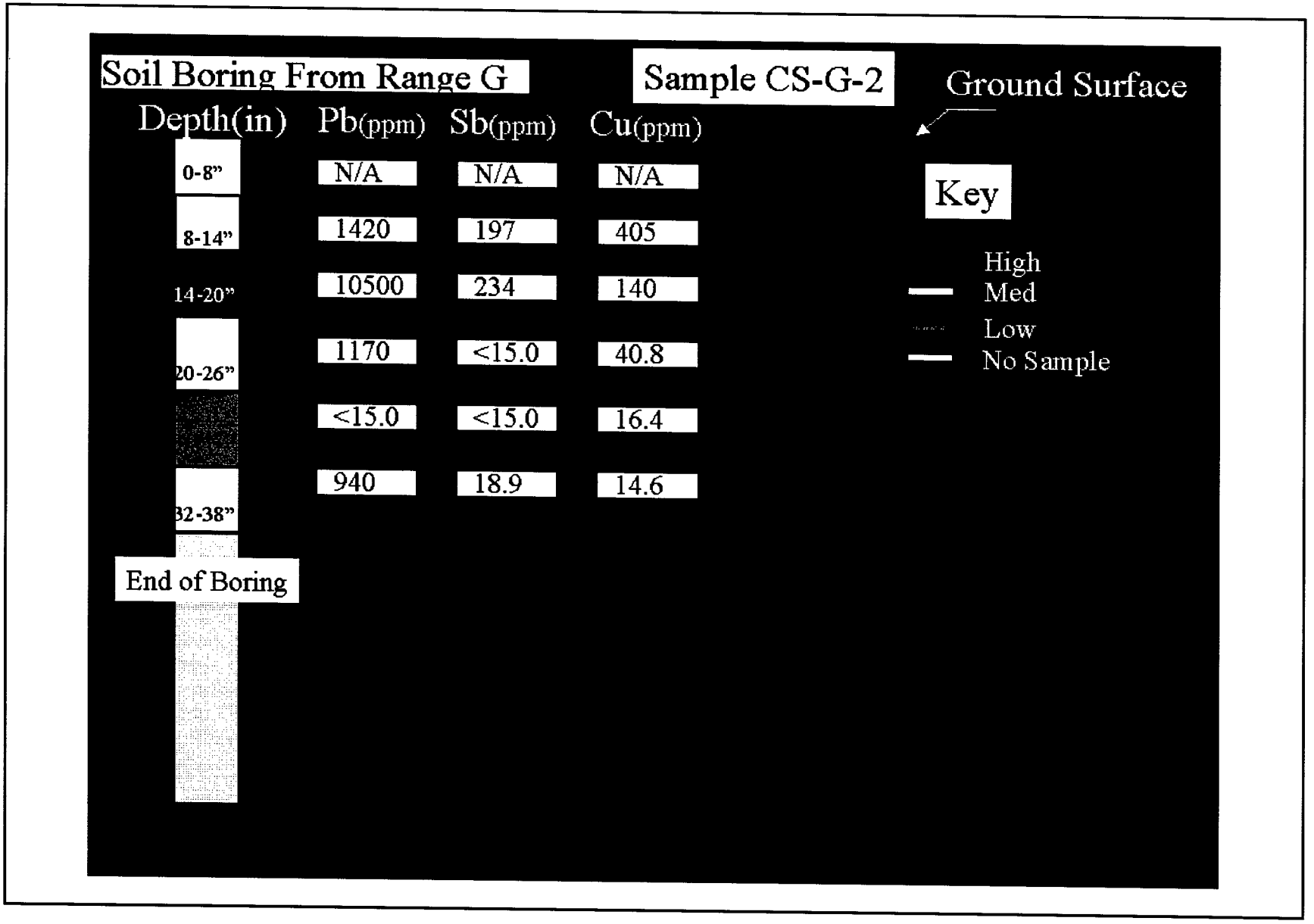

Figure 17. Sampling results for core Sample CS-G-2 from CEMR Range G

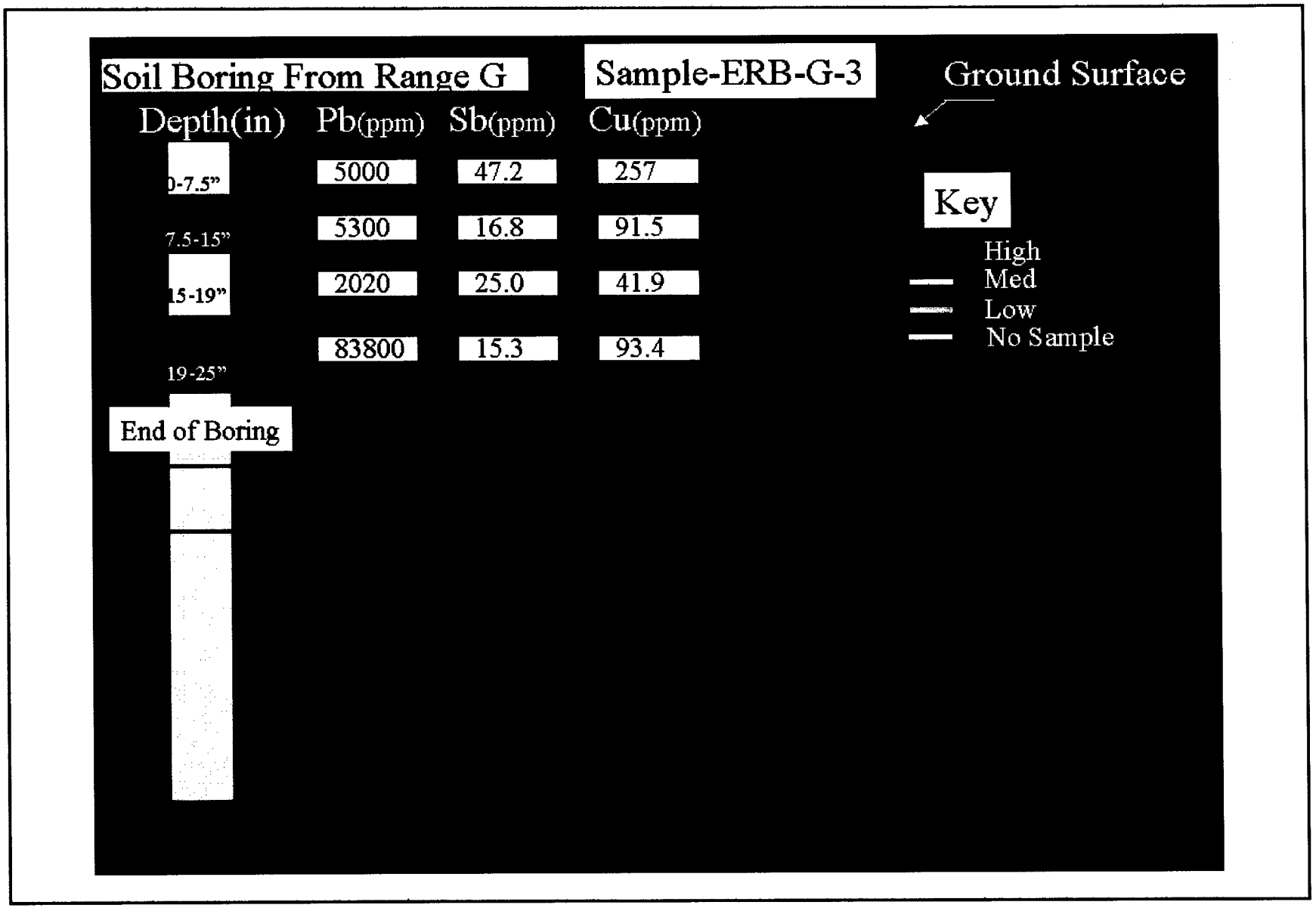

Figure 18. Sampling results for core Sample ERB-G-3 from CEMR Range G

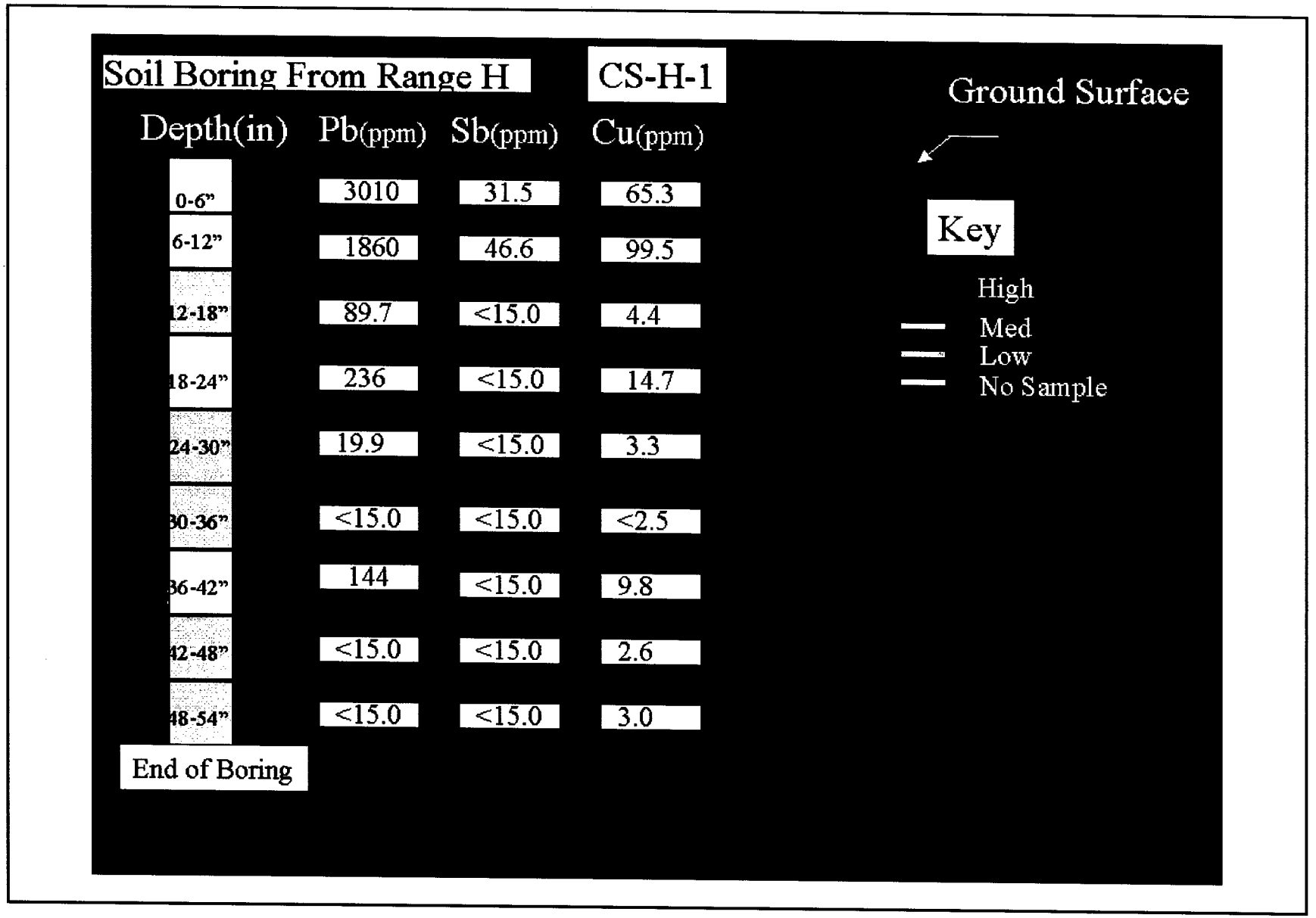

Figure 19. Sampling results for core Sample CS-H-1 from CEMR Range H

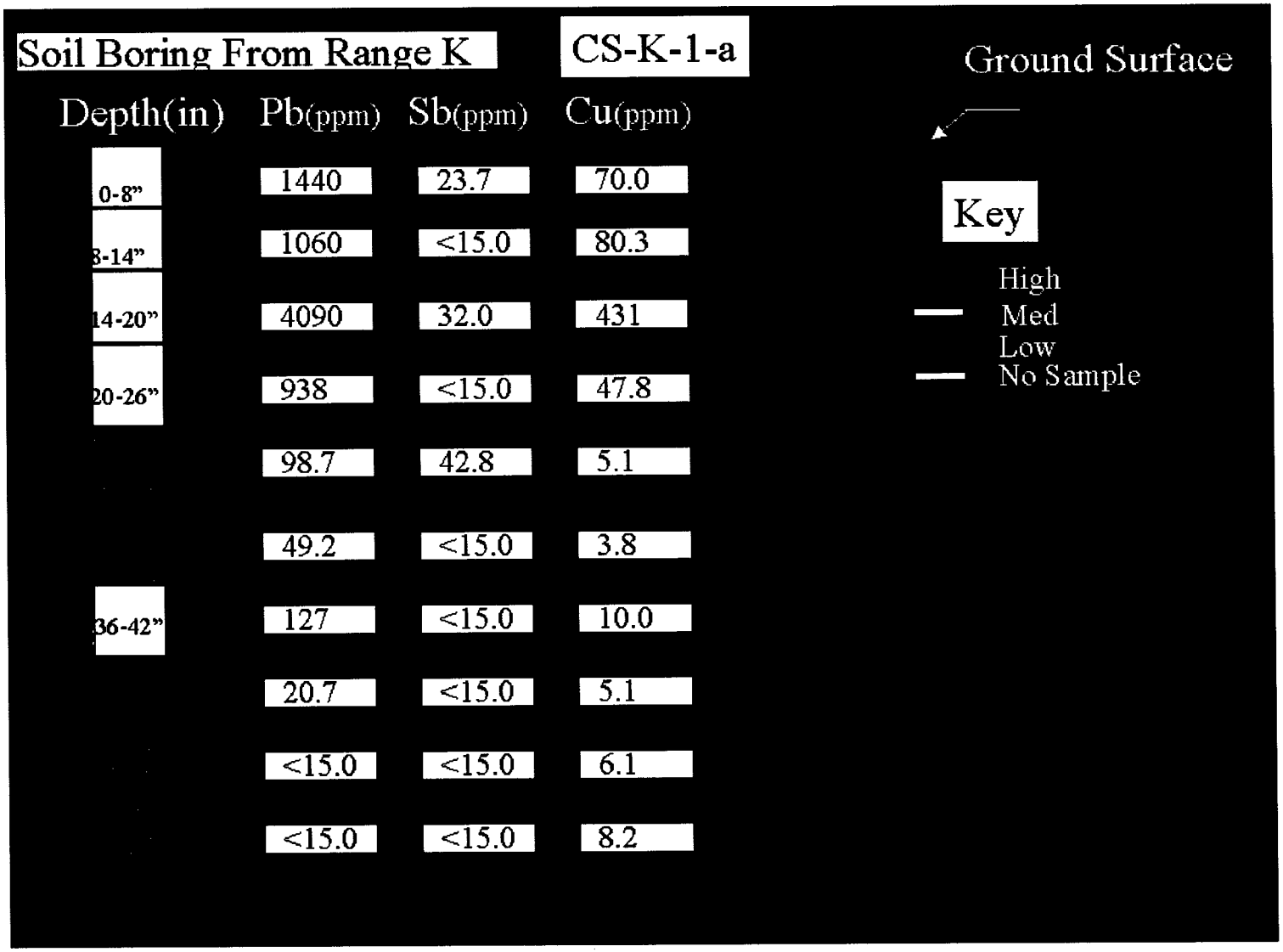

Figure 20. Sampling results for core Sample CS-K-1-a from CEMR Range K. This figure presents the 0- to 152.4-cm (0- to 6-in.) data

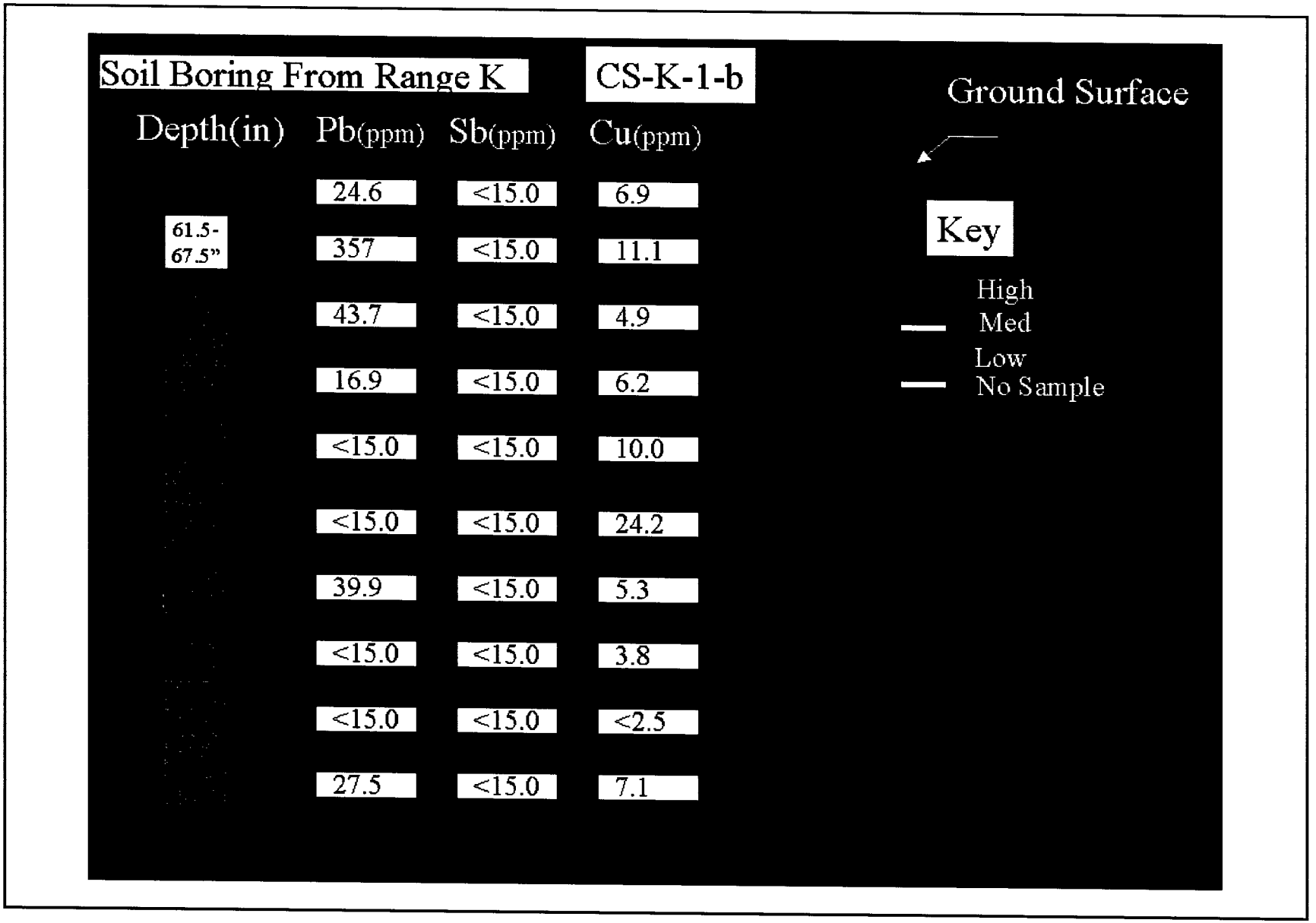

Figure 21. Sampling results for core Sample CS-K-1-b from CEMR Range K. This figure presents the 152.4- to 308.6-cm (60- to 121.5-in.) data

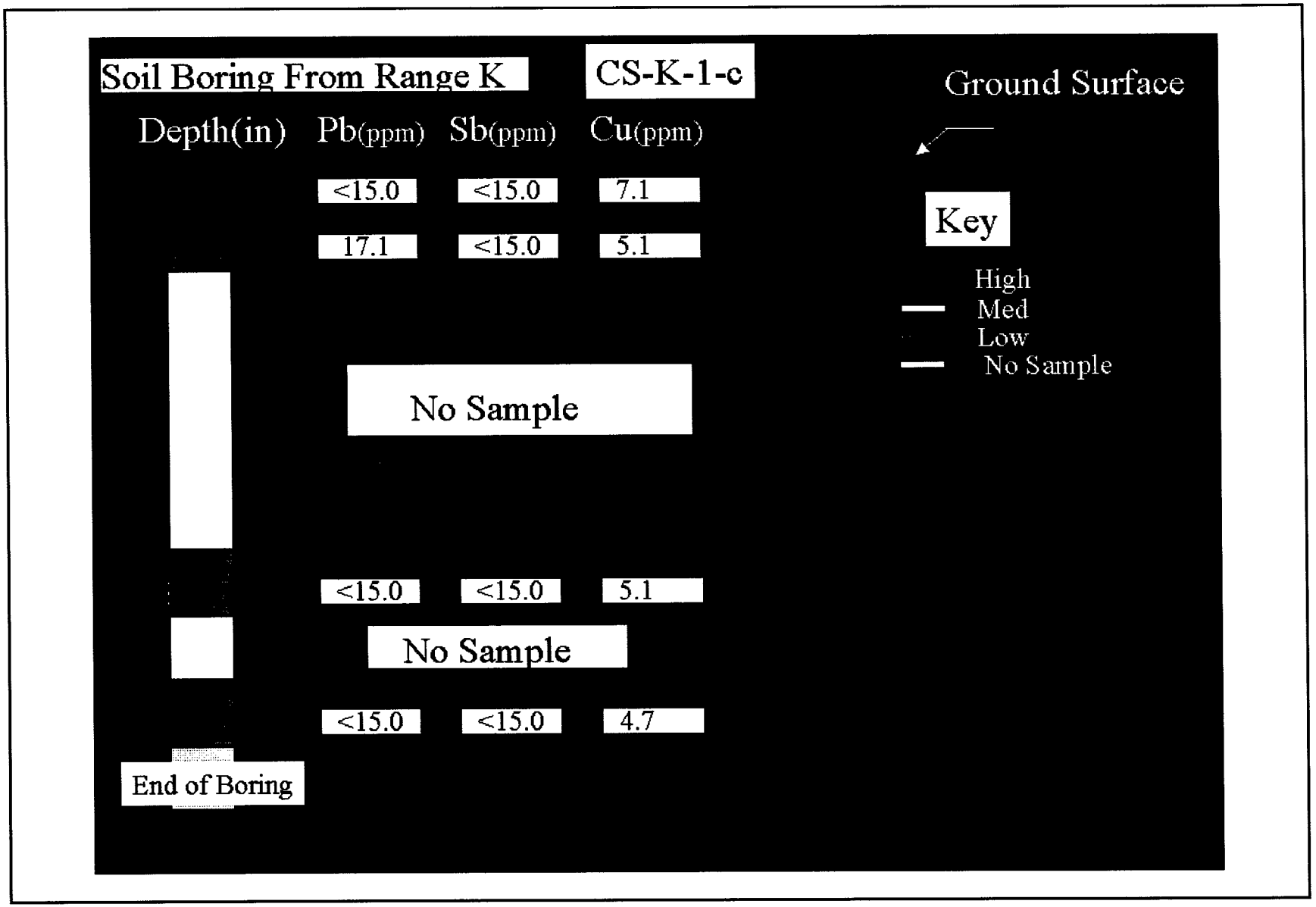

Figure 22. Sampling results for core Sample CS-K-1-c from CEMR Range K. This figure presents the 308.6- to 1691.6-cm (121.5- to 666-in.) data

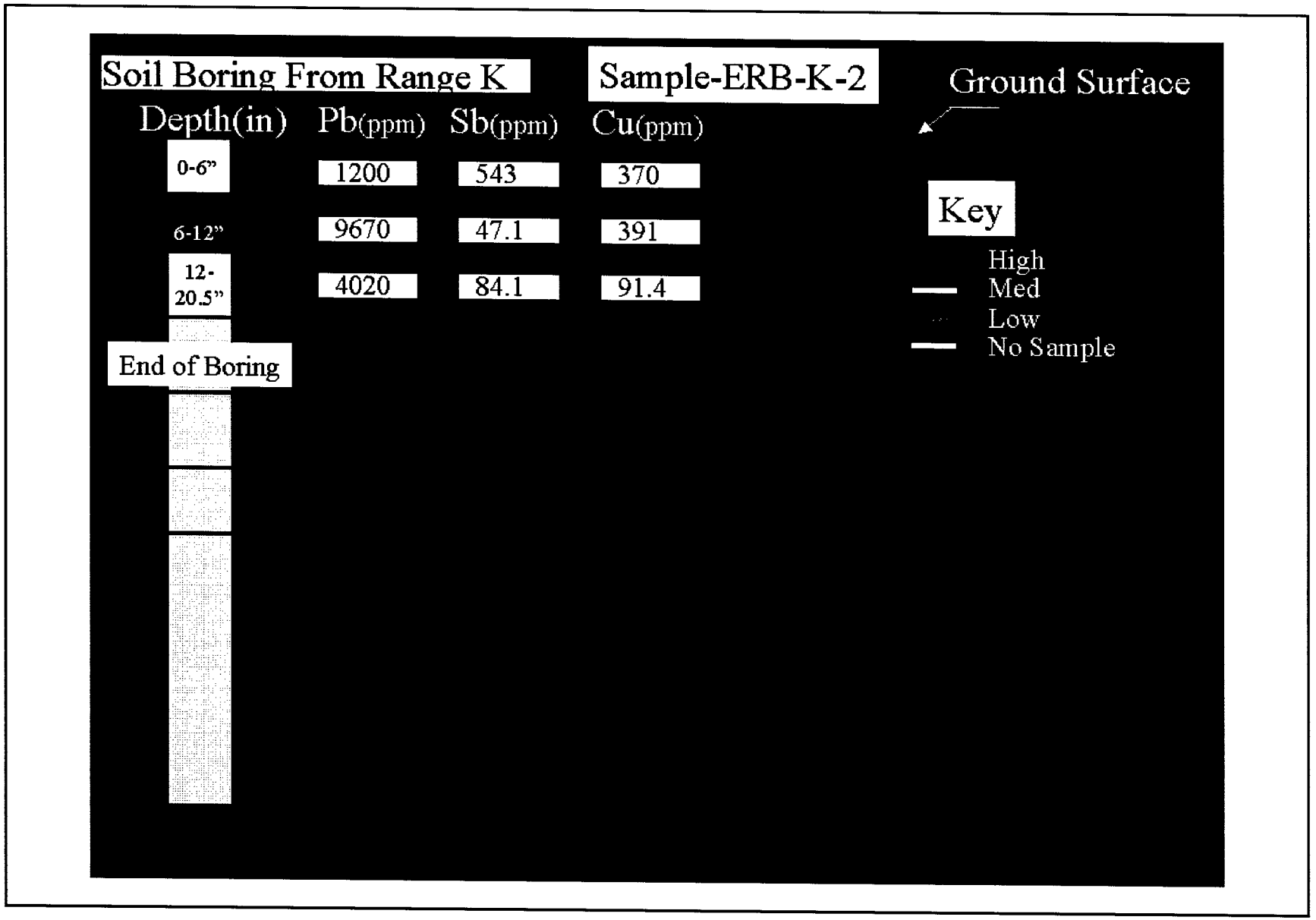

Figure 23. Sampling results for core Sample ERB-K-2 from CEMR Range K

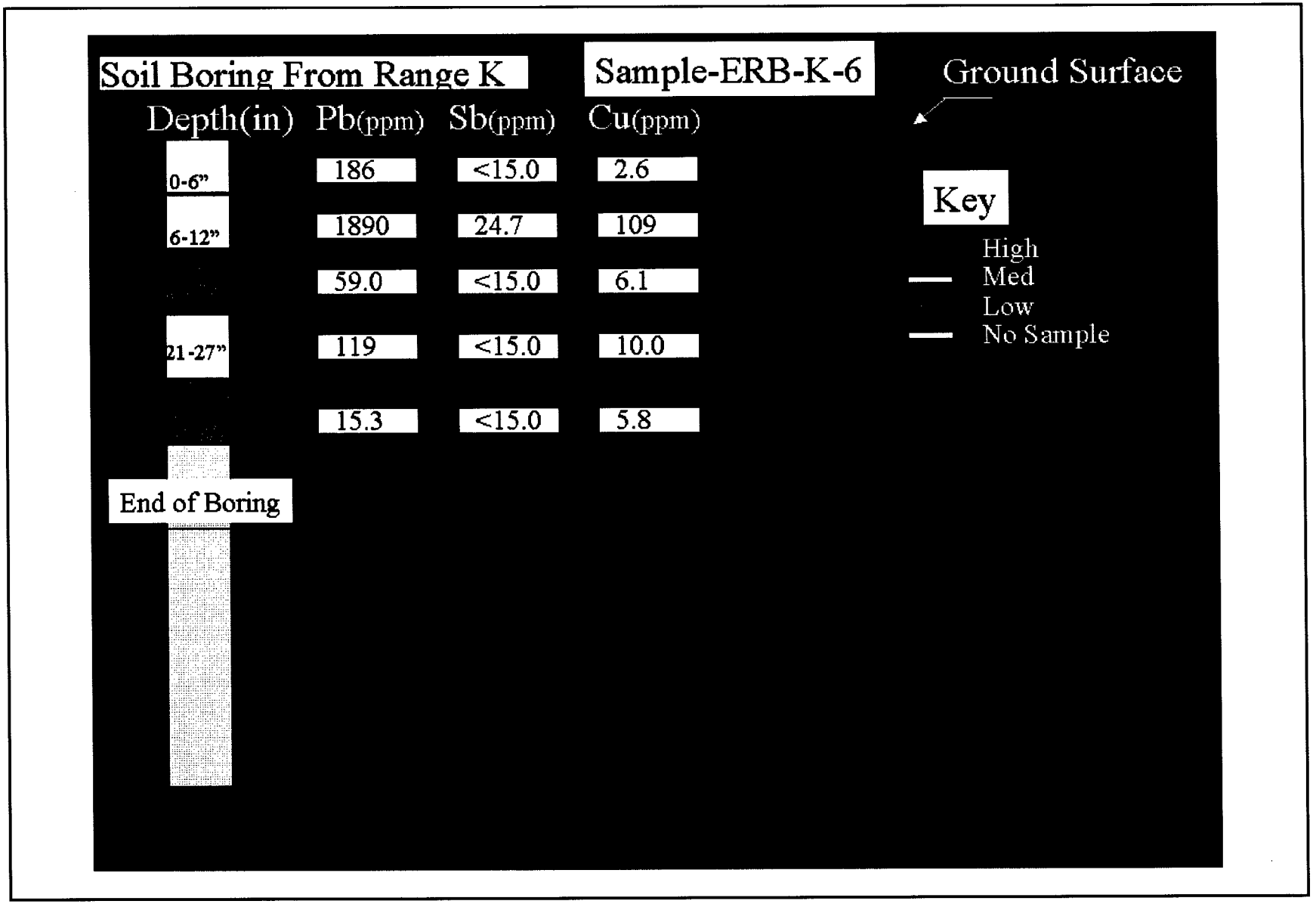

Figure 24. Sampling results for core Sample ERB-K-6 from CEMR Range K

Range H

Sample CS-H-1 was a high-integrity core collected with the drill rig. As shown in Figure 19, sample contamination was not found below 106.7 cm (42 in.). Only minor amounts of lead were detected below 61 cm (24 in.).

Range K

Sample CS-K-1 (a,b,c) (Figures 20-22) is a single sample of high integrity collected with the drill rig. As with samples collected at Range H, contamination at Range K quickly falls off below 50.8 cm (20 in.). At 121.9 cm (48 in.), no detectable lead concentration was measured in the sample. At 152.4-200.7 cm (60-79 in.) and also at 246.4 cm (97 in.), small amounts of lead were measured in the sample. It is suspected that these samples had slightly elevated lead levels as a result of the sampler striking the sides of the hole on descent, meaning that lead from the top of the boring possibly contaminated the lower samples. Note that only small concentrations of lead are found below 170.2 cm (67 in.).

Sample ERB-K-2 (Figure 23) was collected using a hand coring method high upon the berm at Range K. As observed in the sample from range G, this sample is also highly contaminated. Sample ERB-K-6 (Figure 24) was also taken using the hand coring method at the toe of the berm. Note that the lead concentration is very close to the detection limit at 68.6 cm (27 in.).

Second Sampling Activity at CEMR

Due to the problems associated with the first sampling activity, a second sampling effort was attempted. This second sampling effort was attempted to obtain deeper samples at Ranges G, H, and K and to verify the results of the first sampling activity. Results of the second activity are as follows.

During the time period 08 - 12 April 1996, additional samples were collected at CEMR from Ranges G, H, and K. These samples were collected using a hollow stem auger (HSA) drill rig and a split spoon sampler. Core samples were collected with a split spoon sampler and placed in plastic sampling vessels as they were withdrawn from the borehole. The 15.2-cm (6-in.) samples were homogenized in the field and shipped to WES for laboratory analysis. Attempts were made to collect samples continuously (every 15.2 cm (6 in.)) the entire depth of the borehole, except where site conditions prevented sample collection.

In contrast to the first sampling effort, investigatory boreholes were prepared at each range, which assisted in sample collection with the HSA. Once the HSA was placed to sample depth, the chance of sample fallback was greatly reduced by this drilling method. A total of three borings were performed (one from each range). Cores were collected to a depth of 6.1 m (20 ft) at Ranges G and H, and to a depth of 27.4 m (90 ft) at Range K. The boring for Range G was labeled CE-RG-B,

Range H was labeled CE-RH-B, and Range K was labeled CE-RK-B. Sample locations at each range are shown in Figures 8-10.

As with the first sampling effort, all samples were submitted to WES's analytical lab and analyzed for Pb, Cu, Zn, Ba, and Sb according to EPA SW846 (USEPA 1986a) methods. While all the metals were analyzed, results of the Zn and Ba analyses are not presented here due to the low concentration of these contaminants. The maximum concentrations of Zn and Ba were 30.3 ppm and 25.8 ppm, respectively. Results of the analysis are presented graphically in Figures 25-36.

Discussion—Second Sampling Activity

Range G

Results of chemical analysis of the core collected from Range G during the second sampling are presented in Figures 25-27. This core was labeled CE-RG-B. As observed in the first sampling effort, high levels of contamination were measured in the upper layers of the soil near the surface. In the first sampling effort, elevated contamination was detected only to a depth of 0.9 m (3.1 ft). In contrast, during the second sampling effort, contamination was detected at a depth of 1.8 m (6 ft). It should be noted that several samples at depth are missing from this core. Where the data are missing, large rocks were encountered which prevented drilling and would have affected the results. While the rock was removed via an alternative drilling method, no samples were available for chemical analysis at these depths.

Range H

Results of chemical analysis of the core collected from Range H during the second sampling are presented in Figures 28-29. This core is labeled CE-RH-B. In contrast to the first sampling effort, contamination in this core was measured at much lower concentrations. In the first sampling effort, lead contamination was measured in excess of 1,800 mg/kg in the first 30.5 cm (12 in.). The highest concentration measured during the second sampling effort at Range H was 123 mg/kg. While sample drilling methods differ among the first and second sampling effort, both samples were of high quality. The variations between the soil contamination measured during the different sampling efforts cannot be accounted for as a result of the different sampling methods. While the first sampling effort and the second sampling effort are only separated by a linear distance of 3.7 m (12 ft) (as shown in Figure 9), it is suspected that the soil heterogeneities account for the variation in soil contaminant concentration measured at Range H.

Range K

Chemical analyses of the core collected from Range K during the second sampling are presented in Figures 30-36. This core is labeled CE-RK-B. As observed

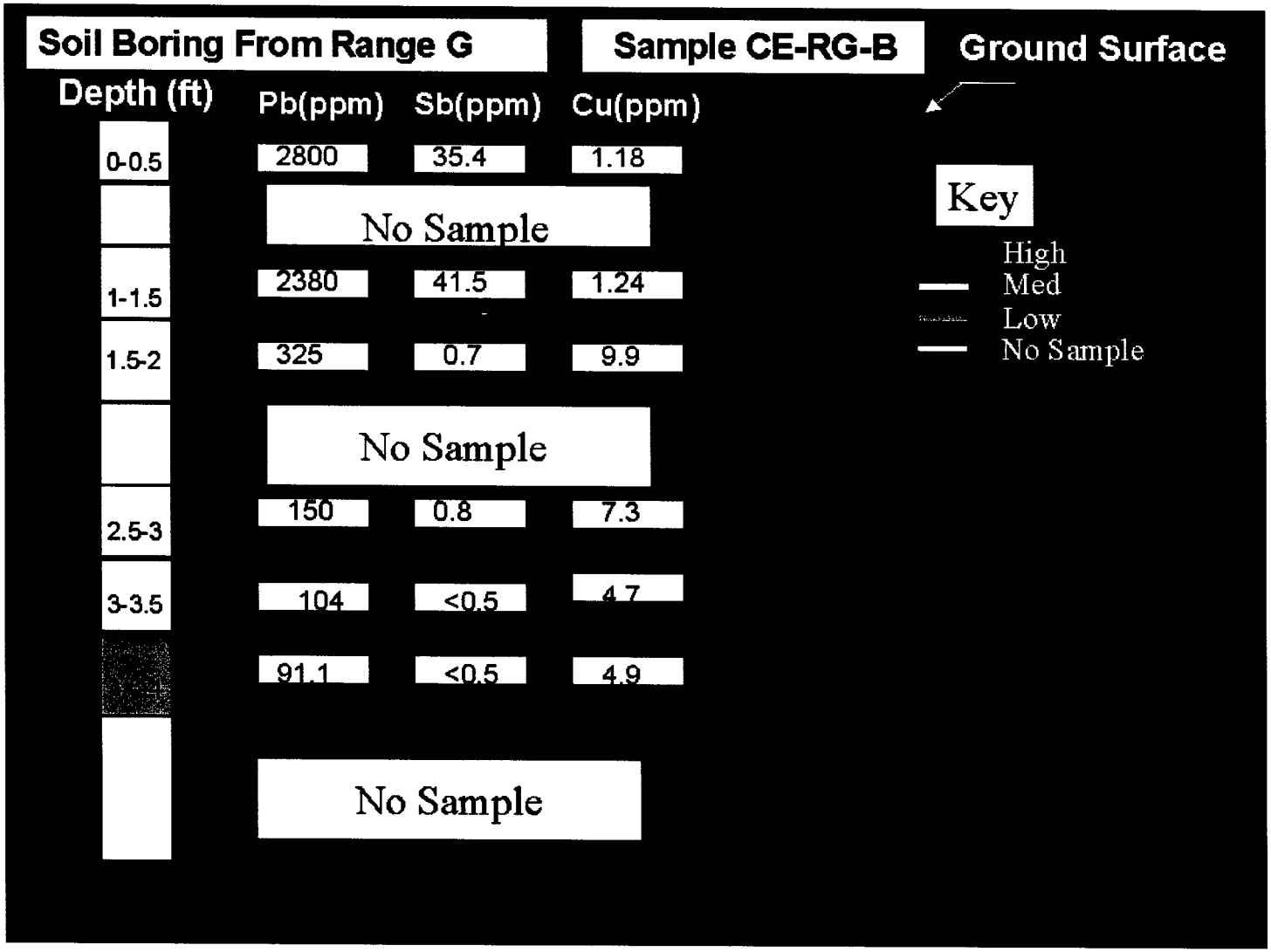

Figure 25. Sampling results for core Sample CE-RG-B from CEMR Range G. This figure presents the 0- to 1.7-m (0- to 5.5-ft) data for the second sampling effort

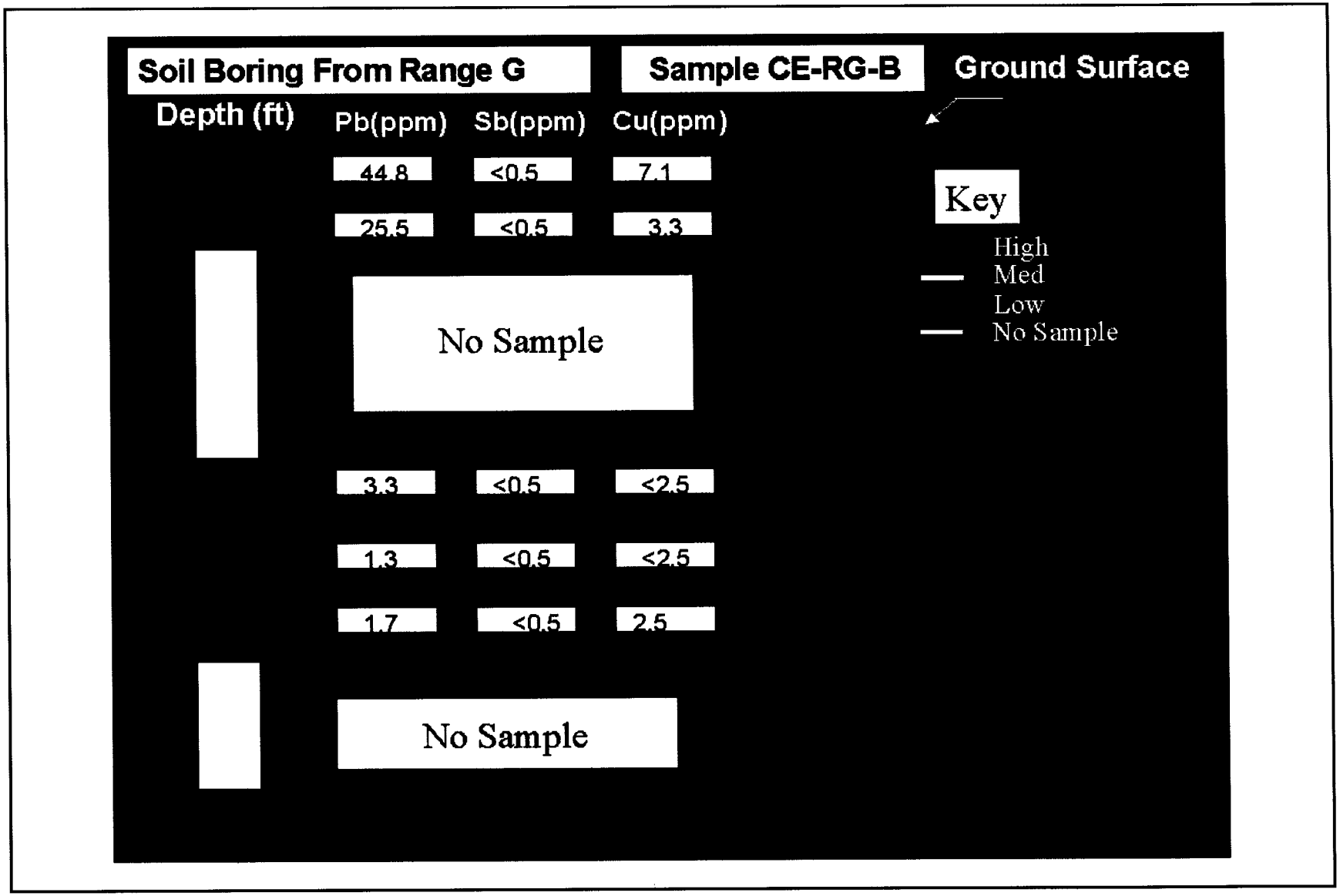

Figure 26. Sampling results for core Sample CE-RG-B from CEMR Range G. This figure presents the 1.7- to 3.4-m (5.5- to 11.0-ft) data for the second sampling effort

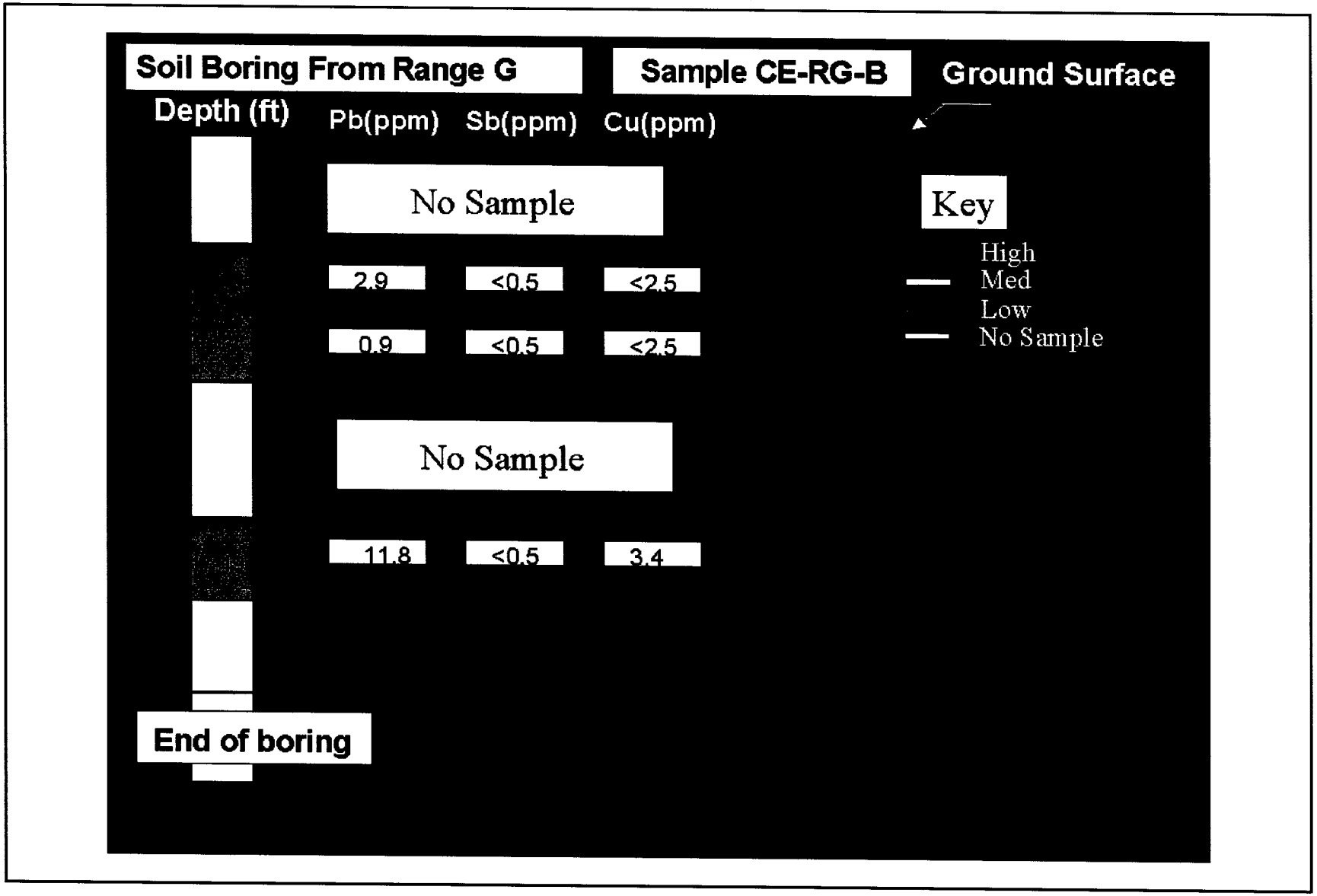

Figure 27. Sampling results for core Sample CE-RG-B from CEMR Range G. This figure presents the 4.3- to 5.8-m (14.0- to 19.0-ft) data for the second sampling effort

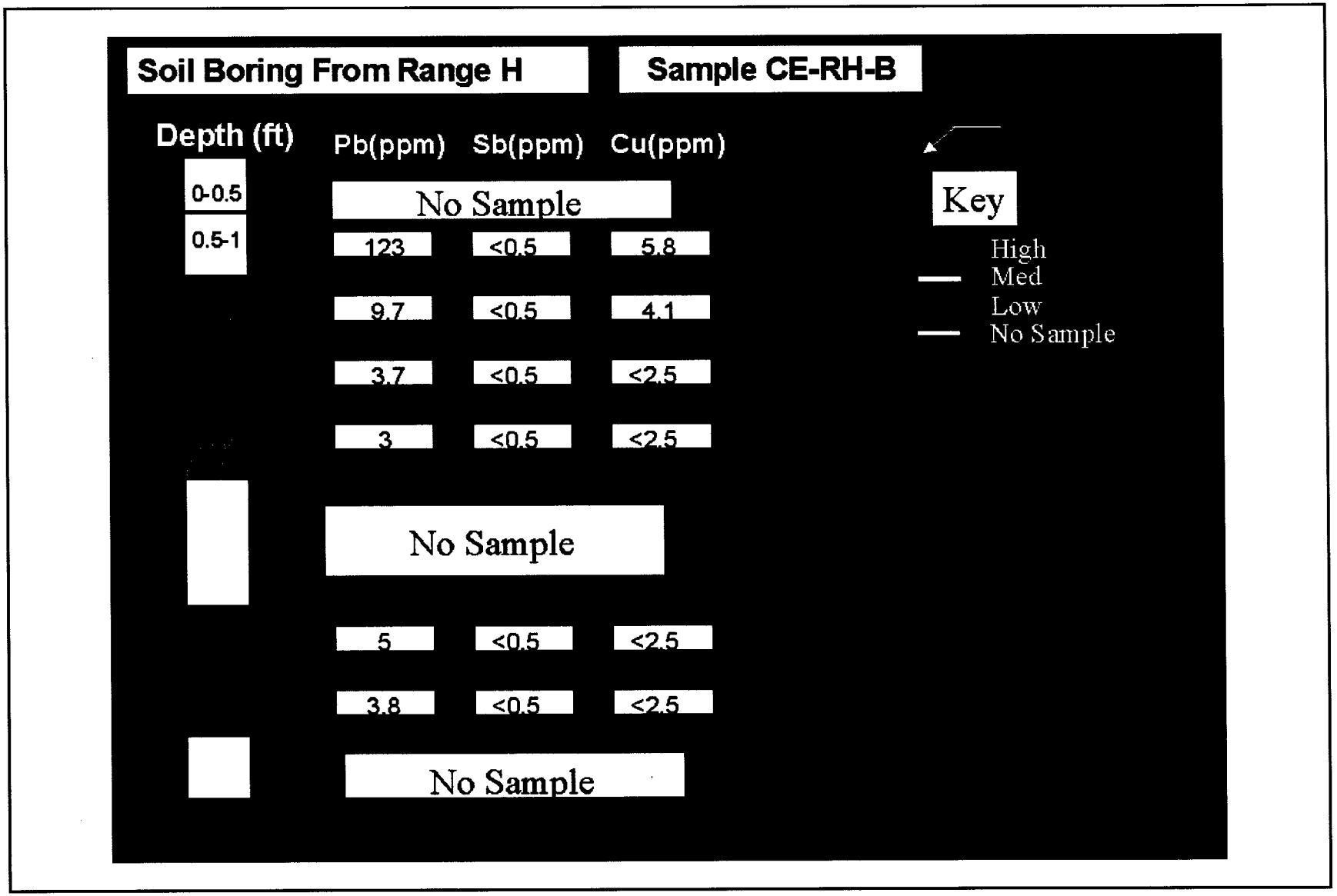

Figure 28. Sampling results for core Sample CE-RH-B from CEMR Range H. This figure presents the 0- to 1.4-m (0- to 4.5-ft)data for the second sampling effort

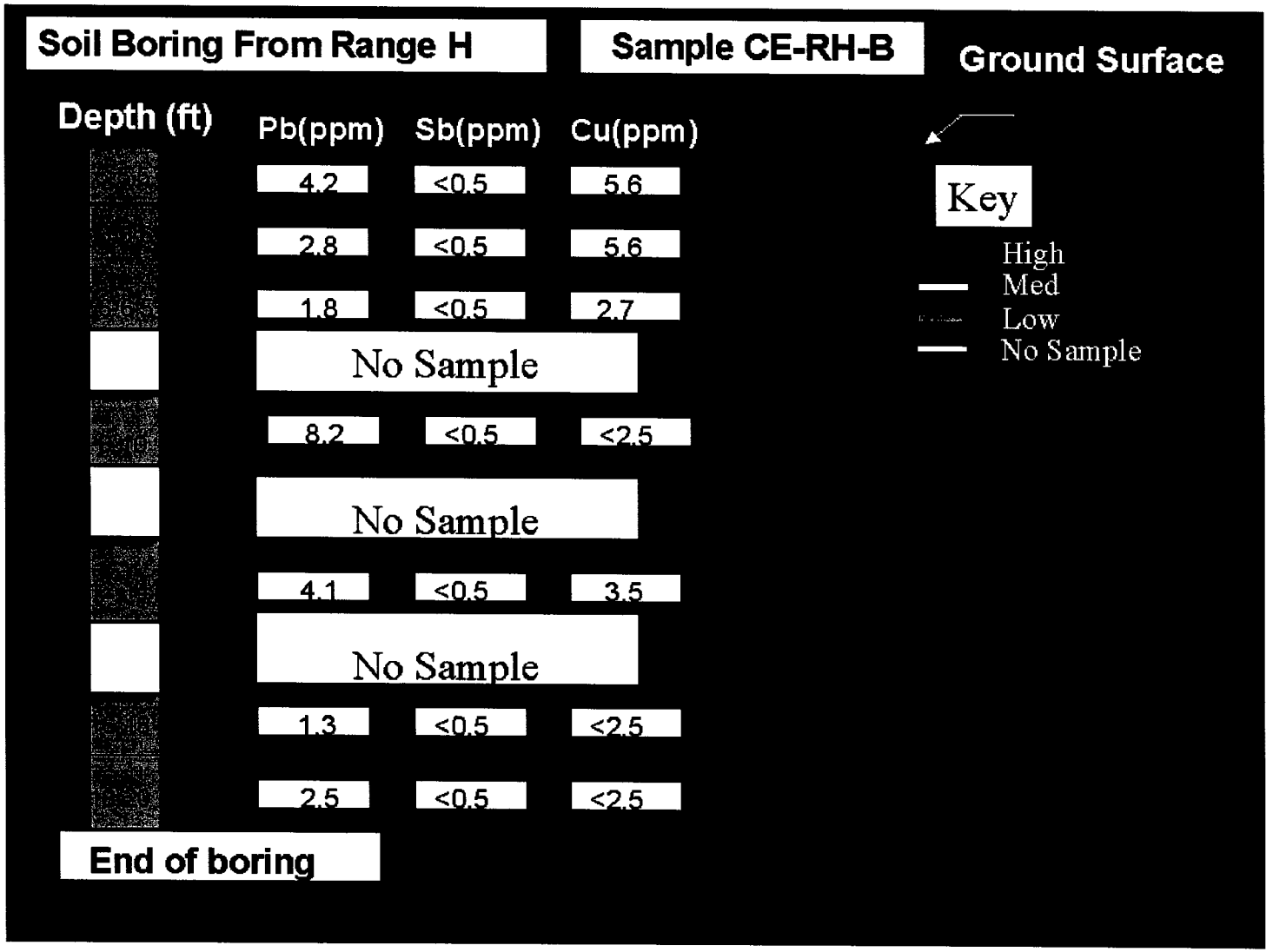

Figure 29. Sampling results for core Sample CE-RH-B from CEMR Range H. This figure presents the 1.5- to 6.1-m (5.0- to 20.0-ft) data for the second sampling effort

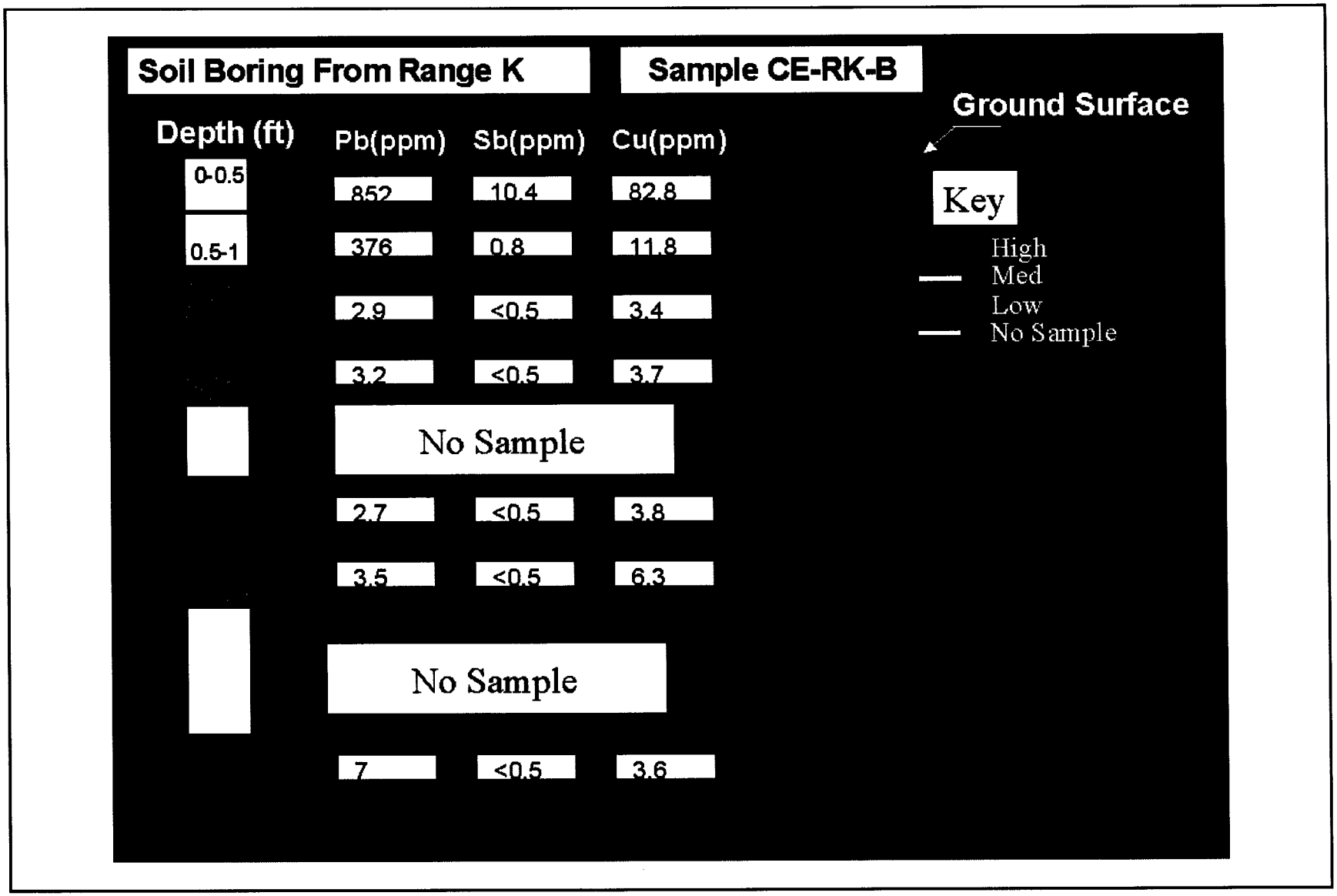

Figure 30. Sampling results for core Sample CE-RK-B from CEMR Range K. This figure presents the 0- to 1.7-m (0- to 5.5-ft) data for the second sampling effort

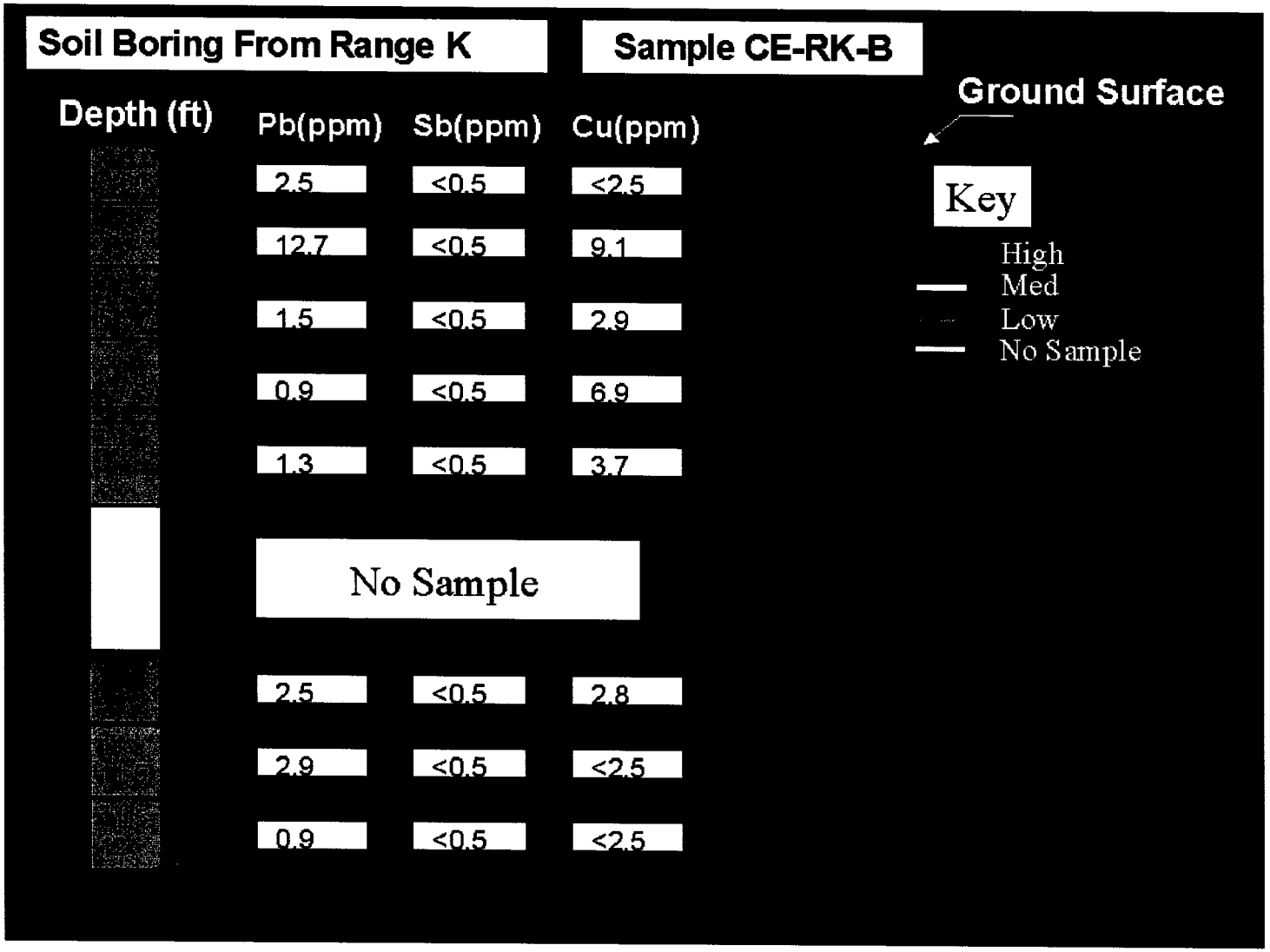

Figure 31. Sampling rresults for core Sample CE-RK-B from CEMR Range K. This figure presents the 1.7- to 3.7-m (5.5- to 12.0-ft) data for the second sampling effort

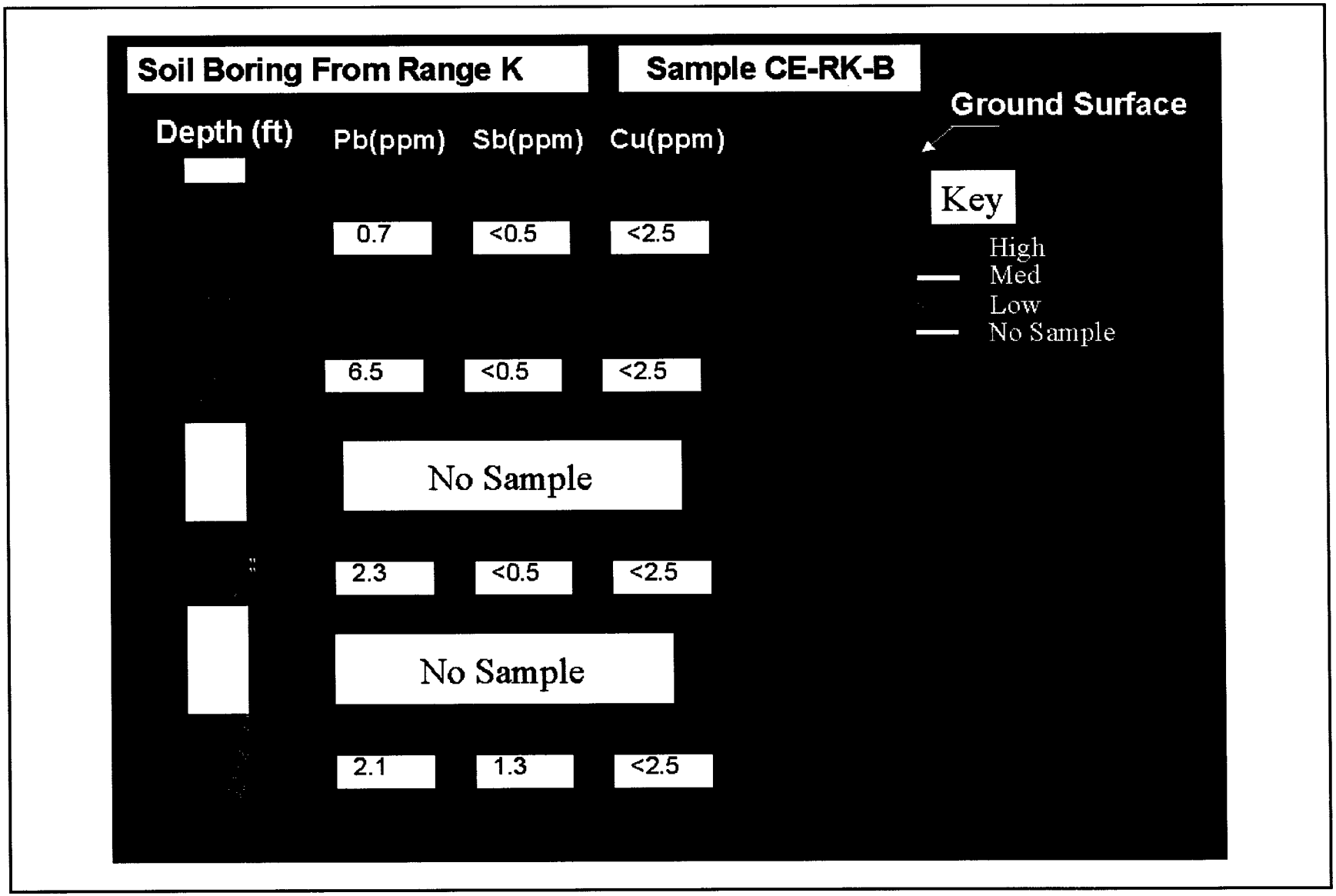

Figure 32. Sampling results for core Sample CE-RK-B from CEMR Range K. This figure presents the 5.8- to 9.7-m (19.0- to 32.0-ft) data for the second sampling effort

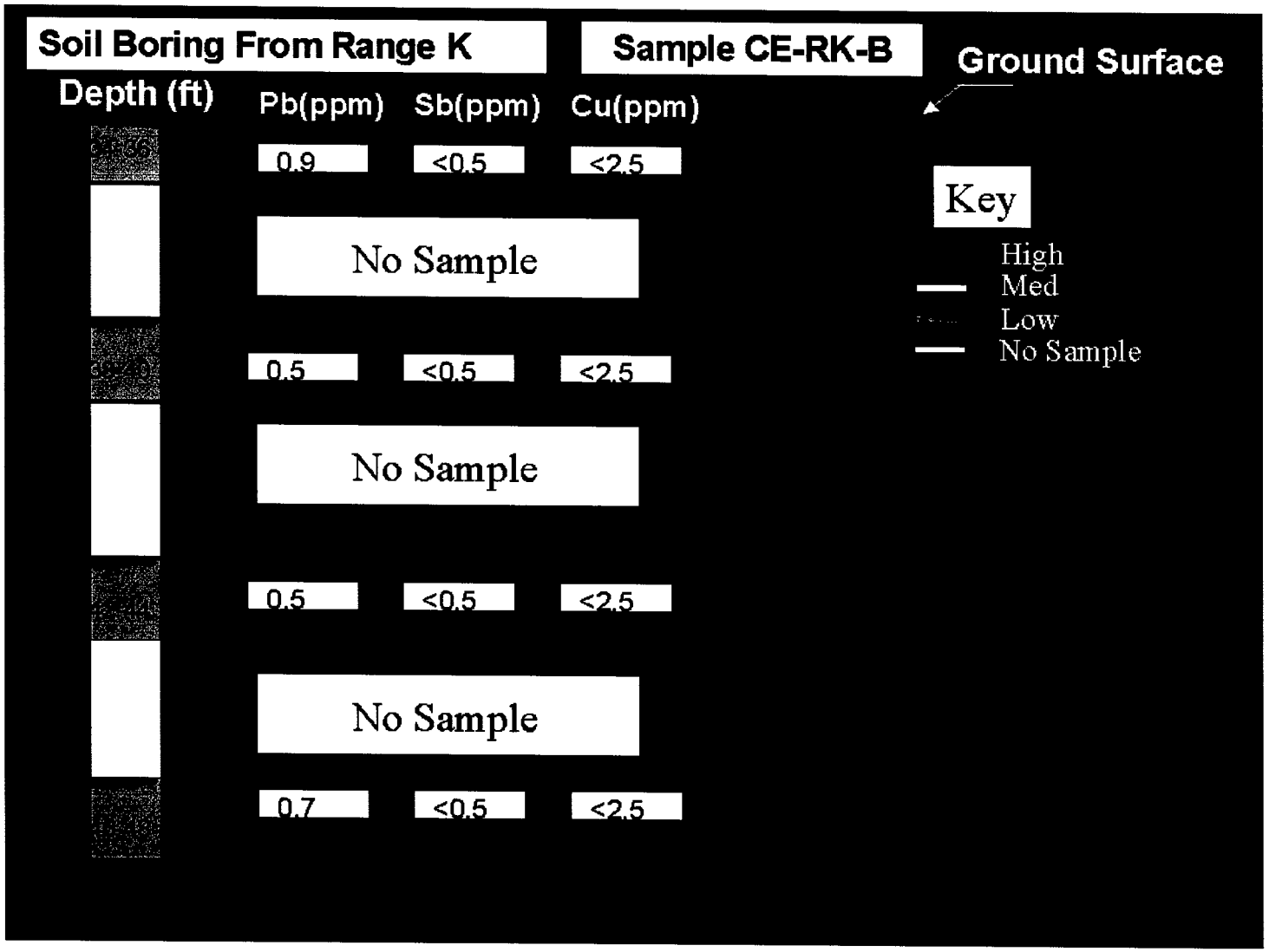

Figure 33. Sampling results for core Sample CE-RK-B from CEMR Range K. This figure presents the 10.4- to 14.6-m (34.0- to 48.0-ft) data for the second sampling effort

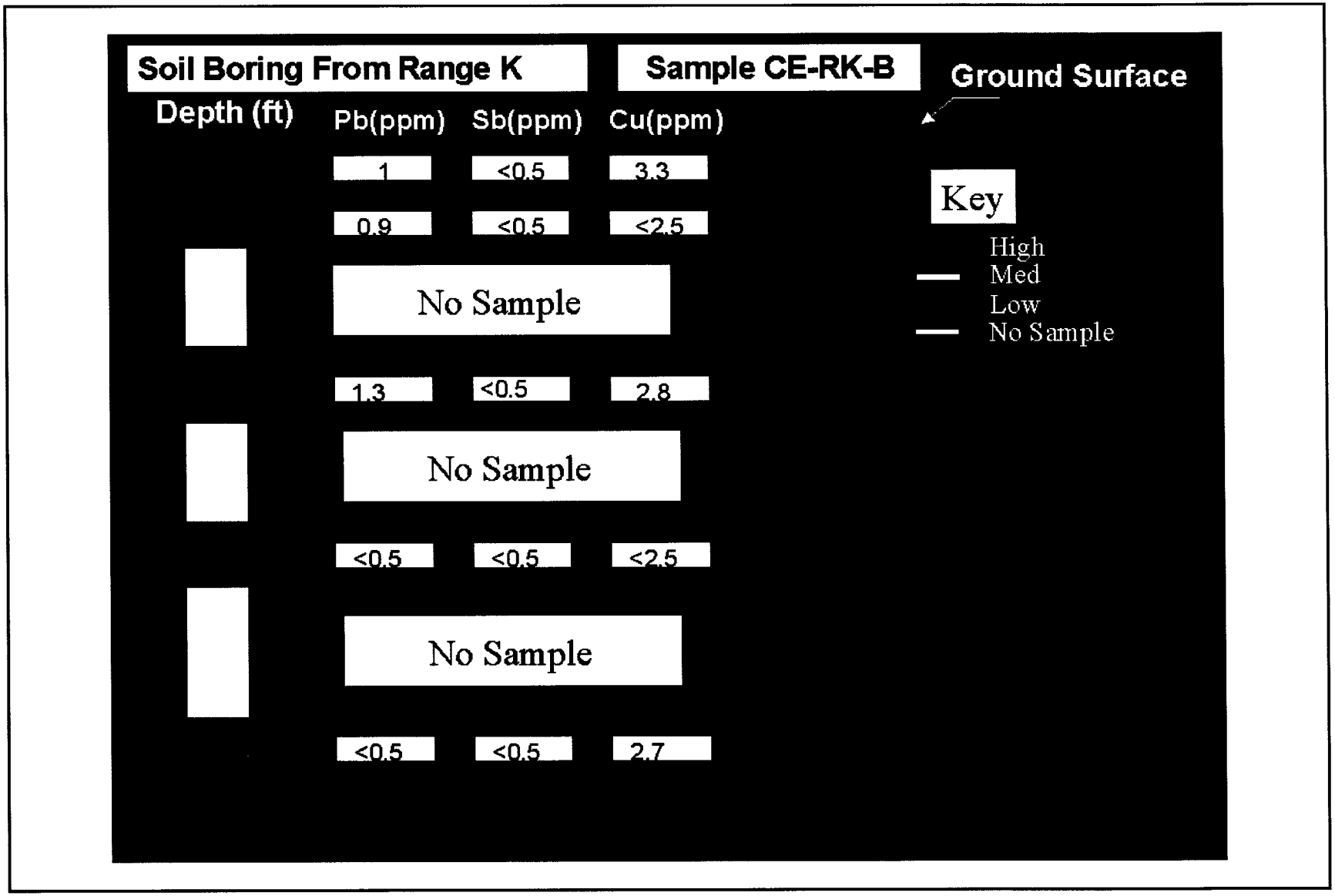

Figure 34. Sampling results for core Sample CE-RK-B from CEMR Range K. This figure presents the 15.2- to 20.1-m (50.0- to 66.0-ft) data for the second sampling effort

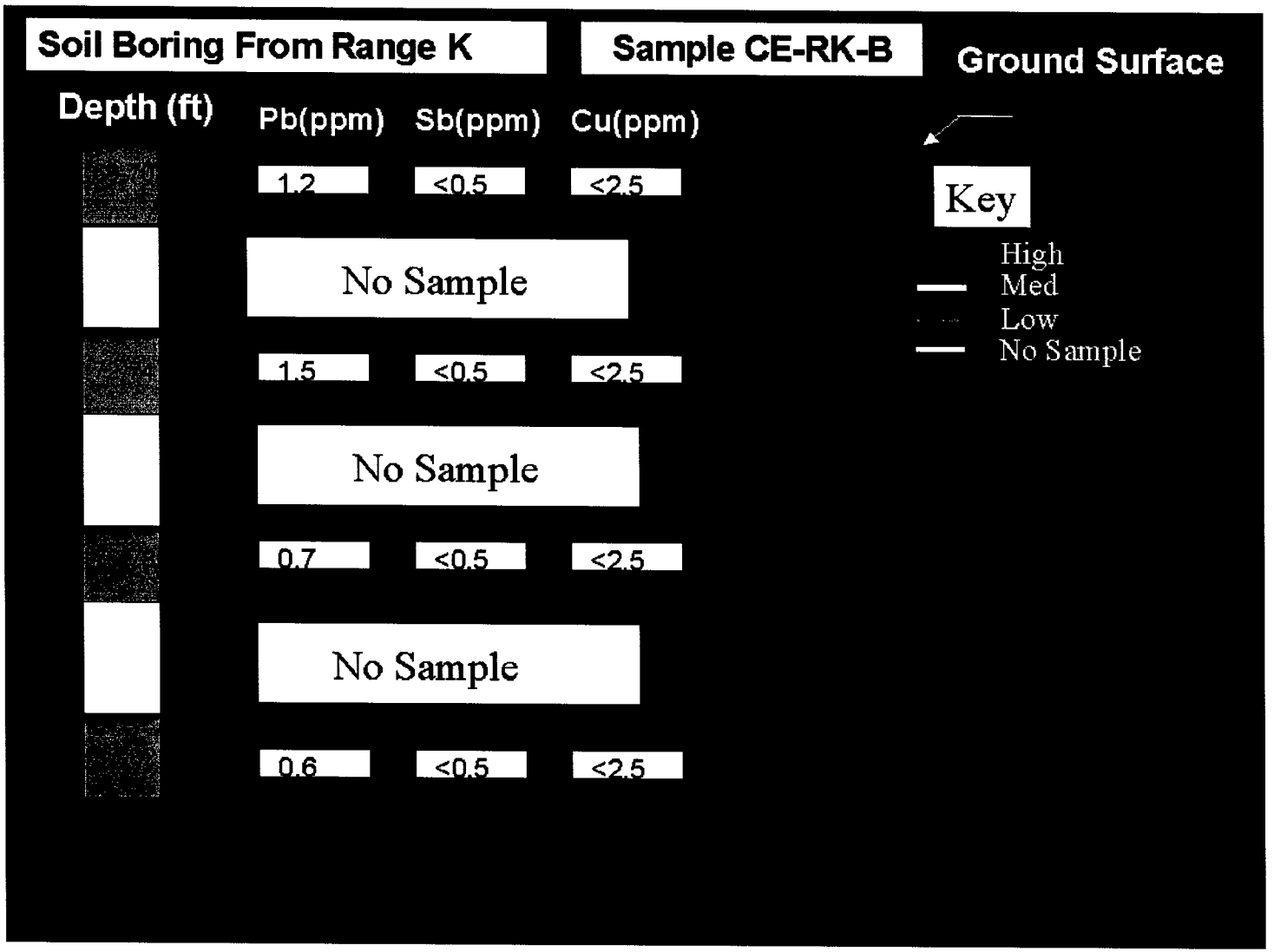

Figure 35. Sampling results for core Sample CE-RK-B from CEMR Range K. This figure presents the 20.7- to 25-m (68.0- to 82.0-ft) data for the second sampling effort

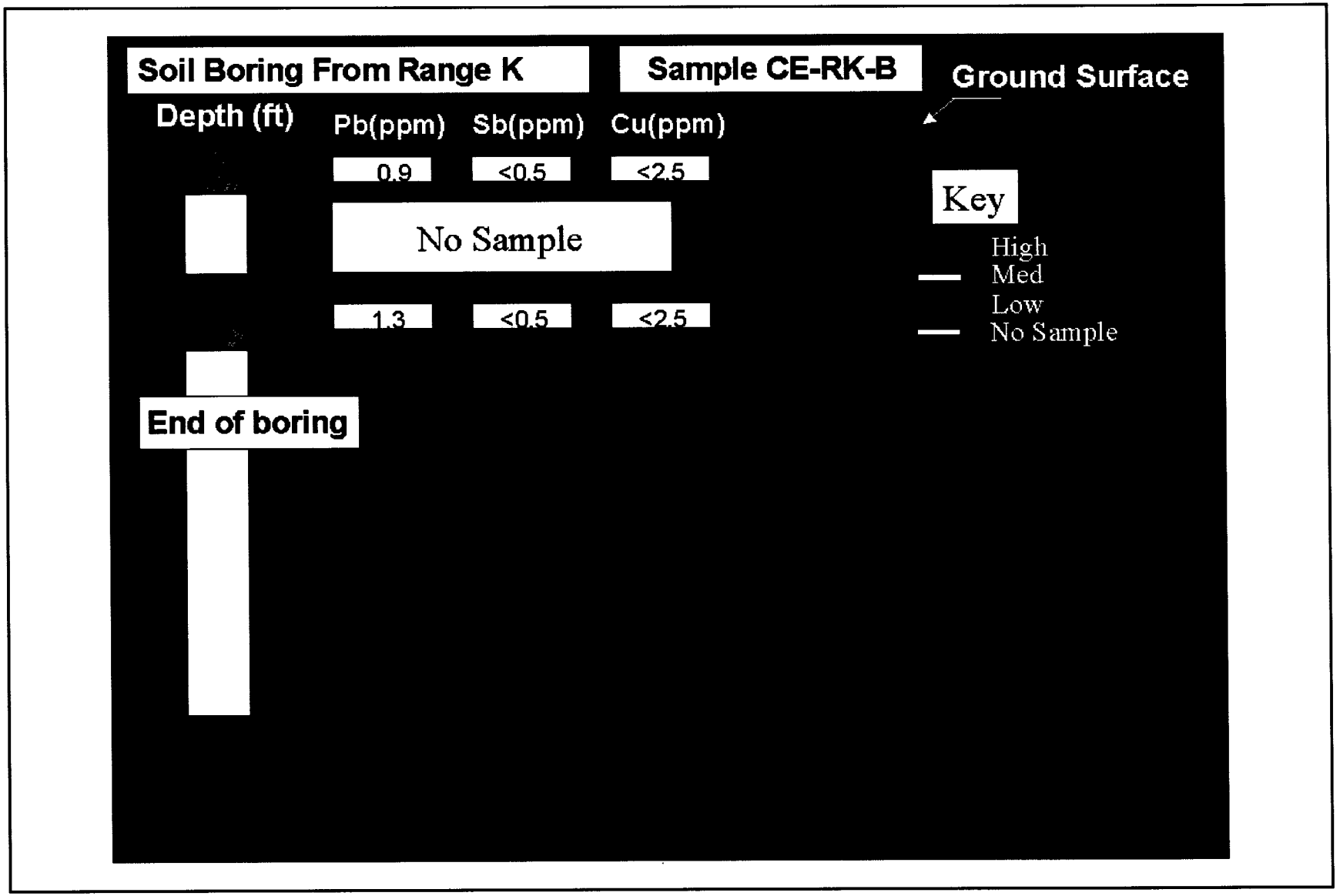

Figure 36. Sampling results for core Sample CE-RK-B from CEMR Range K. This figure presents the 25.6- to 27.4-m (84.0- to 90.0-ft) data for the second sampling effort

when comparing the first and second sampling efforts for Range H, lower contaminant concentrations were observed among the first and second sampling efforts for Range K. Data collected for the second sampling effort indicate high contaminant concentrations measured from the surface to a depth of 0.3 m (1 ft), and only minor contaminant levels measured below 0.3 m (1 ft) at Range K. In contrast, contamination at Range K was measured consistently at elevated concentrations to a depth of 1.2 m (4 ft) at Range K during the first sampling effort. As discussed for the Range H sampling activity, not all variations between the soil contamination measured during the different sampling efforts can be attributed to the difference in the sampling methods.

It is possible that contamination measured below 0.9 m (3 ft) during the first sampling effort could be attributed to the sampling method, but this is unlikely. The 0- to 0.9-m (0- to 3-ft) sample was removed as a single sample during the first sampling effort. Thus, contamination from fallback is not possible. Below 0.9 m (3 ft) in depth, a consistent pattern of decreasing concentration is observed up to a depth of 1.5 m (5 ft) (Figure 20). At 1.5 m (5 ft) in depth, a rock was encountered which prevented the Shelby tube from being pushed and sampling methodologies were modified. As a result (as stated previously) the elevated lead levels measured below 1.5 m (5 ft) in depth could possibly be attributed to the sampling methodology for the first sampling effort.

The samples collected from Range K during the second sampling effort were near the sampling location for the first sampling effort (only 4.6 m (15 ft) to the east, Figure 10). The only explanation offered that could account for the variation in the contaminant levels measured in the soils from 0 to 0.9 m (0 to 3 ft) between the first and second sampling efforts are soil heterogeneities.

Discussion of CEMR Sampling Efforts

Comparing the data from first and second sampling efforts proved to be interesting. Range G had higher and deeper lead levels in the second sampling effort than the first sampling effort. In contrast, Ranges H and K had lower levels of contaminants measured at shallower depths. Combining the information from the three ranges and both sampling efforts, it can be stated with a great deal of confidence based on the sampling results that it is unlikely that any of the metal contaminants have vertically migrated more than 1.8 to 2.1 m (6 to 7 ft) in depth. While vertical metal migration is occurring from the SAR at CEMR, it is occurring at a slow rate. As a result, the lead has not migrated deep into the soil. All deep cores that were collected using the drill rig were collected at the toe of the berms. For these samples, projectile penetration in the soil cannot account for the elevated metal concentrations. These sampling efforts provide information that demonstrates that a more in-depth investigation into the vertical migration issue is warranted.

Historical Well Analysis

A single well was located in the vicinity and down gradient of the SAR where soil sampling took place. This is well AEHA-1A, which is located approximately 304.8 m (1,000 ft) southwest of Range K. Personnel at CEMR provided historical sampling records that were collected for this well in September 1994. Analytical results collected from this well indicate lead concentrations <0.0105 mg/ℓ and copper concentrations < 0.025 mg/ℓ.

5 Results of Other SAR Sampling Activities

Several other SAR have been investigated to determine the extent and depth of migration of the contaminants. During March 1995, three SAR were sampled at Fort Benjamin Harrison located in Indianapolis, Indiana. These ranges consisted of a 25-m (82-ft) zeroing range, an old modified record fire range now used as a skeet range, and a Police Training Range. Results of this sampling activity indicate that Pb and Cu contamination were widespread at the surface but no elevated concentration of Pb and Cu were found below 0.9 m (3 ft) in depth (Bricka 1996a). This soil had a higher clay content than soils from CEMR.

Sampling has also been conducted at a southern Army base located in Louisiana. This sampling activity focused on two zeroing ranges. Results from this sampling indicate that while vast areas of the range demonstrated elevated Pb and Cu levels at the surface, no elevated Pb and Cu levels have been detected below approximately 1.2 m (4 ft) in depth. The two ranges sampled at the southern Army base have the unique feature of a naturally occurring clay layer at approximately 0.9 m (3 ft) in depth. This clay layer has a permeability of less than 1×10^{-7} cm/sec (3.9×10^{-8} in/sec). It is suspected that this clay layer prevents vertical migration of the metals (Bricka 1996b).

Karr, Flynn, and Smith-Rawecki (1990) and Heath et al. (1991) studied an impact berm at the Naval Amphibious Base, Little Creek, Virginia, and an impact berm at the Marine Corps Combat Development Center, Quantico, Virginia. Soil samples were collected to depths of 6 in., and vegetation samples were also collected. Results from these studies indicate that concentrations of Pb and Cu at 6 in. in depth were as high as 23,000 ppm. Levels of Pb and Cu as high as 265 ppm were also measured in the vegetation samples. Heath et al. (1991) state that "results of groundwater sampling and geochemical modeling indicate that lead may cause groundwater pollution at sites with sandy soil, a soil pH less than seven, and shallow groundwater (less than about 10 feet)." This report also states "groundwater modeling indicates that copper or zinc can cause groundwater pollution at sites where the soil pH is less that six, and groundwater is shallow."

Peters (1993) conducted sampling activities at an SAR at the training grounds located at Grafenwohr, Germany. In this study, samples were only collected to a depth of 30.5 cm (12 in.). Results of this sampling activity indicate lead and copper

levels that were measured in the soil at a depth to 30.5 cm (12 in.) in excess of 300 ppm.

In summary, results of these studies indicate that lead and copper levels at SAR will be highly elevated at the surface but will quickly drop as depth increases. The majority of these studies have only been conducted at shallow sampling depths (less than 0.9 m (3 ft), but, when samples were collected at depths of 0.9 m (3 ft) or more, no elevated lead levels were detected.

6 Theory of Metal Migration at CEMR

For metals to migrate vertically from an SAR, two things must occur; first, the metals must be dissolved in the pore water, and secondly, these dissolved metals must migrate via bulk transport. Bulk transport involves the movement of the contaminants from the pore water into the groundwater flowing vertically and horizontally. Soil chemistry, water chemistry, metal speciation, and projectile type will be the main variables affecting the dissolution of the metals. Bulk transport will be influenced by atmospheric precipitation, site topography, wetting and drying cycles, and depth to groundwater.

While SAR projectiles primarily contain lead, copper, and antimony, lead is by far the most toxic and is the greatest environmental concern. Thus, this chapter will focus primarily on lead.

Factors Affecting Pore Water Concentration

One major factor affecting pore water concentration is metal speciation. Metal speciation is influenced by pH and redox potential (Eh) within the soil. Many metal species of lead consist of salt complexes. Most common salts of Pb are relatively insoluble or only sparing soluble, with the notable exceptions of lead nitrate and lead acetate (Table 5). Lead generally occurs in three oxidation states: elemental lead having a valence of "0," divalent lead (+2), and tetravalent lead (+4). Using a Pourbaix diagram (also known as a potential-pH diagram) the various states of lead can be visualized (Figure 37). From Figure 37, it is evident that at natural water pH (3-9) and Eh (0.6-(-0.6)), divalent lead is the predominate valence. (Care must be utilized when interpreting Pourbaix diagrams because these diagrams only consider specific cations and anions at specific concentrations. These diagrams also assume thermodynamic equilibrium). Observing another Pourbaix diagram under similar conditions (Figure 38), but including additional ions (sodium, nitrogen, magnesium, calcium, and chloride ions), we see the vast change in the metal species. Due to the complexity of natural groundwater, it is difficult to apply these simplified drawings directly to SAR; but these diagrams do provide an overview of what may occur, and the variables affecting pore water chemistry.

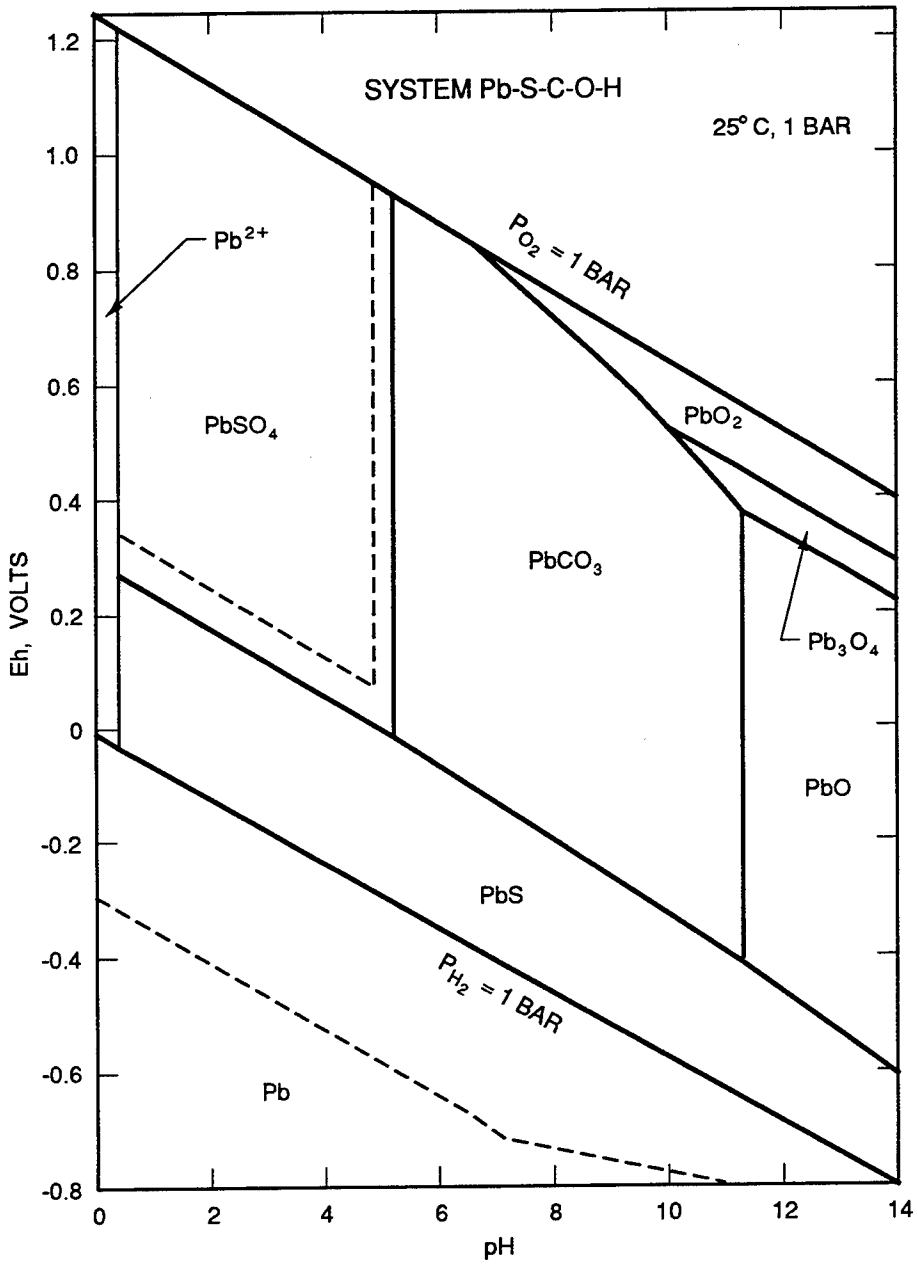

Figure 37. Eh-pH diagram for the Pb-S-OH system (Pb=10^{-6}, S=10^{-3}, and C=10^{-3}) (source: Heath et al. 1991)

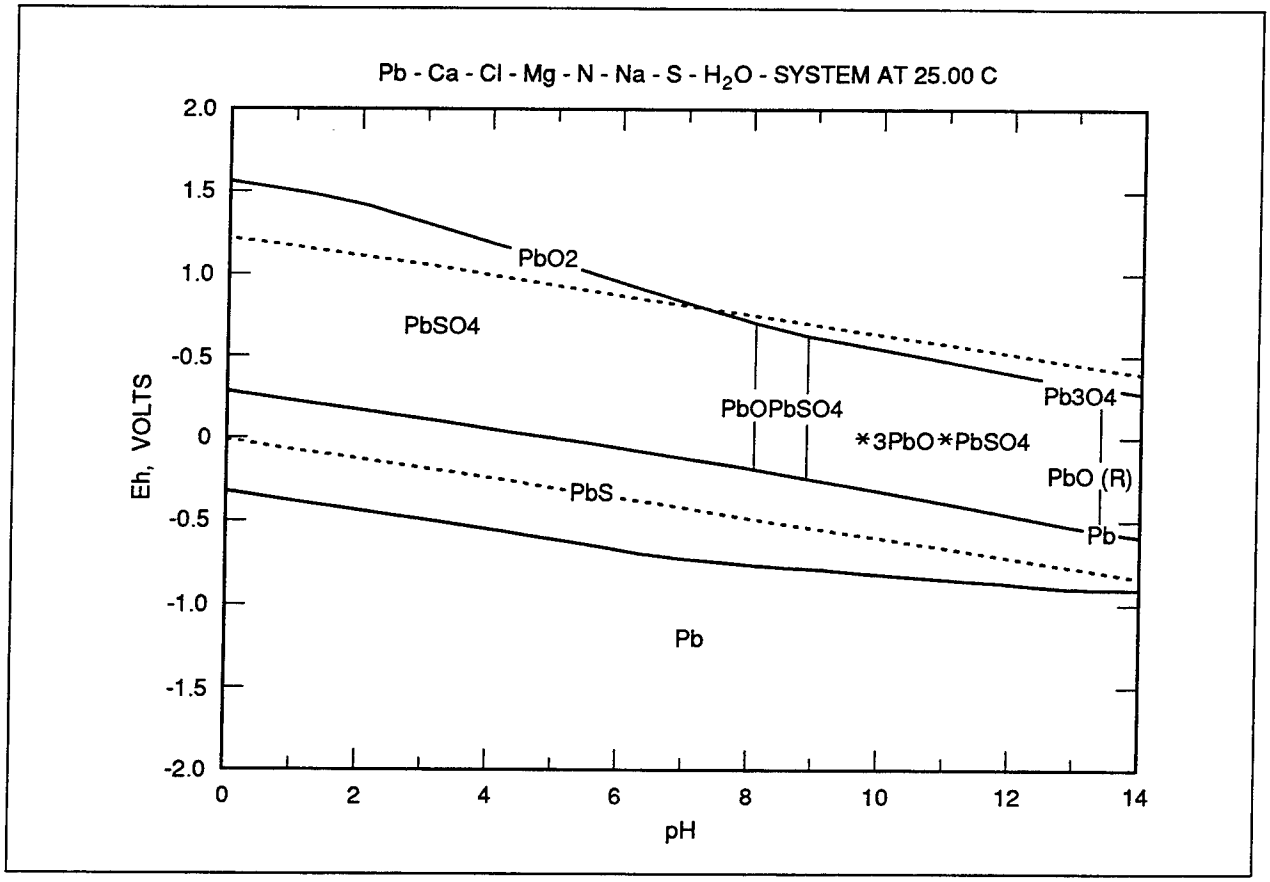

Figure 38. Eh-pH diagram for the Pb-Ca-Cl-Mg-N-Na-S-H2O system at 25 °C (source: Bundy, Bricka, and Morales (1995))

Soil chemistry can also affect lead pore water concentrations. Materials such as complex-forming ligands and chelating agents may increase or decrease the solubility of lead. The effects of dissolved organic matter (represented by fulvic acid) serve to increase the solubility of lead in the pH range of 4 to 6. Figure 39 illustrates how fulvic acid and lead species affect the solubility of lead in groundwaters. Soil organic matter and clays which are insoluble can also serve to complex or sorb lead, lowering the solubility (Allen, Perdue, and Brown 1993; Drever 1988). Soil cation exchange capacity (typically contributed by the clay or organic soil fraction) also significantly influences pore water lead solubility (Figure 40). The decay of soil organic matter such as pine litter may also produce organic acids. These acids will lower soil pH and increase the solubility of lead. Ionic concentration influenced by soil chemistry may also have significant effects on lead solubility (Allen, Perdue, and Brown 1993) as illustrated in Figures 41 and 42.

The type of projectile will also have a significant effect on pore water lead concentration. Generally there are two theories on how the lead is transported from projectiles to pore water. Johnson et al. (1993) report that as the bullet enters the soil, "the lead is molten and soft and sticks to the silicate grains of the soil, thus smearing on the soil surface." The lead in the soil is solubilized from the soil's surface to the pore water. The other theory involves galvanic corrosion effects.

Table 5
Solubilities of Some Common Salts of Lead

Compound	Symbol	Ksp	Sol., g/cc	Color
Lead acetate	$Pb(C_2H_3O_2)$	10.1	--	White
Lead carbonate	$PbCO_2$	3.3×10^{-14}	0.0011	White
Lead chloride	$PbCl_2$	1.6×10^{-5}	0.99	White
Lead chromate	$PbCrO_4$	1.8×10^{-14}	5.8×10^{-6}	Orange
Lead fluoride	PbF_2	3.7×10^{-8}	--	White
Lead hydroxide	$Pb(OH)_2$	1.42×10^{-20}	0.0155	White
Lead nitrate	$Pb(NO_3)$	5.88	56.0	White
Lead orthophosphate	$PB(PO_4)_2$	3×10^{-44}	1.4×10^{-5}	White
Lead di-orthosilicate	$Pb_2Si_2O_7$	insol.	--	White
Lead oxide	PbO	1.2×10^{-15}	0.0017	Yellow-red
Lead oxide (di)	PbO_2	insol.	--	Black, dark br.
Triplumbictetroxide	PB_3O_4	insol.	--	Red
Lead sulfate	$PbSO_4$	1.6×10^{-8}	0.00425	White
Lead sulfide	PbS	8×10^{-28}	0.0006	Black

Source: Peters et al. (1976), West and Astle (1978), Dean (1992).

Most military projectiles are copper jacketed as discussed in Chapter 1. As the projectile enters the soil, the jacket is fractured. The copper in the jacket either remains in contact with the lead core or is separated. Whether or not separation occurs, lead and copper build up in the soil at the SAR after some period of time. When the metals are exposed to moisture through a rain event, an electrical connection in the environment between two dissimilar metals is established, and electron flow occurs between the metals, resulting in galvanic corrosion. With galvanic corrosion, dissolution of the least-resistant metal is increased, and dissolution of the more resistant metal is decreased (Fontana and Greene 1978). As illustrated in Table 6, copper has a higher electromotive force (EMF) (+0.337) than lead (-0.126) and thus is more noble, implying that the dissolution of lead into the pore water would be accelerated.

Little information regarding the corrosion possibility for bullet projectiles at SAR was available when this theory was first considered. To investigate this theory, a study was initiated in the summer of 1995 by WES to examine the corrosion effects of bullets. Preliminary results of this study were released in an internal report, which is attached in its entirety as Appendix D. Results of this study indicate, that as theorized, corrosion is a major factor contributing to the lead pore water concentration.

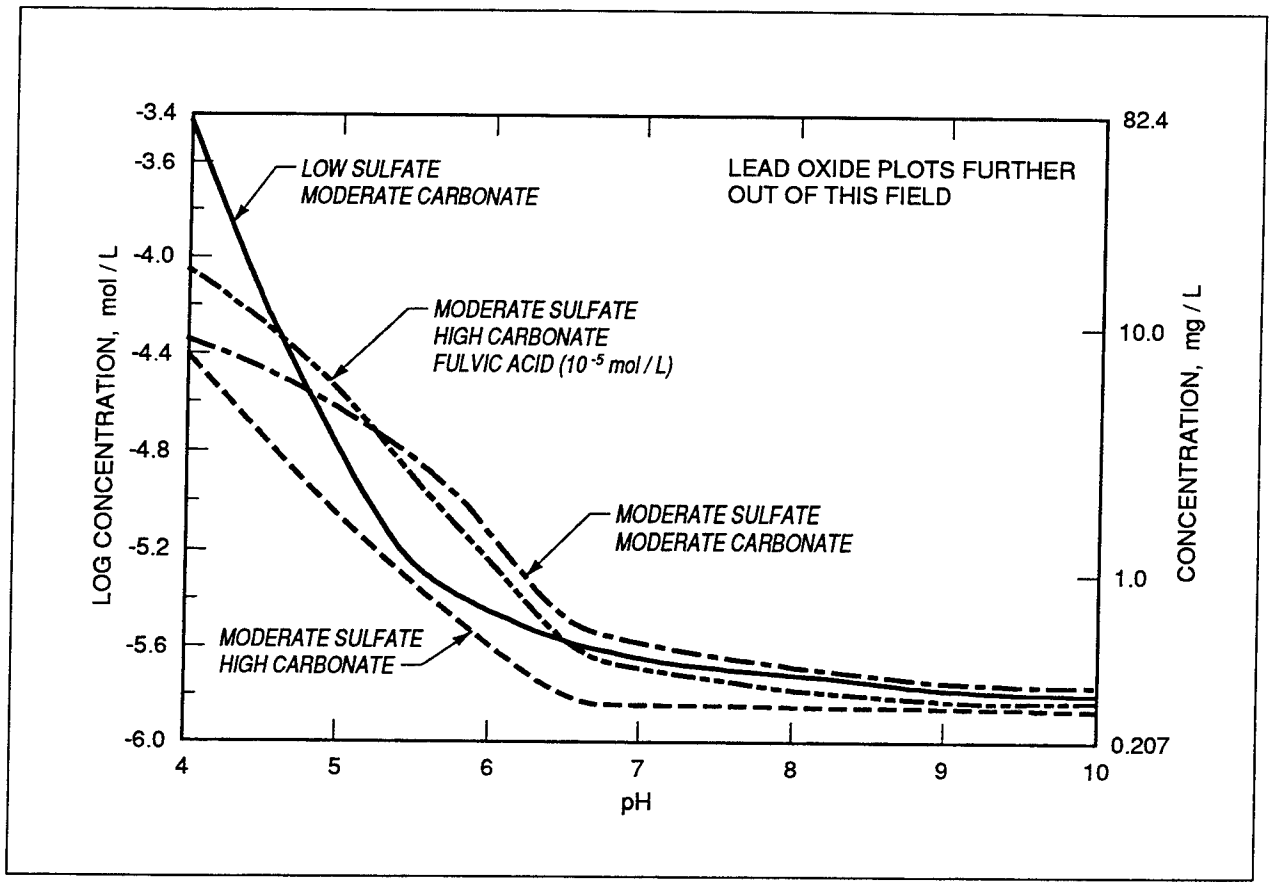

Figure 39. Solubility of lead in three different groundwaters (source: Heath et al. 1991)

Factors Affecting Bulk Transport

Atmospheric precipitation (rainfall) greatly influences the bulk transport of lead, as does site topography. Water must flow through the vadose zone to the aquifer for groundwater contamination to occur. If there is little or no precipitation, there will be no vertical bulk transport of the contaminants. If precipitation is excessive, and this water travels through the vadose zone, contaminants in the pore water will be diluted by the water flow. Site topography affects bulk transport by increasing or decreasing water infiltration to the vadose zone. If the site is significantly sloping, most of the surface water will run off and little infiltration will occur. In contrast, if the site is relatively flat, higher water infiltration will occur.

Wetting and drying cycles of the soil will also affect bulk transport. As the soil dries, an increase in the concentration of the lead in the pore water will occur, increasing metal precipitation and sorption. If the soil becomes completely dry, the lead will be in a solid form, resulting in a change in the metal species. As the soil is re-wetted, additional species transformation will occur which may increase (or decrease) the bulk transport of the lead.

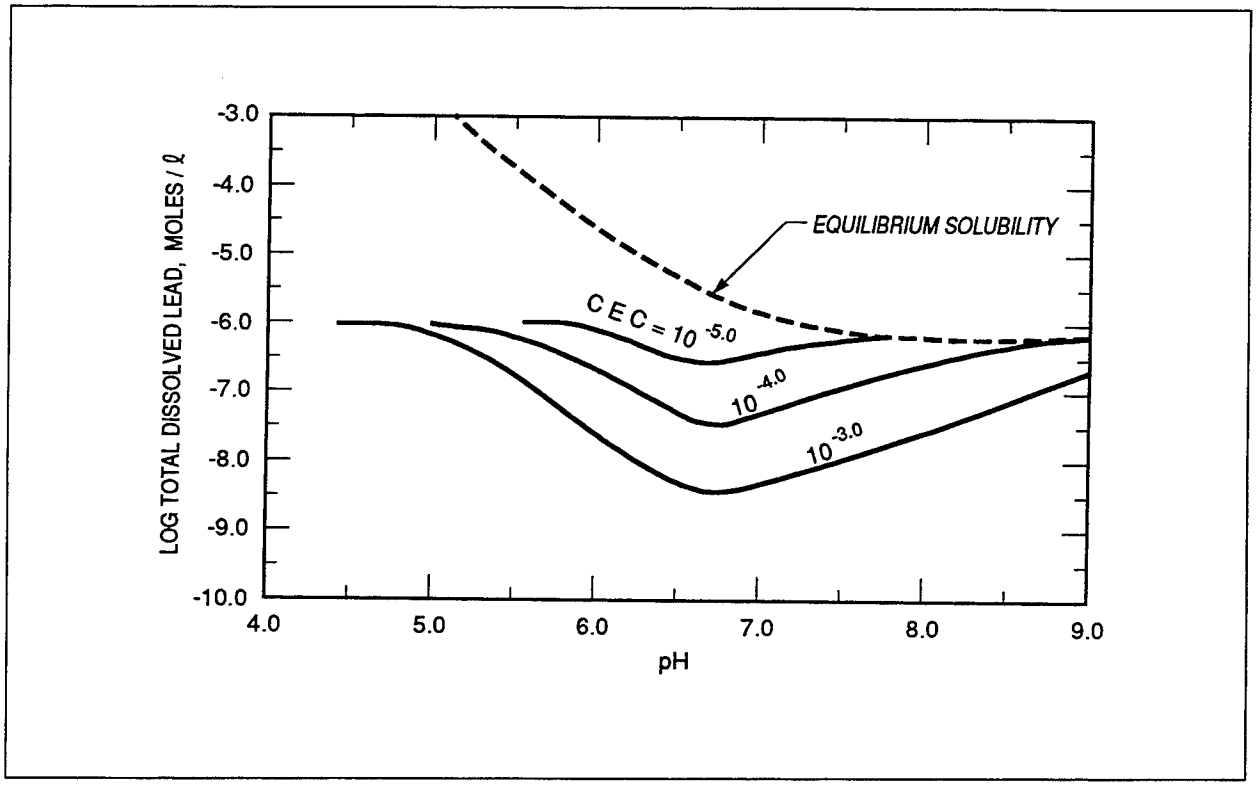

Figure 40. Effects of adsorption by halloysite (a clay) on lead concentration in solution. Contours are equilibrium lead concentrations at different clay concentrations. Clay concentrations are drawn in units of cation exchange capacity (moles of CEC per liter of solution). Dashed line is solubility of PbCO3 (source: Drever 1988)

Depth to groundwater is also a key factor influencing the potential environmental impact of SAR. If groundwater is shallow, the metals have a short travel path to groundwater. Effects of the metals on the groundwater will be observed quickly.

Summary of Theory

Several facts should be highlighted regarding SAR based on the review of the theory:

a. Bulk metal concentrations in the groundwater will never exceed equilibrium pore water concentrations.

b. Low-pH, high-Eh (oxidizing) soils will have high pore water metal concentration.

c. Soils having high solution activities (dissolved mineral or salt concentrations) will have high pore water metal concentrations.

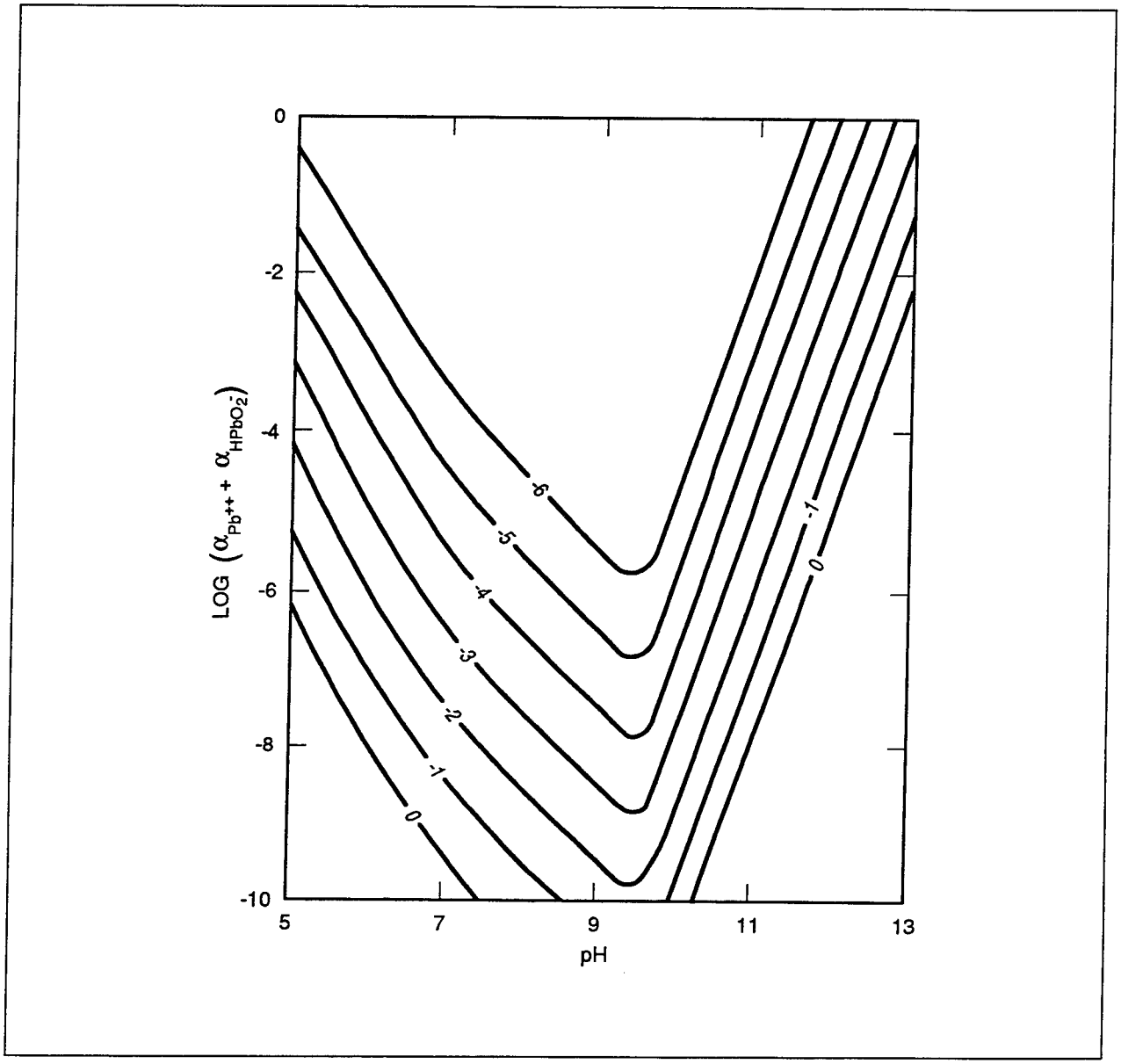

Figure 41. Solubility of lead carbonate as a function of pH for a total activity $aH_2CO_3 + aHCO_3^- + aCO_3^-$ varying from 1 to 10^{-6} (source: Gale, Liu, and Bricka 1994)

d. Soils with high clay content are expected to have lower pore water metal concentrations.

e. Metal species have a significant effect on pore water concentrations.

f. Soil containing high organic matter may have elevated pore water metal concentration if the soil pH is low. If the pH is 6 or above, high soil organic matter will decrease pore water metal concentrations.

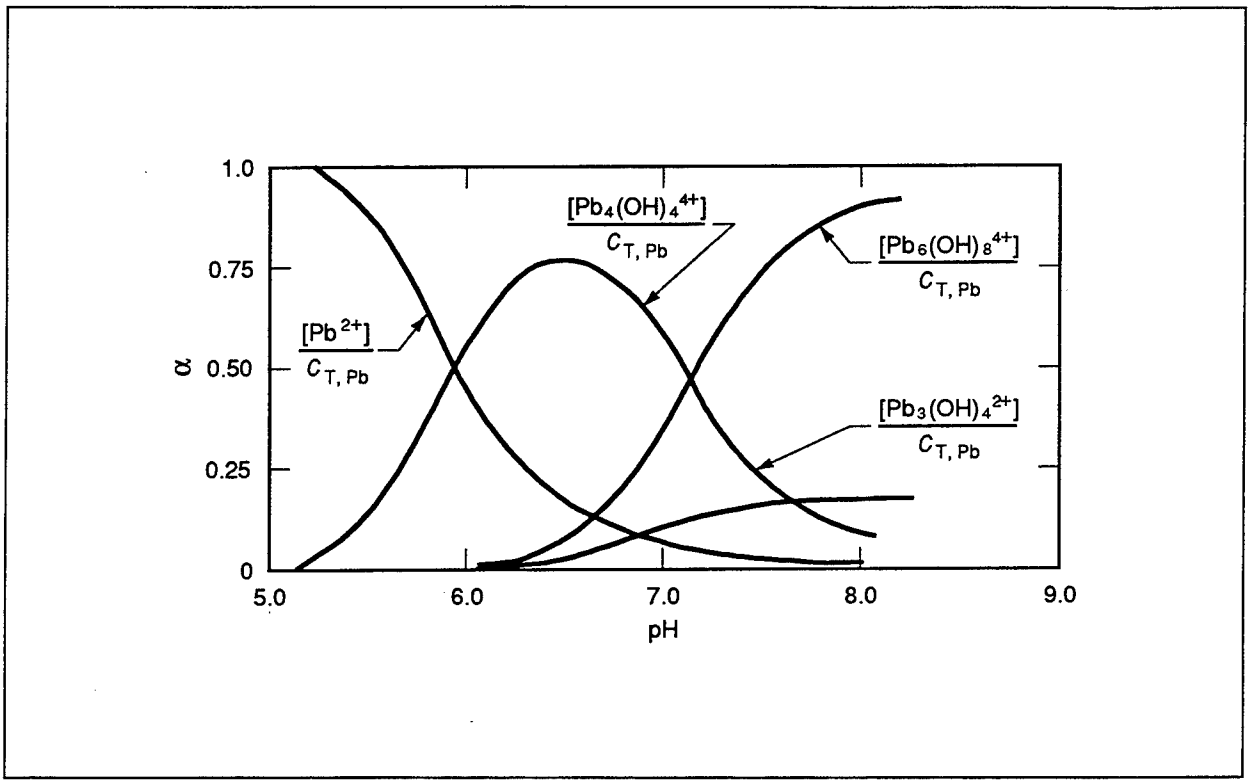

Figure 42. Species distribution of lead in an aqueous Pb(II) solution (source: Snoeyink and Jenkins (1980))

g. High dissolved organic matter will increase pore water metal concentration.

h. Corrosion, occurring with jacketed bullets, will increase pore water metal concentration.

i. It is difficult to predict the effect of wet/dry cycles on pore water metal concentrations.

j. Water infiltration through the vadose zone to groundwater increases metal concentration being transported via bulk transport.

k. Shallow groundwater will be impacted by SAR activities more quickly than deep groundwater.

Table 6
Standard EMF Series of Metals

	Metal-Metal Ion Equilibrium Unit Activity	Electrode Potential Versus Normal Hydrogen Electrode at 25 °C, volts
↑	$Au-Au^{+3}$	+1.498
	$Pt-Pt^{+2}$	+1.2
	$Pd-Pd^{+2}$	+0.987
	$Ag-Ag^{+}$	+0.799
	$Hg-Hg_2^{+2}$	+0.788
	$Cu-Cu^{+2}$	+0.337
Noble or Cathodic		
	H_2-H^{+}	0.000
Active or Anodic		
↓	$Pb-Pb^{+2}$	-0.126
	$Sn-Sn^{+2}$	-0.136
	$Ni-Ni^{+2}$	-0.250
	$Co-Co^{+2}$	-0.277
	$Cd-Cd^{+2}$	-0.403
	$Fe-Fe^{+2}$	-0.440
	$Cr-Cr^{+3}$	-0.744
	$Zn-Zn^{+2}$	-0.763
	$Al-Al^{+3}$	-1.662
	$Mg-Mg^{+2}$	-2.363
	$Na-Na^{+}$	-2.714
	$K-K^{+}$	-2.925

Source: Fontana and Greene (1978).

7 Data Collected for Camp Edwards Small Arms Range Soils

Laboratory analysis was conducted on the soil collected during the first sampling effort to provide some insight on the soil characteristics. Tests were limited to particle size analysis (PSA) and the determination of soil buffering capacity (SBC). PSA testing provides insight into the quantity of fines, sands, and coarse materials in the soil with depth. The SBC test provides information regarding the amount of acidity the soil will be able to buffer.

Particle Size Analysis

Soil particle size analysis consists of dry sieving the soil through a series of U.S. standard sieves ranging in size as listed below. A total of nine soil fractions were generated.

Sieve Size, mm
12.50
6.70
2.00
1.00
0.05
0.25
0.125
0.63

Selected soil samples were tested from the three ranges. Results of this PSA test are presented for Range G in Figure 43, Range H in Figures 44-45, and for Range K in Figures 46-48. Results of this test indicate that for range G material, the soil is very sandy. The top portion of the soil, down 50.8-cm (20 in.) in depth, has more fine material than that below the 50.8 cm (20-in.) depth. Typically, Range G soils contain 14-15 percent fine material as measured by the <0.063-mm fraction in the upper 50.8-cm (20 in.) of soil. Below 50.8 (20 in.), less than 3 percent fines were measured in this fraction. In contrast, Ranges H and K had higher concentrations of fines in the soil. Range H had between 20 and 40 percent fines (<0.063 mm) in all the samples tested down to 160 cm (63 in.) in depth. Range K was a mixture of more coarse and fine material. The Range K soil also contained fines down to about 26 in., but below this depth the soil was relatively coarse.

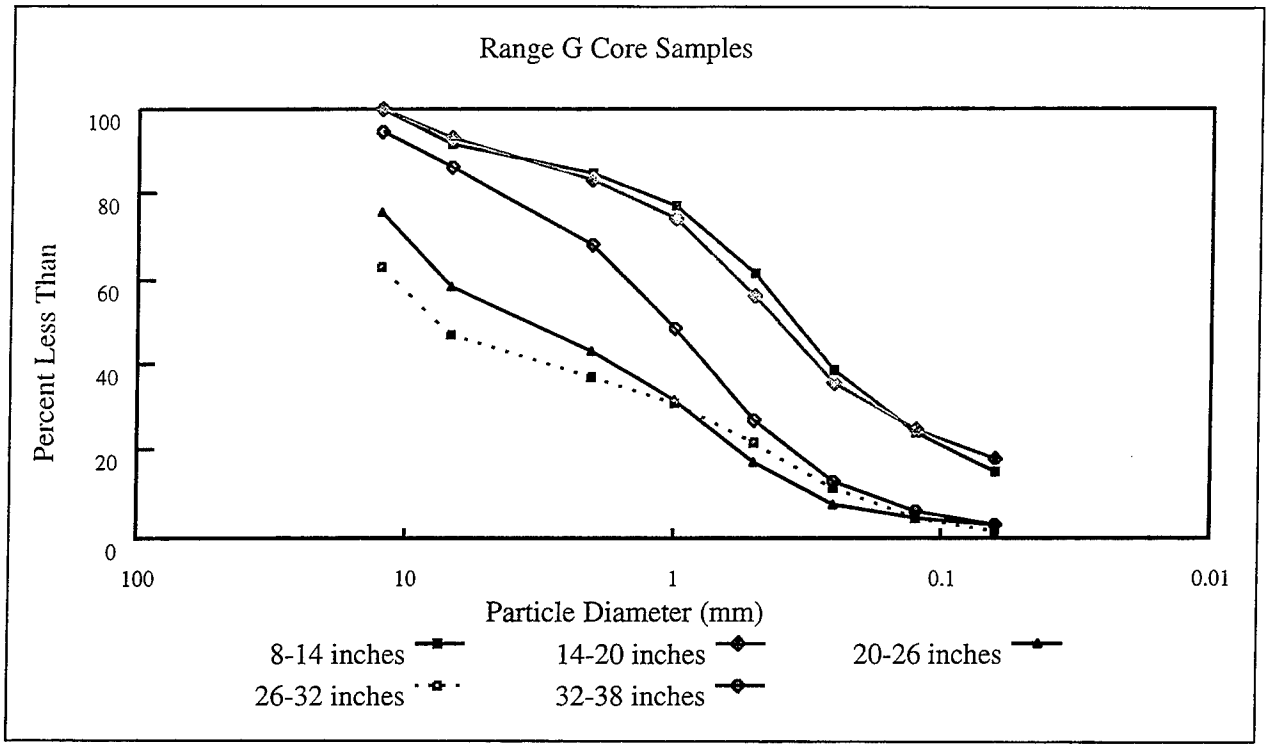

Figure 43. Particle size analysis for core sample CS-G-1 from Range G. This figure presents the 20.3- to 96.5-cm (8- to 38-in.) data

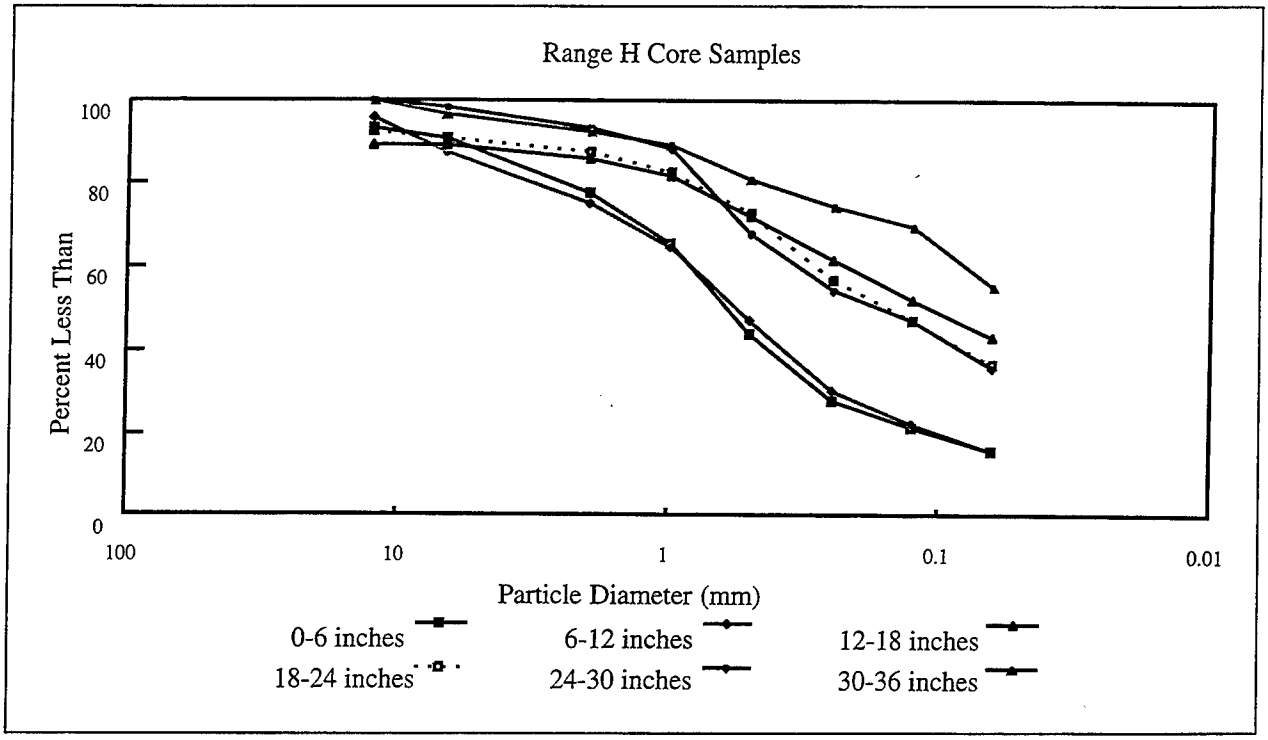

Figure 44. Particle size analysis for core sample CS-H-1 from Range H. This figure presents the 0- to 91.4-cm (0- to 36-in.) data

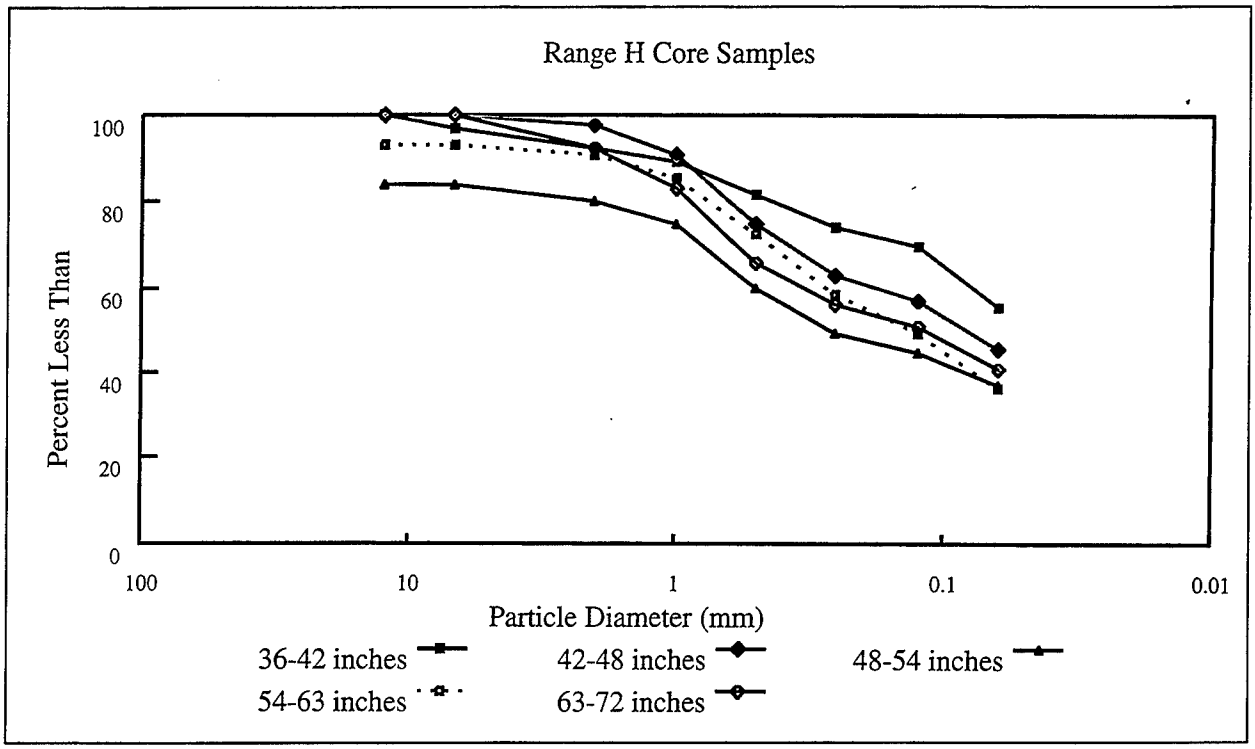

Figure 45. Particle size analysis for core sample CS-H-1 from Range H. This figure presents the 91.4- to 182.9-cm (36- to 72-in.) data

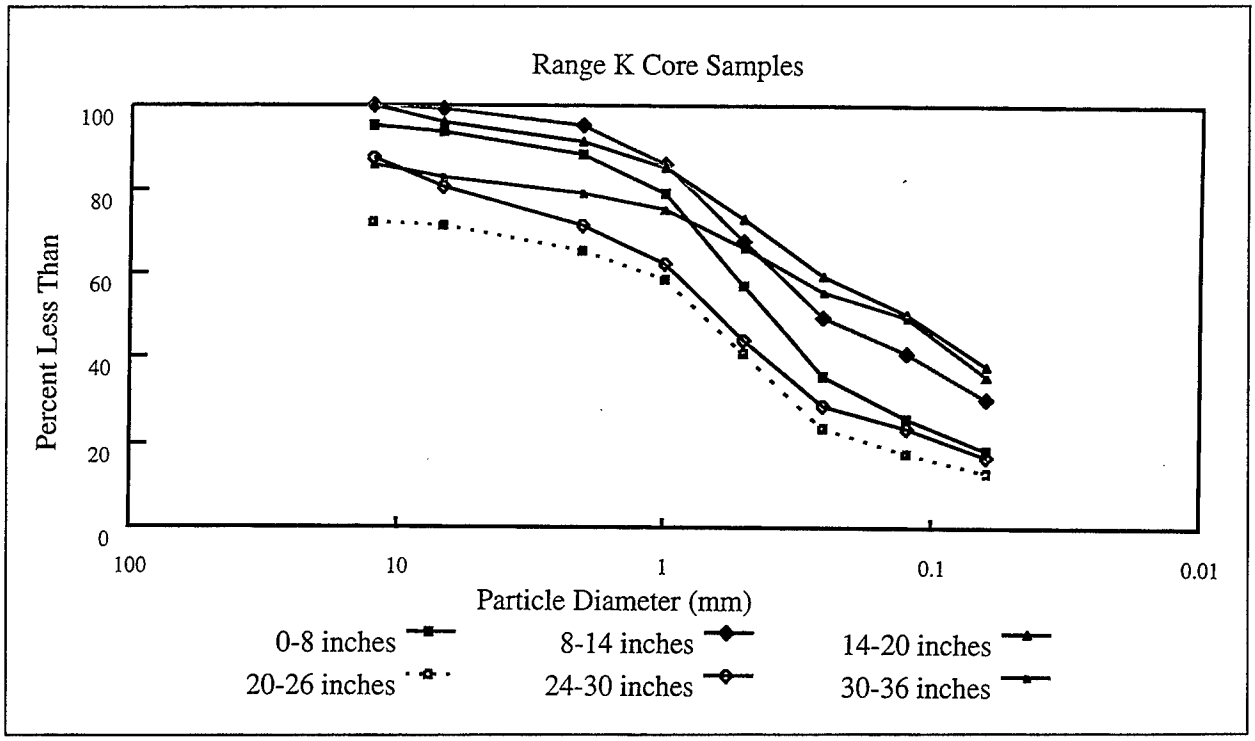

Figure 46. Particle size analysis for core sample CS-K-1 from Range H. This figure presents the 0- to 91.4-cm (0- to 36-in.) data

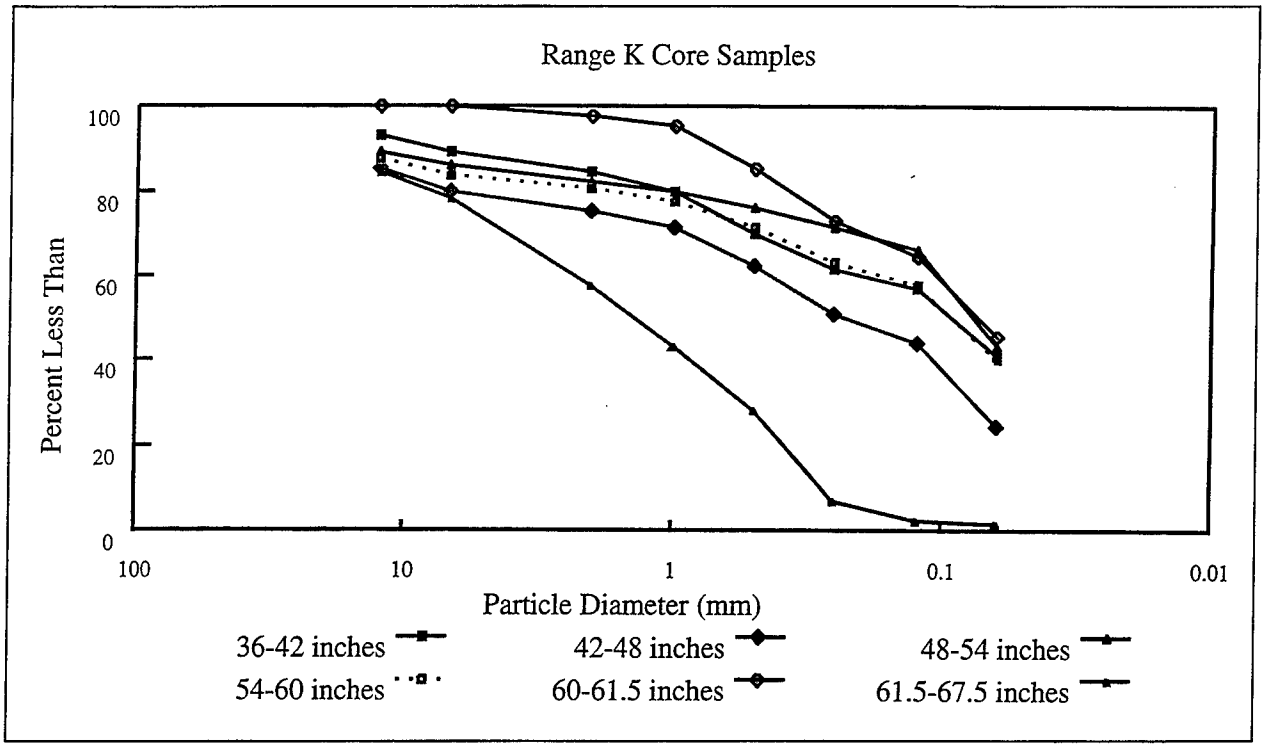

Figure 47. Particle size analysis for core sample CS-K-1 from Range K. This figure presents the 91.4- to 171.5-cm (36- to 67.5-in.) data

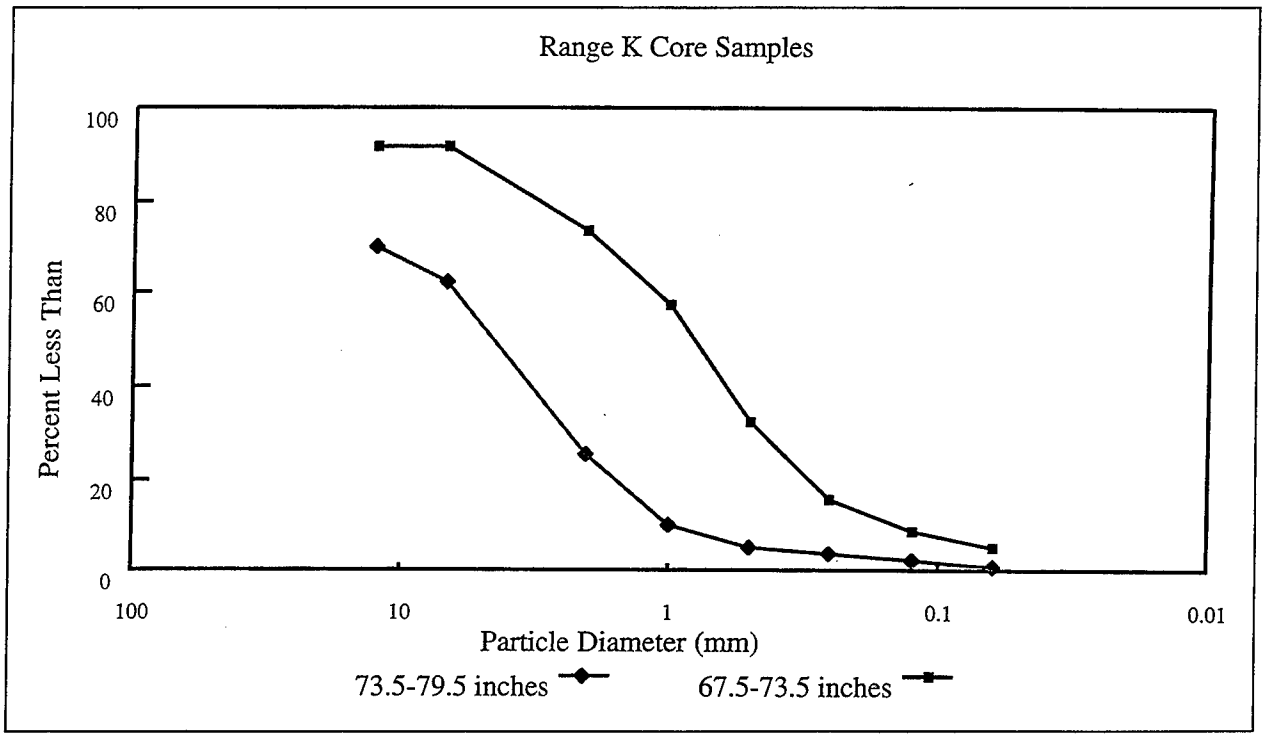

Figure 48. Particle size analysis for core sample CS-K-1 from Range K. This figure presents the 171.5- to 201.9-cm (67.5- to 79.5-in.) data

Soil Buffering Capacity

Soil buffering capacity tests were conducted only on the CS1 and CS2 core samples from Range G during the first sampling effort. The cores were divided into 6-in. sections and SBC tests were conducted on each section of the core. The deepest sample analyzed was the 81.3- to 96.5-cm (32- to 38-in.) CS2 sample. A Metrohm™ 670 Titroprocessor was used to conduct buffering capacity determination for the soil sample using an acid-base addition procedure following the manufacturer's guidelines, briefly described as follows. First, 3-5 g of oven-dried soil was weighed and slurried with 100 ml of water. Then, using a known normality solution of nitric acid, acid was added to the soil slurry at a rate of 0.2 ml/min and the pH of the slurry was recorded. The data reported was the pH versus the moles of acid per gram of soil added.

Figures 49 and 50 present the results for the CS1 and CS2 samples, respectively. It is clear from these figures that there is very little soil buffering capacity until the soil reaches a pH of 4.5 or below. These figures also illustrate that the SBC changes little over the depths tested. Figure 51 presents a comparison of the SBC of soil from the CS1 sample and SBC of soil collected from an SAR at Fort Benjamin Harrison (FBH). The FBH soil has a much higher clay content than the CEMR SAR soils. The FBH soil is more typical of Army SAR soils. Comparing the FBH soil to the CEMR soil, it is evident that CEMR soil has little buffering capacity.

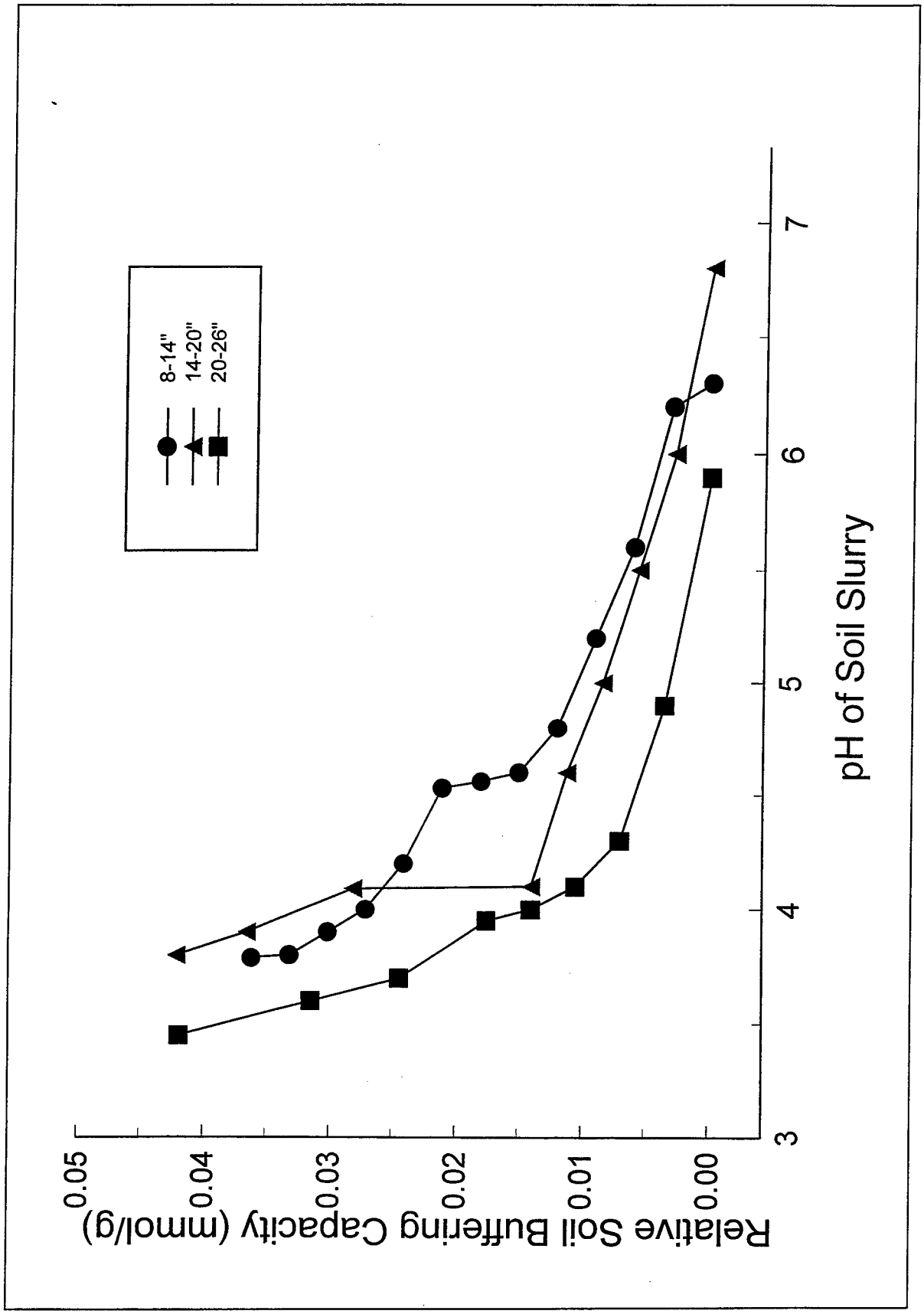

Figure 49. Soil buffering capacity curves for core sample CC-CR-CS1 from Range G. This figure presents the 8- to 26-in. (20.3- to 66-cm) data

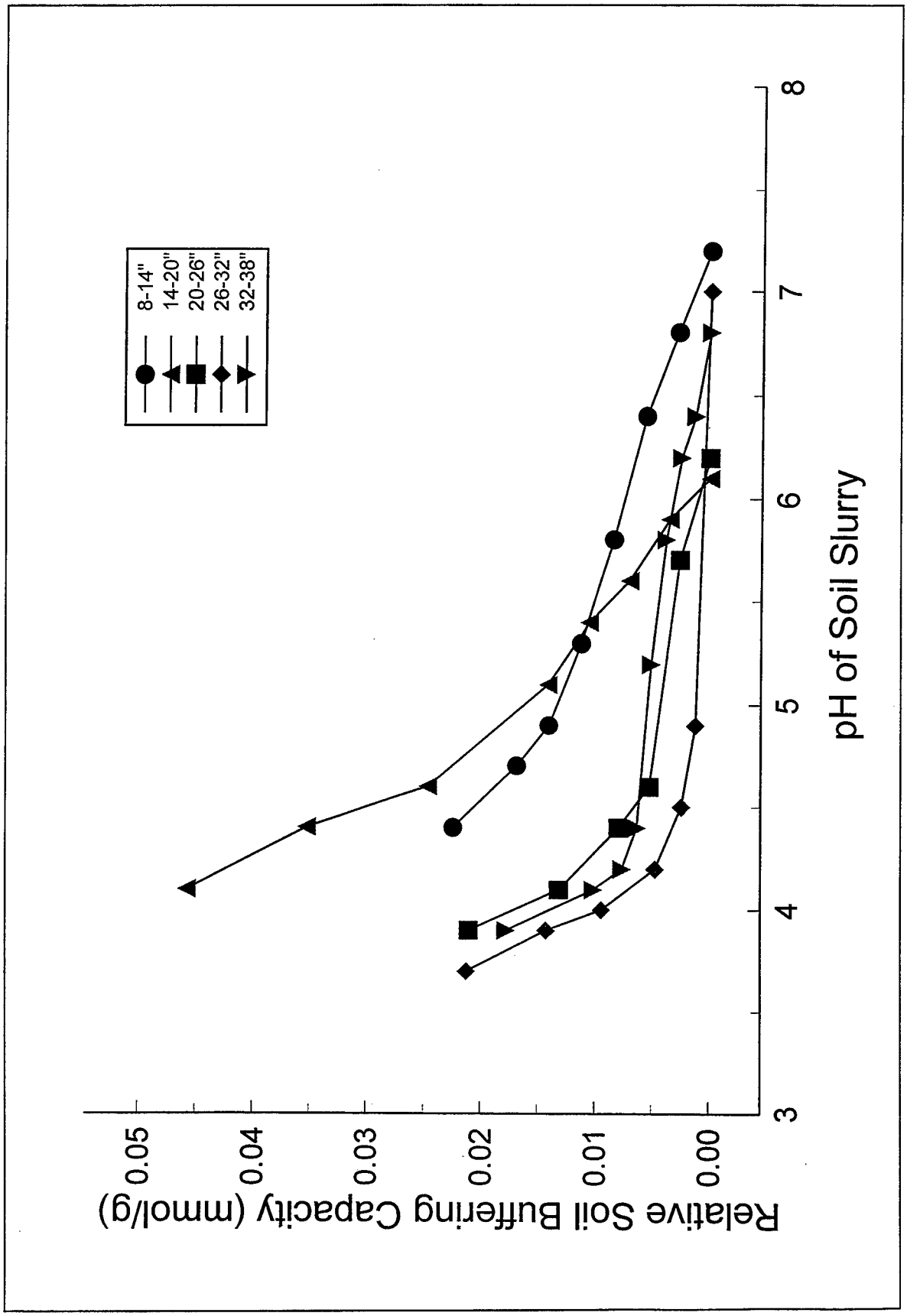

Figure 50. Soil buffering capacity curves for core sample CC-CR-CS2 from Range G. This figure presents the 8- to 38-in. (20.3- to 96.5-cm) data

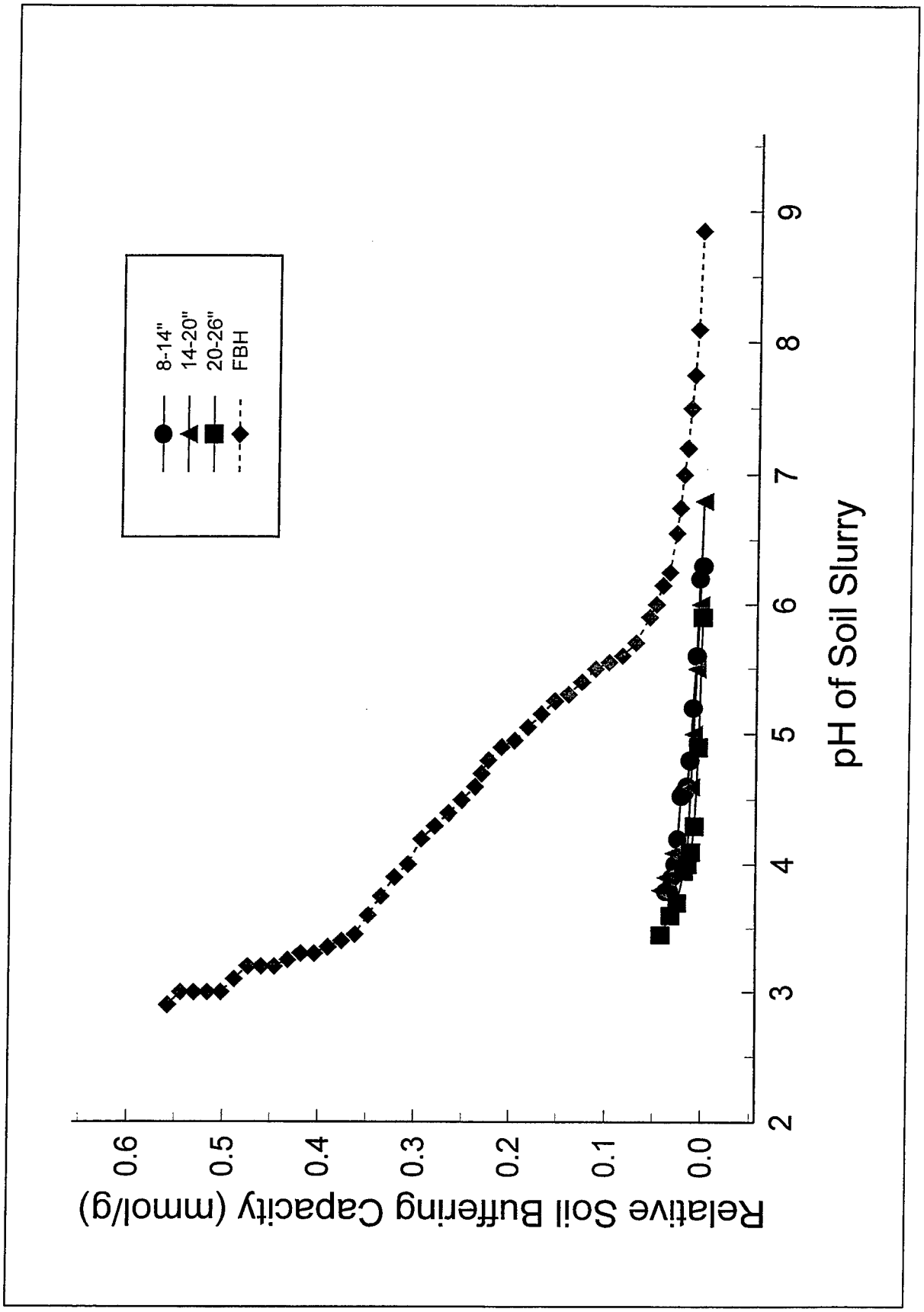

Figure 51. Soil buffering capacity curves for core sample CC-CR-CS1 from Range G and the Fort Benjamin Harrison soil

8 Modeling Efforts

First Modeling Effort

To better understand the potential for vertical migration at the SAR at CEMR, a simple model was used. A one-dimensional form of the advection-dispersion equation for nonreactive dissolved constituents was determined to fit the conditions exhibited at the SARs. Equation 1 was the model chosen to represent site conditions. This model represents the conditions of saturated, homogeneous, isotropic materials under steady-state uniform flow conditions (Freeze and Cherry 1979).

$$\frac{C}{C_o} = \frac{1}{2}\left[\operatorname{erfc}\left(\frac{l-\bar{v}t}{2\sqrt{D_l t}}\right) + \exp\left(\frac{\bar{v}l}{D_l}\right)\operatorname{erfc}\left(\frac{l+\bar{v}t}{2\sqrt{D_l t}}\right)\right] \quad (1)$$

where

l = distance along the flow path

$\bar{v}$ = average linear water velocity

D_l = coefficient of hydrodynamic dispersion in the longitudinal direction

C = contaminant concentration at time t

t = time

C_o = source concentration

The majority of fluid flow at the SAR at CEMR is in the vadose zone and not under saturated conditions. Recognizing this fact, the model will "overpredict" the transport of the contaminants with time. Unsaturated flow models are very complicated and beyond the scope of this first effort. Therefore, it was decided to adjust this model to fit the known site conditions. For this first estimate, it was determined that this model could be used to predict the time required for the contaminants to migrate to the groundwater if corrections were applied to the model

results. Solving Equation 1, without corrections, provides the solution shown by Equation 2 (van Genuchten and Alves 1982).

$$C(x,t) = \frac{1}{2}\operatorname{erfc}\left[\frac{Rx - vt}{2(DRt)^{1/2}}\right] + \frac{1}{2}\exp(vx/D)\operatorname{erfc}\left[\frac{Rx + vt}{2(DRt)^{1/2}}\right] \quad (2)$$

where

C = concentration

R = retardation factor

$R = 1 + (\zeta/\theta)Kd$ ζ = bulk density of the soil, θ = porosity of the soil

x = length of groundwater travel

v = hydraulic conductivity

t = time

D = dispersion coefficient

and the boundary conditions of:

$C(l,0) = 0 \qquad l >= 0$

$C(0,t) = Co \qquad t >= 0$

$C(\infty,t) = 0 \qquad t >= 0$

As shown in Appendix E, the rate of contaminant transport was predicted using two corrections. The first assumed that the contaminant would only migrate vertically if water was present. Using an estimate of 12 days for rain events greater than or equal to 1 in. (Fletcher 1993) and applying this correction to the model, it is estimated that vertical lead migration will take a period in excess of 125 years to impact groundwater at CEMR at 90 ft in depth. This calculation is based on several assumptions. A more accurate method of contaminant migration prediction involves "tuning" the model. Using the fact that after 40 to 50 years, the contamination at the SAR had migrated no deeper than 10 ft and using a reasonable estimate of dispersion and hydraulic conductivity, we calculated that R = 50, as illustrated by the curve shown in Figure 52. Substituting these values into the model and predicting migration to 90 ft (groundwater) we see that breakthrough will not occur for approximately 300 years (Figure 53). While predictions from the two models vary from 125 to 300 years, they both indicate that the lead will migrate to groundwater. Both modeling efforts predict that SAR activities at CEMR will provide a source of lead groundwater contamination in the near term (< 500 years) if no action is taken at the SAR to reduce the lead migration and use of these SAR is continued.

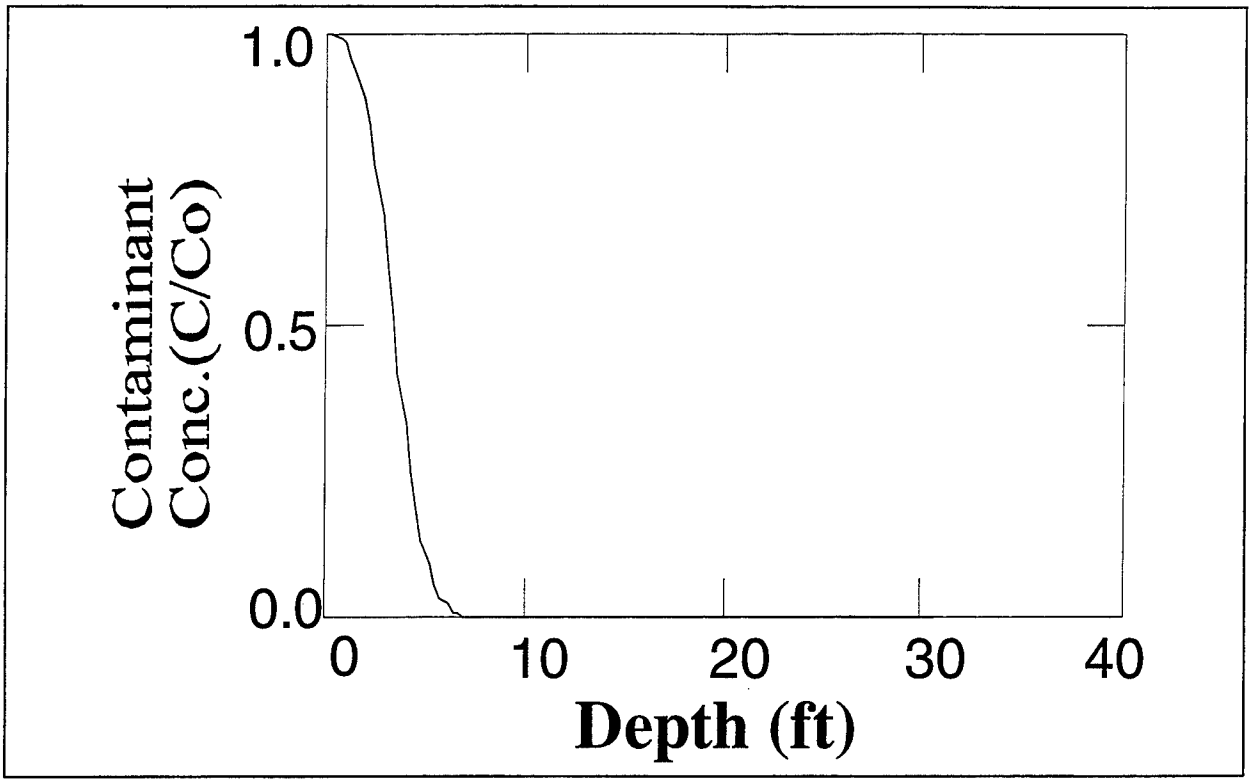

Figure 52. Model prediction of Pb migration at CEMR. This figure was used to "tune the model." Solution variables were D = 0.028 ft^2/day, v = 0.08 ft/day, t = 50 years, and R = 50. The model was run using trial and error to provide the conditions of C/Co = 0 at 3 m (10 ft) of depth (x)

Second Modeling Effort

The result of the first modeling effort was presented to project personnel at CEMR in a briefing held on 26 March 1996. As a result of this meeting, WES was tasked to conduct a more in-depth modeling investigation to provide a more representative prediction of the vertical migration rate of the contaminants and the potential for groundwater impact. The Water Quality and Contaminant Modeling Branch at WES was tasked with this effort, results of which are presented in this chapter.

Model Selection

Existing groundwater models were reviewed to determine the most appropriate model for modeling the vertical contamination from the SAR at CEMR. Limited site data regarding groundwater flow characteristics were available from CEMR in the area around the SAR, and this weighed strongly in model selection. Based on the data provided to WES by the CEMR and the object of this modeling effort, the Multimedia Environmental Pollutant Assessment System (MEPAS) model was selected for use in the second modeling effort.

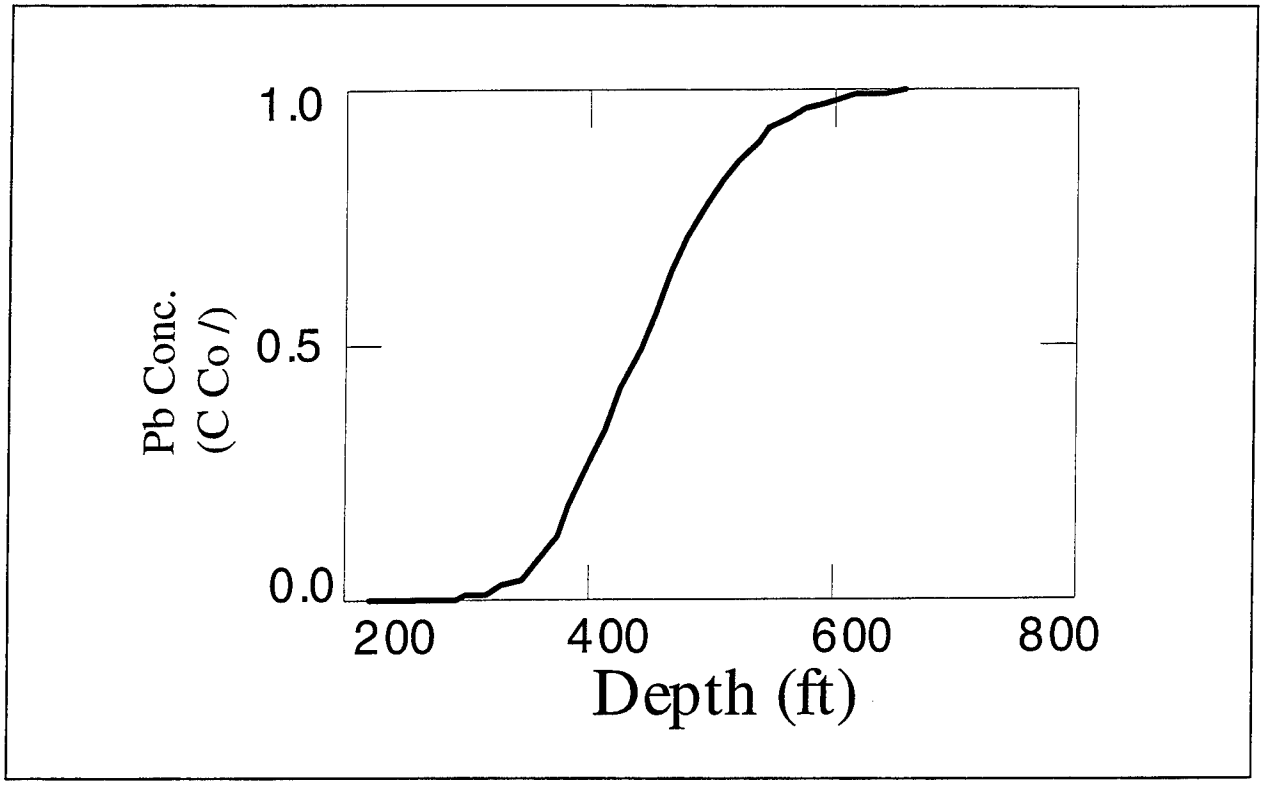

Figure 53. Model prediction of Pb migration at CEMR. This figure uses the solution variables shown in Figure 31 by x = 27.4 m (90 ft) (groundwater depth). The model predicts that it will take 300 years for the Pb to migrate the 27.4 (90 ft)

MEPAS is a physics-based risk computation code that integrates source-term, transport, and exposure models. This model is primarily a screening level model which has been used for the evaluation and ranking of environmental problems for the USEPA (Whelan et al. 1992). The multimedia MEPAS model was developed at the Pacific Northwest Laboratory and can be used to evaluate air, groundwater, surface-water, and overland flow transport pathways. For the CEMR, the primary focus of this second modeling effort was on groundwater contamination.

Objective

The objective of this second modeling effort was to investigate the potential migration of lead to groundwater resources from three SARs at CEMR. Lead was selected as an indication of contaminant migration because it was measured at the greatest levels in the soils and, based on the soil boring, it had the highest rate of migration. Both concentrations and time of arrival were determined for the vertical migration through the vadose (or unsaturated) zone and the transport of the lead in the groundwater to fixed locations at known distances from the SAR.

Background

Utilizing the field data collected during the first and second sampling efforts, the MEPAS model was calibrated and the screening level model was used to determine the degree of groundwater contamination that would occur from the ranges. Input data to the model were purposely held conservative so that the worst-case scenarios could be evaluated.

Due to the fact that firing Range G appeared to have the deepest contaminant migration, this range was modeled in this study. Based on data gathered by the U.S. Army Center for Health Promotion and Preventive Medicine (1994), the conceptional soil structure at Range G used as input to the model is shown in Figure 54. From the figure it can be seen that the majority of transport is through sandy soil. The area of the berm was estimated to be approximately 55 by 168 m (180.5 by 551.2 ft). The other two ranges of interest, H and K, exhibit geological characteristics similar to Range G; thus, contaminant migration at Ranges H and K should be represented adequately by Range G. It is assumed that since the deepest contamination is measured at Range G, this would present the worst-case scenario.

Modeling Assumptions

Several assumptions were made in this modeling process. One assumption was the beginning date for soil loading at the site. For this modeling effort, January 1, 1973 was used as the initialization point. In viewing the output graphs from the model, year 0 on the x-axis corresponds to 1JAN73. Thus, for calibration purposes, 1996 data collected during the second sampling effort were calibrated to the concentrations at year 23. Two area source loading scenarios were investigated. One scenario addresses the case where the range usage was discontinued after 50 years of use but the projectiles were not removed from the berm. The second scenario addresses the case where the range is continued to be used for 1,000 years. The purpose was to provide insight into the difference between short- and long-term continued loading at Range G on groundwater resources. Other assumptions included utilizing the Boston, MA, weather data summaries for Camp Edwards, and groundwater transport was the media investigated (no overland flow or volatilization was considered). Soil chemical and physical parameters were obtained for Range G sampling data when available, and the MEPAS guide was used to provide best guess estimates when better data were unavailable. In addition, a groundwater well receptor was used to determine horizontal migration from the site. The well depth in the aquifer was originally placed at 0.3 m (1 ft) to obtain the highest possible concentration. This depth was varied to 15.2 m (50 ft) in the aquifer, to obtain more realistic concentrations for well withdrawals.

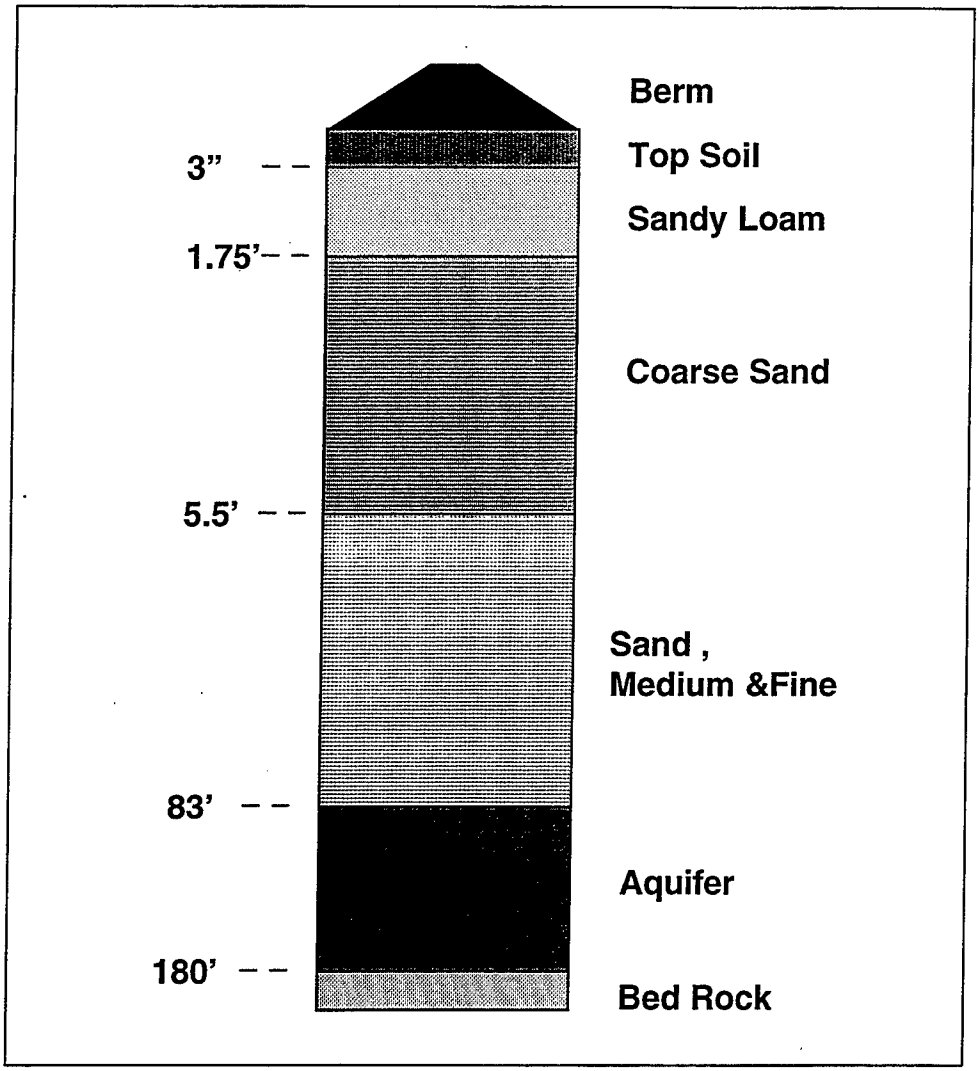

Figure 54. Conceptional soil structure at Range G used as input to the second modeling effort

Model Input Data

Model input is summarized in Appendix F. The appendix lists the values used for the calibration simulation run. The computer run was made for a 50-year loading of lead (each year, 20,000 kg (2.2 tons) were added to the site). In addition to the lead, chloride transport (as sodium salt) was also simulated utilizing the same loading rate. Modeling of the chloride transport was done as a check to make sure the model was operating correctly. Chloride is nonreactive with the soil, so chloride transport will be much faster than lead transport. The values used for the soil parameters of each layer (total porosity, bulk density, field capacity, permeability, darcy velocity, etc.) can be seen in Appendix F as well as the dispersivity values used for the aquifer.

Model Calibration

The model was calibrated through use of soil data collected during the second sampling effort at Range G. Data collected included soil concentrations at various depths at Range G. Model output was collected and compared to data at 0.5-m and 1.7-m (1.75- and 5.5-ft) vertical depths in the soil profile. To match the observed concentrations, the loading rate of lead at the site was varied until an approximate match was obtained. The observed value of lead at the 0.5-m (1.75-ft) level was 2,380 ppm, and the simulated value was 2,802 ppm. At the 1.7-m (5.5-ft) level, the observed value was 44.8 ppm compared to the 45.5-ppm simulated value. Although it is recognized that there is a wide range of values that would enable the calibration of the model, based on yearly precipitation, best estimates of lead loading at the site, and best engineering judgement, the above calibration values appear to be reasonable and prudent.

Model Results

After the model was calibrated and verified, the 50- and 1,000-year loading scenarios were run for both the lead contaminant and the chloride tracer. Figures 55-61 present the chloride data for the 50-year loading scenario. Figures 55-57 show that the chloride front quickly moves through the soil to the groundwater. In fact, chloride breakthrough to the aquifer is observed in less than 6 years at 25.3 m (83 ft) (Figure 57). As a result of the quick transport of chloride, chloride concentrations in the aquifer 4.6 m (15 ft) from the source (in a well screened at 0.3 m (1 ft) reach a maximum of 2,580 ppm in 7-8 years (Figure 58), and at 1.6 km (1 mile) from the source (in a well screened at 15.2 m (50 ft), a maximum concentration of 0.11 ppm is reached in 18 years (Figure 59). As expected, the results for the 1,000-year loading scenario for chloride (Appendix G) generate identical maximum concentrations. The only difference between the 50-year loading and the 1,000-year loading is that the maximum concentrations for the 1,000-year scenario remain elevated for a much longer period of time due to the fact that the source remains constant for an extended period of time.

These chloride data represent the quickest rate of transport because the contaminant has little interaction with the soil (i.e., is weakly sorbed by the soil). As expected, the model predicts that the contaminant quickly moves to the groundwater and is transported by the groundwater to offsite sources in as little as 50 years. This seems conceivable for the sandy material encountered at CEMR; thus, it is felt that the assumptions utilized for the model are reasonable.

Figures 62-68 present the lead data for the 50-year loading scenario. In Figures 62-64 it is evident that the lead front moves through the soil at a much slower rate than the chloride. Lead breakthrough to the aquifer is not observed at measurable concentrations 4.6 m (15 ft) from the source in a well screen at 0.3 m (1 ft) until 350 years (Figure 65). At 1 mile from the source, the maximum concentration observed in a well screened 1.6 km (50 ft) in the aquifer is 1.4 parts per billion

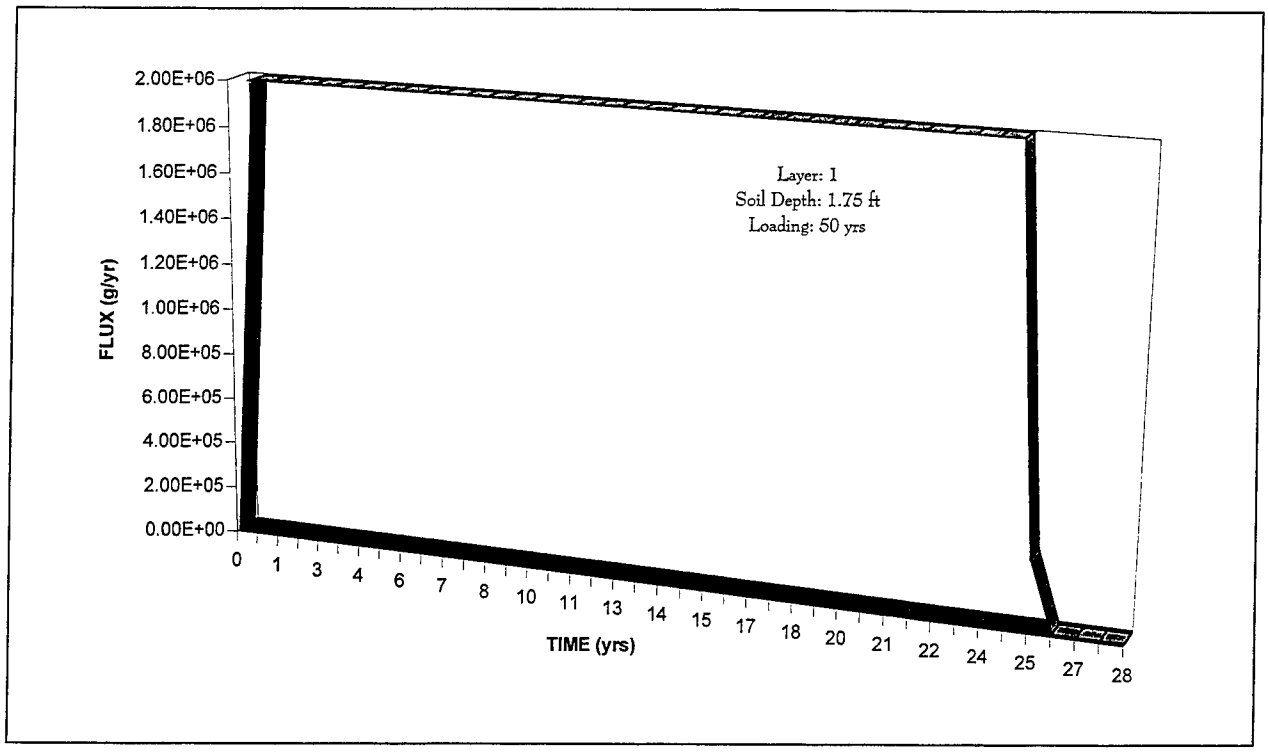

Figure 55. Model prediction for chloride transport through the first soil layer using a 50-year soil loading

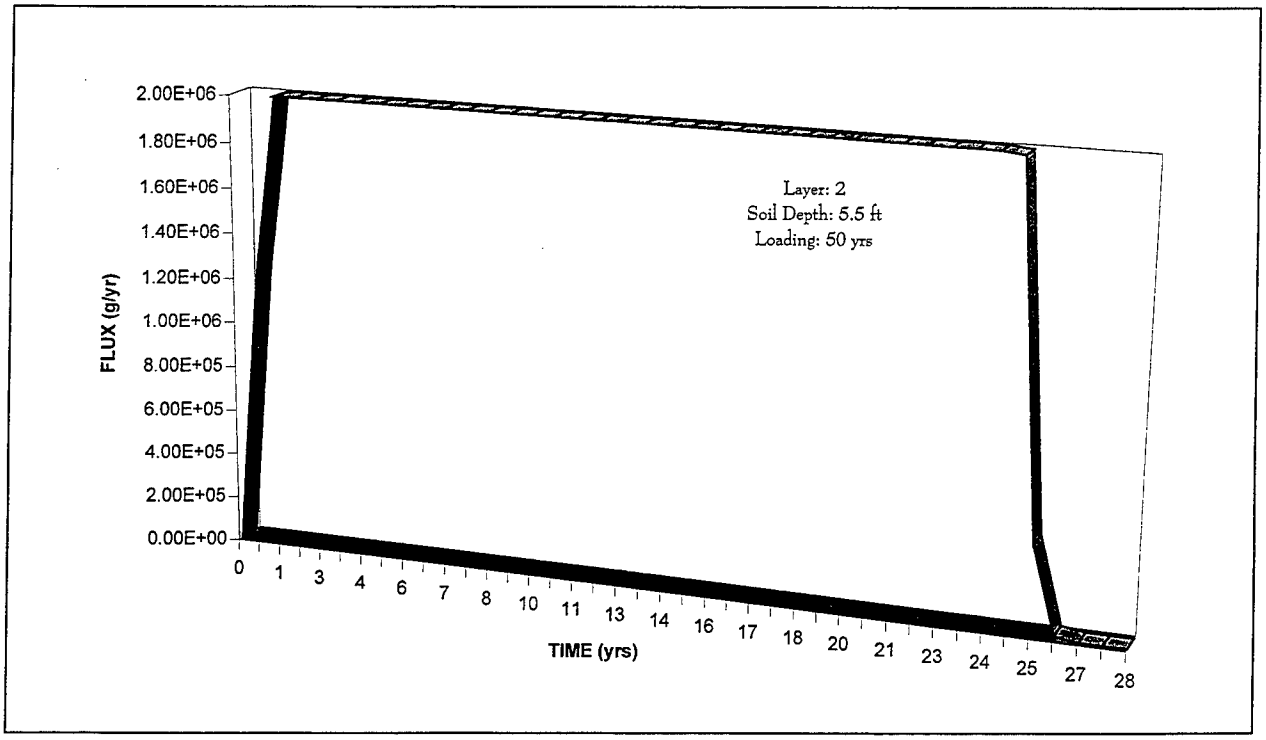

Figure 56. Model prediction for chloride transport through the second soil layer using a 50-year soil loading

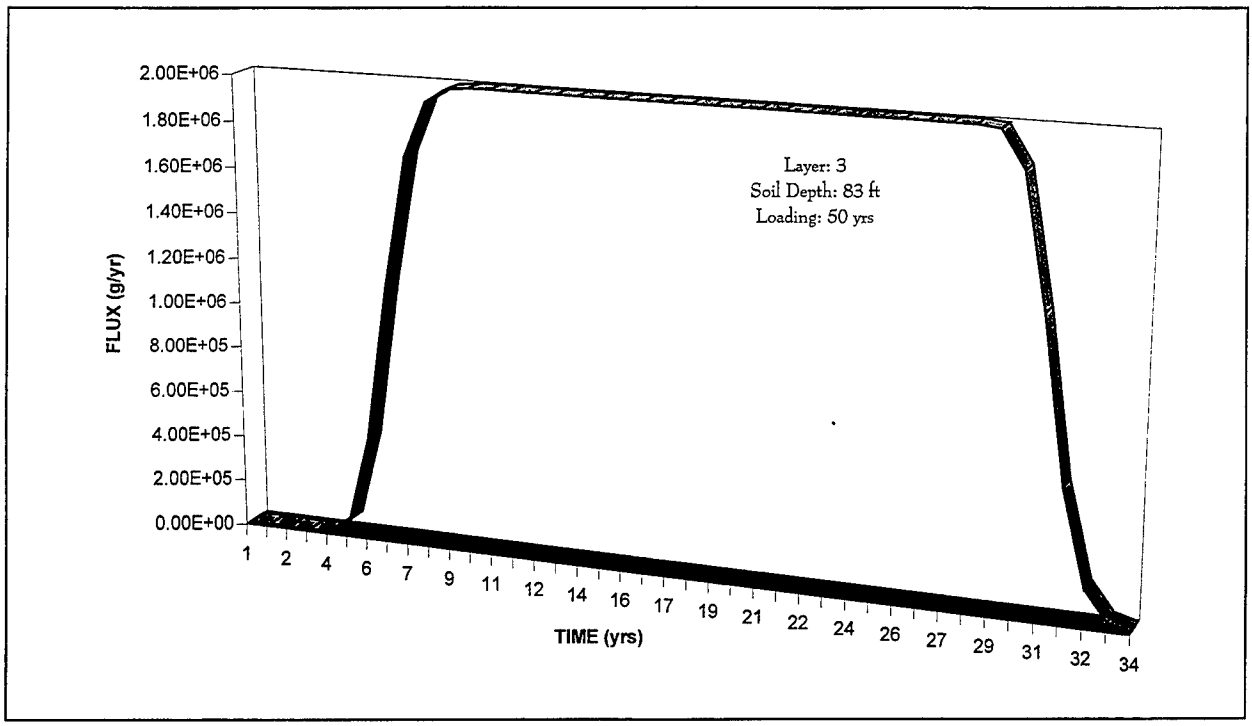

Figure 57. Model prediction for chloride transport through the third soil layer using a 50-year soil loading

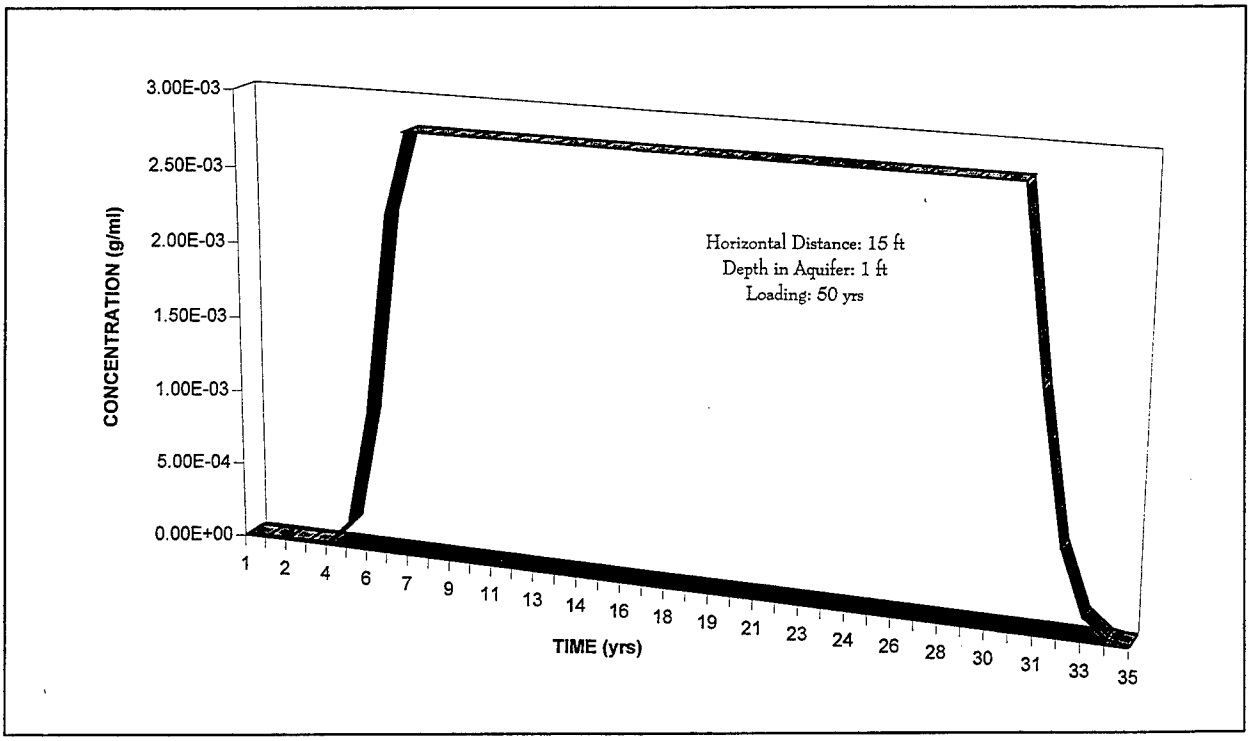

Figure 58. Model prediction for chloride transport in the aquifer using a 50-year soil loading. The receptor is a well located 4.6 m (15 ft) from the range, which is screened at 0.3 (1 ft)

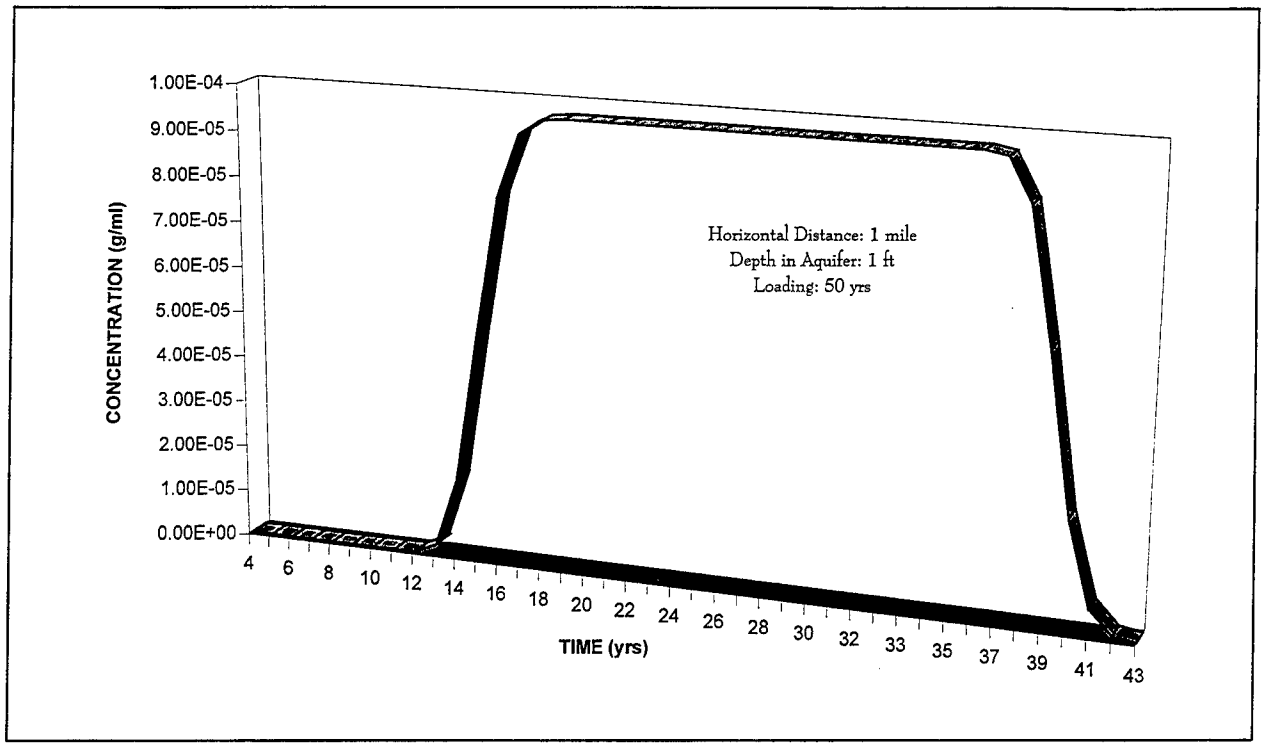

Figure 59. Model prediction for chloride transport in the aquifer using a 50-year soil loading. The receptor is a well located 1.6 km (1 mile) from the range, which is screened at 0.3 m (1 ft)

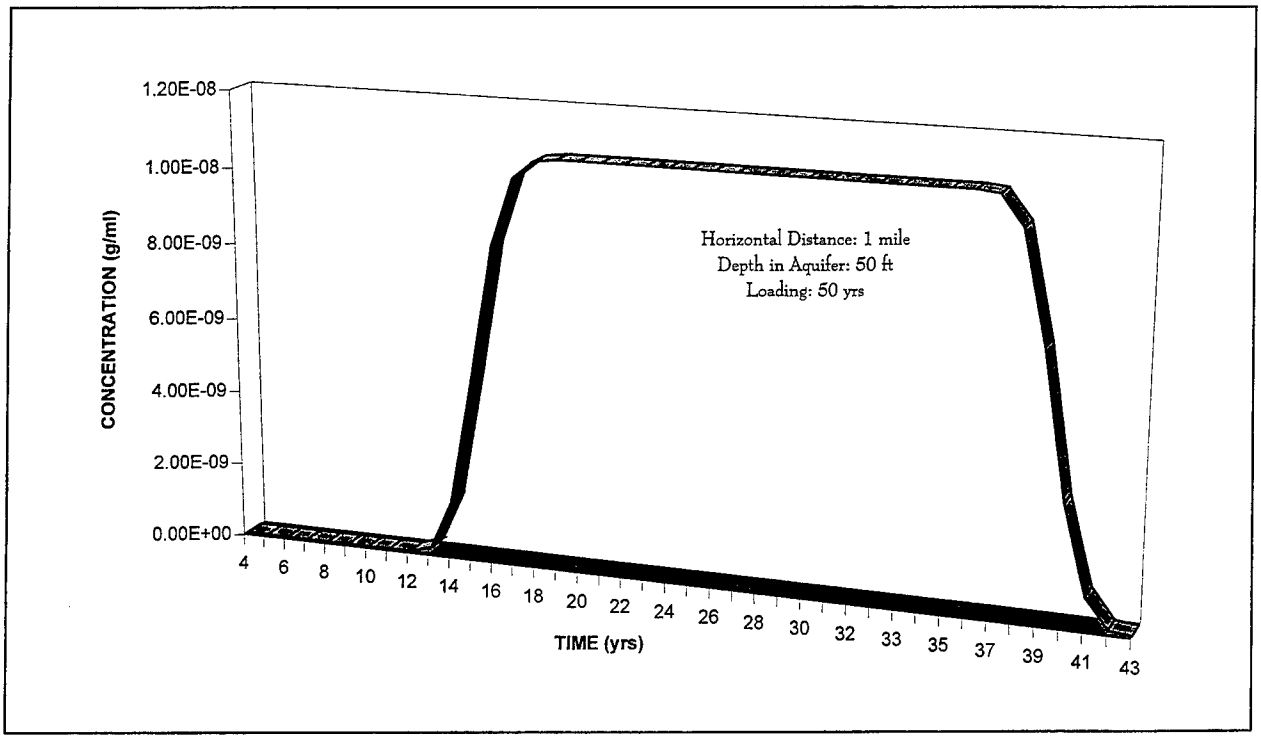

Figure 60. Model prediction for chloride transport in the aquifer using a 50-year soil loading. The receptor is a well located 1.6 km (1 mile) from the range, which is screened at 15.2 m (50 ft)

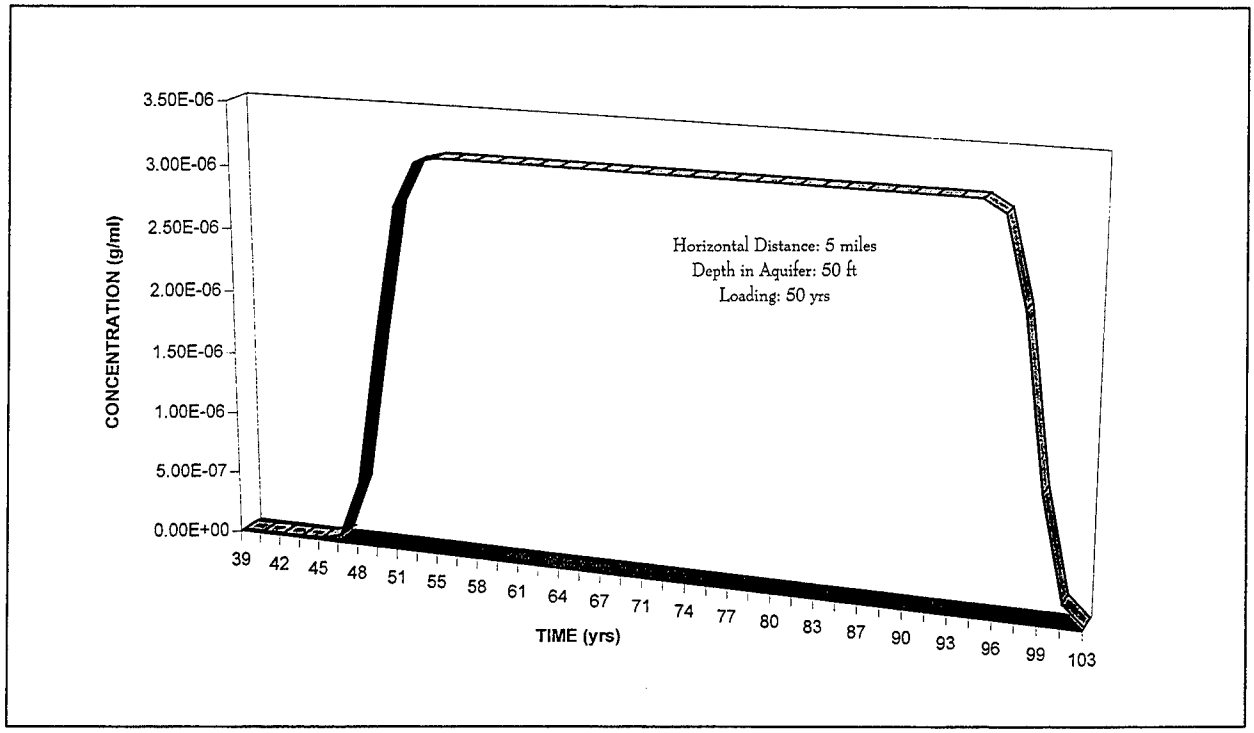

Figure 61. Model prediction for chloride transport in the aquifer using a 50-year soil loading. The receptor is a well located 8 km (5 miles) from the range, which is screened at 15.2 m (50 ft)

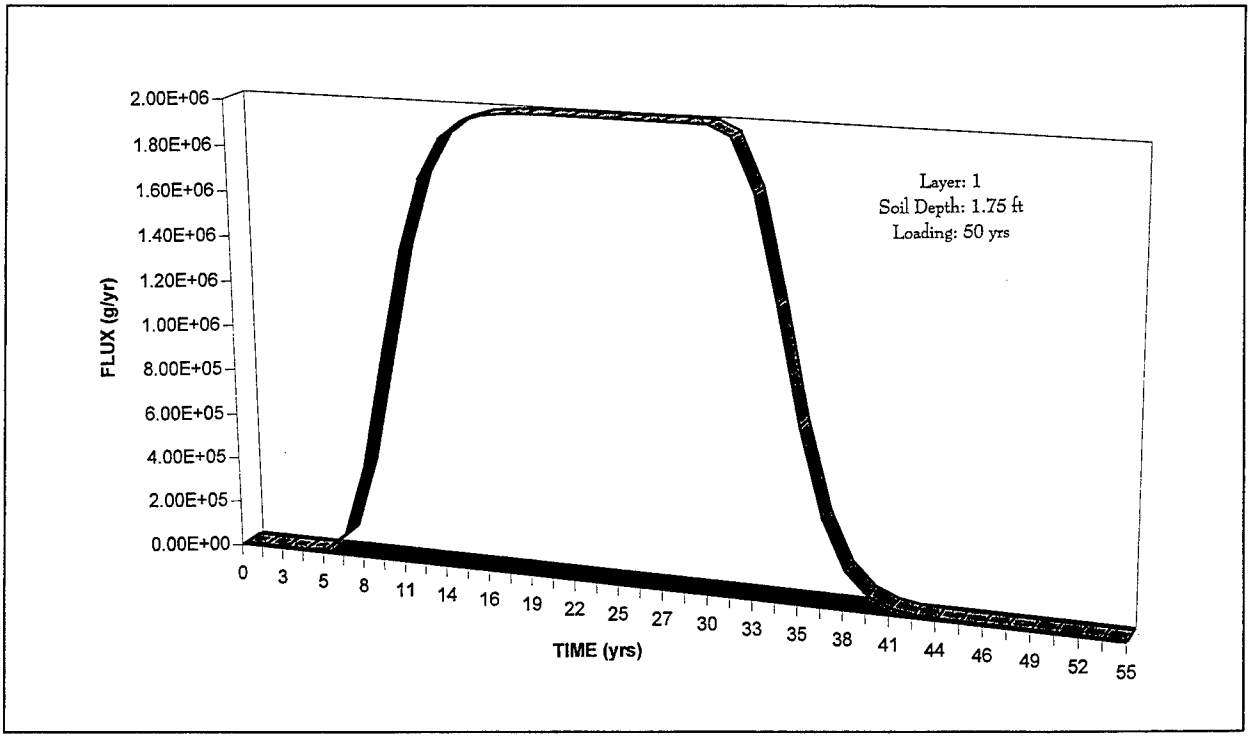

Figure 62. Model prediction for lead transport through the first soil layer using a 50-year soil loading

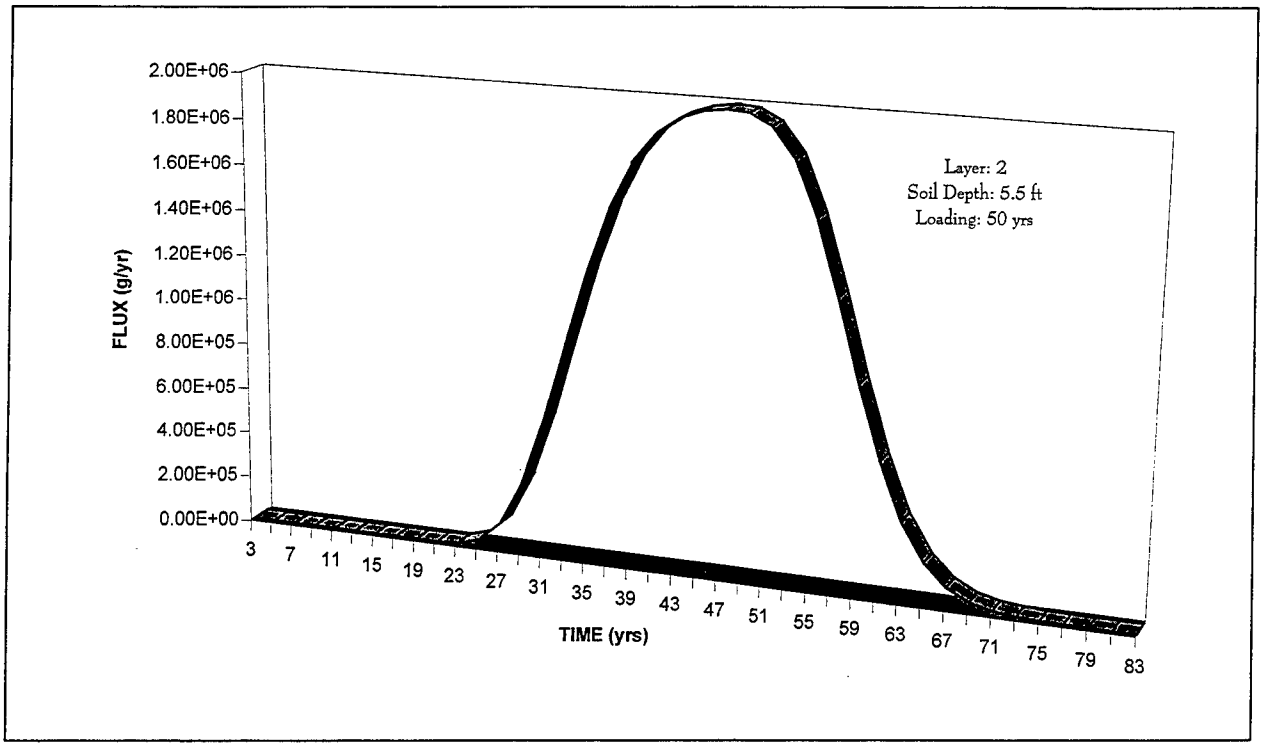

Figure 63. Model prediction for lead transport through the second soil layer using a 50-year soil loading

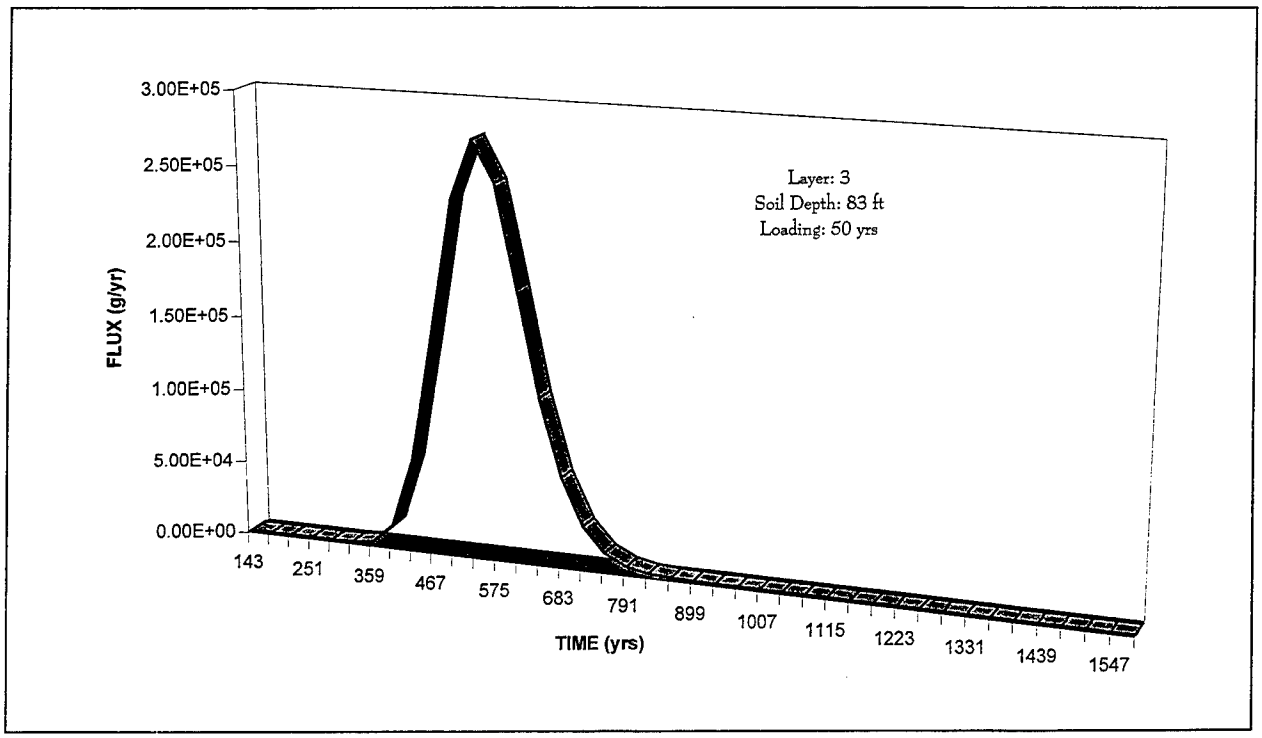

Figure 64. Model prediction for lead transport through the third soil layer using a 50-year soil loading

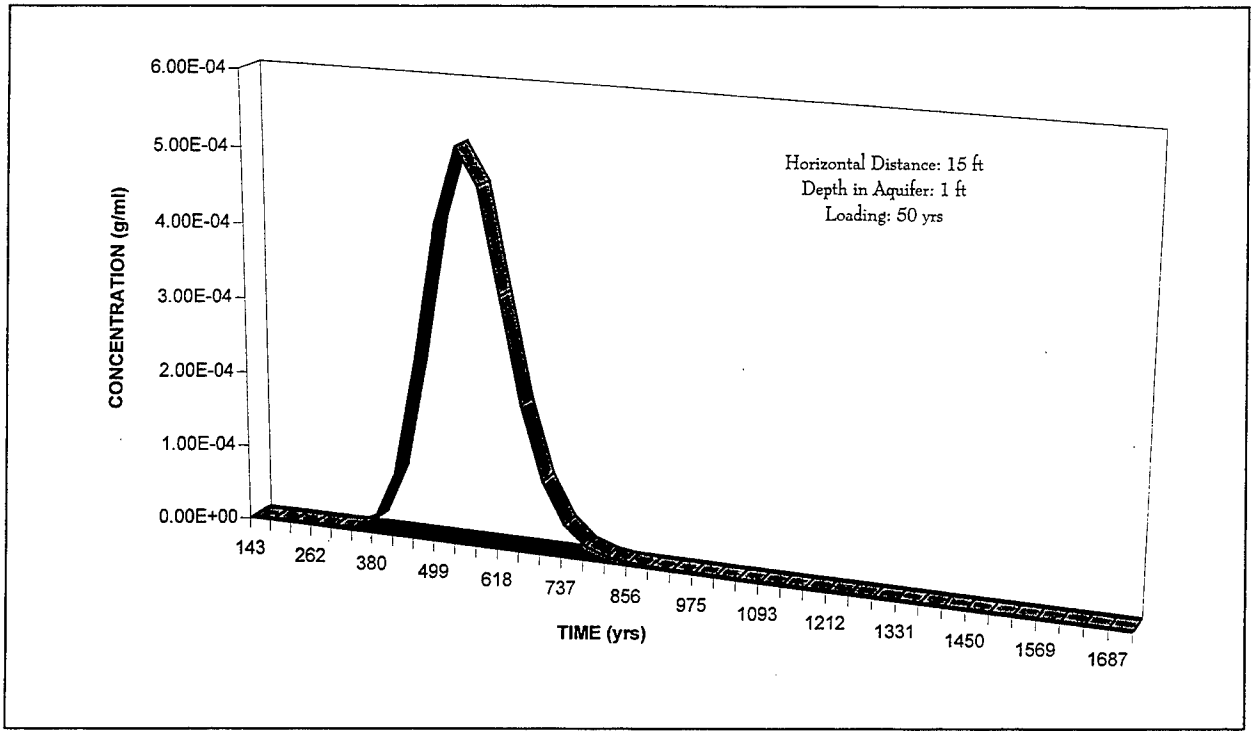

Figure 65. Model prediction for lead transport in the aquifer using a 50-year soil loading. The receptor is a well located 4.6 m (15 ft) from the range, which is screened at 0.3 m (1 ft)

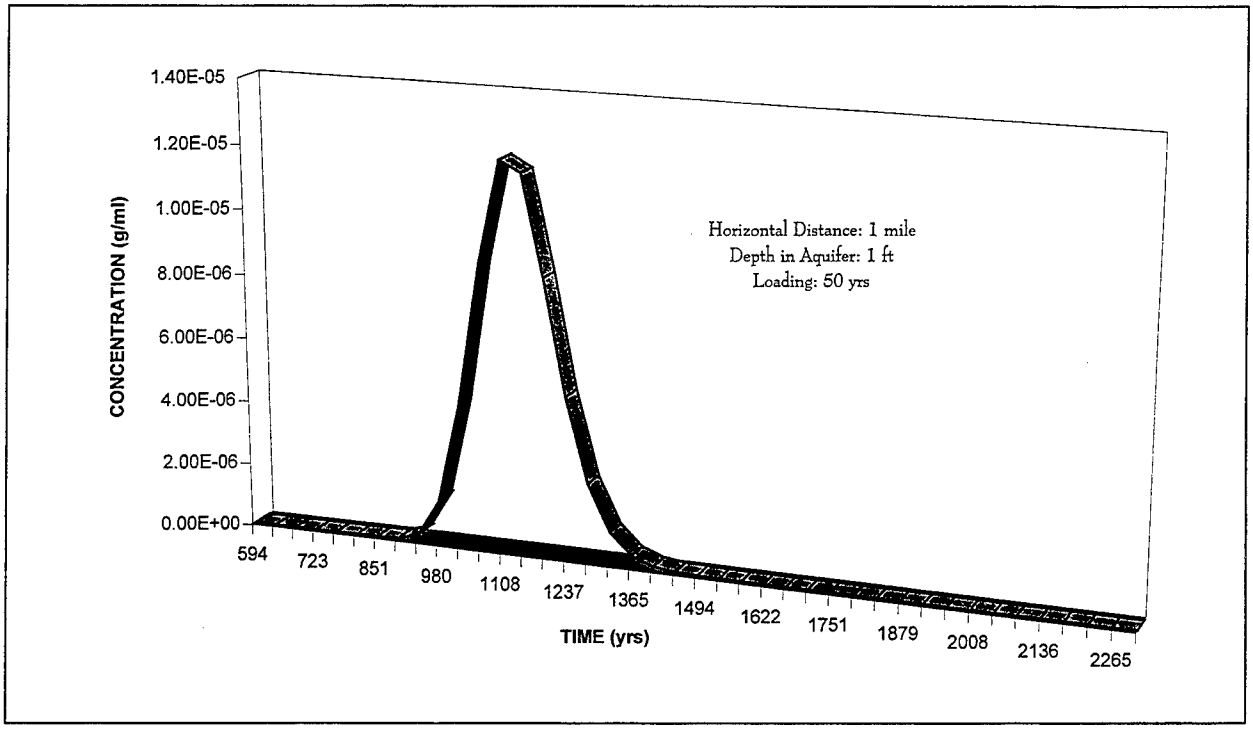

Figure 66. Model prediction for lead transport in the aquifer using a 50-year soil loading. The receptor is a well located 1.6 km (1 mile) from the range, which is screened at 0.3 m (1 ft)

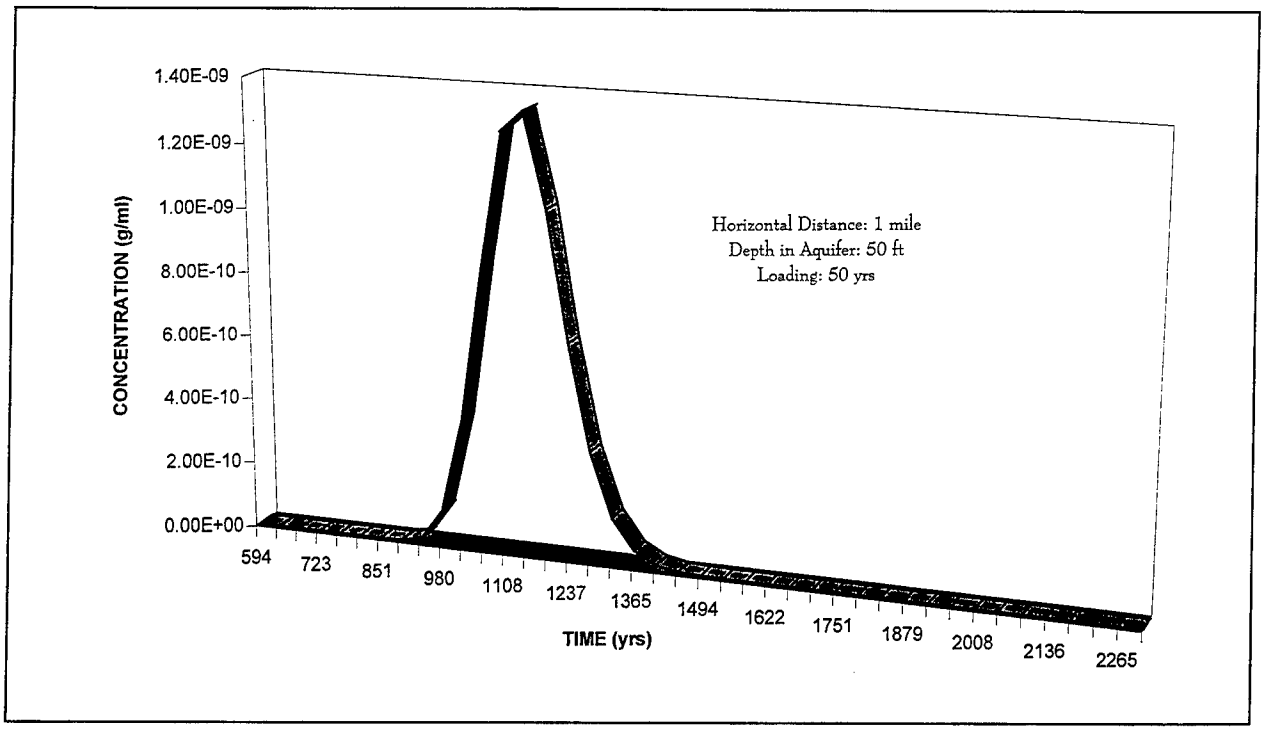

Figure 67. Model prediction for lead transport in the aquifer using a 50-year soil loading. The receptor is a well located 1.6 km (1 mile) from the range and the well is screened at 15.2 m (50 ft)

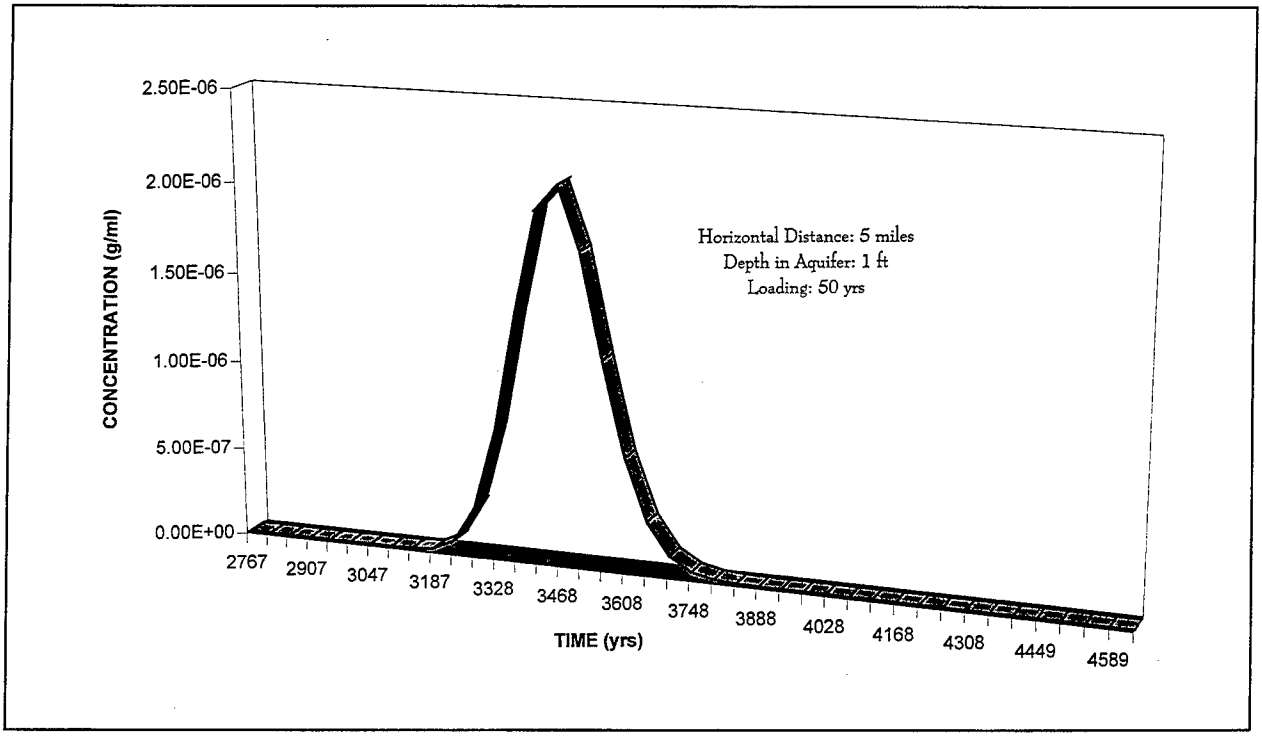

Figure 68. Model prediction for lead transport in the aquifer using a 50-year soil loading. The receptor is a well located 8 km (5 miles) from the range and the well is screened at 0.3 m (1 ft)

(ppb) after a period of 1,044 years (Figure 67). Based on the model results for the lead at a 50-year loading, lead appears to move through the first layer in a period of approximately 35 years. This means that if the use of the range is stopped, it will take a period of at least 35 years for the lead front to move through the 0.5-m-thick (1.75-ft-thick) layer. Thus, if the solubility of the lead contained in the berm is similar to that assumed for the model, and range usage is stopped and/or the lead is removed, lead will not be detected in the deeper layers of the soil.

Figures 69-75 present lead data for the 1,000-year loading scenario. From these figures, it is evident that the lead flux is sustained at the maximum level for extended periods of time when compared to the 50-year loading scenario. As a result of this sustained loading, lead reaches higher maximum values in the aquifer. Unlike the 50-year lead loading where the lead front moves in and out of a soil layer prior to reaching the aquifer, the 1,000-year scenario lead is able to exceed the sorption capacity of the soil (Figure 69). This forces the lead to move to the next soil layer, where the lead exceeds the sorption capacity of that layer (Figure 70) until the lead reaches the aquifer (Figure 72). After all the soil is loaded, the lead continues to feed into the aquifer until an equilibrium solubility is reached. Thus, the concentration reaches a maximum due to the fact that the model assumes constant flow of the aquifer over the 1,000-year period.

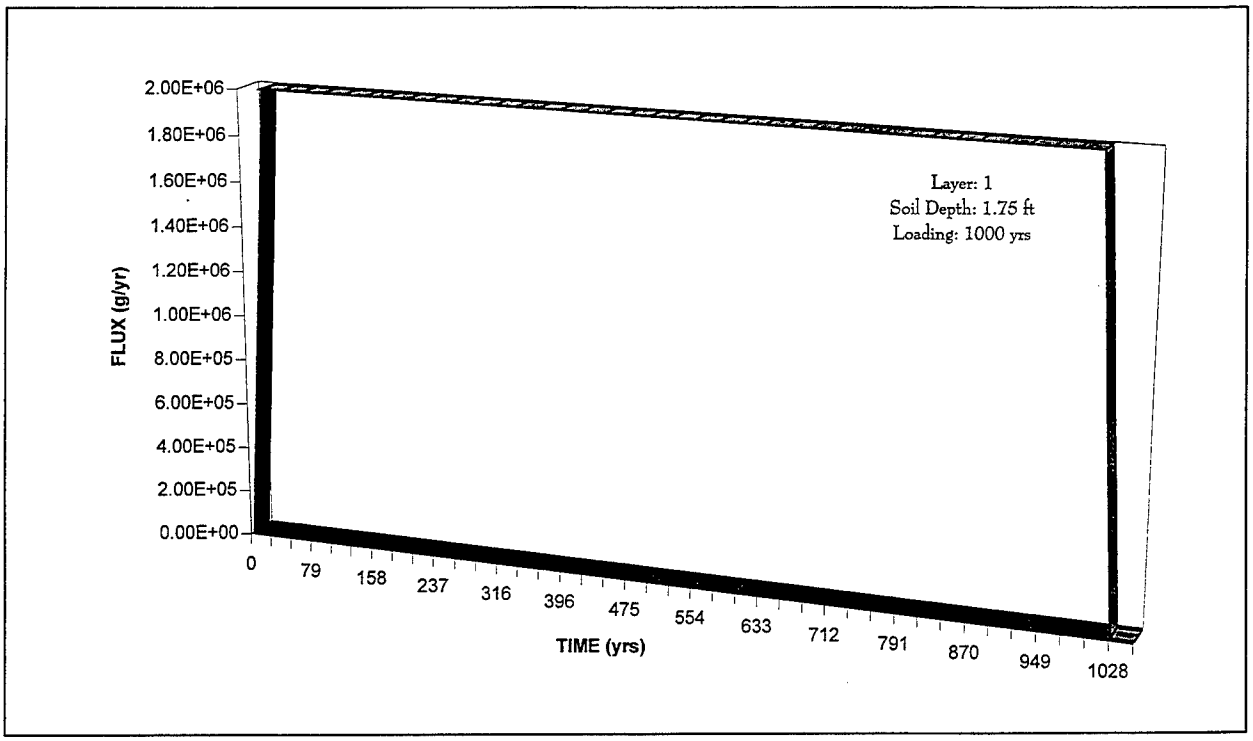

Figure 69. Model prediction for lead transport through the first soil layer using a 1,000-year soil loading

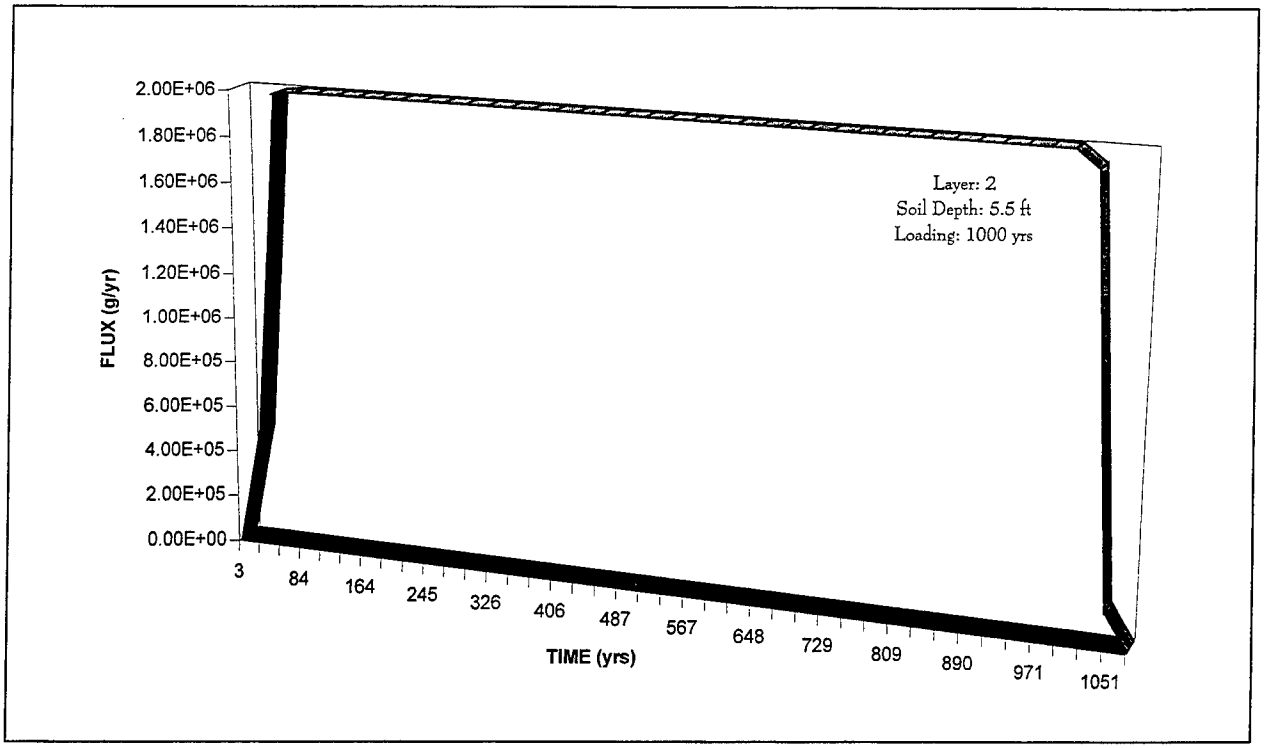

Figure 70. Model prediction for lead transport through the second soil layer using a 1,000-year soil loading

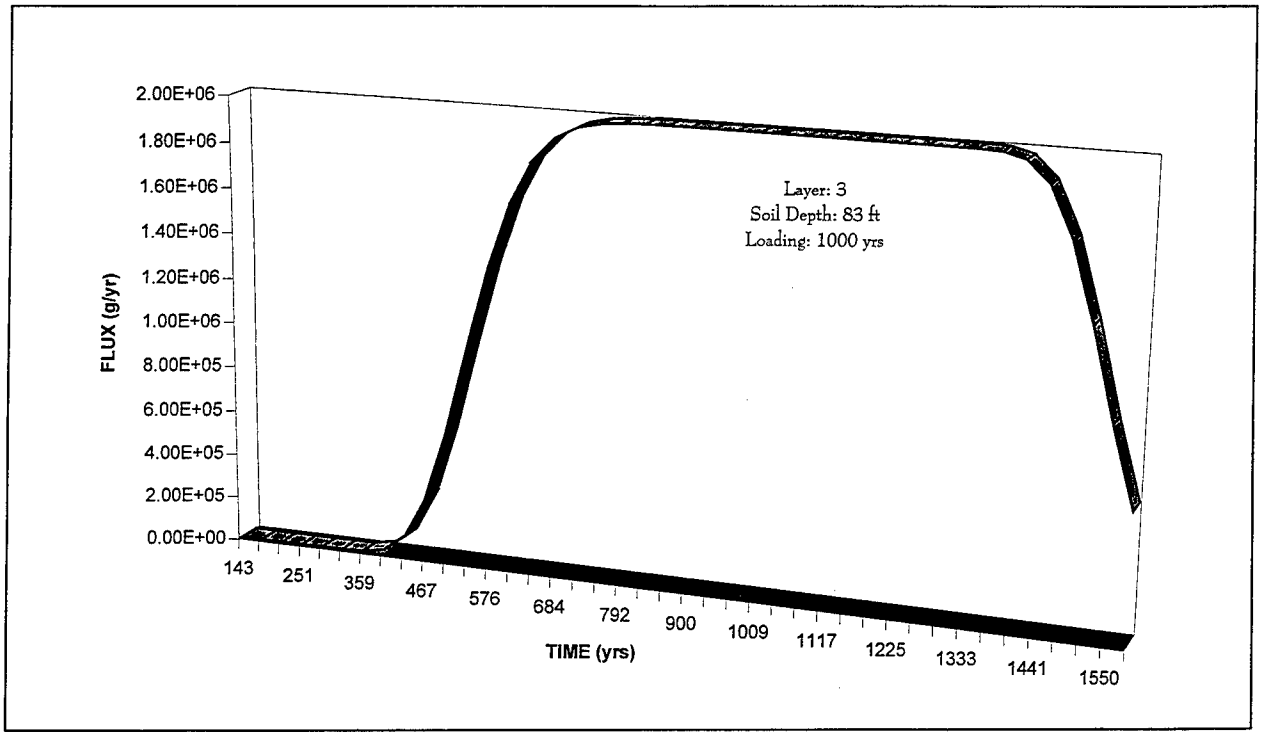

Figure 71. Model prediction for lead transport through the third soil layer using a 1,000-year soil loading

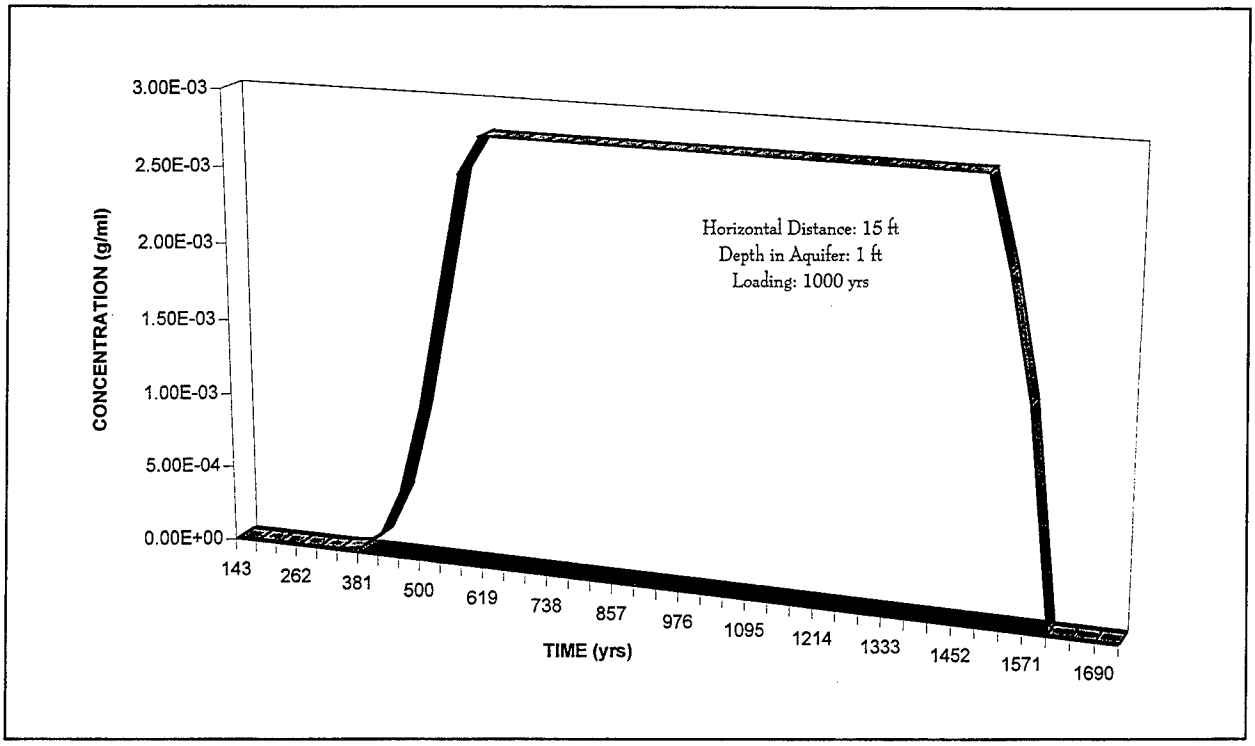

Figure 72. Model prediction for lead transport in the aquifer using a 1,000-year soil loading. The receptor is a well located 4.6 m (15 ft) from the range and the well is screened at 0.3 m (1 ft)

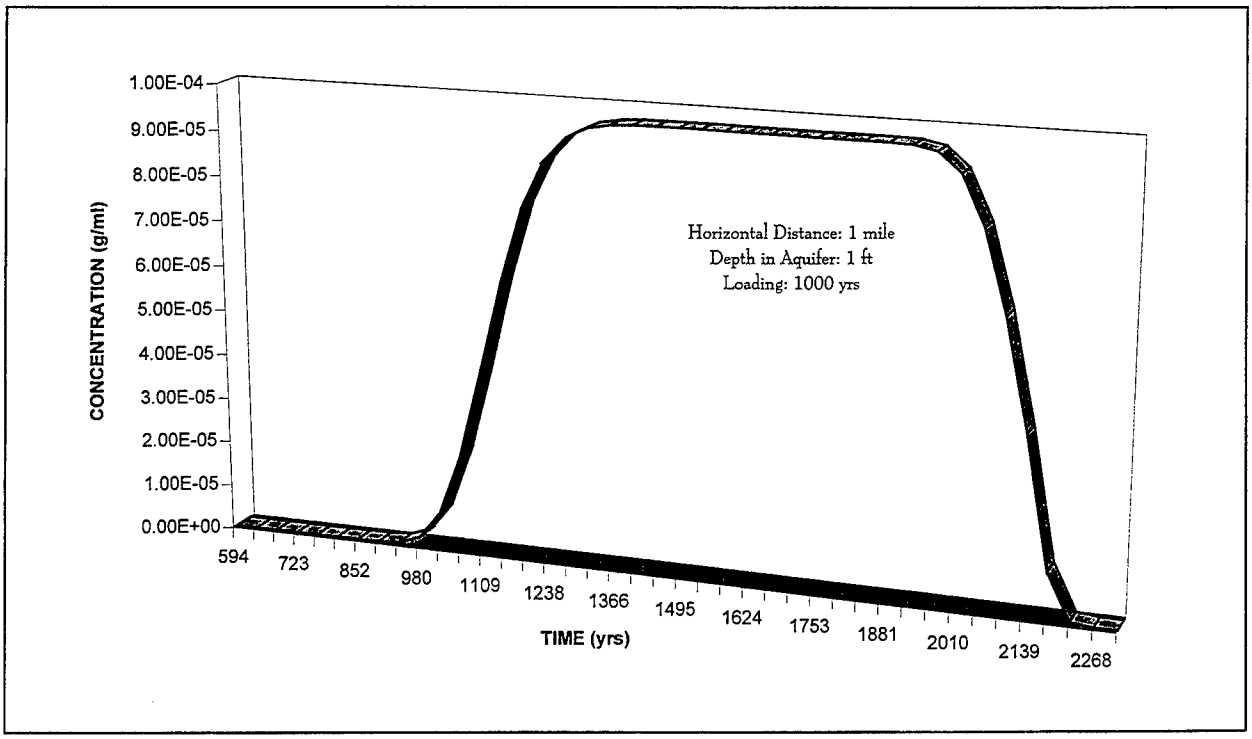

Figure 73. Model prediction for lead transport in the aquifer using a 1,000-year soil loading. The receptor is a well located 1.6 km (1 mile) from the range and the well is screened at 0.3 m (1 ft)

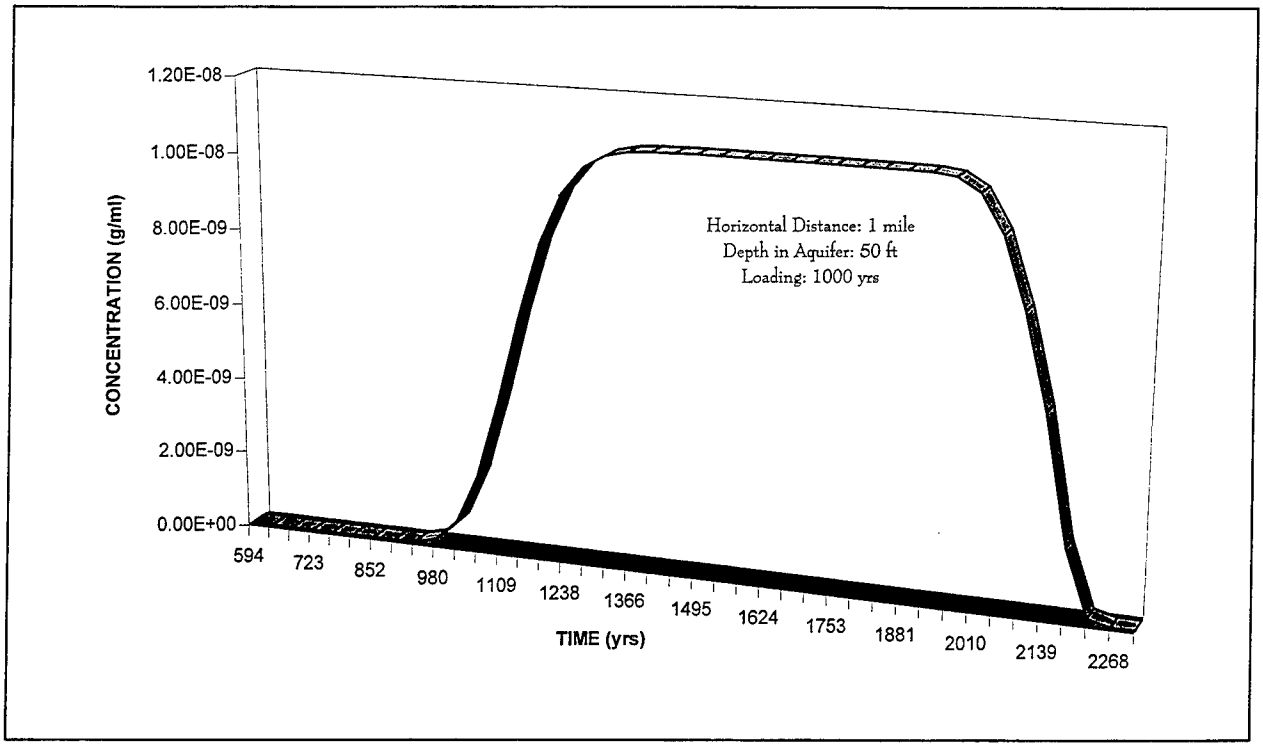

Figure 74. Model prediction for lead transport in the aquifer using a 1,000-year soil loading. The receptor is a well located 1.6 km (1 mile) from the range and the well is screened at 15.2 m (50 ft)

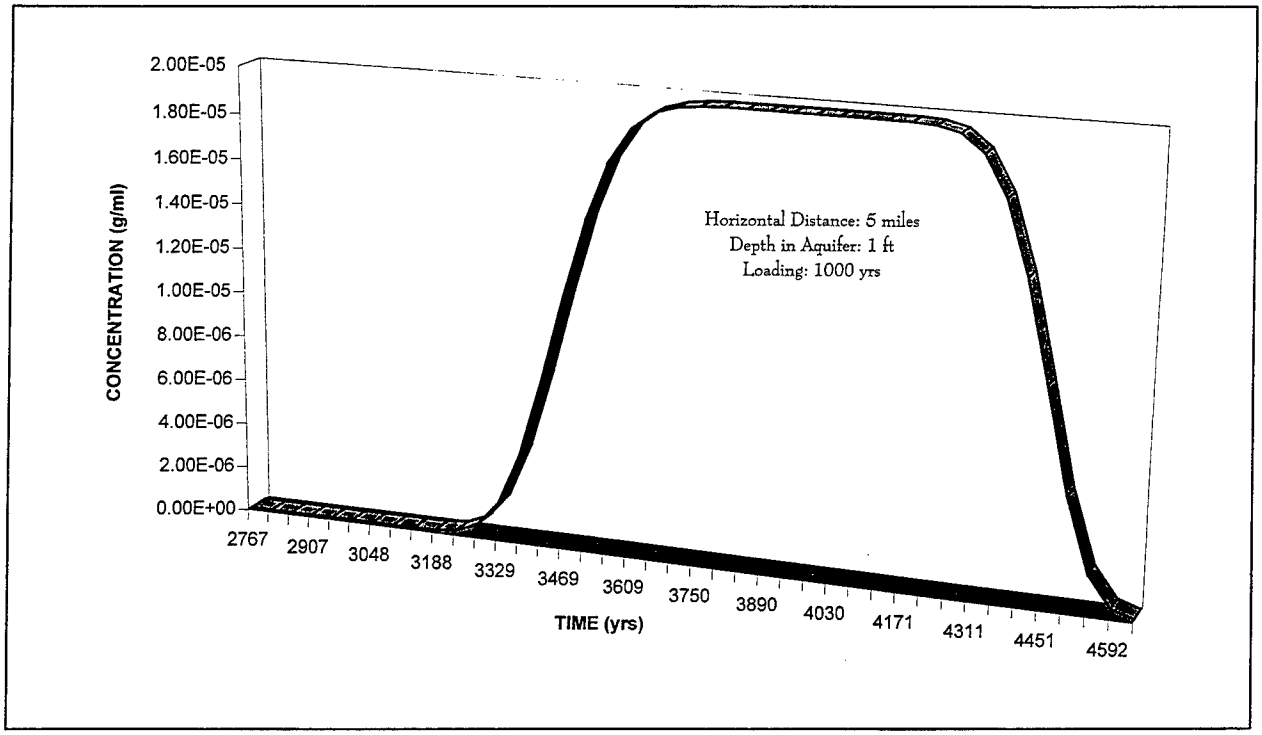

Figure 75. Model prediction for lead transport in the aquifer using a 1,000-year soil loading. The receptor is a well located 8 km (5 miles) from the range and the well is screened at 0.3 m (1 ft)

For comparison, Tables 7-9 present the maximum concentrations for lead in the aquifer at 50- and 1,000-year loading and the chloride at 50 years loading (the 1,000-year maximum concentration for the chloride is identical to the 50-year scenario due to the high rate of transport of the chloride). Maximum values in Table 7 indicate that if use of the ranges is discontinued, the lead levels in the aquifer measured in a well 1 mile from the source and screened at 15.2 m (50 ft) will never exceed the lead drinking water criteria of 15 ppb. Comparing the values in Tables 7 and 8 illustrates that if the range usage is not discontinued, the maximum lead levels measured in the aquifer will increase. These tables also indicate that while chloride transport occurs much quicker than lead, the lead will eventually reach the same maximum values as the chloride.

Model Summary

It should be noted that model predictions indicate that while the small arms activities will have an impact on the groundwater, this impact should be minimal. Such impacts could be eliminated if the contaminated soil is routinely cleaned to remove the lead. Based on model predictions, if such cleanup activities were performed every 50-70 years of range use, groundwater contamination from metals resulting from SAR activities would be prevented.

Table 7
Predicted Maximum Lead Concentration in the CEMR Aquifer Resulting from Contaminant Migration for the SAR, Loading = 50 Years

Minimum Time to Reach Maximum Concentration (Years)	Maximum Concentration (ppm) Scenario (Distance from Source/Well Screen Depth in Aquifer)				
	4.6 m/1 ft 15 ft/1 ft	1.6 km/1 ft 1 mile/1 ft	1.6 km/50 ft 1 mile/50 ft	8 km/1 ft 5 miles/1 ft	5 miles/50 ft
>500	500	--	--	--	--
>1,000	--	12.0	0.0014	--	--
>3,400	--	--	--	2.0	0.60

Note: Model assumes a highly soluble lead salt.

Table 8
Predicted Maximum Lead Concentration in the CEMR Aquifer Resulting from Contaminant Migration for the SAR, Loading = 1,000 Years

Minimum Time to Reach Maximum Concentration (Years)	Maximum Concentration (ppm) Scenario (Distance from Source/Well Screen Depth in Aquifer)				
	4.6 m/1 ft 15 ft/1 ft	1.6 km/1 ft 1 mile/1 ft	1.6 km/50 ft 1 mile/50 ft	8 km/1 ft 5 miles/1 ft	5 miles/50 ft
>500	2,600	--	--	--	--
>1,200	--	95.0	0.01	--	--
>3,500	--	--	--	19.0	3.0

Note: Model assumes a highly soluble lead salt.

Table 9
Predicted Maximum Chloride Concentration in the CEMR Aquifer Resulting from Contaminant Migration for the SAR

Minimum Time to Reach Maximum Concentration (Years)	Loading = 50/1,000 Years Maximum Concentration (ppm) Scenario (Distance from Source/Well Screen Depth in Aquifer)				
	4.6 m/1 ft 15 ft/1 ft	1.6 km/1 ft 1 mile/1 ft	1.6 km/50 ft 1 mile/50 ft	8 km/1 ft 5 miles/1 ft	5 miles/50 ft
>7	2,600	--	--	--	--
>16	--	95.0	0.01	--	--
>50	--	--	--	19.0	3.0

9 Conclusions

Based on the information obtained through this review of the literature, the sampling efforts at CEMR, and the simple modeling efforts, it is suspected that, with time, lead has the potential to migrate to the groundwater. In addition, the pore water concentration of the metals is expected to be high, as observed in the top 3 m (10 ft) of soil. This is due to a low soil pH, low clay content of the soil, low organic matter content of the soil, and an elevated solution activity. Transport of metals through the soil is expected to be relatively quick when compared to other SAR sites with soils having higher clay and organic matter content and lower hydraulic conductivity. At depth to groundwater of approximately 18.3 to 27.4 m (60 to 90 ft), even with conditions which tend to accelerate vertical contaminant migration, model predictions estimate that it will take in excess of 150 to 300 years for the lead to have an impact on the groundwater. This is reinforced by results of well sampling which tend to indicate that the lead has not impacted the groundwater to date as a result of SAR activities at CEMR.

When compared to other SARs which have been sampled, it is suspected that the conditions at the SAR at CEMR are more favorable for contaminant migration. Comparing the SAR data from CEMR with that from other facilities reinforces this theory. Contaminants at the SAR at CEMR have migrated to a depth of approximately 1.5 to 1.8 m (5 to 6 ft), which is twice as far as the contaminant migration observed at other SARs.

It should be noted that while model predictions indicate that small arms activities will have an impact on groundwater, this impact should be minimal. Such impacts could be eliminated if the contaminated soil is routinely cleaned to remove the lead. Based on model predictions, if such cleanup activities were performed every 50-70 years of range use, groundwater contamination from metals resulting from SAR activities would be prevented. With regard to active duty SAR, results from CEMR indicate that soil type and content, environmental conditions, and projectile type and quantity are important factors contributing to the increase or decrease in lead migration rate. SARs that have a higher throughput of troops, are close to groundwater sources, and are near coastal areas may pose a much higher risk to groundwater than that observed at CEMR. It appears as though simple testing procedures such as soil buffering capacity, sequential extraction tests, soil permeability tests, etc. coupled with claimant data, range usage groundwater, and range location data may provide the needed tools to assess the potential risk of SAF ranges. Studies have been initiated to investigate such issues.

10 Recommendations

Based on the findings of this report, it is recommended that additional laboratory tests be performed on the samples collected from the SAR at CEMR. These tests should include the following:

a. Soil buffering capacity - to determine the soil pH and acid neutralization capacity.

b. Sequential extraction testing - to determine the affinity of the soil for the metals.

c. Soil permeability testing - to verify and narrow the U.S. Department of Agriculture (USDA) Soil Survey results.

d. Soil density - to verify and narrow the USDA Soil Survey results.

e. Soil organic content - to verify and narrow the USDA Soil Survey results.

f. Soil/metal partitioning testing - to determine the Kd for the soil and metal.

It is recommended that a more thorough modeling effort be conducted, including regional groundwater modeling. Such an effort may provide information indicating that even if the lead vertically migrates to the groundwater aquifer, dilution by the regional groundwater results in metal concentrations below drinking water health concerns. Such modeling efforts may provide evidence that SAR activities may never significantly impact the groundwater at CEMR.

References

Allen, H., Perdue, E., and Brown, D. (1993). *Metals in groundwater*. Lewis Publishers, Chelsea, MI.

Bricka, R. M. (1996a). "Investigation of physical separation and extraction techniques for metal removal at the Fort Benjamin Harrison small arms training areas," in preparation, U.S. Army Engineer Waterways Experiment Station, Vicksburg, MS.

_____. (1996b). "Investigation of physical separation and extraction techniques for metal removal at southern army facilities in Louisiana," in preparation, U.S. Army Engineer Waterways Experiment Station, Vicksburg, MS.

Bundy, K. J., Bricka, M., and Morales, A. (1995). "Electrochemical measurement of the corrosion of bullets in various soils environments," Draft Report, U.S. Army Engineer Waterways Experiment Station, Vicksburg, MS.

Dean, J. A. (1992). *Lange's handbook of chemistry*. McGraw-Hill, Inc., New York, NY.

Drever, J. (1988). *The geochemistry of natural waters*. 2nd ed., Prentice-Hall, Englewood Cliffs, NJ.

Fletcher, P. (1993). "Soil survey of Barnstable County, Massachusetts," U.S. Department of Agriculture, Soil Conservation Service.

Fontana, M., and Greene, N. (1978). *Materials science and engineering series: Corrosion engineering*. McGraw-Hill, New York, NY.

Freeze, R., and Cherry, J. (1979). *Groundwater*. Prentice-Hall, Englewood Cliffs, NJ.

Gale, R. J., Liu, J. Z., and Bricka, R. M. (1994). "Environmental pollution from lead bullets at the Fort Polk firing ranges," Draft, Electrokinetics Inc., Baton Rouge, LA.

Genuchten, M. T., and Alves, W. J. (1982). "Analytical solutions for the one-dimensional convective-dispersive solute transport equation," U.S. Department of Agriculture, Technical Bulletin No. 1661, U.S. Salinity Laboratory, Riverside, CA.

Heath, J. C., et al. (1991). "Environmental effects of small arms ranges," Technical Note N-1836, Naval Civil Engineering Laboratory, Port Hueneme, CA.

Johnson, J. L., et al. (1993). "Heavy metals removal from small-arms firing ranges," Minerals Metals and Materials Society, Warrendale, PA.

Karr, L., Flynn, D., and Smith-Rawecki, T. (1990). "Characterization of metals in soils and vegetation of small arms impact berms, NAB Little Creek," Memorandum to files, Naval Civil Engineering Laboratory, Port Hueneme, CA.

Kramer, J., and Allen, H. (1988). *Metal speciation: Theory, analysis, and application*. Lewis Publishers, Chelsea, MI.

Martin Marietta Energy Systems. (1992). "Installation restoration program, site assessment, work completion report, chemical spill site in impact area, study area CS-19, Massachusetts Military Reservation, Cape Cod, MA," Report prepared under contract DE-AC05-84OR21400 for the U.S. Department of Energy.

Peters, D. G., Hayes, J. M., and Hieftje, G. M. (1976). *A brief introduction to modern chemical analysis*. Saunders, Philadelphia, PA.

Peters, R. W. (1993). "Feasibility/treatability studies for removal of heavy metals from soils from training ranges at the Grafenwohr Training Area, Germany," Draft, Argonne National Laboratory, Argonne, IL.

Sax, Irving, N. (1984). *Dangerous properties of industrial materials.*" 6th ed., van Nostrand Reinhold, New York, NY.

Snoeyink, V., and Jenkins, D. (1980). *Water chemistry*. John Wiley and Sons, New York, NY.

U.S. Army. (1994a). "U.S. Army Center for Health Promotion and Preventive Medicine, Draft Site Inspection, Geohydrologic Study No. 38-26-0278-95, Propellant Burning at Firing Points (CS-18), Massachusetts Military Reservation, Cape Cod, MA," Aberdeen Proving Ground, MD.

_____. (1994b). "U.S. Army Center for Health Promotion and Preventive Medicine, Draft Site Inspection No. 38-26-1339-95, Site CS-19, Massachusetts Military Reservation, Cape Cod, MA," Aberdeen Proving Ground, MD.

U.S. Army. (1992). "Training ranges," Training Circular TC 25-8, Headquarters, Department of the Army, Washington, DC.

U.S. Army Center for Health Promotion and Preventive Medicine (USCHPPM). (1994). "Draft site geohydrologic study No. 38-26-0278-95 propellant burning at firing points (CS-18) Massachusetts Military Reservation, Cape Cod, Massachusetts, 10-25 October 1994," Aberdeen Proving Ground, Maryland, 90.

U.S. Environmental Protection Agency. (1996). "National primary drinking water regulations," *Code of Federal Regulations*, Vol 40, Part 141.80, Washington, DC.

_____. (1995). "Military munitions rule: Hazardous waste identification and management; explosives emergencies; redefinition of on-site," Washington, DC.

_____. (1986a). "Test methods for evaluation of solid waste: Physical/ chemical methods." SW-846, 4th ed., Office of Solid Waste and Emergency Response, Washington, DC.

_____. (1986b). "Quality criteria for water," Office of Water Regulations and Standards, Washington, DC.

West, R. C., and Astle, M. J. (1978). *CRC handbook of chemistry and physics*. CRC Press, Inc., Boca Raton, FL.

Whelan, G., Buck, J. W., Strenge, D. L., Droppo, J. G., Jr., and Hoopes, B. L. (1992). "Overview of the multimedia environmental pollutant assessment system (MEPAS)." *Hazardous waste and harzardous materials* 9(2), 191-208.

Appendix A
Military Specification for Bullets

MANUFACTURING ENGINEERING
PRODUCT GUIDE BOOK

SECTION E-1

CARTRIDGE: 5.56mm, Ball, M193

WEAPON: Rifle, M16 & M16A1; Port Firing Weapon, M231, Machine Gun, M249

BALLISTIC PERFORMANCE:

VELOCITY:	3250 ± 40 fps at 15 feet, SD 40 fps max
CHAMBER PRESSURE:	Ave ≤55 Kpsi (piezo), Ave + 3 sd ≤ 61 Kpsi
	Ave ≤52 Kpsi (copper), Ave + 3 sd ≤ 58 Kpsi
PORT PRESSURE:	14.4 ± 2 Kpsi (piezo), 15 ± 2 Kpsi (copper)
ACCURACY:	2.00 mean radius max ave at 200 yards
BULLET PULL:	Minimum 35 pounds

TECHNICAL DATA:

SPECIFICATION:	MIL-C-9963
CARTRIDGE:	D10523632; Weight, 182 -14 grains
IDENTIFICATION:	Plain tip
CASE:	C10524200 or 11820451; Weight, 94 -5 grains
CUP:	10542547, 3 Draw (Advisory), or 11828914, 2 draw(Advisory), Weight 115 - 6 grains, CA260 (70/30) annealed, MIL-C-50
BULLET:	C10524197; Weight, 56 - 2 grains
JACKET:	B11735356, Weight, 17.5 - 1 grains
CUP:	B11735355 (Advisory), Weight, 22 - 3 grains CA220 (90/10), Annealed, MIL-L-21768
SLUG:	10542368, Weight 38.5 - 1 grains Lead-Antimony, MIL-L-13283, Grade 1
PRIMER:	Percussion #41, C10534279
CUP:	10534280
ANVIL:	10534281, Tripod
FOIL:	10534282
PELLET:	10534283
MIX:	FA956, C10522388, .365 Grains
PROPELLANT:	10543743, WC844, 28.5 Grains or 11735682, CMR170, 26.5 Grains

-193-

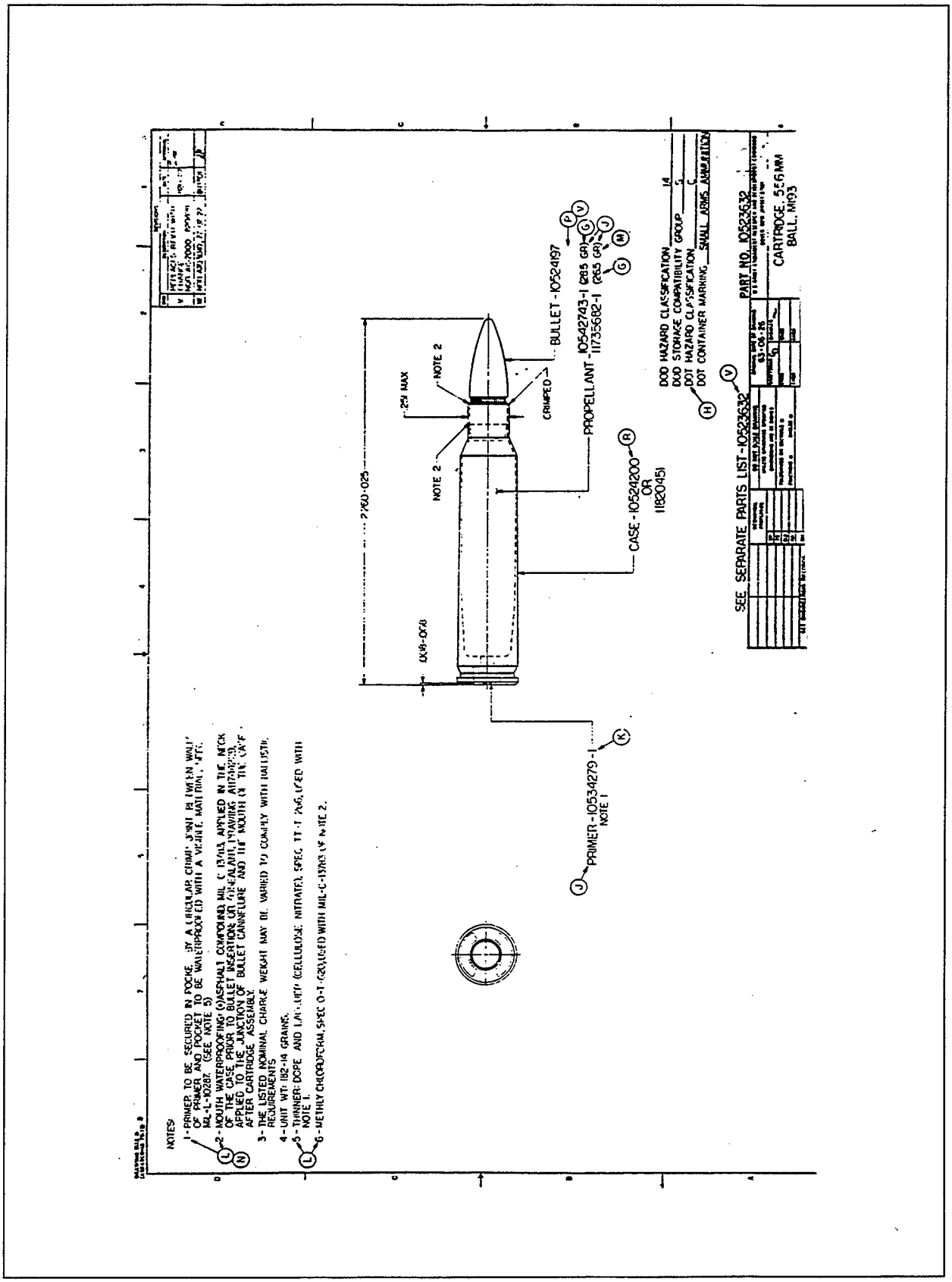
NOTES:
1 - PRIMER TO BE SECURED IN POCKET BY A CIRCULAR CRIMP. JOINT BETWEEN WALL OF PRIMER AND POCKET TO BE WATERPROOFED WITH A VARNISH, MAROON, 4FF, MIL-L-10287. (SEE NOTE 5)
2 - MOUTH WATERPROOFING (ASPHALT COMPOUND) MIL-C-13095, APPLIED IN THE NECK OF THE CASE PRIOR TO BULLET INSERTION OR (VARNISH, AIRDRYING, AMBER) APPLIED TO THE JUNCTION OF BULLET CANNELURE AND THE MOUTH OF THE CASE AFTER CARTRIDGE ASSEMBLY.
3 - THE LISTED NOMINAL CHARGE WEIGHT MAY BE VARIED TO COMPLY WITH BALLISTIC REQUIREMENTS
4 - UNIT WT: 182-14 GRAINS.
5 - THINNER: DOPE AND LACQUER, NITRATE, SPEC TT-T-266, USED WITH NOTE 1.
6 - METHYLCHLOROFORM, SPEC O-T-620 USED WITH MIL-C-13070 IN NOTE 2.
.2760-025
.009-.010
.25 MAX
NOTE 2
NOTE 2
BULLET - 10524197
CRIMPED
PROPELLANT - 10542743-1 (285 GR)
11735682-1 (265 GR)
CASE - 10524200
OR
11820451
PRIMER - 10534279-1
NOTE 1
DOD HAZARD CLASSIFICATION 14
DOD STORAGE COMPATIBILITY GROUP C
DOT HAZARD CLASSIFICATION C
DOT CONTAINER MARKING SMALL ARMS AMMUNITION
SEE SEPARATE PARTS LIST - 10523632
PART NO. 10523632
CARTRIDGE, 5.56MM
BALL, M193

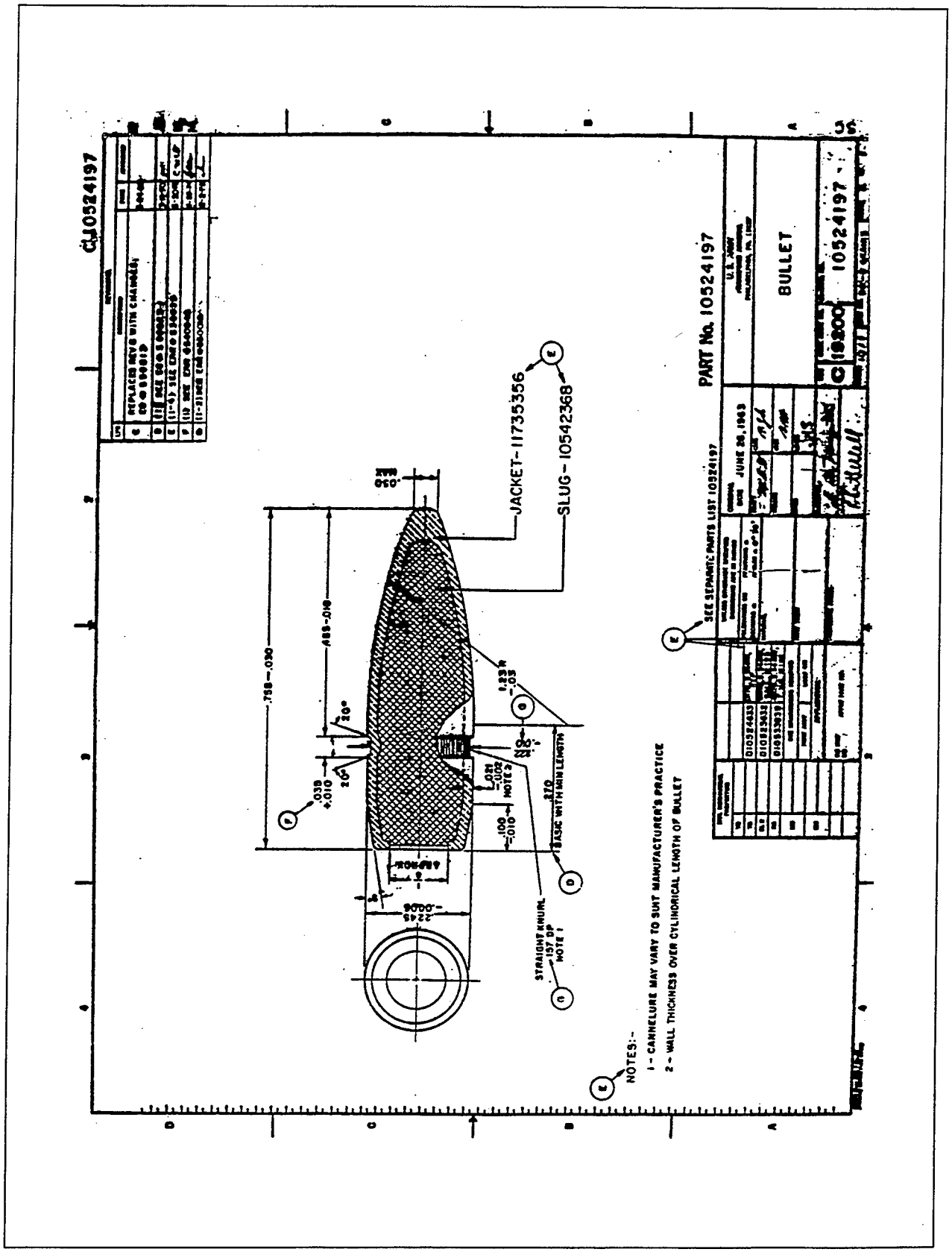
10524197
PART No. 10524197
BULLET
JACKET-11735356
SLUG-10542368
STRAIGHT KNURL
NOTES:-
1 - CANNELURE MAY VARY TO SUIT MANUFACTURER'S PRACTICE
2 - WALL THICKNESS OVER CYLINDRICAL LENGTH OF BULLET

MANUFACTURING ENGINEERING
PRODUCT GUIDE BOOK

SECTION E-2

CARTRIDGE: 7.62mm Ball M80

WEAPON: RIFLE, M14, LAR, G3, L7A2
MACHINE GUN, M60, T65, M219, M134, M240, MLE 1952

BALLISTIC PERFORMANCE:

VELOCITY:	2750 ± 30 Fps at 78 feet
CHAMBER PRESSURE:	Ave ≤ 50 Kpsi, ave + 3 SD or ind ≤ 55 Kpsi (Copper)
	Ave ≤ 365 MPa, ave + 3 SD or ind ≤ 400 MPa (EPVAT)
PORT PRESSURE:	Ave = 12.5 Kpsi ± 2 Kpsi (Copper)
	Ave ≤ 85 MPa and ≥ 60 MPa (EPVAT)
ACCURACY:	Ave Mean Radius at 600 yards ≤ 5.0 " for carton or clip pack, ≤ 7.5" for link pack
ACTION TIME:	4 Millisecond Maximum
BULLET PULL:	60 Pounds minimum

TECHNICAL DATA:

SPECIFICATION:		MIL-C-46931
CARTRIDGE:		C10521998, Weight 392 - 31 grains
	IDENTIFICATION:	Plain Bullet tip
CASE:		D10521997, Weight 190 - 20 Grains
	CUP:	B10522459, Weight 224 - 14 Grains
		Copper Alloy 260, Annealed, MIL-C-50
BULLET:		B8595669, Weight 147 - 3 Grains
	JACKET:	B8595668, Weight 34.5 - 1.5 Grains
	CUP:	B7553579, Weight 44 - 6 Grains
		Copper Alloy Clad Steel, MIL-S-13468
	SLUG:	B8595667, Weight 114.5 - 1.5 Grains
		Lead/Antimony (98/2), MIL-L-13283, Grade 1
PRIMER:		#34, C10522621, Weight 5.43 - .52 Grains (Advis.)
	CUP:	8594095
	ANVIL:	8594096
	FOIL:	8594098
	PELLET:	10522622
	MIX:	FA956
PROPELLANT:		WC846, B10534784, 46 Grains approx
		IMR8138M, B10534783, 41.5 Grains approx (obsolete)
		IMR4475, B10534786, 41 Grains approx (obsolete)

-80-

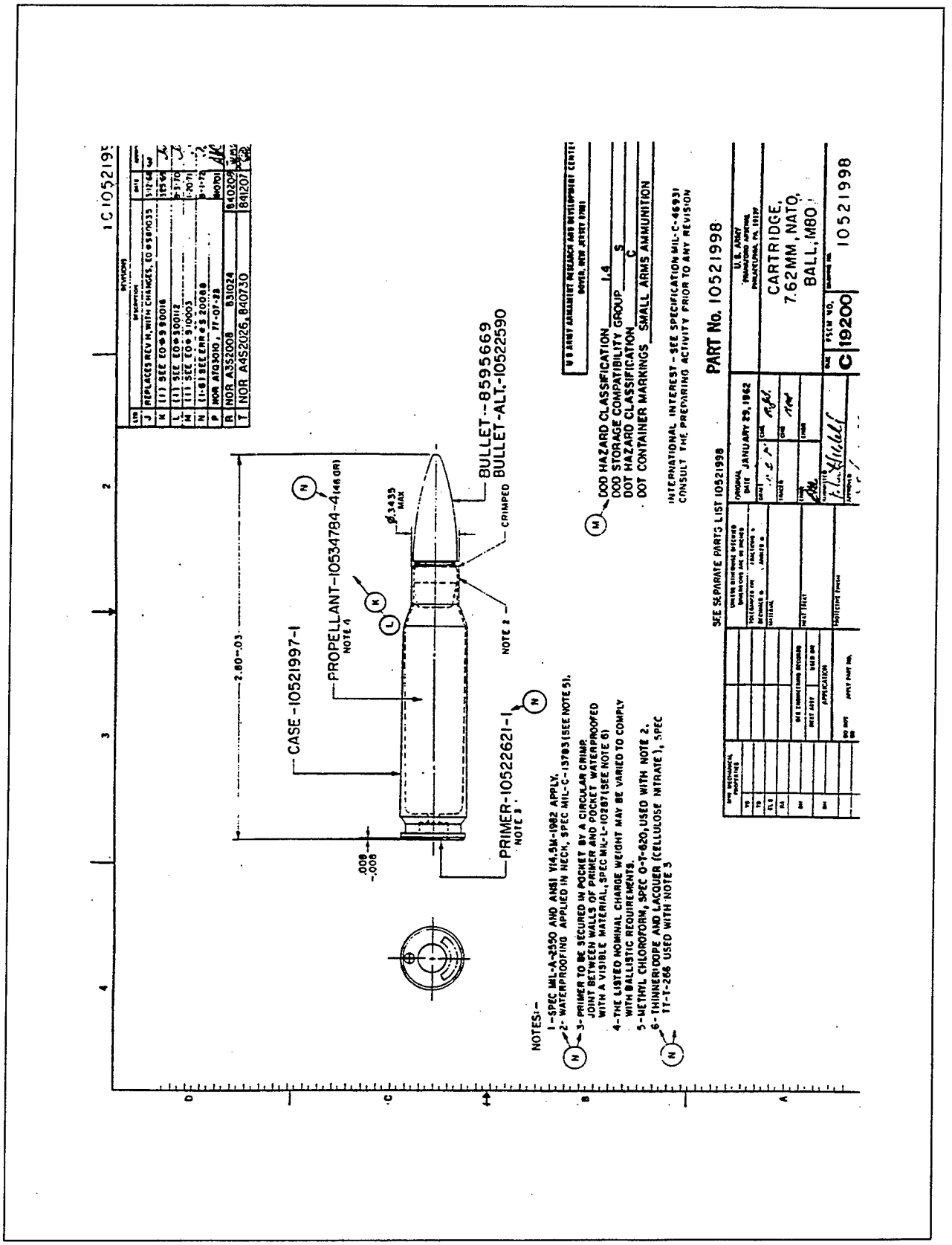
PART No. 10521998
SEE SEPARATE PARTS LIST 10521998
CARTRIDGE, 7.62MM, NATO, BALL, M80
C 19200
10521998
BULLET--8595669
BULLET-ALT.-10522590
CRIMPED
CASE-10521997-1
PROPELLANT-10534784-4(146 GR)
PRIMER-10522621-1
2.80-03
.008
-.008
Ø.3435 MAX
DOD HAZARD CLASSIFICATION 1.4
DOD STORAGE COMPATIBILITY GROUP S
DOT HAZARD CLASSIFICATION C
DOT CONTAINER MARKINGS SMALL ARMS AMMUNITION
INTERNATIONAL INTEREST - SEE SPECIFICATION MIL-C-46931
CONSULT THE PREPARING ACTIVITY PRIOR TO ANY REVISION
NOTES:-
1-SPEC MIL-A-2550 AND ANSI Y14.5M-1982 APPLY.
2- WATERPROOFING APPLIED IN NECK, SPEC MIL-C-13703 (SEE NOTE 5).
3- PRIMER TO BE SECURED IN POCKET BY A CIRCULAR CRIMP JOINT BETWEEN WALLS OF PRIMER AND POCKET WATERPROOFED WITH A VISIBLE MATERIAL, SPEC MIL-L-10287 (SEE NOTE 6)
4-THE LISTED NOMINAL CHARGE WEIGHT MAY BE VARIED TO COMPLY WITH BALLISTIC REQUIREMENTS.
5-METHYL CHLOROFORM, SPEC O-T-620, USED WITH NOTE 2.
6- THINNER: DOPE AND LACQUER (CELLULOSE NITRATE), SPEC TT-T-266 USED WITH NOTE 3
U.S. ARMY ARMAMENT RESEARCH AND DEVELOPMENT CENTER DOVER, NEW JERSEY 07801
U.S. ARMY PRODUCTION BASE MODERNIZATION ACTIVITY PICATINNY ARSENAL, DOVER, N.J. 07801
ORIGINAL DATE JANUARY 29, 1962
DRAWN
TRACED
CHK
APPVD
FSCM NO.
DRAWING NO.
SIZE
REVISIONS
LTR
DESCRIPTION
DATE
APPVD
J REPLACES REV H, WITH CHANGES, TO #5890035
K (11) SEE EO #5900116
L (11) SEE EO #5900112
M (11) SEE EO #5900103
N (11-81) SEE ENR #5 20068
P NOR AFO3010, 17-07-88
R NOR A352008 831024
T NOR A452026, 840730
840209
841207

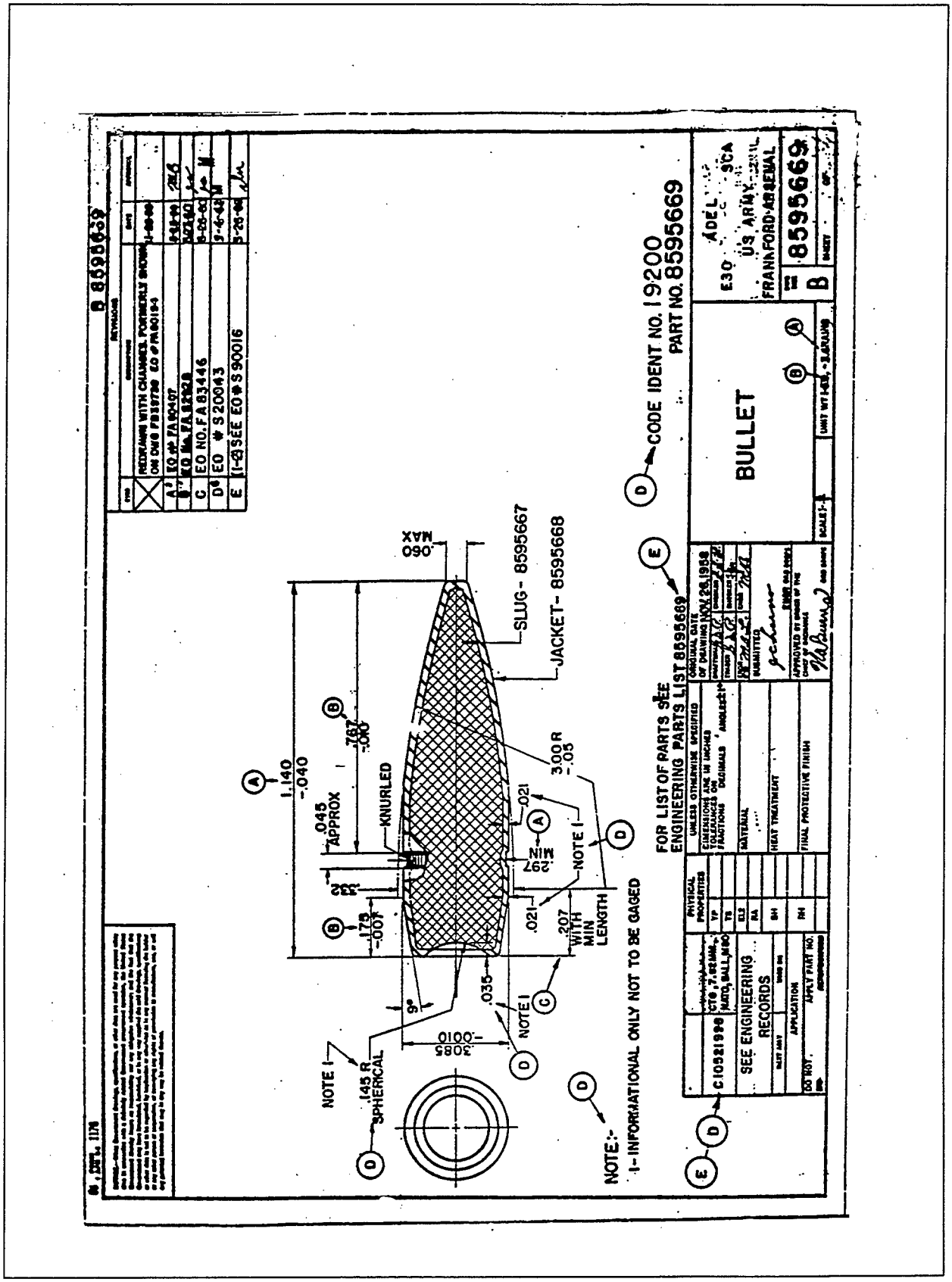
8595669
BULLET
CODE IDENT NO. 19200
PART NO. 8595669
FOR LIST OF PARTS SEE ENGINEERING PARTS LIST 8595669
SLUG - 8595667
JACKET - 8595668
KNURLED
NOTE:-
1 - INFORMATIONAL ONLY NOT TO BE GAGED
SEE ENGINEERING RECORDS
ADEL
USA
ARMY
FRANKFORD ARSENAL

Appendix B
Calculations Showing Prediction of Quantity of Lead Buildup at CEMR Berm on an Annual Basis

Assume

a. Range is 30 lanes wide.

b. Range is only used on weekends.

c. Rounds consist of 5.56 mm, 7.62 mm and 9 mm. 9 mm much larger than 5.56 mm or 7.62 mm so use 7.62 mm as average for all calculations.

d. Troops use 60 rounds/hr.

e. Range used 4 hr/day.

A. Range use

(4 hr/day) (2 days/week) (52 week/year) = 416 hrs/year = useage

B. Rounds fired per year into berm

(30 lanes) (1 Troop/1 lane) (60 rounds/hr/1 Troop) (416 hrs/year)
= 748,800 rounds/year

C. One round of 7.62 mm = 9.655 g @ 0.75% Pb

(748,800 rounds/year) (9.655 g/1 round) (0.75) = 5,422,248 g Pb/year

(5,422,248 g/year) (1 lb/454 g) = 11,943 ≅ 12,000 lb pb/year

≅ 6 Tons

Appendix C
Unified Soil Classification[1]

[1] Source: Merrit, Frederick, S. (1983). *Standard Handbook for Civil Engineers*, McGraw-Hill, New York, NY.

TABLE 7-2 Unified Soil Classification Including Identification and Description[a]

Major division	Group symbol	Typical name	Field identification procedures[b]	Laboratory classification criteria[c]	
A. Coarse-grained soils (more than half of material larger than No. 200 sieve)[d]					
1. Gravels (more than half of coarse fraction larger than No. 4 sieve)[e]					
Clean gravels (little or no fines)	GW	Well-graded gravels, gravel-sand mixtures, little or no fines	Wide range in grain sizes and substantial amounts of all intermediate particle sizes	$D_{60}/D_{10} > 4$ $1 < D_{30}^2/D_{10}D_{60} < 3$ D_{10}, D_{30}, D_{60} = sizes corresponding to 10, 30, and 60% on grain-size curve	
	GP	Poorly graded gravels or gravel-sand mixtures, little or no fines	Predominantly one size, or a range of sizes with some intermediate sizes missing	Not meeting all gradation requirements for GW	
Gravels with fines (appreciable amount of fines)	GM	Silty gravels, gravel-sand-silt mixtures	Nonplastic fines or fines with low plasticity (see ML soils)	Atterberg limits below *A* line or PI < 4	Soils above A line with 4 < PI < 7 are borderline cases, require use of dual symbols
	GC	Clayey gravels, gravel-sand-clay mixtures	Plastic fines (see CL soils)	Atterberg limits above *A* line with PI > 7	
2. Sands (more than half of coarse fraction smaller than No. 4 sieve)[e]					
Clean sands (little or no fines)	SW	Well-graded sands, gravelly sands, little or no fines	Wide range in grain sizes and substantial amounts of all intermediate particle sizes	$D_{60}/D_{10} > 6$ $1 < D_{30}^2/D_{10}D_{60} < 3$	
	SP	Poorly graded sands or gravelly sands, little or no fines	Predominantly one size, or a range of sizes with some intermediate sizes missing	Not meeting all gradation requirements for SW	
Sands with fines (appreciable amount of fines)	SM	Silty sands, sand-silt mixtures	Nonplastic fines or fines with low plasticity (see ML soils)	Atterberg limits above *A* line or PI < 4	Soils with Atterberg limits above *A* line while 4 < PI < 7 are borderline cases, require use of dual symbols
	SC	Clayey sands, sand-clay mixtures	Plastic fines (see CL soils)	Atterberg limits above *A* line with PI > 7	

TABLE 7-2 *(Continued)*

Information required for describing coarse-grained soils:

For undisturbed soils, add information on stratification, degree of compactness, cementation, moisture conditions, and drainage characteristics. Give typical name; indicate approximate percentage of sand and gravel; maximum size, angularity, surface condition, and hardness of the coarse grains; local or geological name and other pertinent descriptive information; and symbol in parentheses. Example: *Silty sand,* gravelly; about 20% hard, angular gravel particles, ½ in. maximum size; rounded and subangular sand grains, coarse to fine; about 15% nonplastic fines with low dry strength; well compacted and moist in place; alluvial sand; (SM).

Major division	Group symbol	Typical names	Identification procedure[f]			Laboratory classification criteria[c]
			Dry strength (crushing characteristics)	Dilatancy (reaction to shaking)	Toughness (consistency near PL)	
B. Fine-grained soils (more than half of material smaller than No. 200 sieve)[d]						
Silts and clays with liquid limit less than 50	ML	Inorganic silts and very fine sands, rock flour, silty or clayey fine sands, or clayey silts with slight plasticity	None to slight	Quick to slow	None	
	CL	Inorganic clays of low to medium plasticity, gravelly clays, sandy clays, silty clays, lean clays	Medium to high	None to very slow	Medium	
	OL	Organic silts and organic silty clays of low plasticity	Slight to medium	Slow	Slight	
Silts and clays with liquid limit more than 50	MH	Inorganic silts, micaceous or diatomaceous fine sandy or silty soils, elastic silts	Slight to medium	Slow to none	Slight to medium	
	CH	Inorganic clays of high plasticity, fat clays	None to very high	None	High	
	OH	Organic clays of medium to high plasticity	Medium to high	None to very slow	Slight to medium	
C. Highly organic soils						
	Pt	Peat and other highly organic soils	Readily identified by color, odor, spongy feel, and often by fibrous texture			

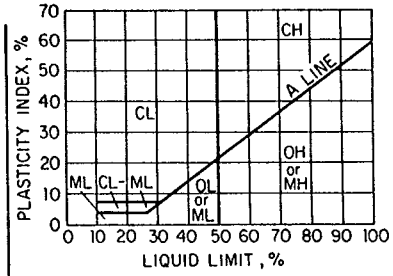

Plasticity chart for laboratory classification of fine-grained soils compares them at equal liquid limit. Toughness and dry strength increase with increasing plasticity index (PI)

Field identification procedures for fine-grained soils or fractions[g]:

Dilatancy (reaction to shaking)

After removing particles larger than No. 40 sieve, prepare a pat of moist soil with a volume of about ½ cu in. Add enough water if necessary to make the soil soft but not sticky.

Place the pat in the open palm of one hand and shake horizontally, striking vigorously against the other hand several times. A positive reaction consists of the appearance of water on the surface of the pat, which changes to a livery consistency and becomes glossy. When the sample is squeezed between the fingers, the water and gloss disappear from the surface, the pat stiffens, and finally it cracks or crumbles. The rapidity of appearance of water during shaking and of its disappearance during squeezing assist in identifying the character of the fines in a soil.

Very fine clean sands give the quickest and most distinct reaction, whereas a plastic clay has no reaction. Inorganic silts, such as a typical rock flour, show a moderately quick reaction.

Dry strength (crushing characteristics)

After removing particles larger than No. 40 sieve, mold a pat of soil to the consistency of putty, adding water if necessary. Allow the pat to dry completely by oven, sun, or air drying, then test its strength by breaking and crumbling between the fingers. This strength is a measure of character and quantity of the colloidal fraction contained in the soil. The dry strength increases with increasing plasticity.

High dry strength is characteristic of clays of the CH group. A typical inorganic silt possesses only very slight dry strength. Silty fine sands and silts have about the same slight dry strength but can be distinguished by the feel when powdering the dried specimen. Fine sand feels gritty, whereas a typical silt has the smooth feel of flour.

Toughness (consistency near PL)

After particles larger than the No. 40 sieve are removed, a specimen of soil about ½ cu in. in size is molded to the consistency of putty. If it is too dry, water must be added. If it is too sticky, the specimen should be spread out in a thin layer and allowed to lose some moisture by evaporation. Then, the specimen is rolled out by hand on a smooth surface or between the palms into a thread about ⅛ in. in diameter. The thread is then folded and rerolled repeatedly. During this manipulation, the moisture content is gradually reduced and the specimen stiffens, finally loses its plasticity, and crumbles when the plastic limit (PL) is reached.

After the thread crumbles, the pieces should be lumped together and a slight kneading action continued until the lump crumbles.

The tougher the thread near the PL and the stiffer the lump when it finally crumbles, the more potent is the colloidal clay fraction in the soil. Weakness of the thread at the PL and quick loss of coherence of the lump below the PL indicate either organic clay of low plasticity or materials such as kaolin-type clays and organic clays that occur below the *A* line.

Highly organic clays have a very weak and spongy feel at PL.

TABLE 7-2 (*Continued*)

Information required for describing fine-grained soils:

For undisturbed soils, add information on structure, stratification, consistency in undisturbed and remolded states, moisture, and drainage conditions. Give typical name; indicate degree and character of plasticity; amount and maximum size of coarse grains; color in wet condition; odor, if any; local or geological name and other pertinent descriptive information; and symbol in parentheses. Example: *Clayey silt,* brown; slightly plastic; small percentage of fine sand; numerous vertical root holes; firm and dry in place; loess; (ML).

---

[a] Adapted from recommendations of Corps of Engineers and U.S. Bureau of Reclamation. All sieve sizes United States standard.
[b] Excluding particles larger than 3 in. and basing fractions on estimated weights.
[c] Use grain-size curve in identifying the fractions as given under field identification.
For coarse-grained soils, determine percentage of gravel and sand from grain-size curve. Depending on percentage of fines (fractions smaller than No. 200 sieve), coarse-grained soils are classified as follows:

Less than 5% fines	GW, GP, SW, SP
More than 12% fines	GM, GC, SM, SC
5% to 12% fines.	Borderline cases requiring use of dual symbols

Soils possessing characteristics of two groups are designated by combinations of group symbols; for example, GW-GC indicates a well-graded, gravel-sand mixture with clay binder.
[d] The No. 200 sieve size is about the smallest particle visible to the naked eye.
[e] For visual classification, the ¼-in. size may be used as equivalent to the No. 4 sieve size.
[f] Applicable to fractions smaller than No. 40 sieve.
[g] These procedures are to be performed on the minus 40-sieve-size particles (about $^1/_{64}$ in.).
For field classification purposes, screening is not intended. Simply remove by hand the coarse particles that interfere with the tests.

Appendix D
Electrochemical Measurement of the Corrosion of Bullets in Various Soils Environments[1]

[1] Bundy, K. J., Bricka, M., and Morales, A. (1995). Internal report, U.S. Army Engineer Waterways Experiment Station, Vicksburg, MS.

ELECTROCHEMICAL MEASUREMENT OF THE CORROSION OF BULLETS IN VARIOUS SOIL ENVIRONMENTS

by

K. J. Bundy*, M. Bricka, and A. Morales
Environmental Restoration Group
Environmental Laboratory
U. S. Army Engineer Waterways Experiment Station
Vicksburg, MS
39180-6199

*Biomedical Engineering Department
Tulane University
New Orleans, LA
70118

for: U.S. Army Engineer Waterways Experiment Station

August 3, 1995

Contract No. DAAL03-91-C-0034
TCN95-092
Scientific Services Program

The views, opinions, and/or findings contained in this report are those of the author(s) and should not be construed as an official Department of the Army position, policy, or decision, unless so designated by other documentation

INTRODUCTION

It appears that one corrosion problem of possibly significant environmental importance, that has been overlooked in the past, is that of spent small arms munitions in soil. For several decades at a great number of military firing ranges, used fired bullets have been accumulating on top of and embedded in soil surfaces. A wide spectrum of soil types and weathering conditions is involved. Typically, bullets consist of a lead alloy slug surrounded by a copper alloy jacket. In armor piercing projectiles, there is, as well, a central cylindrical core of a ferrous alloy. Lead is a well-known neurotoxin and causes other health problems too. Although not harmful to the degree that lead is, copper is also considered to be a toxic metal. Therefore, the release of soluble and precipitated corrosion products into soil is of potential concern, particularly regarding the possibility of their infiltration into ground water. This research project was undertaken in order to assess the feasibility of employing electrochemical techniques to study the rate of corrosion of bullets under a variety of soil chemistry conditions. It complements ongoing studies of the corrosion of bullets using weight loss methods.

LITERATURE SEARCH

Over the years there have been many reports on the corrosion behavior of metals in soil. For the most part, however, these have been concerned with underground structures fabricated from ferrous alloys such as water mains (1), pilings (2), gas pipelines (3), and underground storage tanks(4). Much less is known about the electrochemical dissolution of nonferrous materials in soil environments.

The literature regarding underground corrosion of lead alloys is much sparser than that pertaining to iron and steel, mentioned above. Studies of lead sheathing of concentric neutral underground telecommunication cables have been reported(5)-(7). The extensive NBS soil corrosion research projects (8) utilized lead alloys for a very small percentage of the exposed specimens. Von Baeckmann(9) has reported on the cathodic corrosion of lead in soil. Booth et al.(10) investigated soil characteristics that foster aggressive corrosion in a variety of nonferrous materials including lead and copper. Solid radioactive wastes are sometimes stored in underground containers made of lead, and some research has been reported regarding their corrosion behavior(11)-(12). A literature search turned up only one reference dealing with corrosion of bullets in soil(13), and none in the English language. The study of Shimodaira et al. (13) investigated stress corrosion cracking behavior of brass bullets.

Few of the studies of lead corrosion mentioned above, however, have used electrochemical techniques to monitor the rate of corrosion of these materials, and none have done so for small arms munitions. The purpose of the present investigation is to study the utility and validity of this approach for gauging the severity of corrosion under a range of soil conditions that might be encountered by spent bullets in the field. Electrochemical methods offer the advantage over weight loss tests in that they can be carried out much more quickly. Thus they lend themselves to studies where many different environments are being tested. This work complements ongoing weight loss studies that will be completed in the near future. Ultimately it is hoped that such studies will allow determination of the soil/weathering conditions that pose the greatest hazard for lead release into the soil. This should aid in guiding remediation efforts and/or future efforts in the area of soil treatment to minimize corrosion of bullets.

MATERIALS AND METHODS

Soil Conditions

Soil for testing purposes was obtained from Fort Polk, Louisiana, one of the nation's largest firing ranges. In one series of tests, the soil moisture content was controlled to 15%, which is the typical value of soils in Vicksburg, MS. In a second series of tests, saturated soil was used, corresponding to a moisture content of

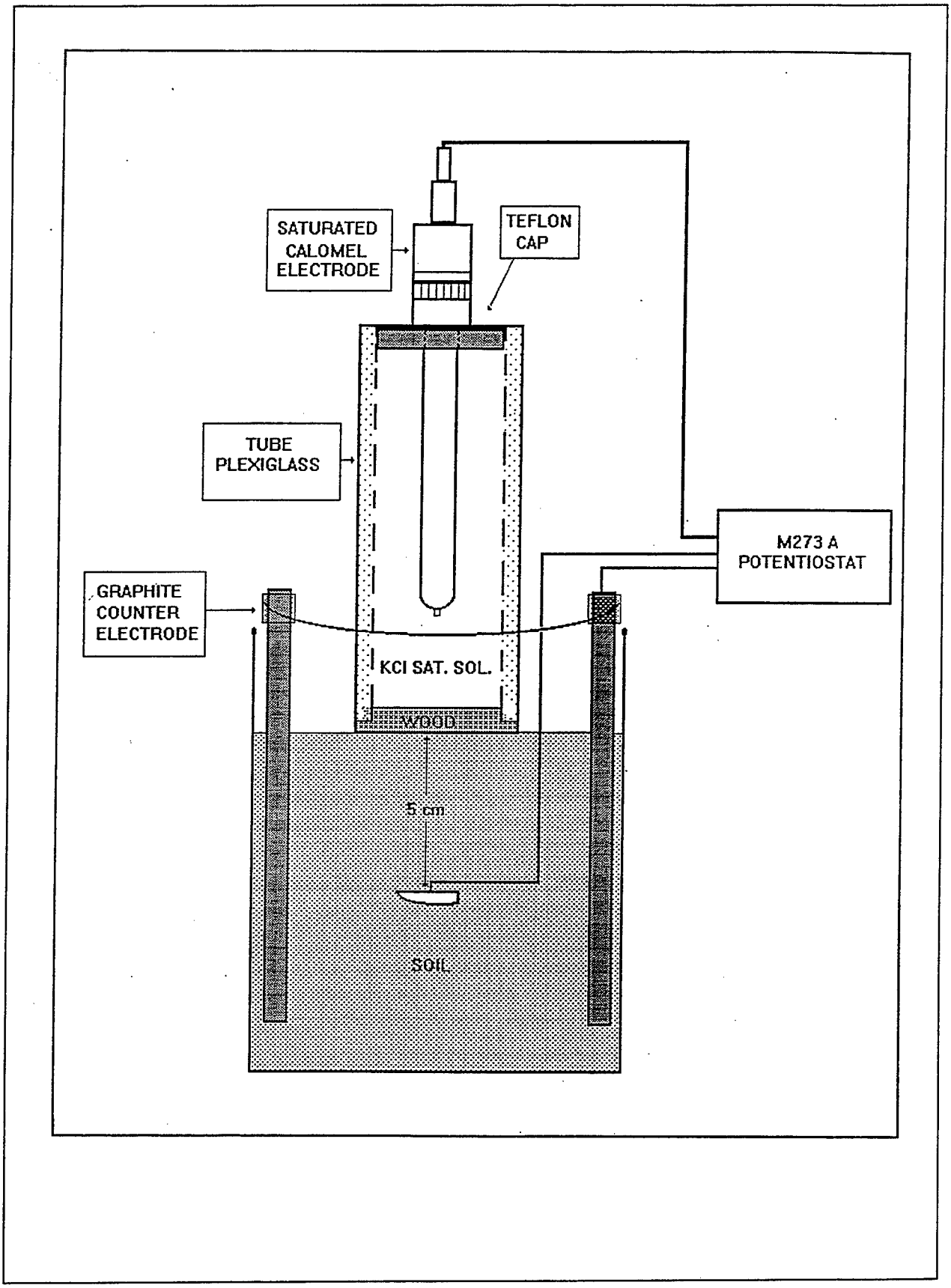
SATURATED
CALOMEL
ELECTRODE
TEFLON
CAP
TUBE
PLEXIGLASS
M273 A
POTENTIOSTAT
GRAPHITE
COUNTER
ELECTRODE
KCl SAT. SOL.
WOOD
5 cm
SOIL

24.5%. Moisture contents were verified using a Denver Instrument Co. IR-100 Moisture Analyzer. The soils were tested at room temperature and exposed to ambient atmospheric oxygen.

In this work, four different soil electrolytes were used (at the two moisture contents mentioned above). It was thought, that this would create a wide range of soil corrosivity useful for the study of the utility of electrochemical techniques. The electrolytes were a) rain water collected at Waterways Experiment Station in Vicksburg, MS, b) artificial sea water (Instant Ocean Synthetic Sea Salt, consisting of, when dissolved, 1.0249 g/kg Na, 0.04 g/kg K, 0.04 g/kg Ca, 0.126 g/kg Mg, 0.02 g/kg HCO3, 1.85 g/kg Cl, 0.26 g/kg SO4, and trace amounts of boron and strontium), c) simulated acid rain (made by taking rain water and adding HNO3 to adjust pH down to 4.09), and d) a 50-50 mixture of sea water and acid rain. Firing ranges in the U.S. are found at locations that represent virtually all climatic, geographical, and soil type conditions. It was considered that the range of soil conditions created in the laboratory would be representative of some portion of these. Additionally, these conditions are a subset of those being used in the wider weight loss measurement project.

Acid rain is composed of a complex mixture of NOx and SOx compounds of anthropogenic and natural origin that have interacted with atmospheric water (14). pH levels have been reported to be in the 3.9-5.5 range (14)-(16). An acid rain mixture based on HNO3 was chosen because of reports that SOx emissions have significantly declined in the past, and this trend is expected to continue in the future(16). This condition was incorporated into the testing program since the destructiveness of acid rain to metallic structures, such as statues and architectural trim, is well known(14)-(17). It seems likely, therefore, that surface and subsurface spent ammunition also could be affected by acid precipitation.

Corrosion Testing and Data Analysis

To perform the corrosion measurements, M16 bullets were used. The "lead" slug is actually a lead-2 weight% antimony alloy. The jacket is made from a copper alloy. The bullets were cut in half axially, and a hole was drilled in the slug. The tip of an insulated copper wire was put in the hole that was then filled with Pb-Sn solder and insulated with silicone rubber sealant. The bullets were cleaned first in an Alconox detergent solution ultrasonically for five minutes, followed by a 10 second tap water rinse. Then another ultrasonic cleaning step for five minutes in ethanol was conducted, followed by another tap water rinse. As the final step, the specimens were rinsed in doubly distilled water for about 10 seconds, and then were air dried. Four specimens were tested in each of the eight moisture/soil electrolyte combinations investigated, for a total of 32 samples measured in total.

Soil with the appropriate electrolyte and moisture content was put in a two liter beaker. The bullet was buried at a depth of about 5 cm beneath the surface. The corrosion behavior of the bullet was measured using electrochemical techniques. An EG&G Model 273A potentiostat operating in a computerized mode was used for this purpose. Graphite rods were used for counter electrodes. A saturated calomel electrode was used for the reference electrode. A salt bridge that consisted of an 8.25 cm diameter pine plug in a plastic tube filled with saturated KCl was employed to make electrical contact with the soil. The salt bridge design was patterned after typical Cu-CuSO4 reference electrodes used in underground corrosion testing of ferrous alloys(18). A schematic of the corrosion cell is shown in Figure 1.

The experimental protocol employed for these measurements was as follows. Using the Headstart software package, free corrosion potential Ec was measured versus time t over a 1000 second period. Over this interval, 200 data points were taken. This was done to assess the stability of the metal/soil interface. The criterion used to assess stabilization was <1 mV/ minute change in potential. After stability was observed, which typically required about 1 hr. of exposure, further corrosion tests were undertaken.

Since soil resistance can be very high, significant artifacts can be introduced in polarization resistance measurements, if this effect (known as IR drop) is not compensated for. To measure the resistance for a given sample/soil electrolyte configuration, the chronoamperometric subroutine of the M270 software

package was used. An 85 mV, 6 msec duration pulse was applied to the free corrosion potential Ec (taken to be the final potential observed in the Ec vs. t measurement), and the resultant current I was measured versus time over a 10 second period. 85 mV divided by the change in current dI observed as the pulse was applied gives a measure of the soil resistance Ro. A typical measurement is shown in Figure 2. The basic theory behind such a test is as follows. The circuit analogy associated with the corroding metal system is, to a first approximation, Ro in series with a parallel RC circuit. This circuit consists of the polarization resistance, discussed below, and the capacitance of the metal/soil electrolyte interface. When a potential is quickly applied, the current flows through the capacitor and Ro. Over time, though, the capacitor charges up, blocking passage of current, which then must flow through Rp + Ro. This results in an RC exponential decay of current versus time. The height of the current spike divided into the applied potential, as mentioned above, gives Ro. The positive feedback option of the M273A potentiostat, along with the M270 IR compensation subroutine software, allowed linear polarization and potentiodynamic polarization curve measurements to be conducted that were compensated for IR drop by subtracting out the contribution of Ro.

Linear polarization measurements were conducted using the linear sweep voltammetry subroutine of the M270 software at a scan rate of 0.1 mV/sec in the approximate range of +/- 25 mV about the corrosion potential. Sliding average smoothing (using a ten point basis) was employed where necessary to minimize noise. Figures 3 and 4 show typical measurements before and after smoothing. The curve fit feature of the software was used to determine the slope of the E vs. I curve at I=0. This slope is known as the polarization resistance, Rp. This parameter is important because according to the Stern Geary equation:

$$Ic = (BaBc)/\{(2.3Rp(Ba + Bc)\} \quad (1)$$

the corrosion current Ic (a parameter directly related to the rate of corrosion) is inversely related to the polarization resistance. The Tafel slopes Ba and Bc must be determined in a separate test, a potentiodynamic polarization curve measurement. The potentiodynamic polarization curve was measured from about 600 mV cathodic to Ec to 600 mV above Ec. A typical measurement is shown in Figure 5. The Tafel constants are the slopes of the potential vs. log |I| curve in the regions where there is a linear relationship between these two parameters. Ba and Bc are the slopes of the anodic and cathodic regions of the curve. These refer to the potential regions above and below Ec, respectively. The Tafel slopes in this investigation were determined by exporting the M270 data to the program Quattro Pro for Windows, and using the linear regression capability of this software.

Three measures of corrosion potential were used to compute an average value of Ec. These were 1) the range of potential observed in the Ec vs. t measurement (or in the final test, if more than one such test was conducted), 2) the potential where the current was zero in the linear polarization test, and 3) the potential of the low current spike observed in the potentiodynamic polarization curve. The extreme points of the potential range of the three measurements above were averaged to obtain a measure of the mean corrosion potential over the course of the measurement interval.

Corrosion rates were also determined in three ways: 1) the linear polarization/ Stern Geary equation method mentioned previously, 2) anodic Tafel extrapolation, and 3) cathodic Tafel extrapolation. In the Tafel extrapolation method, the linear Tafel regions of the potentiodynamic polarization curve (mentioned above) are extrapolated back to Ec. The current at this point is the corrosion current Ic.

One of the recommendations for the future, given later, is to purchase M352 corrosion rate measurement software. The rationale for this recommendation is as follows. The research conducted here made optimal use of the electrochemical software packages that were on hand at WES. However, the M270 package is generally used for polarographic testing, not for corrosion measurements. The Headstart package, although useful for DC corrosion measurements, is far from the state of the art in this area any more. Some of the difficulties encountered with the present software were as follows. Ec vs. t data could not be printed out from the Headstart menu. IR drop could not be directly measured. Headstart has no provision for IR compensation. M270 does, but the routine that directly measures the ohmic resistance was not working,

```
Model 270/250 Research Electrochemistry Software , v.   4.00      Filename:
Pstat:  M273A[96] Ver 201                    CA  CHRONOAMPEROMETRY
File Status:  NORMAL  Date Run:  07-27-95     Time Run:  22:41:43
PT  1                 CP  PASS vs. R        CT  PASS              DT  PASS
IP   -0.126 vs. R     ET  1 S                E1   -0.041 vs. R
E2   -0.126 vs. R     TP   5.295E-02         T1   5.295E-02
T2   1.001E+01        CR  AUTO               NP  200
RU   0.000E+00        IR  NONE               FL  NONE
RT  HIGH STABILITY    REF 0.24150 SCE        WRK HMDE
AR   1.000E+00        OC  -0.126
```

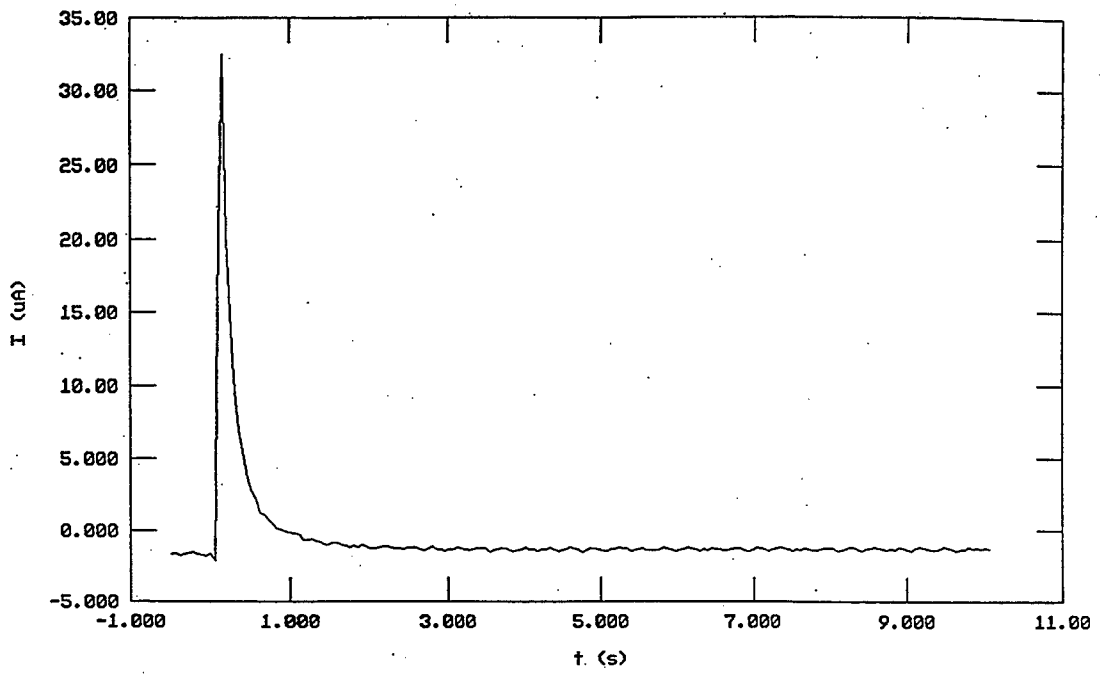

Figure 2. Chronoamperometric Measurement Used for IR Drop Compensation (Specimen 4, Fort Polk Soil, 15% Sea Water)

Model 270/250 Research Electrochemistry Software , v. 4.00 Filename:
Pstat: M273A[96] Ver 201 LSV LINEAR SWEEP VOLTAMMETRY
File Status: NORMAL Date Run: 07-25-95 Time Run: 23:45:29

PT 1	CP PASS vs. R	CT PASS	DT PASS
IP -0.305 vs. R	ET 1 S	FP -0.255 vs. R	
SI 1.000E-03	SR 1.000E-04	ST 1.000E+01	AM 4/4
CR 1 MA	NP 51	RU 7.083E+04	IR ENTERED
FL I 5.3Hz	RT HIGH STABILITY	REF 0.24150 SCE	WRK HMDE
AR 1.000E+00	OC -0.305		

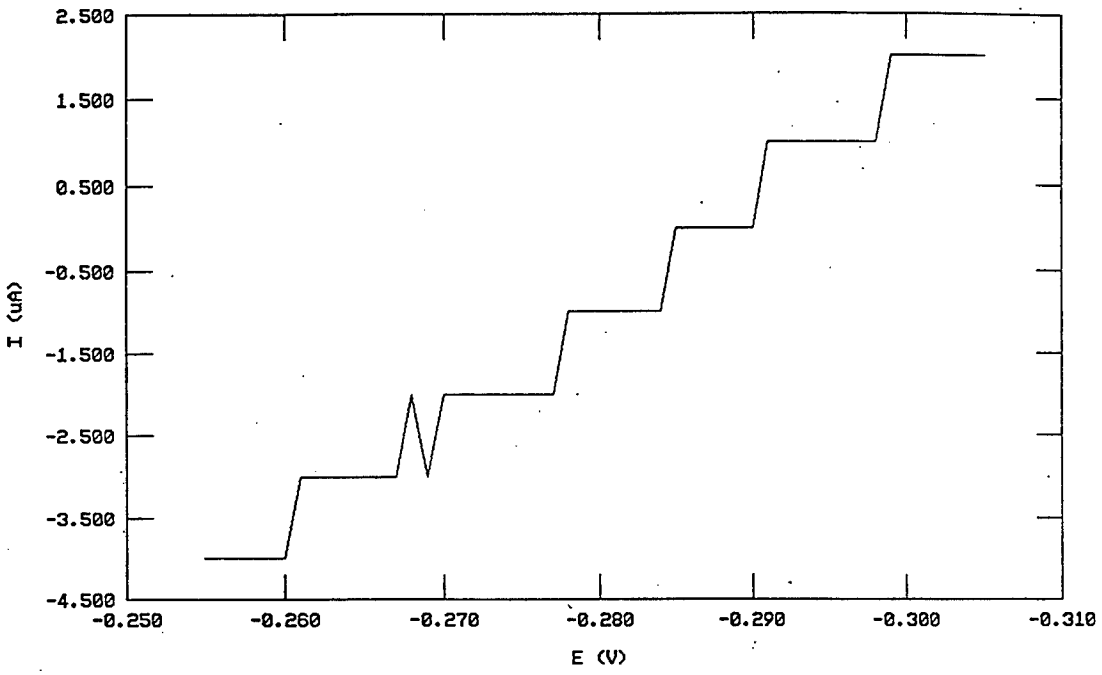

Figure 3. Linear Polarization Measurement Before Curve Smoothing (Specimen 3, Fort Polk Soil , 15% Rain Water)

```
Model 270/250 Research Electrochemistry Software , v.   4.00      Filename:
Pstat:  M273A[96] Ver 201                LSV LINEAR SWEEP VOLTAMMETRY
File Status:  EDITED  Date Run:  07-25-95  Time Run:  23:45:29
PT  1                 CP  PASS vs. R      CT  PASS                DT  PASS
IP   -0.305 vs. R     ET  1 S             FP   -0.255 vs. R
SI   1.000E-03        SR   1.000E-04      ST   1.000E+01          AM  4/4
CR  1 MA              NP  51              RU   7.083E+04          IR  ENTERED
FL  I 5.3Hz           RT  HIGH STABILITY  REF 0.24150 SCE        WRK HMDE
AR   1.000E+00        OC  -0.305
```

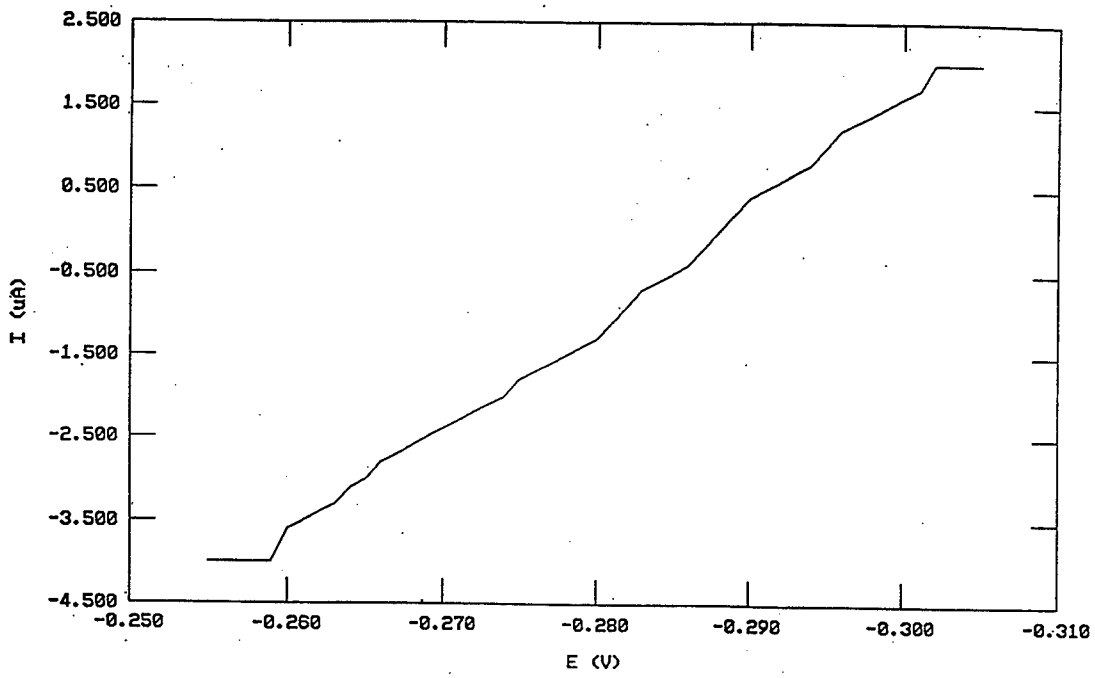

Figure 4. Linear Polarization Measurement After Curve Smoothing (Specimen 3, Fort Polk Soil , 15% Rain Water)

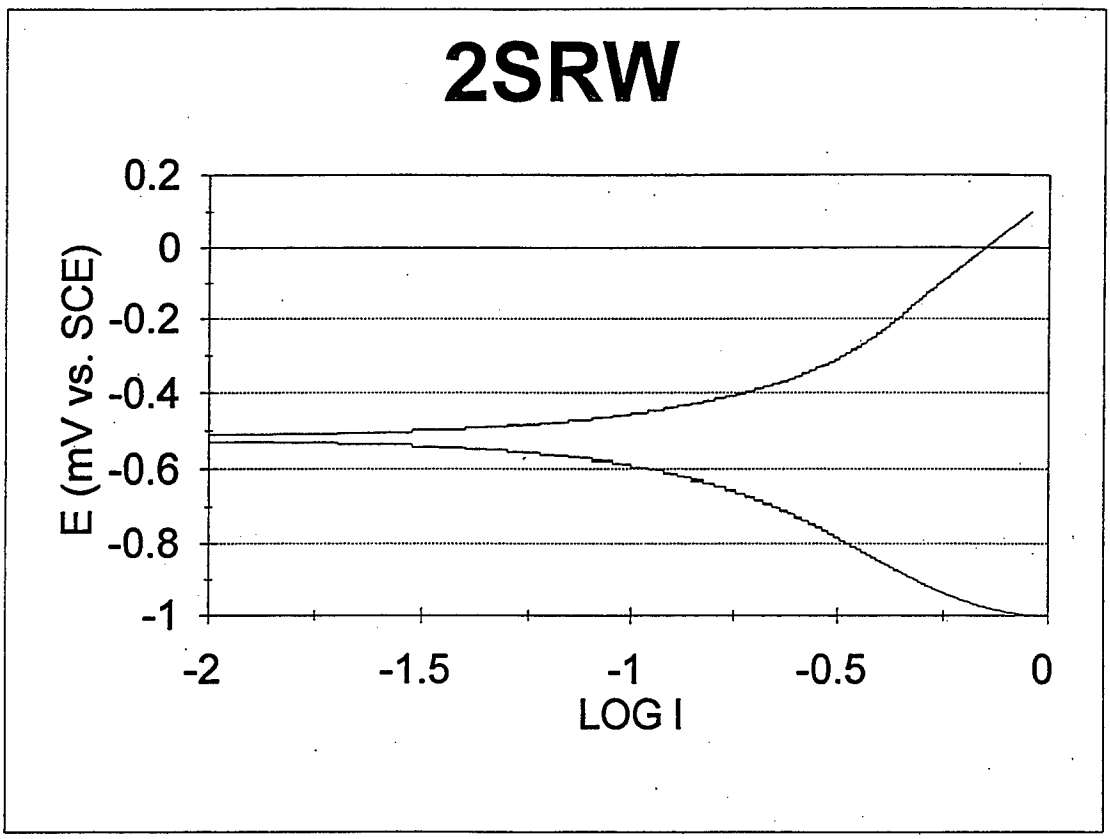

Figure 5. Potentiodynamic Polarization Curve, Specimen 2, Fort Polk Soil, Saturated with Rain Water (0 on the Horizontal Axis Corresponds to 1 mA)

necessitating the indirect procedure described above. The process of exporting the data to Quattro Pro for graphical plotting and regression analysis to obtain the Tafel slopes was time consuming. The latter process also could be potentially prone to significant error if the operator did not have significant experience in electrochemical data analysis. Each of the calculations done in the research described here is automatically provided for with one key stroke in the M352 package. In addition, the M352 has an electrochemical modeling capability that can be used to a certain extent to predict corrosion behavior under conditions other than those of the test (such as different temperatures for example).

Pourbaix Diagram Calculations

Before the experiments were run, various calculations were performed in an attempt to predict the corrosion products that would form due to the corrosion of bullets in soil. This was done using the HSC chemical calculation software program. Pourbaix diagrams, also known as potential-pH diagrams, were calculated for a variety of assumed pore water chemistry conditions. A Pourbaix diagram is based on Nernst equation and solubility product data. It shows the thermodynamically stable soluble ionic forms and insoluble salt forms of a metal in a given electrolyte as a function of electrode potential and pH of the environment. Pourbaix diagrams for both lead and copper were computed.

Since pore water chemistry values of the actual environments tested in this investigation were not available, estimates of the environment were made using data from Romanoff's work(8). The soils selected from the NBS series to simulate Fort Polk soil were number 27, corresponding to Miller clay from Bunkie, Louisiana and number 29 New Orleans muck. Pourbaix diagrams were calculated assuming a wide variety of pore water electrolyte chemistry. The environments considered included sea water, rain water, acid rain, 0.1M nitric acid, and acid rain plus sea water. The procedure for selecting the pore water chemistry for the rain water and sea water environments was as follows. It was noted that the reported ionic content of rain water(19) collected in Amarillo, Texas was much lower than that found in chemical analyses of soil pore water reported by Romanoff(8). The interference would then be that, at least under steady state conditions, water falling as rain would leach constituents from the soil into the pore water. Thus for the rain water environment, the Miller clay pore water analysis (8) for Na, Ca, Mg, HCO3, Cl, and SO4 was used. No values for nitrate content were reported by Romanoff. To provide some estimate, the 118 ppm soil nitrate value reported elsewhere was employed (20). A comparison between the reported chemistry of Miller clay pore water and sea water revealed that only Na and Cl were more concentrated in sea water than in pore water. Thus, again, it might be inferred that sea water in the soil would leach out Ca, Mg, HCO3, SO4, and NO3 to the pore water levels mentioned above (8),(20). Na and Cl levels would be present in excess of that present in pore water and would be found at the values characteristic of sea water (given previously).

The procedure for selecting the pore water chemistry to use in the Pourbaix diagram calculations for the acid rain, nitric acid, and sea water plus acid rain environments was as follows. The pH of the acid precipitation was considered to be 4.5. It was assumed that this was present as HNO3. It was noted that this would represent negligible additional nitrate loading of the soil water. Thus it was not thought the direct composition of the acid rain would affect the pore water chemistry to a significant degree. Yet it certainly was considered possible that the electrolyte composition would be changed by the lowered pH compared to that typical of the Miller clay, since presumably more ions would be leached out at lower pH. Thus the pore water chemistry of the New Orleans muck (a more acidic soil type than the Miller clay) was used to simulate the acid rain. The same was done for the nitric acid environment, except that here the added nitrate burden was significant and was accounted for. The acid rain plus sea water environment was also simulated by the ionic composition of New Orleans muck. Excess Na and Cl was taken into account as explained above, except that 50-50 dilution of the sea water by the fresh water acid rain was used.

Besides considering the effects of the electrolyte solutions above on pore water chemistry as affected by leaching, the Pourbaix diagrams for the solutions themselves (sea water, rain water, acid rain, and nitric acid) were simulated. The Cu and Pb Pourbaix diagrams for pure water were also calculated. Additional soil types were examined as far as simulating rain water leaching soil chemistry using the Romanoff data.

The soils studied in this phase of the research included Fargo clay loam, Merced silt loam, and Montezuma clay adobe.

RESULTS

As mentioned above, the parameters measured in this investigation were corrosion potential Ec, corrosion current Ic, soil resistance Ro, and the anodic and cathodic Tafel slopes Ba and Bc respectively. The numerical values obtained for these parameters in the various soil environments tested here are given in Tables A1-A3 in the appendix. The average values of the four measurements of Ic under the eight soil conditions investigated are shown in Figures 6 and 7. Figure 6 displays the data at the two moisture contents in the order of expected corrosivity, i.e. from lowest to highest: rain water (RW), acid rain (AR), sea water /acid rain (SWAR), and sea water (SW). The same data is also shown in Figure 7 where in each environment the corrosion currents are shown at the two different moisture contents.

Figures 8 and 9 present the soil resistance data in the same format as employed for Ic. It was noted that the corrosion current data appeared to be inversely related with soil resistance. To demonstrate this point more clearly, corrosion current is plotted versus Ro in Figure 10. Figure 11 shows the corrosion potential measurements at the 15% and saturated moisture contents. Figure 12 shows the influence of moisture content on Ec in the different soil environments. Comparing Figures 8 and 9 with 11 and 12, it appeared that here too there might be a relation between Ec and Ic. To examine this possibility, corrosion current is plotted versus corrosion potential in Figure 13.

The anodic Tafel slope data measured in this project is shown in Figures 14 and 15 that give, respectively, the values for the two different moisture contents in the different soil electrolytes and the slopes in the different environments as influenced by the two different moisture contents. Figures 16 and 17 provide the analogous data for the cathodic Tafel slopes.

A representative Pourbaix diagram is shown in Figure 18. Note that conventionally Pourbaix diagrams are plotted relative to a standard hydrogen electrode (SHE). The conversion between a potential measured versus a saturated calomel electrode (SCE) and the hydrogen scale is:

$$E(SHE) = E(SCE) + 0.242 \text{ v}$$

For the tests that were conducted here, the range of Ec noted was approximately -1000 to 0 mV (SCE). At pH values of 1 (0.1M HNO_3), 4.1 (acid rain), 5.6 (rain water in equilibrium with atmospheric carbon dioxide), and 7 (sea water), the most important solid and dissolved corrosion products that would be stable in this observed range of potential are given in Table 1.

DISCUSSION

Figures 6 and 7 demonstrate that the electrochemically measured corrosion current Ic provides a ranking of the rate of corrosion that intuitively corresponds to the expected severity of the environmental conditions imposed on the bullets. In both the 15% and saturated moisture environments, from lowest to highest corrosion rate, the ranking was rain water, acid rain, sea water/acid rain, sea water. A considerable range of corrosion current was observed in these tests, over 1500 microamps, indicating that the test objective to span a wide range of soil corrosivities was met.

From these measurements it is clear that the most influential variable affecting the corrosion of bullets in soil, of the ones tested in this project, is the soil chloride content. The lowered pH due to acid rain compared to rain water does have a significant effect and more than doubles the rate of corrosion. The sea water environment, though, created a corrosion current almost an order of magnitude greater than the acid rain, however. The sea water/acid rain mixture was about half as corrosive as the sea water alone, as might be expected from the 50% dilution factor. As Figure 7 shows, the moisture content is a significant factor,

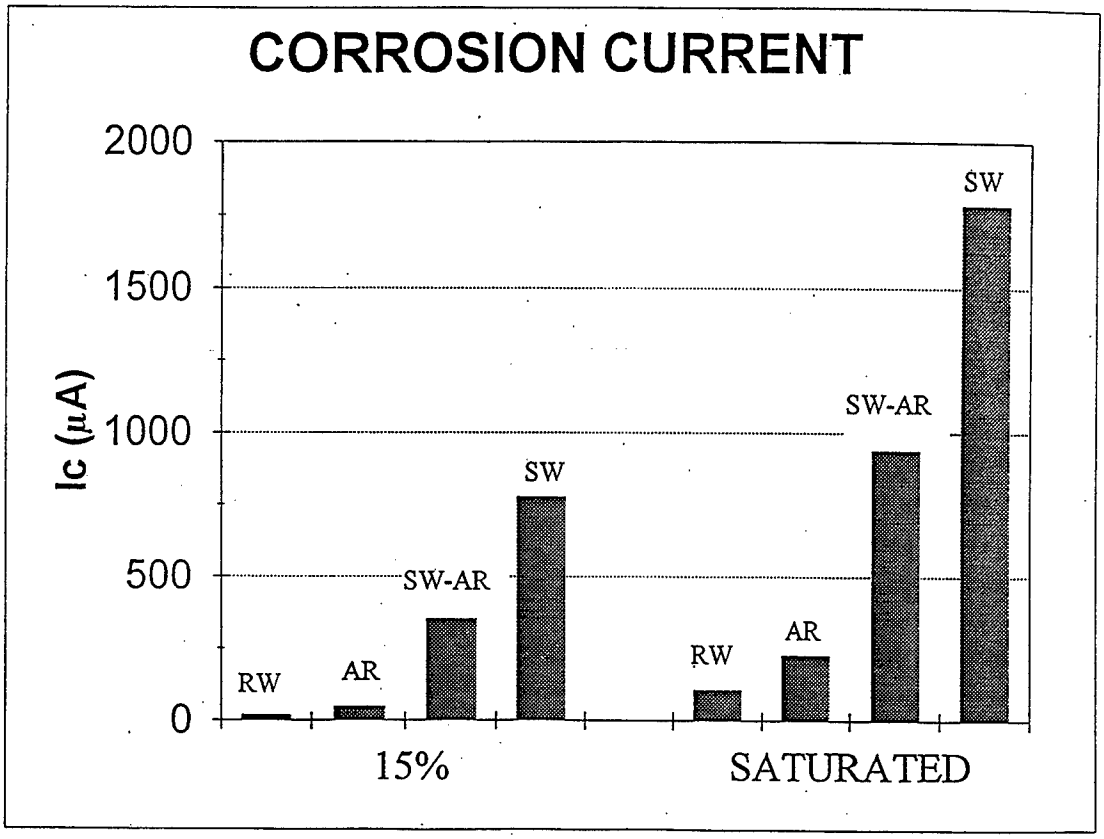

Figure 6. Corrosion Current Ic of Bullets in Fort Polk Soil at 15% and Saturated Moisture Contents for Various Electrolytes.
(RW - rain water, AR - acid rain, SW - sea water, SW-AR - sea water /acid rain mixture)

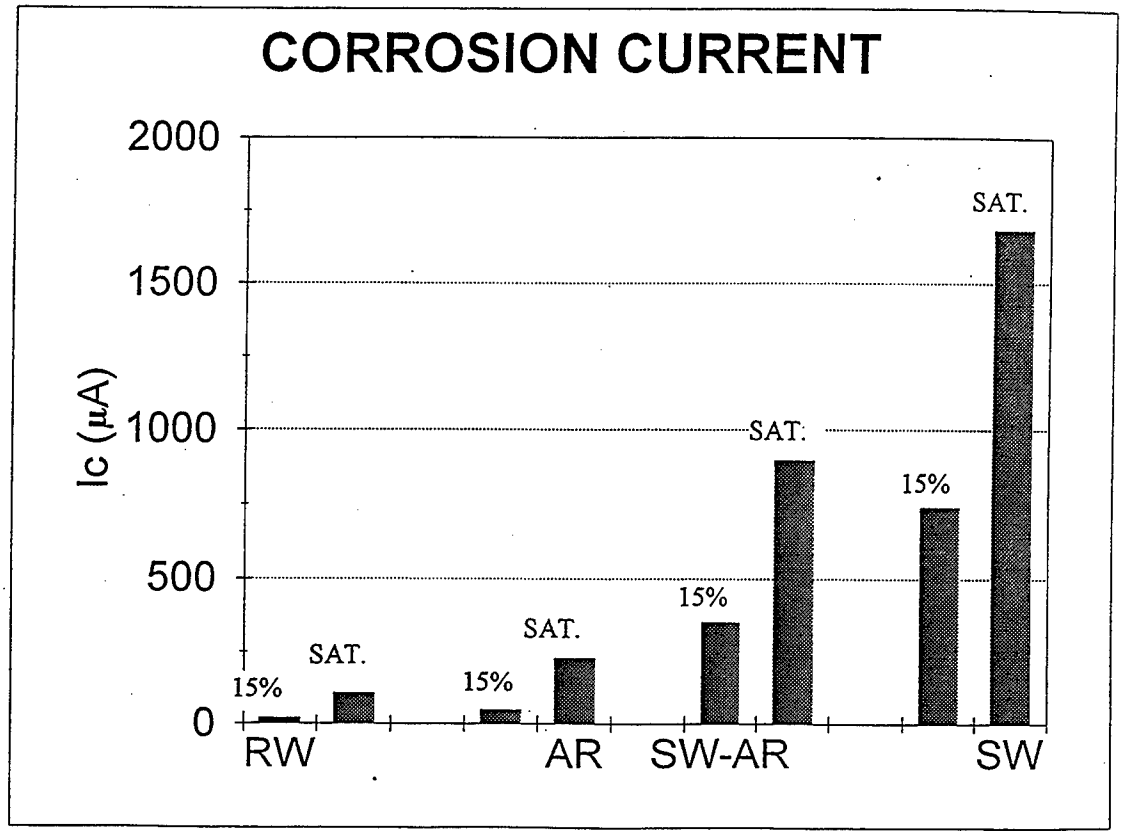

Figure 7. Corrosion Current Ic of Bullets in Fort Polk Soil with Various Electrolytes at 15% and Saturated Moisture Contents.
(RW - rain water, AR - acid rain, SW - sea water, SW-AR - sea water /acid rain mixture)

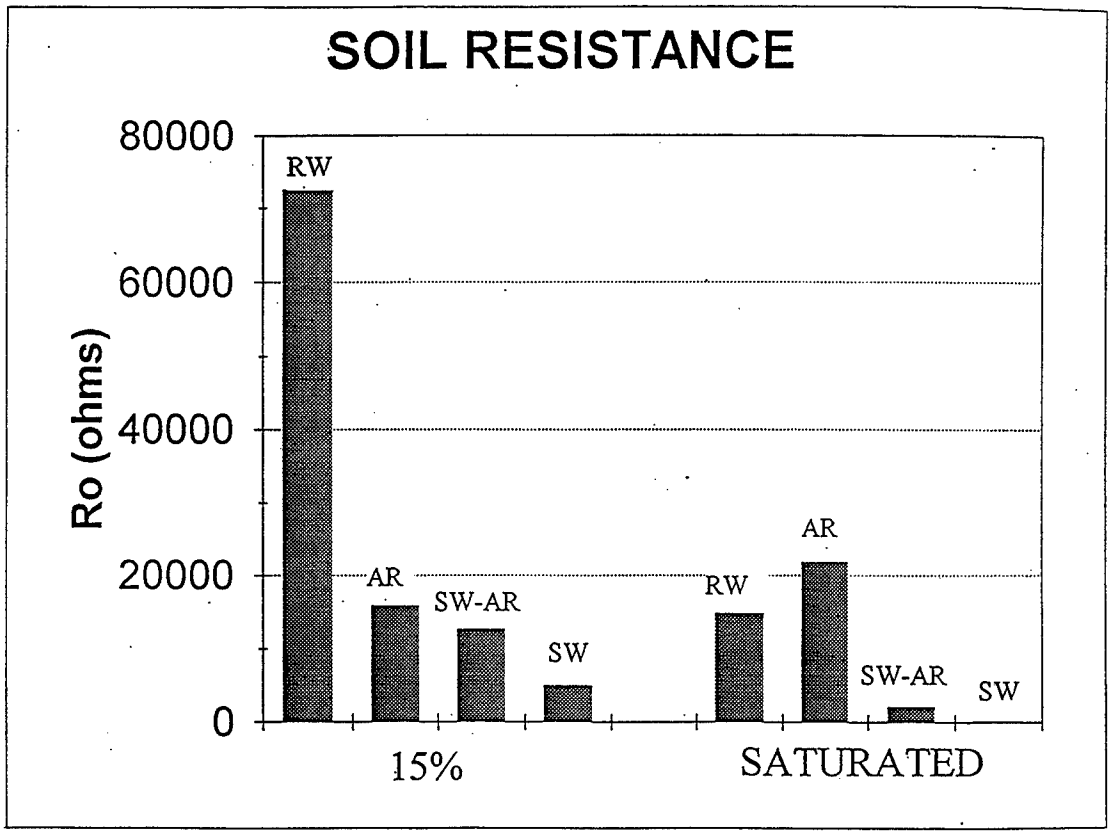

Figure 8. Ohmic Resistance Ro of Fort Polk Soil at 15% and Saturated Moisture Contents for Various Electrolytes.
(RW - rain water, AR - acid rain, SW - sea water, SW-AR - sea water /acid rain mixture)

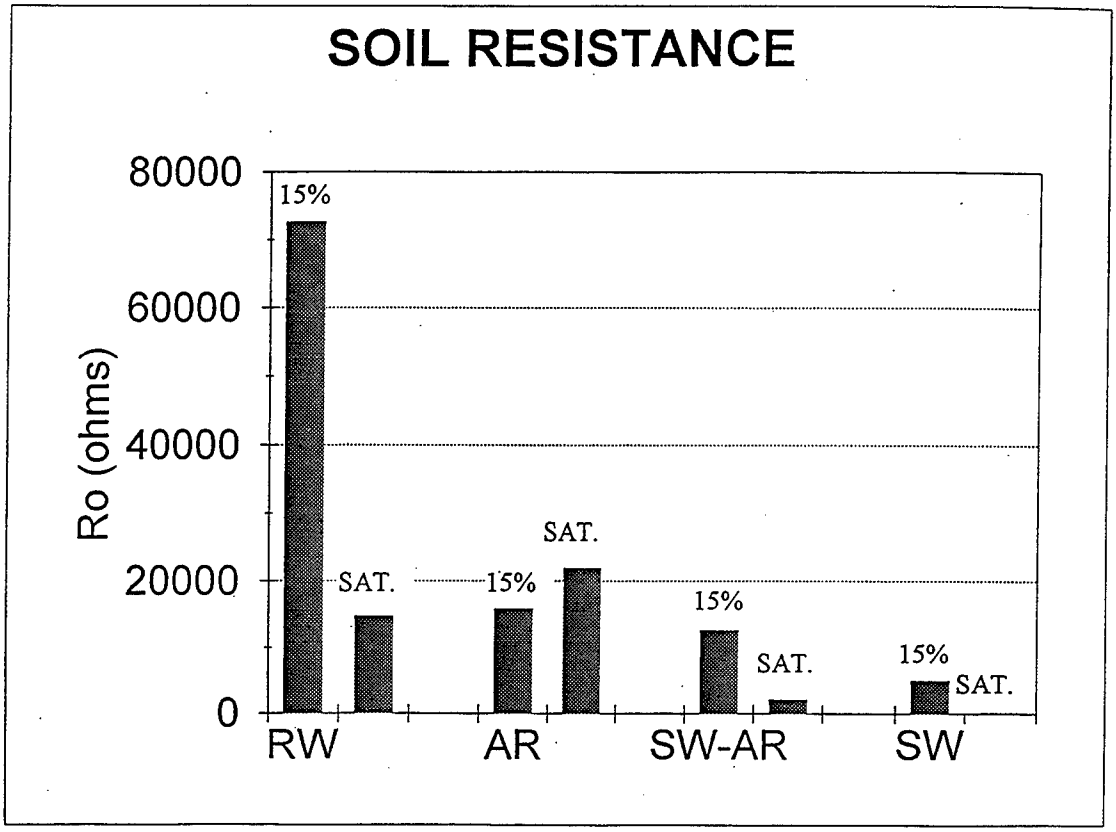

Figure 9. Ohmic Resistance Ro of Fort Polk Soil with Various Electrolytes at 15% and Saturated Moisture Contents.
(RW - rain water, AR - acid rain, SW - sea water, SW-AR - sea water /acid rain mixture)

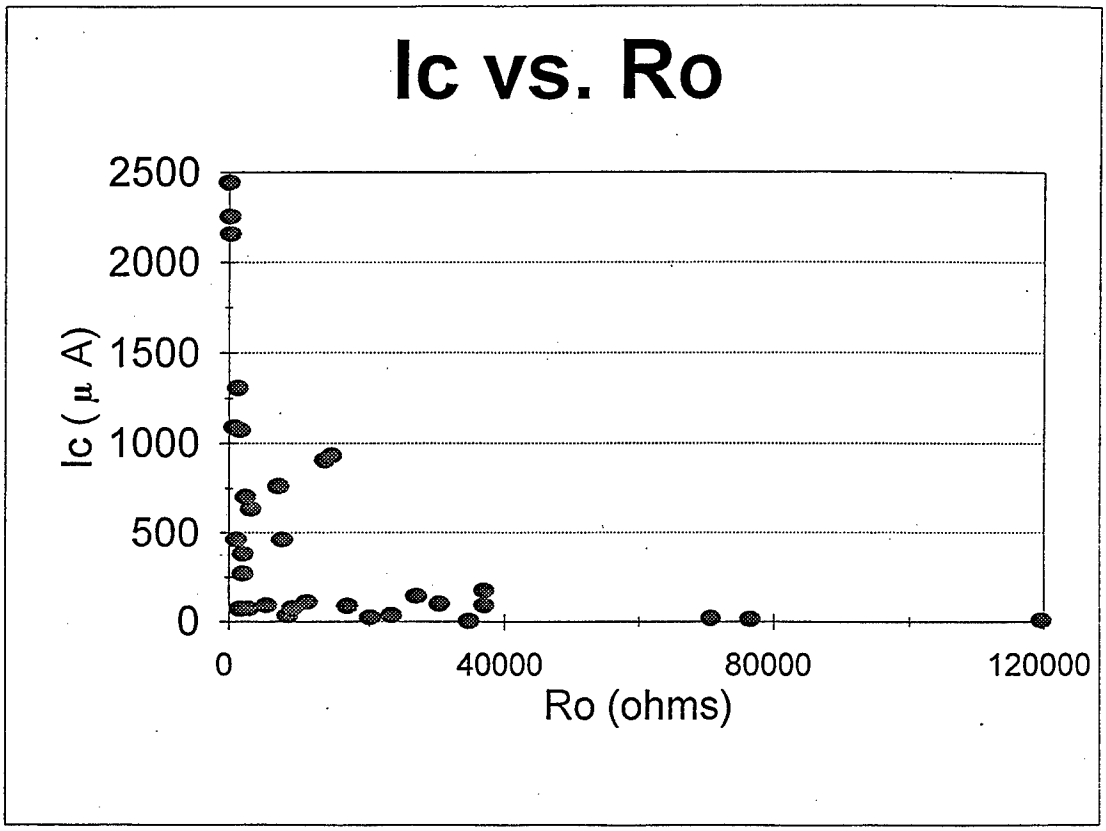

Figure 10. Corrosion Current Ic of Bullets in Fort Polk Soil Versus Ohmic Resistance Ro for Various Soil Electrolytes and Moisture Contents.

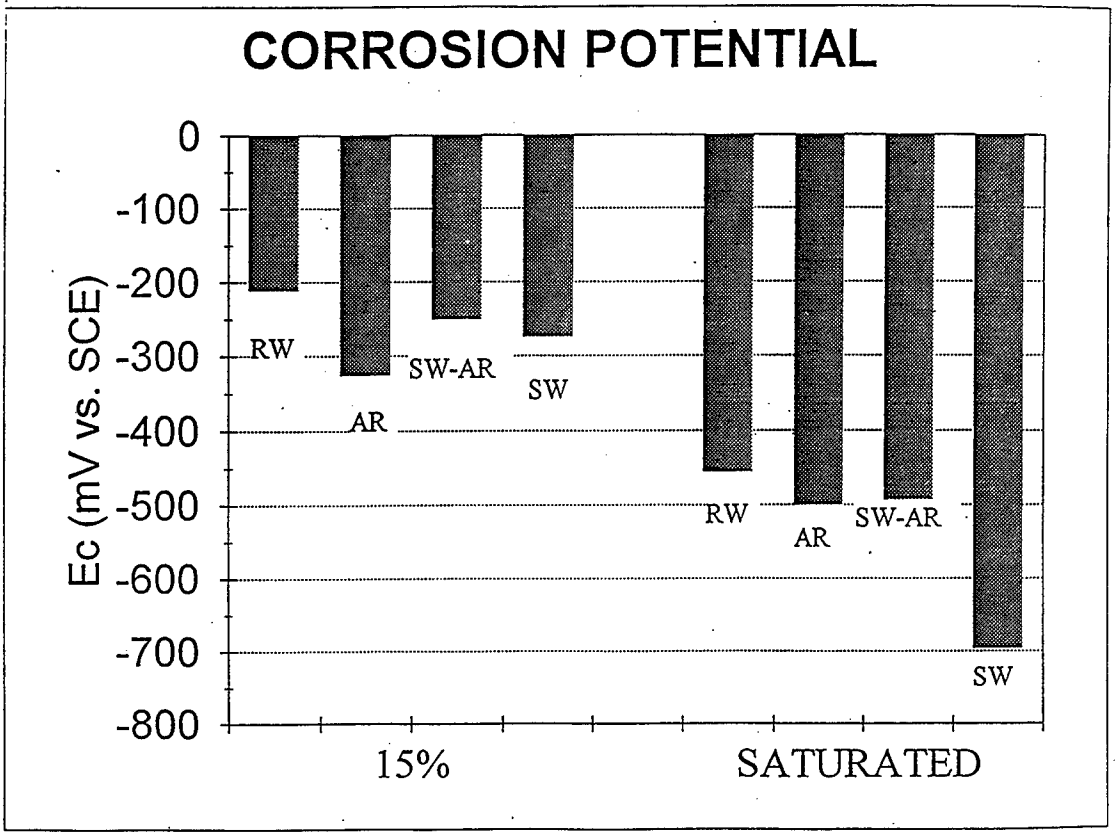

Figure 11. Corrosion Potential Ec of Bullets in Fort Polk Soil at 15% and Saturated Moisture Contents for Various Electrolytes.
(RW - rain water, AR - acid rain, SW - sea water, SW-AR - sea water /acid rain mixture)

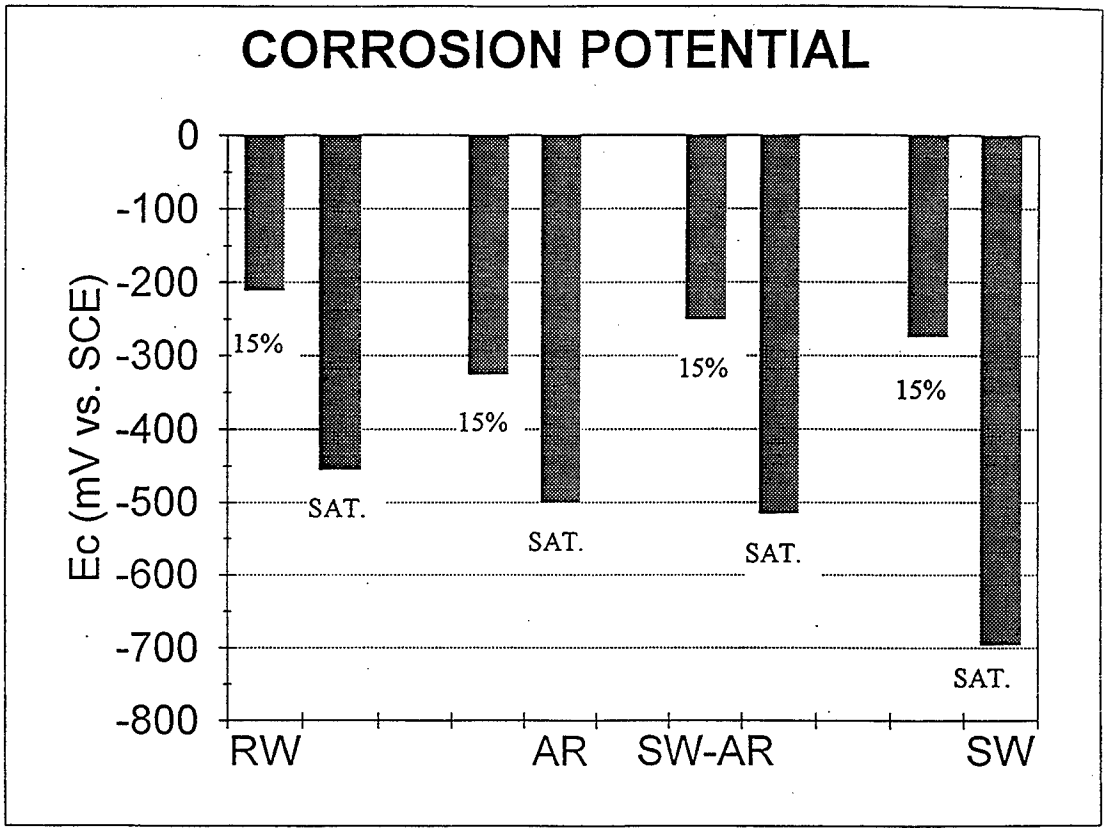

Figure12. Corrosion Potential Ec of Bullets in Fort Polk Soil with Various Electrolytes at 15% and Saturated Moisture Contents.
(RW - rain water, AR - acid rain, SW - sea water, SW-AR - sea water /acid rain mixture)

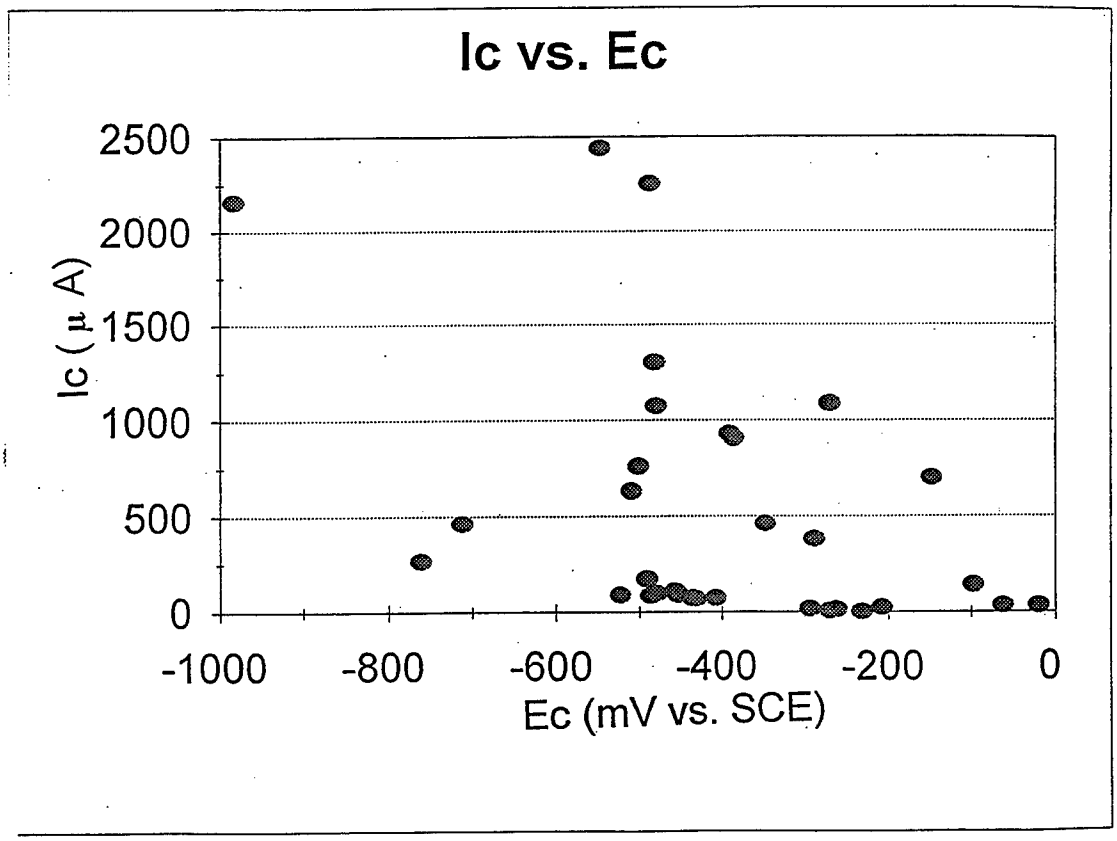

Figure 13. Corrosion Current Ic Versus Corrosion Potential Ec for Various Soil Electrolytes.

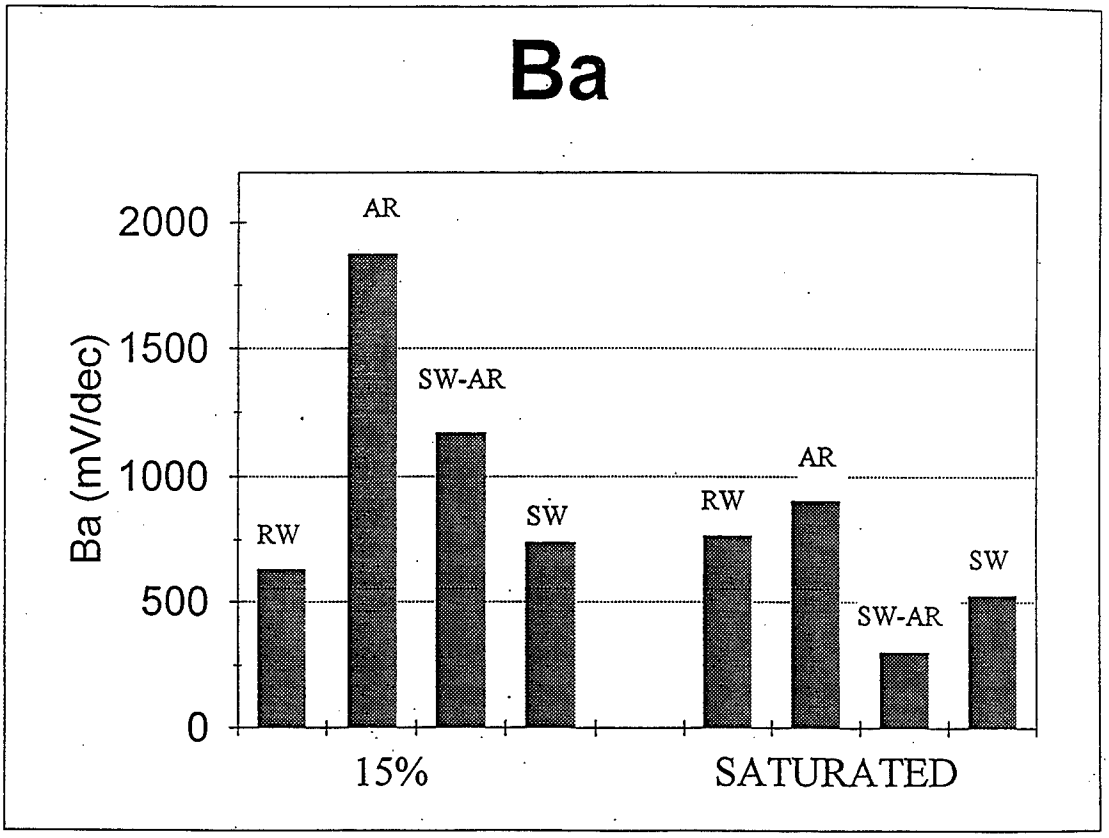

Figure 14. Anodic Tafel Slope Ba of Bullets in Fort Polk Soil at 15% and Saturated Moisture Contents for Various Electrolytes.
(RW - rain water, AR - acid rain, SW - sea water, SW-AR - sea water /acid rain mixture)

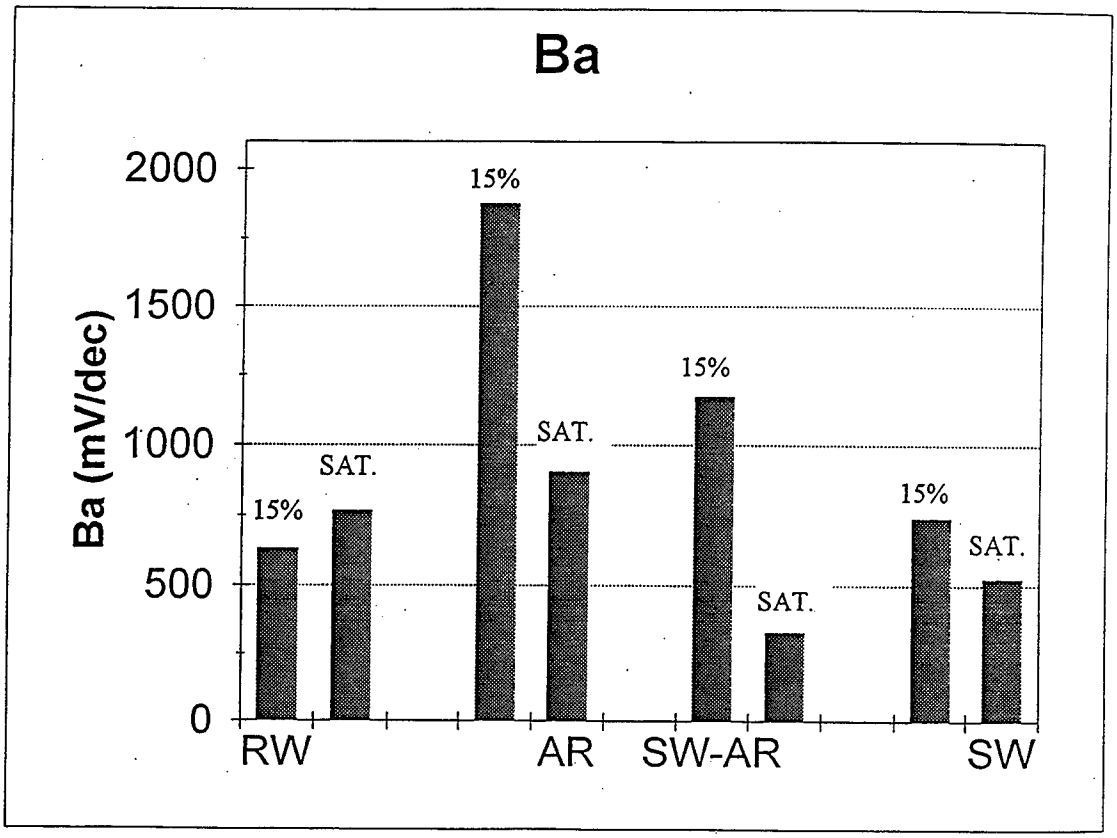

Figure 15. Anodic Tafel Slope Ba of Bullets in Fort Polk Soil with Various Electrolytes at 15% and Saturated Moisture Contents.
(RW - rain water, AR - acid rain, SW - sea water, SW-AR - sea water /acid rain mixture)

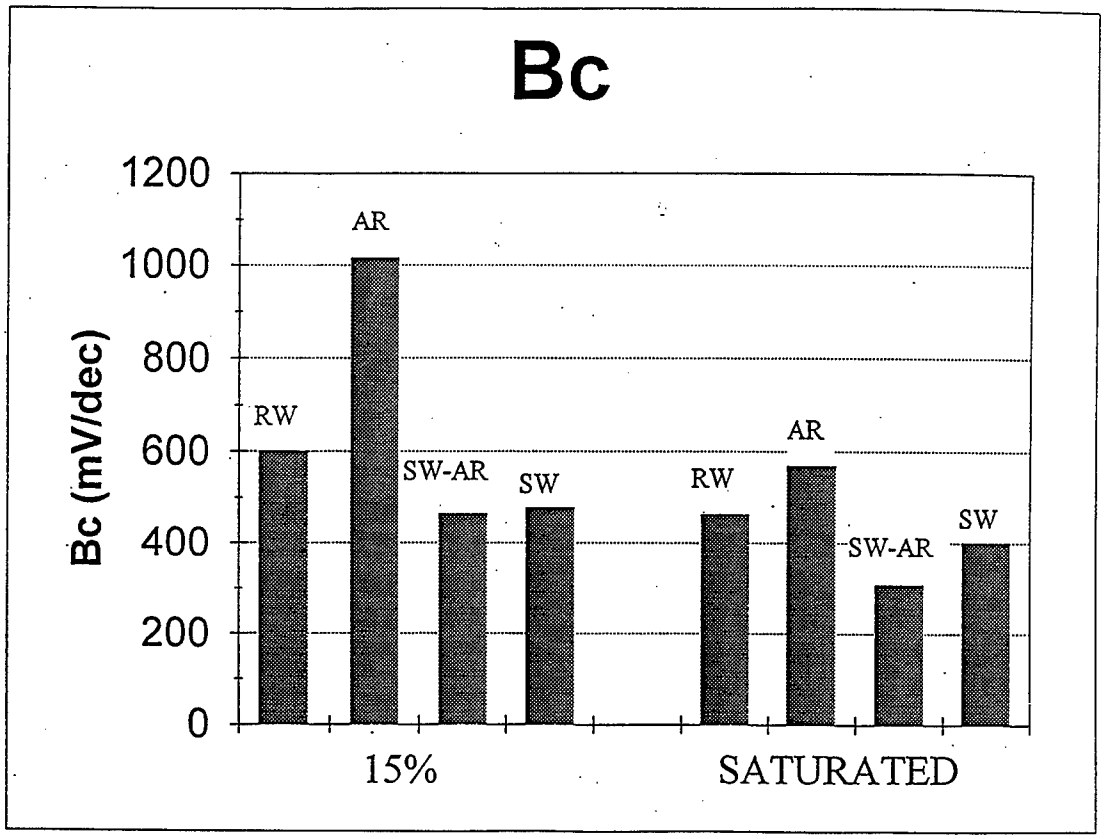

Figure 16. Cathodic Tafel Slope Bc of Bullets in Fort Polk Soil at 15% and Saturated Moisture Contents for Various Electrolytes.
(RW - rain water, AR - acid rain, SW - sea water, SW-AR - sea water /acid rain mixture)

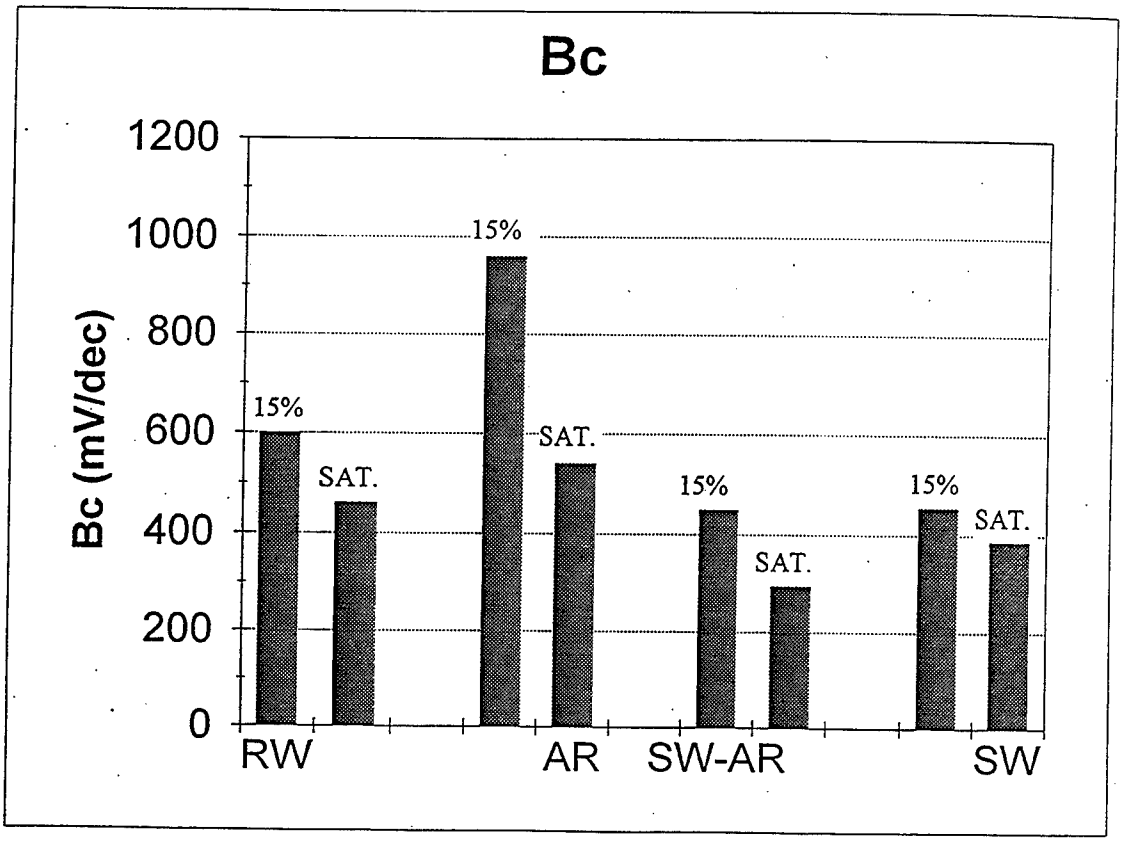

Figure 17. Cathodic Tafel Slope Bc of Bullets in Fort Polk Soil with Various Electrolytes at 15% and Saturated Moisture Contents.
(RW - rain water, AR - acid rain, SW - sea water, SW-AR - sea water /acid rain mixture)

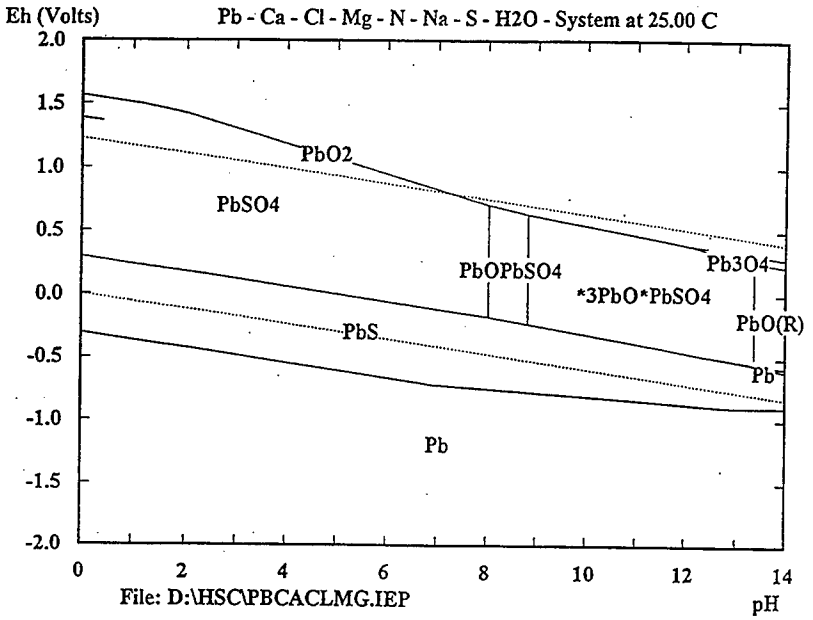

	Molality m mol / kg		Pressure p bar
Ca	9.600E-03	Ca	1.000E+00
Cl	1.690E-02	Cl	1.000E+00
Mg	7.800E-03	Mg	1.000E+00
N	1.900E-03	N	1.000E+00
Na	2.150E-02	Na	1.000E+00
S	1.500E-02	S	1.000E+00
Pb	1.000E+00	Pb	1.000E+00

Figure 18 Pourbaix Diagram for Lead Inmersed in Acid Rain Pore Water Leachate.

Table 1. Corrosion Products According to Pourbaix Diagrams for Lead and Copper in Different Environments.

Environment	E (mV vs. SCE)	Corrosion Product
NA	-1000 to 0	Cu is stable
NA	-1000 to -342	Pb is stable
NA	-342 to 0	Pb (II)
AR	-1000 to -542	Cu is stable
AR	-542 to -142	Cu_2S
AR	-142 to 0	CuCl
AR	-542 to -42	Cu (II)
AR	-42 to 0	Cu (I)
AR	-1000 to -642	Pb is stable
AR	-642 to -142	PbS
AR	-142 to 0	$Pb\ SO_4$
AR	-642 to 0	Pb (II)
RW	-1000 to -642	Cu is stable
RW	-642 to -242	Cu_2S
RW	-242 to -42	CuCl
RW	-42 to 0	Cu_2O
RW	-642 to -42	Cu (II)
RW	-42 to 0	Cu (I)
RW	-1000 to -692	Pb is stable
RW	-692 to -242	PbS
RW	-242 to 0	$PbOPbSO_4$
RW	-692 to 0	$Pb_4\ (OH)_4$ (IV)
SW	-1000 to -842	Cu is stable
SW	-842 to -492	$Cu_2\ S$
SW	-492 to -142	CuS
SW	-142 to 0	CuCl
SW	-842 to 0	Cu(I)
SW	-1000 to -942	Pb is stable
SW	-942 to -242	PbS
SW	-242 to 0	$Pb\ CO_3$

NA- 0.1 M nitric acid, AR- acid rain , RW- rain water, and SW-sea water

also, as would be expected. Ic of the saturated compared to 15% moisture condition was at least doubled for all the soil electrolytes examined.

The soil resistance would be expected to decline as the concentration of dissolved substances increased, due to the increasing contribution of the salts to environmental conductivity. This pattern was observed for the 15% moisture content, see Figure 8. From most resistive to least resistive, the soil electrolytes ranked: rain water, acid rain, sea water/acid rain, and sea water. Under saturated conditions, this same pattern was basically repeated, although the acid rain environment was anomalously higher than the rain water. This could possibly be due to random variations resulting from the relatively small number of measurements conducted here. Perhaps, too, in some cases, the contact with the soil along the surface of the graphite counter electrodes was poor in some of the tests with an acid rain environment, leading to higher resistance. Figure 9 shows that, except for the acid rain anomaly mentioned above, as the soil becomes more moist, its resistance drops precipitously.

Since some of the same variables that decrease soil resistance increase Ic, the relation between Ro and Ic is of interest. It is well known that for steel pipelines, soils of decreased resistivity are highly corrosive. Figure 10 shows the Ic values that we have measured here plotted versus the measured soil resistance values. For bullets in soil, it appears that a similar relation between Ic and Ro exists as for steel. Below about 15,000 ohms, over 70% of the Ic values exceeded 250 microamps. Of the 11 specimens in more highly resistive soils (above 15,000 ohms), not one sample had an Ic value exceeding 250 microamps. This is an important finding because it directly relates to field measurements. Soil resistivity can be readily measured under field conditions, and such measurements could serve, to a point, as a metric of the corrosivity of the soil.

Figure 11 shows that, at a given moisture content, the corrosion potentials in the various environments are rather similar. Also, there is not a consistent ranking of Ec between the two moisture contents, nor is there a pattern of Ec values that clearly seems related to the corrosivity of the environment. This is, to some degree, expected in that the corrosion current Ic is a much more direct measure of corrosion rate than Ec is. On the other hand, both Figures 11 and 12 clearly show that potential declines with increased moisture content. Interestingly, at 15% moisture content, Ec is near the expected corrosion potential of the copper cathode, if it were not galvanically coupled. On the other hand, at saturation, the Ec value of the bullet/jacket couple is near where the open circuit potential of lead would be expected to be. In terms of mixed potential theory for galvanic couples, this means that, in the drier soil, Ec is cathodically controlled, and in the wetter soil it is anodically controlled.

Figure 13 shows corrosion current Ic plotted versus corrosion potential Ec. This graph shows that Ec is not a good predictor of Ic, yet there is some relationship between the two. At potentials more noble than about -300 mV vs. SCE, less than 30% of the samples had an Ic value exceeding 250 microamps. Below -300 mV, on the other hand, almost 60% of the samples had Ic values greater than 250 microamps. This could also be a significant finding, in that potential is also a parameter relatively easily measured in the field.

The anodic Tafel slopes in Figures 14 and 15 range from about 300 to 1800 mV/decade. There is no clear pattern relating Ba to environmental corrosiveness or moisture content. The cathodic Tafel slopes shown in Figure 16 display a consistent ranking at both moisture contents- from highest to lowest: acid rain, rain water, sea water, sea water/acid rain. This ranking is not directly related to environmental corrosivity though. Figure 17 shows that Bc is lowered slightly as the moisture content increases. The range of Bc values observed was from about 300 to 1000 mV/decade. The value for an aqueous electrolyte with an electrode under charge transfer control is about 30-120 mV/decade. This means that, in these soil environments, there was a mass transport limitation for the cathodic reaction. The corrosion rate was thus under diffusion control.

The Pourbaix diagram results for the acid rain, rain water, and sea water environments shown in Table 1 indicate that basically the same corrosion products form in each case, although the potential range of stability varies somewhat for each environment. For Cu from lower to higher potentials, sulfides, chlorides

and oxides are stable. For Pb, sulfides are formed at lower potentials, and sulfates, carbonates and oxides are formed at higher potentials. Conceivably, soil or other field treatments might be devised which could form the more noble potential phases on the bullet surfaces. The inference from Figure 13 is that corrosion rate would be lowered in this manner. This strategy would have to be very carefully verified in the laboratory in long term tests and in actual pilot studies in the field, before it could be shown to be a practical means for lowering the rate of corrosion of bullets in the field.

RECOMMENDATIONS FOR FURTHER RESEARCH

This research project has revealed many possible avenues for future research activities to produce more knowledge regarding corrosion of bullets in soil. These are delineated in this section. The areas for future research fall into several categories: correlations between electrochemical and weight loss measurements, soil metal content analysis, soil corrosivity parameters, effects of soil chemistry on corrosion, corrosion mechanisms, field studies, soil treatment, and publications. These are discussed below.

Correlations between Electrochemical and Weight Loss Measurements

1. Chronoamperometric experiments should be conducted to test the applicability of Faraday's law to the corrosion of bullets. Faraday's law relates weight loss due to corrosion W to time t:

$$W=k*(Iave)*t \qquad (2)$$

where Iave is the average corrosion current during the interval, and k is the electrochemical equivalent. In a chronoamperometric experiment, a programmed corrosion current is selected, and the potentiostat applies the appropriate potential to achieve the current. Since high currents on the order of 1 amp can be selected, this represents a much accelerated test compared to free corrosion. It thus provides a rapid means of correlating electrochemical measures of corrosion with those from weight loss tests.

2. The electrochemical methodology developed in this project should be used to track Ic behavior in soil over the same time intervals as used in the weight loss tests (3 and 6 months). Assuming that a good correlation was observed in 1 above, integrating the current measured over time to get an average value of current will allow electrochemically predicted weight loss to be compared with the gravimetric value.

3. The 3 and 6 month weight loss experiments should be completed. The data should be analyzed to predict average corrosion rates for the various soil electrolyte and moisture conditions simulated. Where possible corrosion product observations and chemical analysis should be made.

4. The experimental protocol developed here should be used to study the complete range of soil conditions being tested in the weight loss experiments. This will allow full study of the correlation between electrochemically measured corrosion rates and those determined by weight loss measurements in 3 above.

5. Although a low leak rate KCl salt bridge was used for the tests conducted here, a salt bridge filled with KNO3 should probably be used for the conduct of repeated measurements over time in the same soil chamber. This will minimize the gradual introduction of corrosive chlorides into the soil.

Soil Metal Content Analysis

6. The soil loading of bullet metals after corrosion has occurred in weight loss experiments should be measured. These experiments may serve two purposes. First if the chemical analyses of the metals are conducted in such a manner as to reveal concentration gradients spatially, some insight into the rate of transport of metals away from the direct site of the bullet corrosion may be achieved. This would be an extremely important consideration in evaluating the hazards in the field that are being created by bullet corrosion. Secondly by measuring the contents of copper, antimony, lead, etc. in the soil, this would help to get insight into 1) whether galvanic effects are significant (leading to the corrosion of one alloy,

presumably lead, predominating over the other) and 2) whether selective leaching is occurring. Selective leaching is the dissolution of alloying elements in a metal in amounts greater than their composition in the bulk alloy. Thus soil metal content analysis would help to gain understanding of the corrosion mechanisms involved in bullet corrosion.

Soil Corrosivity Parameters

7. Besides moisture content, which has been tested in this investigation to a certain extent, a number of other variables (1),(2),(4),(7), (10),(21),(22) have been shown to be implicated in the corrosion of metallic structures in soil, e.g. pH, resistivity, and redox potential. The results of the present investigation, where resistance of the soil rather than its resistivity has been determined, give a strong suggestion that a correlation will be found between bullet corrosion rates and soil resistivity (since the latter can be expected to strongly depend on soil moisture and salt content). The redox potential differentiates between aerobic and anaerobic soil conditions. The latter support the activity of sulfate reducing bacteria (e.g., Desulfovibrio desulfuricans) that are known to affect the corrosion of metals in soils. Fungi have also been reported to be corrosive to lead(23). The following soil parameters: pH, resistivity, and redox potential should be measured in the environments that we employed in the present testing program in order to further characterize aspects of the environments that may be related to corrosion rate. These measurements should follow applicable ASTM standards, e. g. (24)-(25), if they are available. An important motivation for studying this topic is that these parameters can readily be measured in field environments.

8. For the same reason, the parameters mentioned in 7 above should also be measured in the full range of environments presently being studied in the weight loss tests. This will allow correlations between soil corrosiveness for bullets and pH, soil resistivity, and redox potential, if they exist, to be determined. This will ultimately help in assessing the possibility of corrosion at field sites.

Effects of Soil Chemistry on Corrosion

9. Soil chemistry, particularly that of pore water, can also have a substantial influence on the corrosivity of soil. Carbonates, chlorides, sulfates, and sulfides have been identified as being particularly important. To characterize pore water chemistry, pore water should be removed by centrifugation, vacuum filtration or other suitable methods. The chloride, sulfide, sulfate, carbonate, and nitrate contents of the environments that were used in this summer testing program should be measured. These measurements should follow standard analytical techniques employed for these purposes. Correlations should be sought between the corrosion rates that have been measured in this project and the salt content of the pore water.

10. The soil chemistry parameters mentioned in 9 above also should be measured for the full range of conditions being used in the weight loss tests, in order to obtain a better understanding of the influence of soil chemistry on and its correlation with bullet corrosion.

11. New Pourbaix diagrams based on the salt contents measured in 9 and 10 should be calculated. This may help to identify pH and chemical concentration conditions which protect against corrosion. In turn this may help in the development of methods of soil treatment to ameliorate the problems associated with bullet corrosion.

Corrosion Mechanisms

12. Studies of corrosion mechanisms, particularly using AC impedance methods, should be pursued. For example, these will allow determination of the degree to which charge transfer and diffusion control are involved in the corrosion of bullets in the soil. The influence of the crevice that may exist between the copper and lead portions of the bullet may be ascertained. Also, the impact of galvanic corrosion on the behavior of bullets in the soil can be found.

13. The corrosion of armor piercing projectiles was not addressed in this investigation. The three metal galvanic corrosion problem in such projectiles should be studied using electrochemical and weight loss techniques.

Field Studies

14. Field surveys of the variables that have been found in the above testing to be related to bullet corrosion should be conducted. These may include soil potential surveys and measurement of soil properties such as resistivity, redox potential, and pH. This will allow sites where bullet corrosion is most severe to be identified.

15. To verify the predictions in 14 above, metal contents of soil field samples should be measured. Care should be taken to do such tests at firing ranges where the time history of usage of the area is known. This should be done because, without such information, metal transport processes through the soil away from the bullets would be a confounding variable.

Chemical Treatment

16. Investigations of chemical treatment strategies to make the soil less corrosive should be carried out. These should be based on E-pH analyses and other chemical stability and speciation considerations. In developing such strategies, the amphoteric nature of lead should be kept in mind. Lead is attacked by both acidic and basic environments (26). Minimum attack occurs in the pH 5-10 range. Such studies should have both a laboratory simulation component and, for promising strategies, a field testing component.

Equipment Purchases

Several pieces of equipment should be purchased to assist this project to proceed:

17. The M352 software package available from EG&G Princeton Applied Research Corporation should be bought for reasons which have been described in an earlier section of this report.

18. A soil resistivity meter that can be employed for measuring at field sites should be purchased because this research project has shown that this parameter is probably a good predictor for soil corrosivity to bullets. The Terrameter SAS 300C (from Terraplus) and the Sting R1 (from Advanced Geosciences, Inc.) appear suitable for this purpose.

19. An electrometer or other device suitable for measuring potentials in the field should be purchased.

Publications

20. A paper based on this research project should be prepared and submitted to an archival environmental journal.

CONCLUSION

The project conducted here has been concerned with measuring the rates of corrosion of bullets in soil under a range of conditions. The utility of electrochemical techniques for this purpose has been validated in this investigation. Corrosion current Ic was found to be very sensitive to the soil environmental conditions. The corrosion rate was seen to increase as pH decreased and as moisture and chloride contents increased. The most influential of these parameters on soil corrosivity for bullets was seen to be the chloride content. Ic was also seen to be related to soil resistance and free corrosion potential. High resistance and noble values of potential are associated with low rates of corrosion. Conversely highly conductive soils and those

where Ec is lower foster high rates of corrosion. These findings are important because both soil resistivity and potential can be straightforwardly measured under field conditions.

Pourbaix diagram calculations were conducted in this work, and the results suggest that surface or soil treatments might be devised to lower the rate of corrosion of bullets in soil. This approach would have to be very carefully validated in laboratory and field experiments before it could be put into routine use. This project has spawned several recommendation for future research in various areas to give further insight into bullet corrosion and to correlate the results of electrochemical and weight loss measurement approaches to corrosion testing. These include both laboratory and field experiments. The tests proposed involve corrosion measurements, soil metal content and dissolved salt analysis, measurement of soil corrosivity parameters, studies of mechanisms of bullet corrosion, and the investigation of soil treatments. Through use of electrochemical testing techniques in association with weight loss measurements, chemical analyses of soils, and other types of soil measurements, it is hoped that further insight into the problems associated with bullet corrosion and how to prevent or minimize it can be obtained.

REFERENCES

1. J. D. Palmer, "Environmental Characteristics Controlling the Soil Corrosion of Ferrous Piping," in Effects of Soil Characteristics on Corrosion, ASTM STP 1013, V. Chaker and J. D. Palmer, Eds., American Society for Testing and Materials, Phil., 1989, pp. 5-17.

2. E. Escalante, "Measuring the Corrosion of Metals in Soil," in Corrosion Testing and Evaluation: Silver Anniversary Volume, ASTM STP 1000, R. Baboian and S. W. Dean, Eds., American Society for Testing and Materials, Phil., 1990, pp. 112-124.

3. J. R. Scully and K. J. Bundy, Electrochemical Methods for Measurement of Pipe Steel Corrosion Rates in Soil," Materials Performance, 24(4), 1985, pp. 18-25.

4. V. Chaker, "Corrosion Testing in Soils- Past, Present, and Future," in Corrosion Testing and Evaluation: Silver Anniversary Volume, ASTM STP 1000, R. Baboian and S. W. Dean, Eds., American Society for Testing and Materials, Phil., 1990, pp. 95-111

5. J. L. Pintado and F. Montero, Underground Biodeterioration of Medium Tension Electrical Cables," Int. Biodeterioration and Biodegradation, 29, 1992, pp. 357-365.

6. K. G. Compton, "Mechanisms in the Underground Corrosion of the Concentric Neutral of URD Cable," Materials Performance, 20(3), 1981, pp. 15-19.

7. K. E. Sawyer, "Some Fundamentals of Lead Cable Corrosion," in Proc. 4th Ann. Appalachian Underground Corrosion Short Course, R. E. Hanna, Ed., Tech. Bull. 56, West Va. U., 1959, pp. 171-187.

8. M. Romanoff, Underground Corrosion, NBS Circular 579, U. S. Government Printing Office, Washington D. C., 1957.

9. W. G. von Baeckmann, "Kathodishe Korrosion von Blei im Erdboden," Werkstoffe und Korrosion, 20(7), 1969, pp. 578-583.

10. G. H. Booth, A. W. Cooper, and A. K. Tiller, "Criteria of Soil Aggressiveness Towards Buried Metals, III. Verification of Predicted Behaviour of Selected Soils, " Brit. Corr. J., 2(3), 1967, pp. 116-118.

11. J. R. Devine, "A Review of the Hanford Site Soil Corrosion Applicable to Solid Waste Containers," U. S. DOE Office of Environmental Restoration and Waste Management, WHC-EP-0408, DE91017742, 1991.

12. C. M. Case, J. O. Davis, J. C. Heidker, and M. R. Whitbeck, "Studies of Infiltration and Lead-Soil Interactions at the Radioactive Waste Management Site in Area 5 of the Nevada Test Site," U. S. DOE Nevada Field Office, DOE/NV/10384-13, DE 93 002867, 1992.

13. S. Shimodaira, K. Hashimoto, S. Mijahara, and T. Matsui, "Stress Corrosion Cracking of Fired Bullets of Brass," Corr. Eng., 16(6), 1967, pp. 119-25.

14. J. E. Bridge and F. P. Fairchild, Northeast Damage Report of the Long Range Transport and Deposition of Air Pollutants, Northeast Regional Task Force on Atmospheric Deposition, A8420997A, 1981.

15. F. A. Record, D. V. Bubenick, and R. J. Kindja, Acid Rain Information Book, Noyes Data Corp., Park Ridge, NJ, 1982.

16. M. Freemantle, "The Acid Test for Europe," Chemical and Engineering News, May 1, 1995, pp. 10-17.

17. H. H. Lawson, Outdoor Atmospheres, Chapter 28 in Corrosion Tests and Standards: Applications and Interpretations, R. Baboian, Ed. , Manual MNL 20, ASTM, Phil., 1995, pp. 289-294.

18. C. M. Calhoun, "Basic Measuring Instruments and Their Application," Fundamentals of Underground Corrosion and Cathodic Protection, National Academy of Sciences- National Research Council, Washington, D.C., Publication 1097, 1963, pp. 13-30.

19. D. Carroll, Rainwater as a Chemical Agent of Geological Processes- a Review, Geological Survey Water Supply Paper 1535-G, U.S. Govt. Printing Office, Washington, D.C., 1962.

20. V. Chaker and J. D. Palmer, Eds., Effects of Soil Characteristics on Corrosion, ASTM STP 1013, American Society for Testing and Materials, Phil., 1989, p. 148.

21. E. Escalante, "Concepts of Underground Corrosion," in Effects of Soil Characteristics on Corrosion, V. Chaker and J. D. Palmer, Eds., ASTM STP 1013, American Society for Testing and Materials, Phil., 1989, pp. 81-94.

22. J. D. Palmer, "Field Soil Corrosivity Testing- Engineering Considerations," in Corrosion Testing and Evaluation: Silver Anniversary Volume, ASTM STP 1000, R. Baboian and S. W. Dean, Eds., American Society for Testing and Materials, Phil. , 1990, pp. 125-138.

23. S. M. Siegal, B. Z. Siegal, and K. E. Clark, "Bio-corrosion: Solubilization and Accumulation of Metals by Fungi," Water, Soil, and Air Pollution, 9, 1983, pp. 229-236.

24. Standard Test Method for Measuring pH of Soil for Use in Corrosion Testing, ASTM Standard G51-92.

25. Standard Method for Field Measurement of Soil Resistivity Using the Wenner Four-Electrode Method, ASTM Standard G57-78.

26. M. J. Schiff, "What is Corrosive Soil," 18th Western States Corrosion Seminar, May 1-3, 1984, Pomona, CA, NACE, 1984, pp. 33/1-33/8.

APPENDIX: Ic, Ec, Ro, Ba, and Bc Data for Various Soil Environments

Table A1.

Soil Resistivity Ro, Range of Corrosion Potential Ec, Corrosion Current Ic, and Tafel Slopes Ba and Bc for Various Soil Environments and Moisture Content

Specimen No.	Moisture Content	Environment	Ro (ohms)	Ec (mV vs. SCE)	Ic (μA)	Ba (mV/dec)	Bc (mV/dec)
1	15%	RW	23266	-55 to +14	34.09	449	420.2
2	15%	RW	76666.67	-303 to -220	14.2	481.4	584.8
3	15%	RW	70833	-298 to -288	19.41	992.4	615.5
4	15%	RW	119718.31	-273 to -265	71.86	598.9	782.0
1	saturated	RW	9189	-480 to -391	76.24	503.6	187.9
2	saturated	RW	36957	-520 to -462	175.7	949.2	637.2
3	saturated	RW	11184	-495 to -422	110.0	805.9	504.0
4	saturated	RW	1623.38	-525 to -446	71.86	807.8	526.2

RW- rain water, AR- acid rain, SW-AR - sea water/acid rain, SW- sea water

cont. Table A1

Specimen No.	Moisture Content	Environment	Ro (ohms)	Ec (mV vs. SCE)	Ic (μA)	Ba (mV/dec)	Bc (mV/dec)
1	15%	AR	5484	-550 to -358	92.03	5472.4	1468.7
2	15%	AR	34694	-268 to -197	3.93	458.5	669.6
3	15%	AR	2833	-425 to -392	74.65	922.0	672.2
4	15%	AR	20238.09	-250 to -164	24.01	651.9	1250.8
1	saturated	AR	3172	-600 to -421	634.42	941.7	154.4
2	saturated	AR	36,957	-610 to -437	91.17	588.8	465.4
3	saturated	AR	30,357	-520 to -439	99.74	973.1	792.8
4	saturated	AR	17,000	-525 to -446	87.67	1,117.4	865.2

RW- rain water, AR- acid rain, SW-AR - sea water/acid rain, SW- sea water

cont. Table A1

Specimen No.	Moisture Content	Environment	Ro (ohms)	Ec (mV vs. SCE)	Ic (μA)	Ba (mV/dec)	Bc (mV/dec)
1	15%	SW-AR	8500	-90 to -34	35.42	2719.2	253.8
2	15%	SW-AR	26,984	-105 to-92	144.9	270.2	468.7
3	15%	SW-AR	7203	-540 to-462	761.88	465.9	445.0
4	15%	SW-AR	7727.2	-472 to -222	464.06	1231.8	690.9
1	saturated	SW-AR	1635	-520 to -441	1075.55	347.2	295.5
2	saturated	SW-AR	3696	-475 to -297	907.7	339.1	314.0
3	saturated	SW-AR	1288	-488 to -477	1305.9	291.4	321.8
4	saturated	SW-AR	1847.8	-950 to -473	463.94	341.9	302.3

RW- rain water, AR- acid rain, SW-AR - sea water/acid rain, SW- sea water

cont. Table A1

Specimen No.	Moisture Content	Environment	Ro (ohms)	Ec (mV vs. SCE)	Ic (μA)	Ba (mV/dec)	Bc (mV/dec)
1	15%	SW	833	-400 to -142	1090.42	1760.9	383.3
2	15%	SW	2073	-450 to -127	383.0	259.8	241.9
3	15%	SW	14655	-430 to -352	932.11	700.7	569.7
4	15%	SW	2428.5	-170 to -125	703.87	242.8	717.8
1	saturated	SW	224	-750 to -227	2253.78	657.4	320.4
2	saturated	SW	43.6	-700 to -397	2443.7	497.3	620.8
3	saturated	SW	274	-1497 to -471	2157.6	454.7	454.7
4	saturated	SW	2023.8	-1040 to -484	270.15	499.5	207.3

Table A2

Corrosion Potentials (mV vs. SCE)Measured by Different Methods for Various Soil Environments and Moisture Contents

Specimen No.	Moisture Content	Environment	Ec vs. t (mV vs. SCE)	LPSG(mV/SCE)	PDP (mV/SCE)
1	15%	RW	-55 to -50	+14	+5.0
2	15%	RW	-303 to -296	-240	-220
3	15%	RW	-298 to -292	-288	-293
4	15%	RW	-271 to -268	-273	-265
1	saturated	RW	-224 to -416	-391	-480
2	saturated	RW	-470	-462	-520
3	saturated	RW	-428 to -422	-433	-495
4	saturated	RW	-396 to -385	-407	-480

RW- rain water, AR- acid rain, SW-AR - sea water/acid rain, SW- sea water
Ec vs. t - corrosion potential versus time
LPSG - linear polarization / Stern Geary method
PDP - low current spike on potentiodynamic polarization curve

Table A3

Corrosion Current (μ A) Measured by Different Methods for Various Soil Environments and Moisture Contents.

Specimen No.	Moisture Content	Environment	LPSG(μA)	ATE (μA)	CTE (μA)
1	15%	RW	31.247	23.714	47.315
2	15%	RW	12.51	1080	19.20
3	15%	RW	22.23	17.78	18.23
4	15%	RW	7.48	4.69	12.36
1	saturated	RW	98.65	50.12	79.94
2	saturated	RW	203.89	206.91	116.36
3	saturated	RW	161.92	96.47	71.48
4	saturated	RW	85.34	81.85	48.39

RW- rain water, AR- acid rain, SW-AR - sea water/acid rain, SW- sea water
LPSG- linear polarization/Stern Geary Method
CTE- cathodic Tafel extrapolation
ATE - anodic Tafel Extrapolation

cont. Table A3:

Specimen No.	Moisture Content	Environment	LPSG(μA)	ATE (μA)	CTE (μA)
1	15%	AR	115.64	74.99	85.47
2	15%	AR	3.98	2.99	4.82
3	15%	AR	96.85	77.92	49.17
4	15%	AR	11.15	9.47	51.40
1	saturated	AR	1653.50	168.53	78.22
2	saturated	AR	161.05	56.23	56.23
3	saturated	AR	114.16	110.07	74.99
4	saturated	AR	79.72	110.07	73.21

RW- rain water, AR- acid rain, SW-AR - sea water/acid rain, SW- sea water
LPSG- linear polarization/Stern Geary Method
CTE- cathodic Tafel extrapolation
ATE - anodic Tafel Extrapolation

cont. Table A3:

Specimen No.	Moisture Content	Environment	LPSG(μA)	ATE (μA)	CTE (μA)
1	15%	SW-AR	25.32	54.56	26.37
2	15%	SW-AR	94.43	155.48	184.78
3	15%	SW-AR	1264.65	653.53	367.47
4	15%	SW-AR	372.59	261.02	758.58
1	saturated	SW-AR	1009.83	1216.82	1000
2	saturated	SW-AR	255.18	1000	1467.80
3	saturated	SW-AR	1619.69	859.43	1438.45
4	saturated	SW-AR	578.99	606.19	206.64

RW- rain water, AR- acid rain, SW-AR - sea water/acid rain, SW- sea water
LPSG- linear polarization/Stern Geary Method
CTE- cathodic Tafel extrapolation
ATE - anodic Tafel Extrapolation

cont. Table A3:

Specimen No.	Moisture Content	Environment	LPSG(μA)	ATE (μA)	CTE (μA)
1	15%	SW	2639.97	380.19	251.19
2	15%	SW	830.61	187.80	130.55
3	15%	SW	556.31	1077.98	1162.03
4	15%	SW	978	240.12	893.48
1	saturated	SW	3121.42	1980.34	1659.59
2	saturated	SW	164.4.47	3082.40	4084.24
3	saturated	SW	3040.76	1301.03	2130.34
4	saturated	SW	525.5	157.53	127.43

RW- rain water, AR- acid rain, SW-AR - sea water/acid rain, SW- sea water
LPSG- linear polarization/Stern Geary Method
CTE- cathodic Tafel extrapolation
ATE - anodic Tafel Extrapolation

Appendix E
Model Calculations

First Run

First Run

L = 90 ft

D_p = 0.28 ft^2/day

V = 0.28 ft/day

R = 4 ← estimate

R = 1 + (ς/Θ) kd — Source: Perry's Handbook for Chem "E"

ς = sand = 2.2 sg. = 144 lb/ft^3

clay = 1.5 sg. = 95 lb/ft^3

I'll use an estimate of 100 lb/ft^3

Θ = loess = 0.40 - 0.5 — Source: Perry's Handbook for Chem "E"

sand = 0.3 - 0.5

limestone = 0.2 - 0.5

I'll use an estimate of 0.4 = Θ

Kd for Pb = 4.5 - 7,640 — Source: Myers "Estimating Contaminant Losses From Components of Soils" 1995, pg B:9

I'll use an estimate of 10 mℓ/g - 100 mℓ/g this give an R ≅ 4

Permeability = 2.0 in/hr USDA Soil Survey

(2.0 in/hr) (2.54 cm/in) (1 hr/60 min) (1 min/60 sec) = 1.4×10^{-3} cm/sec
= Sand Materials

$R = 1 + (\varsigma/\Theta)\, kd$

$\Theta = 0.4$

$\varsigma = 1.55\ g/cm^3$

$R = 1 + (1.55/0.4)\,(kd)$

@ kd	R	
1	4.8	Use R at 4-40
10	39.8	
100	388.5	

Now Run Model
Under saturated conditions the model predicts breakthrough

at m = 15 this is = 1500 days

Using 12 days of rain, we get

(1500 days) (12/365) = 45,625 days ≅ 125 years

Use 125 days till breakthrough

To calculate concentration at breakthrough

Assume $PbCO_3$ $PbSO_4$ = Species
PbO_2 PbO_2

We'll use the most mobile function @ 0.99 g/100$\mu\ell$ solubility

(0.99 g/100 mℓ) (1000 mℓ/1 ℓ) (1000 mg/g) (1 ℓ/1 kg) = 9.900 mg/ℓ

Least soluble fraction solubility is:

(0.00011 g/100 cc) (1000 mℓ/1 ℓ) (1000 mg/1 g) = 1.1 ppm

Use Figure off graph = 0.85 = C/CO

I'll assume the Pb in the porewater is ≅ 9.9 ppm or high, rounding up we get 10 ppm of lead which is resolvabilized in the pore water.

Conc =
(10 ppm) (0.85) = 8.5 ppm's

FINITE LENGTH MODEL (CLEARY AND ADRIAN (1973) AS CITED BY Van GENUCHTEN AND AVES (1982.). BREAKTHROUGH CURVE MODEL

Eignevalues

Velocity is numerically equal to dispersion

$L := 2743 \cdot cm$ <-- Cap thickness 90ft

$D_p := 0.28 \cdot \frac{ft^2}{day}$ Dispersion Coefficient $L = 89.993 \cdot ft$

$v := 0.28 \cdot \frac{ft}{day}$ Average Pore Water Velocity

$R := 4$ <— Lead Retardation Factor (assumed)

$m := 7 .. 15$

$t := 100 \cdot day$ < – Time Index (days)

$T_m := m \cdot t$

$$E_m := 1 - erf\left(\frac{R \cdot L - v \cdot T_m}{\sqrt{4 \cdot D_p \cdot R \cdot T_m}}\right)$$

$A_m := \frac{1}{2} \cdot E_m$

$$E = \begin{bmatrix} 0 \\ 0 \\ 0 \\ 0 \\ 0 \\ 0 \\ 3.459 \cdot 10^{-5} \\ 0.001 \\ 0.016 \\ 0.091 \\ 0.295 \\ 0.644 \\ 1.059 \\ 1.433 \\ 1.7 \end{bmatrix}$$

$C_m := A_m$ <-- Dimensionless concentration

$$T = \begin{bmatrix} 0 \\ 0 \\ 0 \\ 0 \\ 0 \\ 0 \\ 6.048 \cdot 10^{7} \\ 6.912 \cdot 10^{7} \\ 7.776 \cdot 10^{7} \\ 8.64 \cdot 10^{7} \\ 9.504 \cdot 10^{7} \\ 1.037 \cdot 10^{8} \\ 1.123 \cdot 10^{8} \\ 1.21 \cdot 10^{8} \\ 1.296 \cdot 10^{8} \end{bmatrix} \cdot \text{time}$$

	C_m
7	$1.729 \cdot 10^{-5}$
8	$6.589 \cdot 10^{-4}$
9	0.008
10	0.046
11	0.148
12	0.322
13	0.53
14	0.716
15	0.85

A-D Breakthrough Curve:

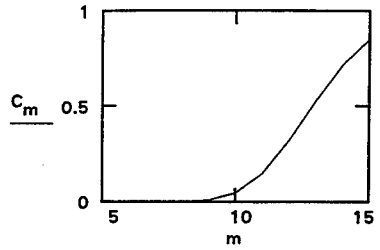

Fig 1

M = 10

T = 1000 days 3,9 years

Second Run

a. Tune model so we get breakthrough @ 10 ft in 50 years (the life of ranges)

Use L = ?ft

DP = 0.28 ft^2/day

V = 0.28 ft/day hydraulic conductivity = 0.01

R = ?

t = 50

By trial and error

@ R = 50 L = 8 ft and hydraulic conductivity = 0.01

See Figure 2

Rerun using these parameters gives Figure 3, where breakthrough occurs in 300 years

SEMIINFINITE MODEL (van GENUCHTEN AND AVES 1982.). BREAKTHROUGH CURVE PREDICTIONS

$L := 2743 \cdot cm$ $L = 89.993 \cdot ft$ <-- Distance to water table

Assume velocity is numerically equal to dispersion

$D_p := 0.028 \cdot \frac{ft^2}{day}$ Dispersion Coefficient

$v := 0.028 \cdot \frac{ft}{day}$ Average Pore Water Velocity

$v = 9.878 \cdot 10^{-6} \cdot \frac{cm}{sec}$ <-- 0.01 X hydraulic conductivity

$t := 50 \cdot yr$ <-- time period of analysis

$R := 50$ <-- Lead Retardation Factor (assumed)

$m := 1 .. 100$

$z_m := m \cdot 1 \cdot ft$

$$A_m := \left(1 - erf\left(\frac{R \cdot z_m - v \cdot t}{\sqrt{4 \cdot D_p \cdot R \cdot t}}\right)\right) + \exp\left(\frac{v \cdot z_m}{D_p}\right) \cdot \left(1 - erf\left(\frac{R \cdot z_m + v \cdot t}{\sqrt{4 \cdot D_p \cdot R \cdot t}}\right)\right)$$

$C_m := \frac{1}{2} \cdot A_m$ <-- Dimensionless concentration (C/C_o)

$tt_m := \frac{m \cdot 100}{365}$ <-- time in years } not needed

Breakthrough Curve
R=50
v=1X10^{-5} cm/sec:

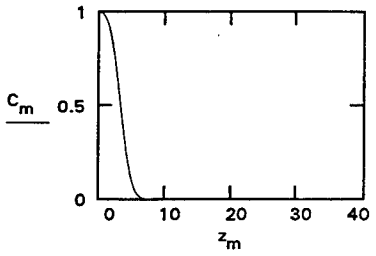

Fig 2

SEMIINFINITE MODEL (van GENUCHTEN AND AVES 1982.). BREAKTHROUGH CURVE PREDICTIONS

$L := 2743 \cdot cm$ $L = 89.993 \cdot ft$ <-- Distance to water table

Assume velocity is numerically equal to dispersion

$D_p := 0.028 \cdot \frac{ft^2}{day}$ Dispersion Coefficient

$v := 0.028 \cdot \frac{ft}{day}$ Average Pore Water Velocity

$v = 9.878 \cdot 10^{-6} \cdot \frac{cm}{sec}$ <-- 0.01 X hydraulic conductivity

$R := 50$ <-- Lead Retardation Factor (assumed)

$m := 800, 850 .. 2400$

$t := 100 \cdot day$ <-- Time Index (days)

$T_m := m \cdot t$

$$A_m := \left(1 - \operatorname{erf}\left(\frac{R \cdot L - v \cdot T_m}{\sqrt{4 \cdot D_p \cdot R \cdot T_m}}\right)\right) + \exp\left(\frac{v \cdot L}{D_p}\right) \cdot \left(1 - \operatorname{erf}\left(\frac{R \cdot L + v \cdot T_m}{\sqrt{4 \cdot D_p \cdot R \cdot T_m}}\right)\right)$$

$C_m := \frac{1}{2} \cdot A_m$ <-- Dimensionless concentration (C/C_0)

$tt_m := \frac{m \cdot 100}{365}$ <-- time in years

Breakthrough Curve
R=10
v=1X10^{-5} cm/sec:

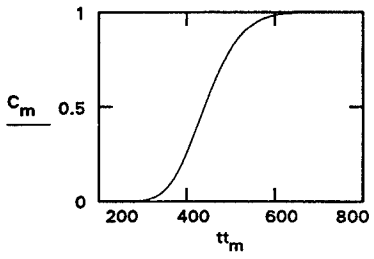

Fig 3

Other Calculations

SEMIINFINITE MODEL (van GENUCHTEN AND AVES 1982.). BREAKTHROUGH CURVE PREDICTIONS

$L := 2743 \cdot cm$ $L = 89.993 \cdot ft$ <-- Distance to water table

Assume velocity is numerically equal to dispersion

$D_p := 0.28 \cdot \frac{ft^2}{day}$ Dispersion Coefficient

$v := 0.28 \cdot \frac{ft}{day}$ Average Pore Water Velocity

$v = 9.878 \cdot 10^{-5} \cdot \frac{cm}{sec}$ <-- 0.1 X hydraulic conductivi

$R := 10$ <— Lead Retardation Factor (assumed)

$m := 15 .. 45$

$t := 100 \cdot day$ < -- Time Index (days)

$T_m := m \cdot t$

$$A_m := \left(1 - \operatorname{erf}\left(\frac{R \cdot L - v \cdot T_m}{\sqrt{4 \cdot D_p \cdot R \cdot T_m}}\right)\right) + \exp\left(\frac{v \cdot L}{D_p}\right) \cdot \left(1 - \operatorname{erf}\left(\frac{R \cdot L + v \cdot T_m}{\sqrt{4 \cdot D_p \cdot R \cdot T_m}}\right)\right)$$

$C_m := \frac{1}{2} \cdot A_m$ <-- Dimensionless concentration (C/C_o)

$tt_m := \frac{m \cdot 100}{365}$ <-- time in years

Breakthrough Curve
R=10
$v = 1X10^{-4}$ cm/sec:

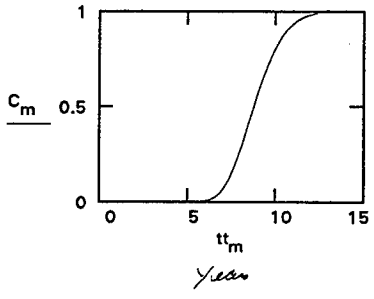

SEMIINFINITE MODEL (van GENUCHTEN AND AVES 1982.). BREAKTHROUGH CURVE PREDICTIONS

$L := 2743 \cdot cm$ $L = 89.993 \cdot ft$ <-- Distance to water table

Assume velocity is numerically equal to dispersion

$D_p := 0.028 \cdot \frac{ft^2}{day}$ Dispersion Coefficient

$v := 0.028 \cdot \frac{ft}{day}$ Average Pore Water Velocity

$v = 9.878 \cdot 10^{-6} \cdot \frac{cm}{sec}$ <-- 0.01 X hydraulic conductivi

$R := 10$ <-- Lead Retardation Factor (assumed)

$m := 50, 60 .. 500$

$t := 100 \cdot day$ <-- Time Index (days)

$T_m := m \cdot t$

$$A_m := \left(1 - erf\left(\frac{R \cdot L - v \cdot T_m}{\sqrt{4 \cdot D_p \cdot R \cdot T_m}}\right)\right) + \exp\left(\frac{v \cdot L}{D_p}\right) \cdot \left(1 - erf\left(\frac{R \cdot L + v \cdot T_m}{\sqrt{4 \cdot D_p \cdot R \cdot T_m}}\right)\right)$$

$C_m := \frac{1}{2} \cdot A_m$ <-- Dimensionless concentration (C/C_o)

$tt_m := \frac{m \cdot 100}{365}$ <-- time in years

Breakthrough Curve
R=10
v=1X10^{-5} cm/sec:

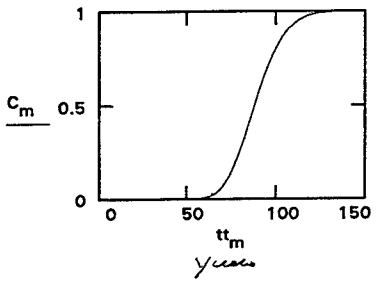

SEMIINFINITE MODEL (van GENUCHTEN AND AVES 1982.). BREAKTHROUGH CURVE PREDICTIONS

$L := 2743 \cdot cm$ $L = 89.993 \cdot ft$ <-- Distance to water table

Assume velocity is numerically equal to dispersion

$D_p := 0.28 \cdot \frac{ft^2}{day}$ Dispersion Coefficient

$v := 0.28 \cdot \frac{ft}{day}$ Average Pore Water Velocity

$v = 9.878 \cdot 10^{-5} \cdot \frac{cm}{sec}$ <-- 0.1 X hydraulic conductivi

$R := 15$ <-- Lead Retardation Factor (assumed)

$m := 20 .. 70$

$t := 100 \cdot day$ < -- Time Index (days)

$T_m := m \cdot t$

$$A_m := \left(1 - erf\left(\frac{R \cdot L - v \cdot T_m}{\sqrt{4 \cdot D_p \cdot R \cdot T_m}}\right)\right) + \exp\left(\frac{v \cdot L}{D_p}\right) \cdot \left(1 - erf\left(\frac{R \cdot L + v \cdot T_m}{\sqrt{4 \cdot D_p \cdot R \cdot T_m}}\right)\right)$$

$C_m := \frac{1}{2} \cdot A_m$ <-- Dimensionless concentration (C/C_o)

$tt_m := \frac{m \cdot 100}{365}$ <-- time in years

Breakthrough Curve
R=15
$v = 1X10^{-4}$ cm/sec:

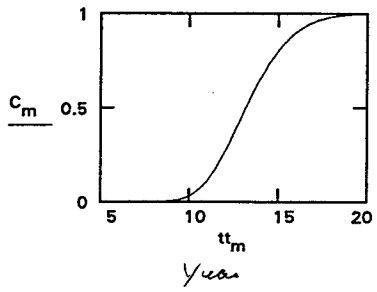

SEMIINFINITE MODEL (van GENUCHTEN AND AVES 1982.). BREAKTHROUGH CURVE PREDICTIONS

$L := 2743 \cdot cm$ $L = 89.993 \cdot ft$ <-- Distance to water table

Assume velocity is numerically equal to dispersion

$D_p := 0.028 \cdot \frac{ft^2}{day}$ Dispersion Coefficient

$v := 0.028 \cdot \frac{ft}{day}$ Average Pore Water Velocity

$v = 9.878 \cdot 10^{-6} \cdot \frac{cm}{sec}$ <-- 0.01 X hydraulic conductivi

$R := 15$ <-- Lead Retardation Factor (assumed)

$m := 100, 110 .. 800$

$t := 100 \cdot day$ < -- Time Index (days)

$T_m := m \cdot t$

$$A_m := \left(1 - erf\left(\frac{R \cdot L - v \cdot T_m}{\sqrt{4 \cdot D_p \cdot R \cdot T_m}}\right)\right) + \exp\left(\frac{v \cdot L}{D_p}\right) \cdot \left(1 - erf\left(\frac{R \cdot L + v \cdot T_m}{\sqrt{4 \cdot D_p \cdot R \cdot T_m}}\right)\right)$$

$C_m := \frac{1}{2} \cdot A_m$ <-- Dimensionless concentration (C/C_0)

$tt_m := \frac{m \cdot 100}{365}$ <-- time in years

Breakthrough Curve
R=15
v=1X10^{-5} cm/sec:

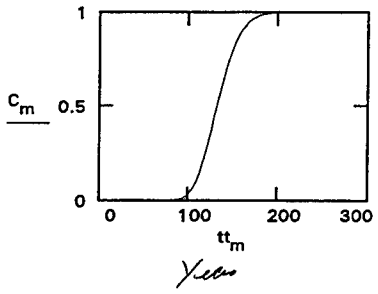

SEMIINFINITE MODEL (van GENUCHTEN AND AVES 1982.). BREAKTHROUGH CURVE PREDICTIONS

$L := 2743 \cdot cm$ $L = 89.993 \cdot ft$ <-- Distance to water table

Assume velocity is numerically equal to dispersion

$D_p := 0.28 \cdot \frac{ft^2}{day}$ Dispersion Coefficient

$v := 0.28 \cdot \frac{ft}{day}$ Average Pore Water Velocity

$v = 9.878 \cdot 10^{-5} \cdot \frac{cm}{sec}$ <-- 0.1 X hydraulic conductivit

$R := 20$ <-- Lead Retardation Factor (assumed)

$m := 30 .. 100$

$t := 100 \cdot day$ < -- Time Index (days)

$T_m := m \cdot t$

$$A_m := \left(1 - \operatorname{erf}\left(\frac{R \cdot L - v \cdot T_m}{\sqrt{4 \cdot D_p \cdot R \cdot T_m}}\right)\right) + \exp\left(\frac{v \cdot L}{D_p}\right) \cdot \left(1 - \operatorname{erf}\left(\frac{R \cdot L + v \cdot T_m}{\sqrt{4 \cdot D_p \cdot R \cdot T_m}}\right)\right)$$

$C_m := \frac{1}{2} \cdot A_m$ <-- Dimensionless concentration (C/C_0)

$tt_m := \frac{m \cdot 100}{365}$ <-- time in years

Breakthrough Curve
R=20
v=1X10^{-4} cm/sec:

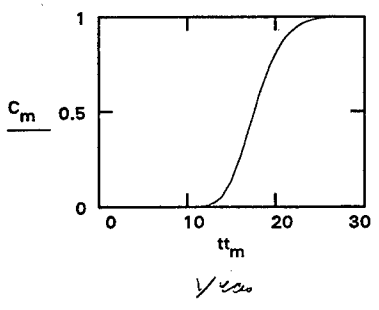

SEMIINFINITE MODEL (van GENUCHTEN AND AVES 1982.). BREAKTHROUGH CURVE PREDICTIONS

$L := 2743 \cdot cm$ $L = 89.993 \cdot ft$ <-- Distance to water table

Assume velocity is numerically equal to dispersion

$D_p := 0.028 \cdot \frac{ft^2}{day}$ Dispersion Coefficient

$v := 0.028 \cdot \frac{ft}{day}$ Average Pore Water Velocity

$v = 9.878 \cdot 10^{-6} \cdot \frac{cm}{sec}$ <-- 0.01 X hydraulic conductivit

$R := 20$ <— Lead Retardation Factor (assumed)

$m := 100, 110 .. 1000$

$t := 100 \cdot day$ < -- Time Index (days)

$T_m := m \cdot t$

$$A_m := \left(1 - erf\left(\frac{R \cdot L - v \cdot T_m}{\sqrt{4 \cdot D_p \cdot R \cdot T_m}}\right)\right) + \exp\left(\frac{v \cdot L}{D_p}\right) \cdot \left(1 - erf\left(\frac{R \cdot L + v \cdot T_m}{\sqrt{4 \cdot D_p \cdot R \cdot T_m}}\right)\right)$$

$C_m := \frac{1}{2} \cdot A_m$ <-- Dimensionless concentration (C/C_o)

$tt_m := \frac{m \cdot 100}{365}$ <-- time in years

Breakthrough Curve
R=20
v=1X10^{-5} cm/sec:

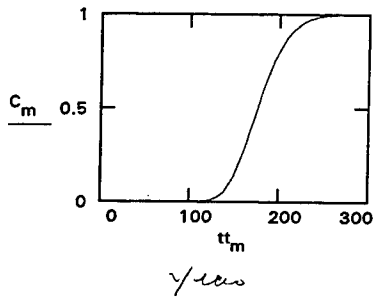

years

SEMIINFINITE MODEL (van GENUCHTEN AND AVES 1982.). BREAKTHROUGH CURVE PREDICTIONS

$L := 2743 \cdot cm$ $L = 89.993 \cdot ft$ <-- Distance to water table

Assume velocity is numerically equal to dispersion

$D_p := 0.28 \cdot \frac{ft^2}{day}$ Dispersion Coefficient

$v := 0.28 \cdot \frac{ft}{day}$ Average Pore Water Velocity

$v = 9.878 \cdot 10^{-5} \cdot \frac{cm}{sec}$ <-- 0.1 X hydraulic conductivit

$R := 30$ <— Lead Retardation Factor (assumed)

$m := 50 .. 150$

$t := 100 \cdot day$ < -- Time Index (days)

$T_m := m \cdot t$

$$A_m := \left(1 - erf\left(\frac{R \cdot L - v \cdot T_m}{\sqrt{4 \cdot D_p \cdot R \cdot T_m}}\right)\right) + \exp\left(\frac{v \cdot L}{D_p}\right) \cdot \left(1 - erf\left(\frac{R \cdot L + v \cdot T_m}{\sqrt{4 \cdot D_p \cdot R \cdot T_m}}\right)\right)$$

$C_m := \frac{1}{2} \cdot A_m$ <-- Dimensionless concentration (C/C_0)

$tt_m := \frac{m \cdot 100}{365}$ <-- time in years

Breakthrough Curve
R=30
v=1X10^{-4} cm/sec:

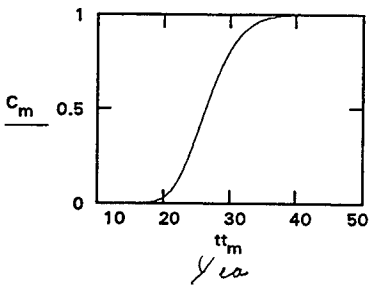

SEMIINFINITE MODEL (van GENUCHTEN AND AVES 1982.). BREAKTHROUGH CURVE PREDICTIONS

$L := 2743 \cdot cm$ $L = 89.993 \cdot ft$ < -- Distance to water table

Assume velocity is numerically equal to dispersion

$D_p := 0.028 \cdot \frac{ft^2}{day}$ Dispersion Coefficient

$v := 0.028 \cdot \frac{ft}{day}$ Average Pore Water Velocity

$v = 9.878 \cdot 10^{-6} \cdot \frac{cm}{sec}$ <-- 0.01 X hydraulic conductivity

$R := 30$ <— Lead Retardation Factor (assumed)

$m := 500, 510 .. 1400$

$t := 100 \cdot day$ < -- Time Index (days)

$T_m := m \cdot t$

$$A_m := \left(1 - erf\left(\frac{R \cdot L - v \cdot T_m}{\sqrt{4 \cdot D_p \cdot R \cdot T_m}}\right)\right) + \exp\left(\frac{v \cdot L}{D_p}\right) \cdot \left(1 - erf\left(\frac{R \cdot L + v \cdot T_m}{\sqrt{4 \cdot D_p \cdot R \cdot T_m}}\right)\right)$$

$C_m := \frac{1}{2} \cdot A_m$ <-- Dimensionless concentration (C/C_0)

$tt_m := \frac{m \cdot 100}{365}$ <-- time in years

Breakthrough Curve
R=30
$v = 1X10^{-5}$ cm/sec:

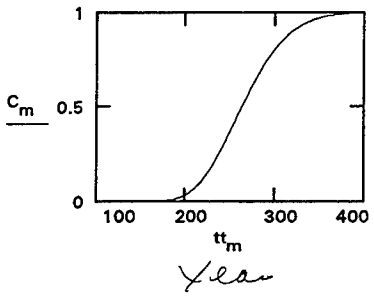

SEMIINFINITE MODEL (van GENUCHTEN AND AVES 1982.). BREAKTHROUGH CURVE PREDICTIONS

$L := 2743 \cdot cm$ $L = 89.993 \cdot ft$ <– Distance to water table

Assume velocity is numerically equal to dispersion

$D_p := 0.28 \cdot \frac{ft^2}{day}$ Dispersion Coefficient

$v := 0.28 \cdot \frac{ft}{day}$ Average Pore Water Velocity

$v = 9.878 \cdot 10^{-5} \cdot \frac{cm}{sec}$ <– 0.1 X hydraulic conductivit

$R := 50$ <— Lead Retardation Factor (assumed)

$m := 70 .. 250$

$t := 100 \cdot day$ < – Time Index (days)

$T_m := m \cdot t$

$$A_m := \left(1 - erf\left(\frac{R \cdot L - v \cdot T_m}{\sqrt{4 \cdot D_p \cdot R \cdot T_m}}\right)\right) + \exp\left(\frac{v \cdot L}{D_p}\right) \cdot \left(1 - erf\left(\frac{R \cdot L + v \cdot T_m}{\sqrt{4 \cdot D_p \cdot R \cdot T_m}}\right)\right)$$

$C_m := \frac{1}{2} \cdot A_m$ <– Dimensionless concentration (C/C_o)

$tt_m := \frac{m \cdot 100}{365}$ <– time in years

Breakthrough Curve
R=50
v=1X10^{-4} cm/sec:

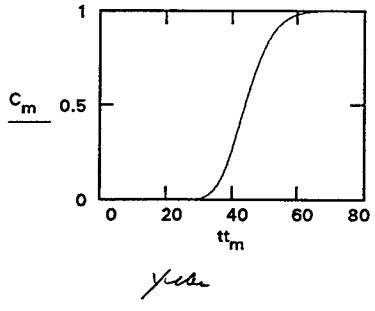

SEMIINFINITE MODEL (van GENUCHTEN AND AVES 1982.). BREAKTHROUGH CURVE PREDICTIONS

$L := 2743 \cdot cm$ $L = 89.993 \cdot ft$ <-- Distance to water table

Assume velocity is numerically equal to dispersion

$D_p := 0.28 \cdot \frac{ft^2}{day}$ Dispersion Coefficient

$v := 0.28 \cdot \frac{ft}{day}$ Average Pore Water Velocity

$v = 9.878 \cdot 10^{-5} \cdot \frac{cm}{sec}$ <-- 0.1 X hydraulic conductivity

$R := 75$ <-- Lead Retardation Factor (assumed)

$m := 100 .. 350$

$t := 100 \cdot day$ < -- Time Index (days)

$T_m := m \cdot t$

$$A_m := \left(1 - erf\left(\frac{R \cdot L - v \cdot T_m}{\sqrt{4 \cdot D_p \cdot R \cdot T_m}}\right)\right) + \exp\left(\frac{v \cdot L}{D_p}\right) \cdot \left(1 - erf\left(\frac{R \cdot L + v \cdot T_m}{\sqrt{4 \cdot D_p \cdot R \cdot T_m}}\right)\right)$$

$C_m := \frac{1}{2} \cdot A_m$ <-- Dimensionless concentration (C/C_0)

$tt_m := \frac{m \cdot 100}{365}$ <-- time in years

Breakthrough Curve
R=50 75
v=1X10^{-4} cm/sec:

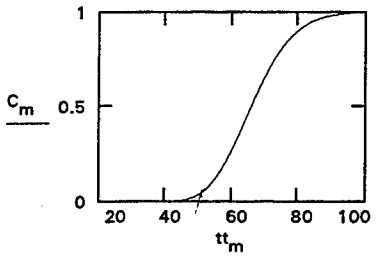

SEMIINFINITE MODEL (van GENUCHTEN AND AVES 1982.). BREAKTHROUGH CURVE PREDICTIONS

$L := 2743 \cdot cm$ $L = 89.993 \cdot ft$ <-- Distance to water table

Assume velocity is numerically equal to dispersion

$D_p := 0.028 \cdot \frac{ft^2}{day}$ Dispersion Coefficient

$v := 0.028 \cdot \frac{ft}{day}$ Average Pore Water Velocity

$v = 9.878 \cdot 10^{-6} \cdot \frac{cm}{sec}$ <-- ~~0.1~~ 0.01 X hydraulic conductivity

$R := 75$ <-- Lead Retardation Factor (assumed)

$m := 1000, 1100 .. 3500$

$t := 100 \cdot day$ < -- Time Index (days)

$T_m := m \cdot t$

$$A_m := \left(1 - erf\left(\frac{R \cdot L - v \cdot T_m}{\sqrt{4 \cdot D_p \cdot R \cdot T_m}}\right)\right) + \exp\left(\frac{v \cdot L}{D_p}\right) \cdot \left(1 - erf\left(\frac{R \cdot L + v \cdot T_m}{\sqrt{4 \cdot D_p \cdot R \cdot T_m}}\right)\right)$$

$C_m := \frac{1}{2} \cdot A_m$ <-- Dimensionless concentration (C/C_o)

$tt_m := \frac{m \cdot 100}{365}$ <-- time in years

Breakthrough Curve
R=~~50~~ 75
$v = 1X10^{-5}$ cm/sec:

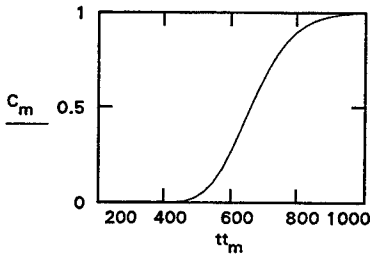

Appendix F
Model Input for a Typical Run[1]

[1] This run is for Range G, chloride and lead transport, using a 50-year soil loading. The receptor is a well located 100 ft from the range and the well is screened at 1 ft.

```
**************************11/17/1995 VERSION 4.2**************************

      RADCON -- WATERBORNE TRANSPORT COMPONENT for the Multimedia
            Environmental Pollutant Assessment System (MEPAS):
            Models movement of radionuclides and other chemicals
            in groundwater, surface water, and overland pathways.

            Battelle, Pacific Northwest Laboratory (PNL)
            P.O. Box 999, Richland, WA 99352

            Developed for the U.S. Department of Energy


       Input file for this run is EDWARDS .WIN
********************************************************************************
              Modeling Scenario Number  1
********************************************************************************

Name of Facility     = Camp Edwards - SAR
Name of Waste Unit   = CEMR
Transport Scenario   = Transport Pathway
Exposure Scenario    = NNYNNNNNNN
Usage Location Number =  1
Usage Location Medium =  1
Usage Location Name  =

TLIFE is the duration of release for each contaminant expressed in years.
TDIFF is the time difference in years between the start date for risk
calculations and the date when a contaminant was first released into
the environment (WS-TRISK minus WS-CDATE).


        Constituent        TLIFE    TDIFF        TFINAL
          Name             (years)  (years)      (years)

        LEAD             5.000E+01 0.000E+00    1.000E+04
        CHLORATE         5.000E+01 0.000E+00    1.000E+04

#       Constituent      NUM

 1      LEAD             2
 2      CHLORATE           2

Known Darcian Infiltration Rate from Site (VLEACH)  = 9.140E-02 cm/day


********************************************************************************

 Station                    = Boston
 Altitude in Meters           =   42.7
 Latitude in Degrees          =   42.2
 Height of Wind Measurement in Meters =   6.10
 Temperature Data is Given in Degrees : F
```

****

MONTH	TEMPERATURE	PRECIPITATION VOLUME (IN)	WIND (MPH)	CLOUDINESS (TENTHS)	NUMBER OF PRECIPITATION EVENTS
1	2.88E+01	3.62E+00	1.38E+01	6.20E+00	1.14E+01
2	2.94E+01	3.38E+00	1.38E+01	6.20E+00	1.05E+01
3	3.71E+01	3.86E+00	1.37E+01	6.40E+00	1.19E+01
4	4.72E+01	3.61E+00	1.32E+01	6.60E+00	1.13E+01
5	5.79E+01	3.22E+00	1.22E+01	6.60E+00	1.15E+01
6	6.72E+01	3.15E+00	1.15E+01	6.30E+00	1.06E+01
7	7.27E+01	3.15E+00	1.10E+01	6.20E+00	9.20E+00
8	7.10E+01	3.60E+00	1.08E+01	5.70E+00	9.90E+00
9	6.41E+01	3.19E+00	1.13E+01	5.60E+00	8.70E+00
10	5.40E+01	3.29E+00	1.20E+01	5.60E+00	9.10E+00
11	4.37E+01	3.91E+00	1.29E+01	6.40E+00	1.09E+01
12	3.28E+01	3.65E+00	1.36E+01	6.30E+00	1.16E+01

Total Water Available for Snowmelt Sediment Flux is = 2.76E+01 cm

Source-Term Type (ISTYPE) = 1
Source-Term Flux Boundary Conditions (ISOURC) = 3
Liquid Impoundment Index (IPOND) = 2
Source-Term Decay Index (IDECAY) = 2
Direct Discharge Surface Water Index (IDDSW) = 0
Number of Parent Constituents (NUMCON) = 2

Source-Term Configuration (ISCONF) = 4
Number of Media (NMED) = 4
Number of Integration Time Steps (NTIMES) = 40

Medium # 1 Equals Medium Type (MED) # 1
Medium # 2 Equals Medium Type (MED) # 1
Medium # 3 Equals Medium Type (MED) # 1
Medium # 4 Equals Medium Type (MED) # 3

Length of Release Unit (AL1 OR CLEN) = 5.49E+03 cm
Width of Release Unit (B1) = 1.68E+03 cm

Water concentration units are: ATTO (1.000E-18) Ci OR g

Constituent	CAS ID	Half-Life (Years)	Initial Conc. (ml/g)	Equilibrium Coeff. (g/ml)	Solubility limit	Surface Constituent Inventory (g OR Ci)
LEAD	7439921	1.00E+20	-9.99E+01	-9.99E+01	1.00E+23	1.00E+08
CHLORATE	7775099	1.00E+20	-9.99E+01	-9.99E+01	1.00E+23	1.00E+08

Constituent Flux (g/yr or Ci/yr) and Time (Years) at the Release Unit

Constituent #		Flux	Time	Constituent #		Flux	Time
1	1	2.00E+06	0.000E+00	1	2	2.00E+06	5.000E+01
2	1	2.00E+06	0.000E+00	2	2	2.00E+06	5.000E+01

New Constituent Flux (g/yr or Ci/yr) and Time (Years) at the Release Unit

Constituent #		Flux	Time	Constituent #		Flux	Time
1	1	2.00E+06	0.000E+00	1	2	2.00E+06	5.000E+01
2	1	2.00E+06	0.000E+00	2	2	2.00E+06	5.000E+01

The New Duration of Time that Constituents are Released from the Release Unit

#	Constituent	New TLIFE (Years)
1	LEAD	5.000E+01
2	CHLORATE	5.000E+01

Modeling Medium # 1
Medium Type (MED) = 1
Source Configuration = 4
Source Term Discharge Type = 1
PARTIALLY SATURATED ZONE

Thickness of Unsaturated Layer (H1) = 5.33E+01 cm
X-Direction Dispersivity (A1) = 5.33E-01 cm
Bulk Density (R2) = 1.40E+00 g/cm**3
Total Porosity (AN4) = 4.42E-01 (fraction)
Field Capacity (AN5) = 1.75E-01 (fraction)
Permeability (X2) = 6.22E+01 cm/day
Darcy Velocity (VLEACH) = 2.12E-01 cm/day
Soil-Type Coefficient (A2) = 4.90E+00

Moisture Content (AN5) = 28.36 %
Pore water velocity (U) = 7.49E-01 cm/day

NO	PARENT	HALFLIFE YEARS	KD ML/G	CENTERLINE ESTIMATED RETARDATION FACTOR	CENTERLINE ADVECTIVE TIME TO PEAK YEARS	TRAVEL TIME YEARS
1	LEAD	1.000E+20	1.000E+01	5.037E+01	9.594E+00	9.818E+00
2	CHLORATE	1.000E+20	0.000E+00	1.000E+00	1.905E-01	1.949E-01

Constituent	CAS ID	Half-Life (Years)	Initial Conc. (ml/g)	Equilibrium Coeff. (g/ml)	Solubility limit	Surface Constituent Inventory (g OR Ci)

```
LEAD       7439921 1.00E+20  2.80E-03 -9.99E+01    1.00E+23   1.00E+08
CHLORATE   7775099 1.00E+20  2.80E-03 -9.99E+01    1.00E+23   1.00E+08


                                  Mass Released      Mass Passed
                        Solution  From Source        This Medium
 Name     CASID   RATIO(a)  Method   (g or Ci)          (g or Ci)
-------- -------- --------- -------- ------------ --------------------

LEAD     7439921  1.919E-01 NUMERICAL  1.000E+08    8.910E+07 ( 89.1%)
CHLORATE 7775099  3.810E-03 NUMERICAL  1.000E+08    9.814E+07 ( 98.1%)

(a) RRATIO= 3.000E+01.  RATIO is the estimated time to peak divided by the
    duration of time over which the contaminant enters this medium.  When
    RATIO >= RRATIO, the equation for an instantaneous release is used,
    otherwise the numerical solution for a time varying release is used.


Modeling Medium #          2
Medium Type (MED)        = 1
Source Configuration     = 4
Source Term Discharge Type = 1
PARTIALLY SATURATED ZONE



Thickness of Unsaturated Layer (H1) =  1.12E+02 cm
X-Direction Dispersivity (A1)      =  1.12E+00 cm
Bulk Density (R2)                  =  1.60E+00 g/cm**3
Total Porosity (AN4)               =  3.80E-01 (fraction)
Field Capacity (AN5)               =  9.00E-02 (fraction)
Permeability (X2)                  =  5.70E+02 cm/day
Darcy Velocity (VLEACH)            =  2.12E-01 cm/day
Soil-Type Coefficient (A2)         =  4.05E+00



Moisture Content (AN5)  = 18.66 %
Pore water velocity (U) =  1.14E+00 cm/day


                                  CENTERLINE   CENTERLINE
                                  ESTIMATED    ADVECTIVE
NO  PARENT    DECAY RATE    KD    RETARDATION  TIME TO PEAK  TRAVEL TIME
              YEARS         ML/G  FACTOR       YEARS         YEARS

1  LEAD      6.931E-21  1.000E+01  8.675E+01    2.305E+01     2.338E+01
2  CHLORATE  6.931E-21  0.000E+00  1.000E+00    2.657E-01     2.695E-01


                                  Mass Released      Mass Passed
                        Solution  From Source        This Medium
 Name     CASID   RATIO(a)  Method   (g or Ci)          (g or Ci)
```

```
-------- -------- --------- -------- ------------ --------------------

LEAD     7439921  4.222E-01 NUMERICAL   1.000E+08    8.846E+07 ( 88.5%)
CHLORATE 7775099  5.009E-03 NUMERICAL   1.000E+08    9.814E+07 ( 98.1%)

(a) RRATIO= 3.000E+01. RATIO is the estimated time to peak divided by the
    duration of time over which the contaminant enters this medium. When
    RATIO >= RRATIO, the equation for an instantaneous release is used,
    otherwise the numerical solution for a time varying release is used.


Modeling Medium #          3
Medium Type (MED)        = 1
Source Configuration     = 4
Source Term Discharge Type = 1
PARTIALLY SATURATED ZONE


Thickness of Unsaturated Layer (H1) =  2.36E+03 cm
X-Direction Dispersivity (A1)       =  2.37E+01 cm
Bulk Density (R2)                   =  1.64E+00 g/cm**3
Total Porosity (AN4)                =  3.80E-01 (fraction)
Field Capacity (AN5)                =  9.00E-02 (fraction)
Permeability (X2)                   =  5.70E+02 cm/day
Darcy Velocity (VLEACH)             =  2.12E-01 cm/day
Soil-Type Coefficient (A2)          =  4.05E+00


Moisture Content (AN5)  = 18.66 %
Pore water velocity (U) =  1.14E+00 cm/day


                                    CENTERLINE   CENTERLINE
                                    ESTIMATED    ADVECTIVE
NO PARENT   DECAY RATE    KD        RETARDATION  TIME TO PEAK  TRAVEL TIME
           YEARS      ML/G          FACTOR       YEARS         YEARS

1 LEAD     6.931E-21  1.000E+01  8.890E+01   4.996E+02   5.048E+02
2 CHLORATE 6.931E-21  0.000E+00  1.000E+00   5.621E+00   5.678E+00


                          Mass Released     Mass Passed
                 Solution From Source       This Medium
 Name    CASID   RATIO(a) Method  (g or Ci)      (g or Ci)
-------- -------- -------- -------- ------------ --------------------

LEAD     7439921  6.246E+00 NUMERICAL   1.000E+08    8.848E+07 ( 88.5%)
CHLORATE 7775099  1.054E-01 NUMERICAL   1.000E+08    9.814E+07 ( 98.1%)

(a) RRATIO= 3.000E+01. RATIO is the estimated time to peak divided by the
    duration of time over which the contaminant enters this medium. When
```

RATIO >= RRATIO, the equation for an instantaneous release is used,
otherwise the numerical solution for a time varying release is used.

Modeling Medium # 4
Medium Type (MED) = 3
Source Configuration = 4
Source Term Discharge Type = 1
SATURATED ZONE AT A WELL

NO	PARENT	DECAY RATE YEARS	KD ML/G	RETARDATION FACTOR	CENTERLINE ESTIMATED TIME TO PEAK YEARS	CENTERLINE ADVECTIVE TRAVEL TIME YEARS
1	LEAD	6.931E-21	1.000E+01	6.767E+01	1.049E+01	1.103E+01
2	CHLORATE	6.931E-21	0.000E+00	1.000E+00	1.550E-01	1.629E-01

Darcy Velocity (DARCYV) = 1.23E+01 cm/day
Pore-water Velocity (U) = 5.13E+01 cm/day
Aquifer Thickness (H1) = 5.49E+03 cm
X-Direction Dispersivity (A1) = 1.52E+02 cm
Y-Direction Dispersivity (A2) = 5.03E+01 cm
Z-Direction Dispersivity (A3) = 3.81E-01 cm
Bulk Density (R2) = 1.60E+00 g/cm**3
Total Porosity (AN4) = 3.80E-01 (fraction)
Effective Porosity (AN5) = 2.40E-01 (fraction)
Length of Burial Area (AL1) = 5.49E+03 cm
Width of Burial Area (B1) = 1.68E+03 cm
Depth of Release Unit Below Water Table (HW) = 0.00E+00 cm
Centerline Downgradient Distance from
Center of Source (X2) = 3.05E+03 cm ≈ 100ft
Perpendicular Distance Off Flow Centerline (Y2) = 0.00E+00 cm
Angle Between Flow Direction and Receptor
Direction (ANGLE) = 0.00E+00 deg
Depth Below Watertable of Calculated
Concentration at Receptor (Z1) = 3.05E+01 cm ≈ 1ft

Name	CASID	RATIO(a)	Solution Method	Mass Released From Source (g or Ci)
LEAD	7439921	7.284E-03	NUMERICAL	1.000E+08
CHLORATE	7775099	2.656E-03	NUMERICAL	1.000E+08

(a) RRATIO= 3.000E+01. RATIO is the estimated time to peak divided by the duration of time over which the contaminant enters this medium. When RATIO >= RRATIO, the equation for an instantaneous release is used, otherwise the numerical solution for a time varying release is used.

****

Times are given as years since the start of risk calculations (WS-TRISK)

Concentration for LEAD when risk calculations begin (0.0 yrs) is:
0.000E+00 (g/ml or Ci/ml)

Concentration for CHLORATE when risk calculations begin (0.0 yrs) is:
0.000E+00 (g/ml or Ci/ml)

****

Times are given as years since the start of risk calculations (WS-TRISK)

Maximum Constituent Concentrations:

Name	CASID	Type(a)	Maximum Concentration (g/mL or Ci/mL)	Time (Years)
LEAD	7439921	PEAK	6.147E-04	581.0
CHLORATE	7775099	PEAK	2.651E-03	37.6

(a)
PEAK: The maximum concentration occurs as a peak concentration at the given time.

****

Appendix G
Model Predictions for Chloride Using a 1,000-Year Loading

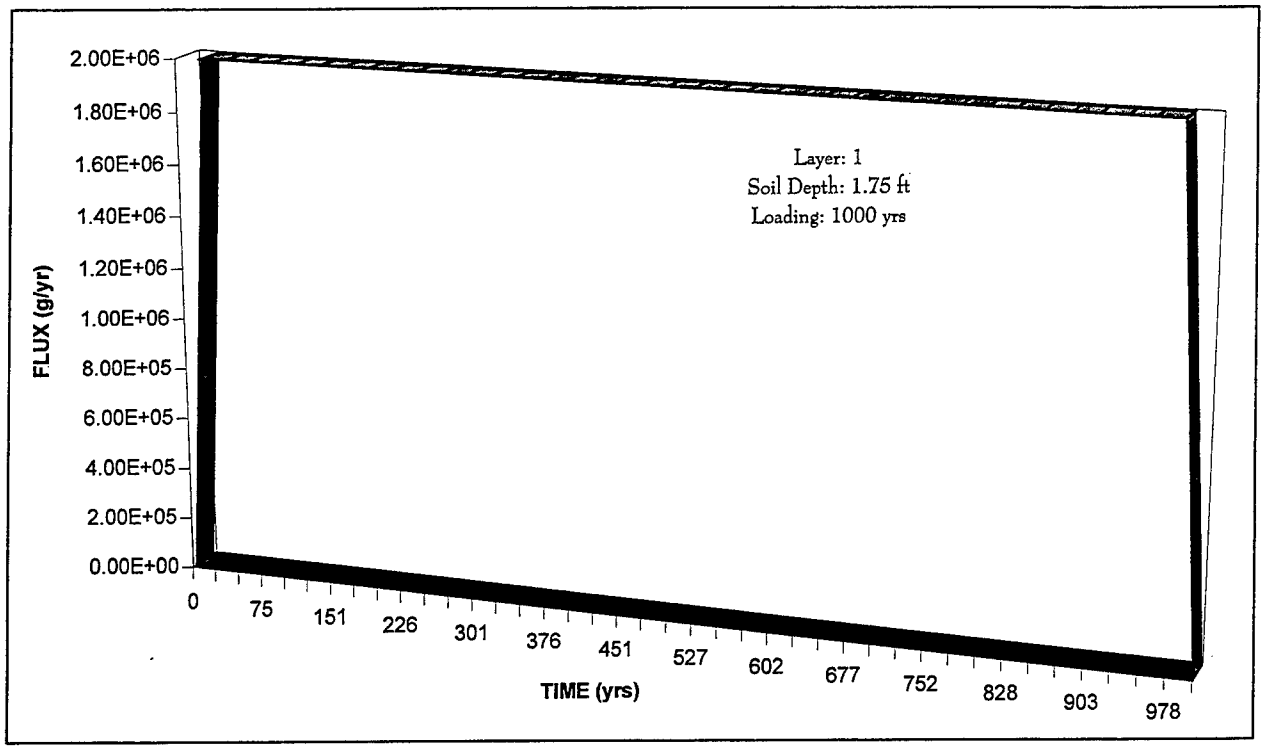

Figure G1. Model prediction for chloride transport through the first soil layer using a 1,000-year soil loading

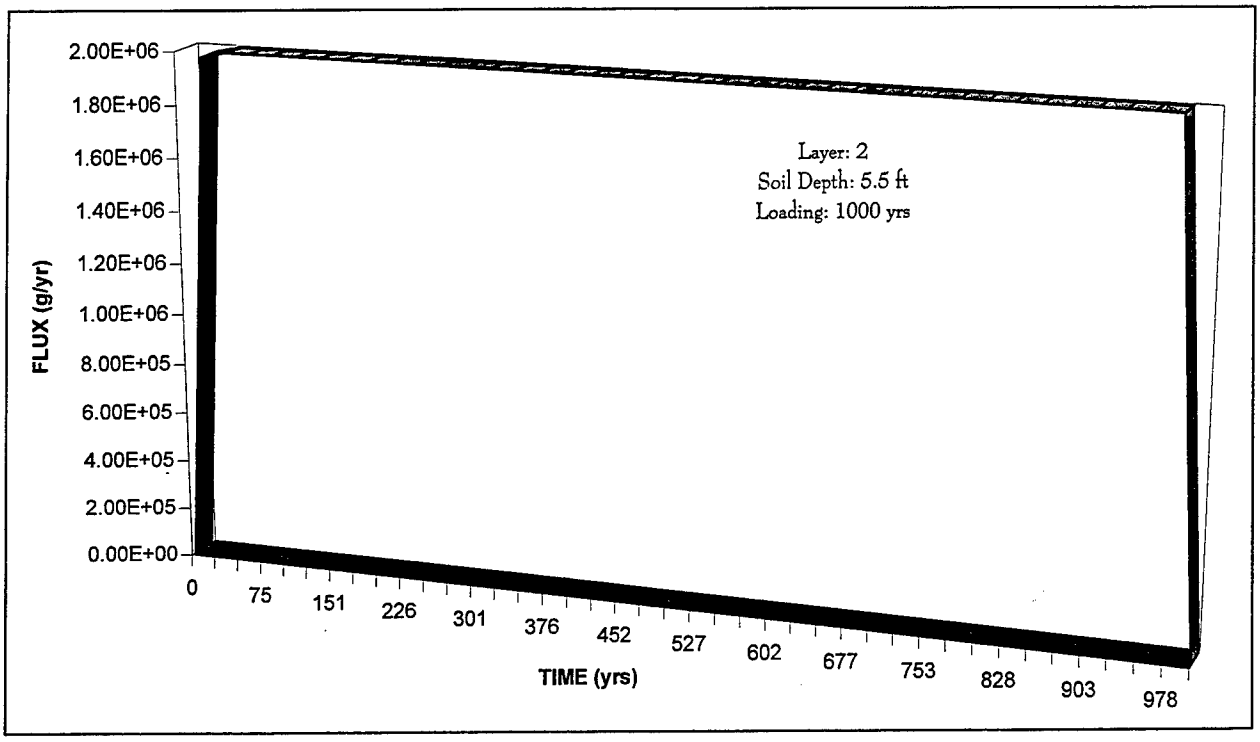

Figure G2. Model prediction for chloride transport through the second soil layer using a 1,000-year soil loading

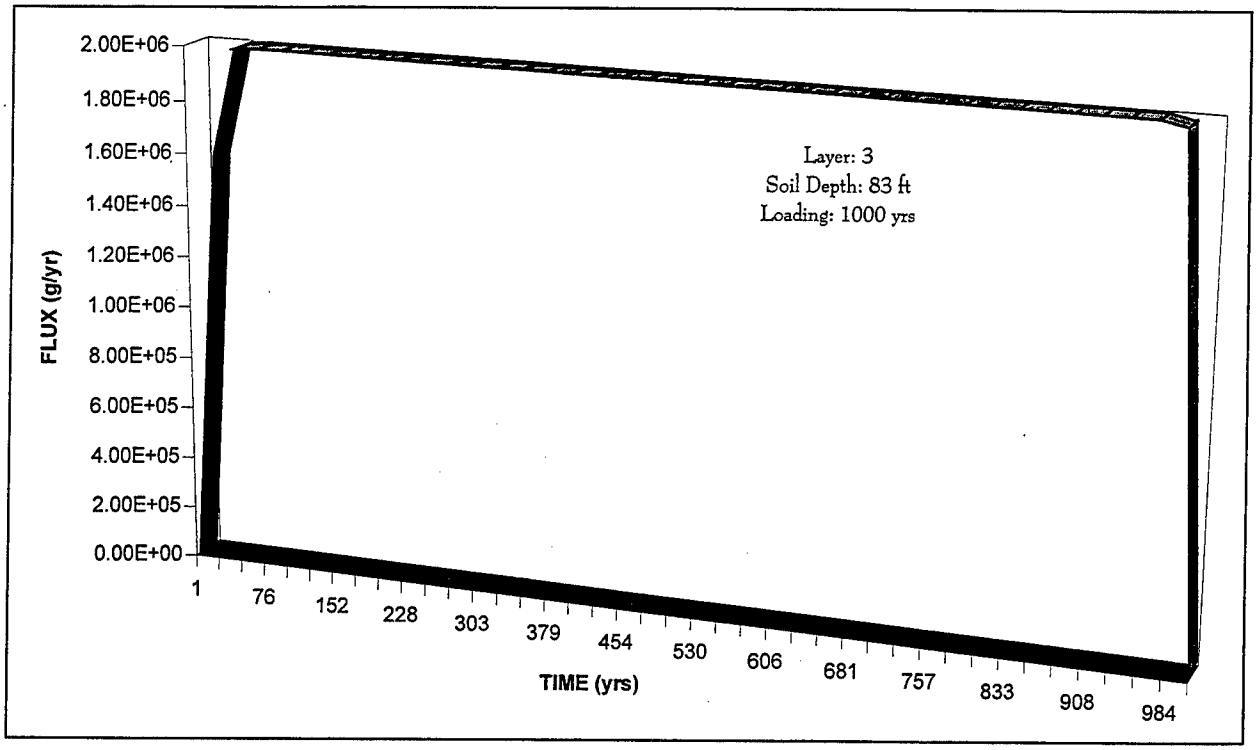

Figure G3. Model prediction for chloride transport through the third soil layer using a 1,000-year soil loading

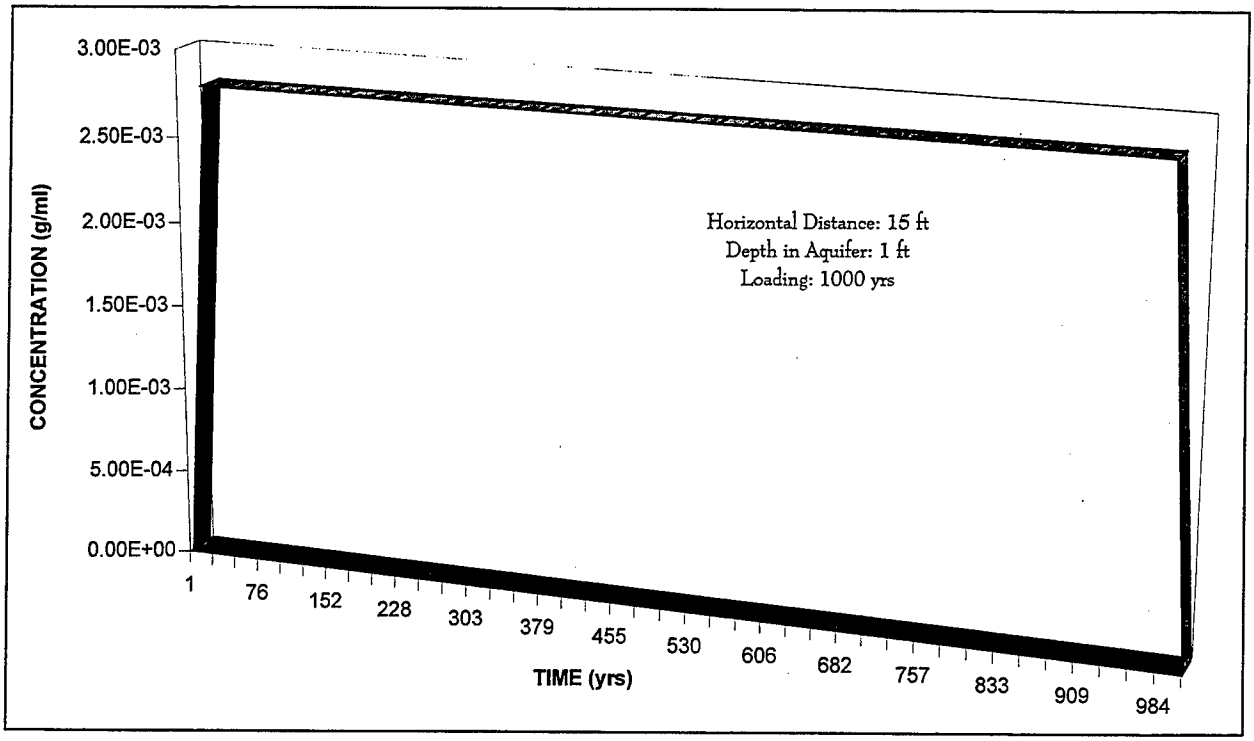

Figure G4. Model prediction for chloride transport in the aquifer using using a 1,000-year soil loading. The receptor is a well located 15 ft from the range and the well is screened at 0.3 m (1 ft)

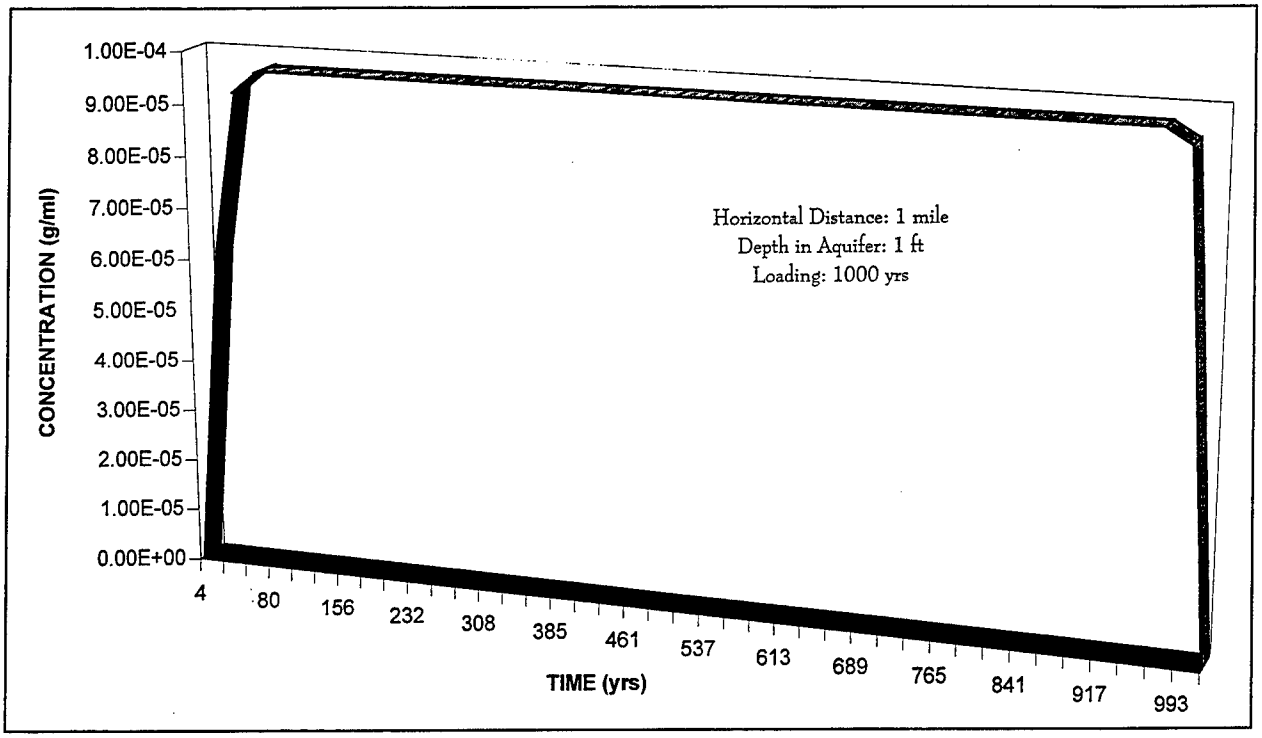

Figure G5. Model prediction for chloride transport in the aquifer using a 1,000-year soil loading. The receptor is a well located 1.6 km (1 mile) from the range and the well is screened at 0.3 m (1 ft)

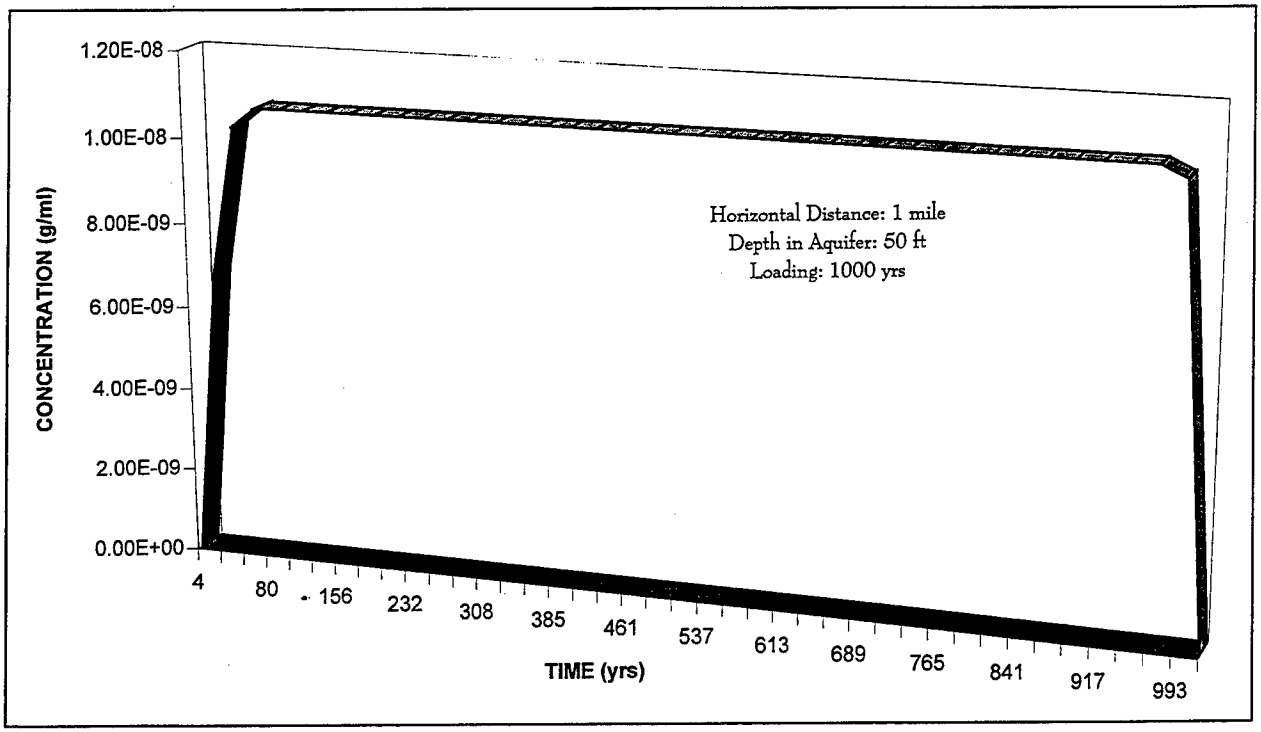

Figure G6. Model prediction for chloride transport in the aquifer using using a 1,000-year soil loading. The receptor is a well located 1.6 km (1 mile) from the range and the well is screened at 15.2 m (50 ft)

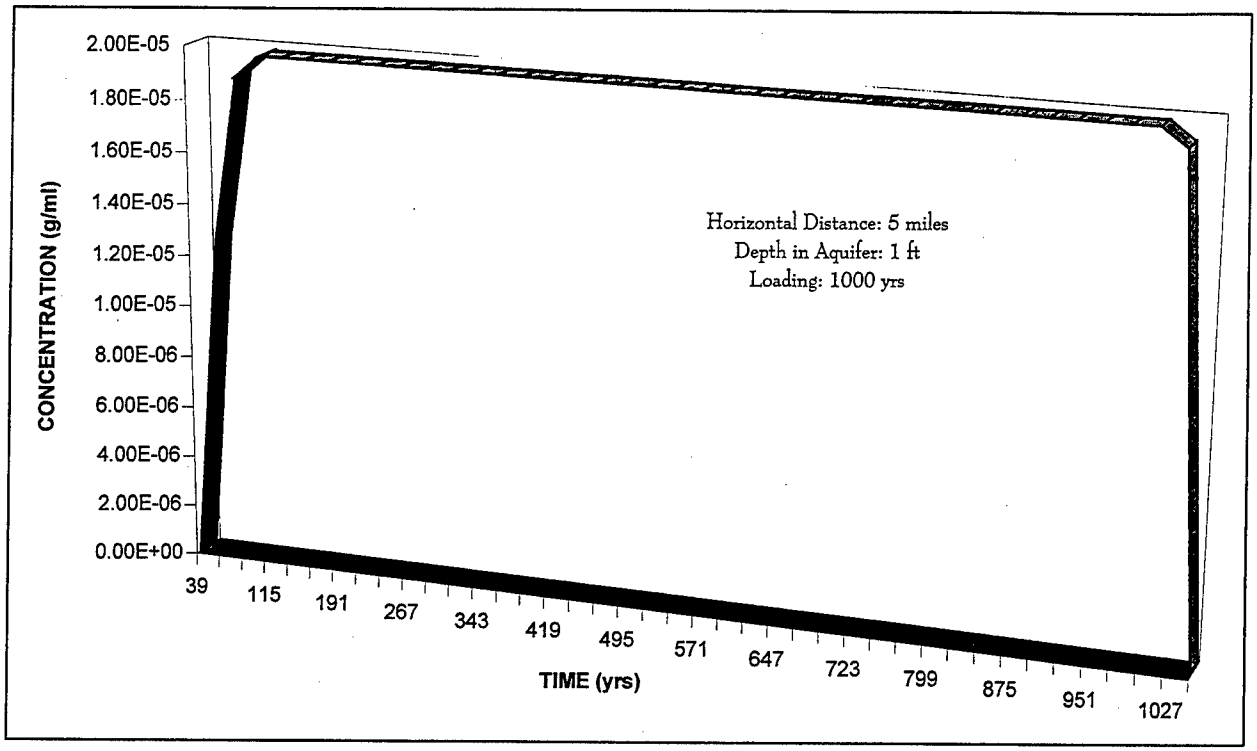

Figure G7. Model prediction for chloride transport in the aquifer using a 1,000-year soil loading. The receptor is a well located 8 km (5 miles) from the range and the well is screened at 0.3 m (1 ft)

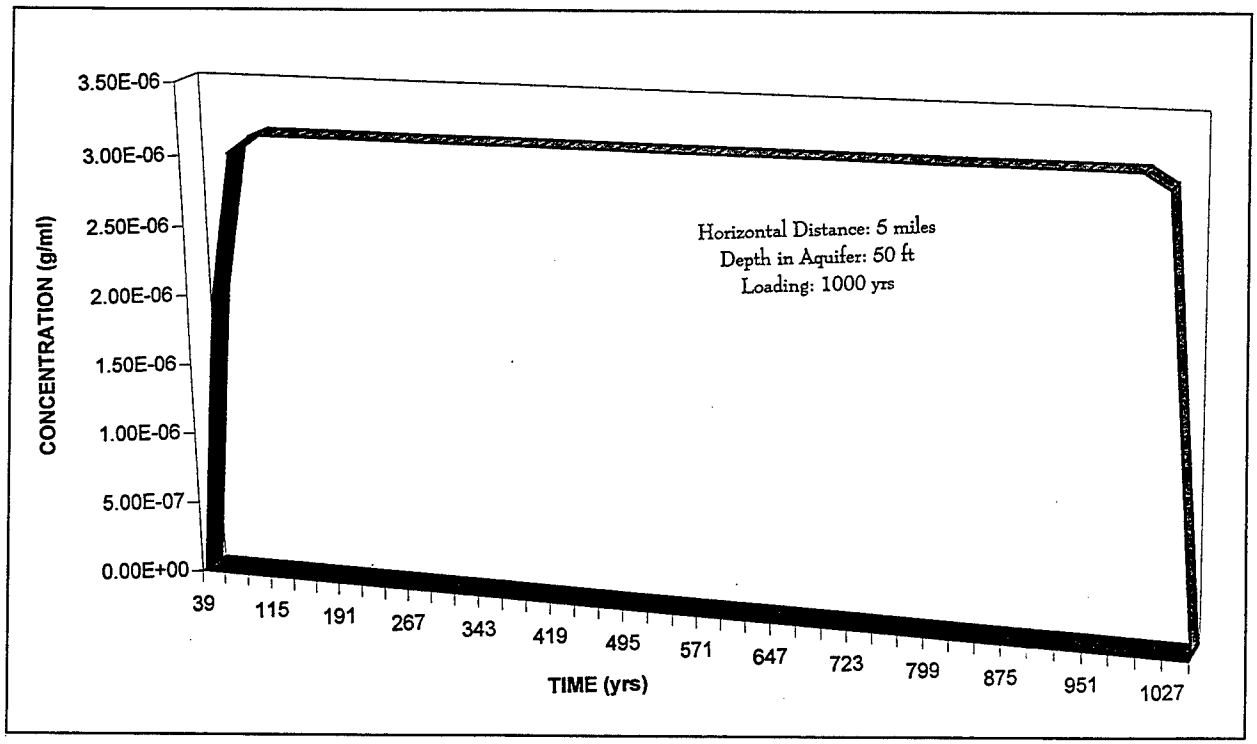

Figure G8. Model prediction for chloride transport in the aquifer using a 1,000-year soil loading. The receptor is a well located 8 km (5 miles) from the range and the well is screened at 15.2 m (50 ft)

REPORT DOCUMENTATION PAGE

Form Approved
OMB No. 0704-0188

Public reporting burden for this collection of information is estimated to average 1 hour per response, including the time for reviewing instructions, searching existing data sources, gathering and maintaining the data needed, and completing and reviewing the collection of information. Send comments regarding this burden estimate or any other aspect of this collection of information, including suggestions for reducing this burden, to Washington Headquarters Services, Directorate for Information Operations and Reports, 1215 Jefferson Davis Highway, Suite 1204, Arlington, VA 22202-4302, and to the Office of Management and Budget, Paperwork Reduction Project (0704-0188), Washington, DC 20503.

1. AGENCY USE ONLY *(Leave blank)*	2. REPORT DATE	3. REPORT TYPE AND DATES COVERED
	March 1998	Final report

4. TITLE AND SUBTITLE
Vertical Migration Potential of Metal Contaminants at Small Arms Firing Ranges, Camp Edwards Military Reservation, Massachusetts

5. FUNDING NUMBERS

6. AUTHOR(S)

R. Mark Bricka, Yilda B. Rivera, Patrick N. Deliman

7. PERFORMING ORGANIZATION NAME(S) AND ADDRESS(ES)

U.S. Army Engineer Waterways Experiment Station
3909 Halls Ferry Road, Vicksburg, MS 39180-6199

8. PERFORMING ORGANIZATION REPORT NUMBER
Technical Report
IRRP-98-3

9. SPONSORING/MONITORING AGENCY NAME(S) AND ADDRESS(ES)

Army National Guard Bureau
Massachusetts Military Reservation;
U.S. Army Corps of Engineers
Washington, DC 20314-1000

10. SPONSORING/MONITORING AGENCY REPORT NUMBER

11. SUPPLEMENTARY NOTES

Available from National Technical Information Services, 5285 Port Royal Road, Springfield, VA 22161.

12a. DISTRIBUTION/AVAILABILITY STATEMENT

Approved for public release; distribution is unlimited.

12b. DISTRIBUTION CODE

13. ABSTRACT (Maximum 200 words)

The primary goal of the United States Military is to train and equip troops to maintain military readiness. Training range areas represent a major element in keeping the Army ready to accomplish this mission. Training ranges represent considerable investments in time, money, and other resources. Small arms training ranges (SARs) represent a large portion of this investment.

Projectiles utilized as part of small arms training range activities have accumulated at many SARs for a number of years. These projectiles are composed of toxic metals such as lead, copper, and antimony. Such metals may pose a threat to the environment through contaminant migration.

Environmental personnel at Camp Edwards, an Army National Guard training area located at the Massachusetts Military Reservation (CEMR), recognized the potential for small arms activities to adversely affect the environment. To better understand the migration of the metals and the potential threat of the metals to groundwater, CEMR initiated investigations to study such metal migration. This report presents the results of this investigation.

(Continued)

14. SUBJECT TERMS	15. NUMBER OF PAGES
See reverse.	198
	16. PRICE CODE

17. SECURITY CLASSIFICATION OF REPORT	18. SECURITY CLASSIFICATION OF THIS PAGE	19. SECURITY CLASSIFICATION OF ABSTRACT	20. LIMITATION OF ABSTRACT
UNCLASSIFIED	UNCLASSIFIED		

13. (Concluded).

This report presents the results of the following: an overview of factors which affect metal migration from small arms training areas, soil sampling conducted at the CEMR small arms ranges, and modeling efforts to predict the time of impact of the metal migration on groundwater. As part of this study, soil borings were collected to a depth of 27.4 m (90 ft), and borings were analyzed for five metals in 15.2-cm (6-in.) sections. In addition, limited soil properties were also analyzed in the laboratory. These results indicate that the metal contaminants are migrating vertically but have not been transported to a depth greater than 1.8 m (6 ft) at any of the ranges. Modeling efforts predict that measurable concentrations of lead are not expected until after 350 years.

14. Subject Terms.

Bullets
Camp Edwards
Firing ranges
Groundwater
Groundwater contamination
Heavy metals
Impact areas
Lead
Massachusetts Military Reservation
Metal contamination
Modeling
Projectiles
Small arms training
Soil contamination
Soil sampling